



Analyzing the Influence of Urban Morphology on Thermal Microclimate in a Temperate Maritime Climate

Amer Habib AL-Sudani

BSc, Msc (University of Baghdad)

A Thesis Submitted in Accordance with the Requirements of the
University of Liverpool for the Degree of Doctor in Philosophy
(PhD)

Faculty of Humanities and Social Sciences

School of Architecture

September 2018

Table of Content

TABLE OF CONTENT	3
LIST OF FIGURES	8
LIST OF TABLES	15
LIST OF EQUATIONS	17
ABSTRACT	19
ACKNOWLEDGEMENTS	21
CONFERENCES	23
LIST OF ABBREVIATIONS AND SYMBOLS	25
CHAPTER ONE	27
1 THE INTRODUCTION OF RESEARCH	29
1.1 INTRODUCTION.....	29
1.2 RESEARCH BACKGROUND	29
1.3 PROBLEM STATEMENT	30
1.4 RESEARCH QUESTIONS, AIM AND OBJECTIVES	31
1.5 THE SCOPE OF THE STUDY	32
1.6 OVERVIEW OF THESIS STRUCTURE	33
CHAPTER TWO	35
2 LITERATURE REVIEW	37
2.1 INTRODUCTION.....	37
2.2 THE URBAN MORPHOLOGY.....	37
2.2.1 <i>The configuration of urban space</i>	38
2.2.2 <i>The types of urban space</i>	41
2.2.3 <i>The analysis of urban space</i>	43
2.2.4 <i>The description of urban form</i>	45
2.3 THE URBAN CLIMATE.....	49
2.3.1 <i>Surface temperature</i>	51
2.3.2 <i>Air temperature</i>	54
2.3.3 <i>Urban – Orientation – Climate relationship</i>	55
2.4 THE RESEARCHES OF URBAN-CLIMATE RELATIONSHIP	57

2.5	CONCLUSIONS	66
CHAPTER THREE		67
3	CHAPTER THREE: RESEARCH METHODOLOGY	69
3.1	INTRODUCTION	69
3.2	THE STUDY AREA CONTEXT	70
3.2.1	<i>The case study</i>	75
3.3	FIELD MEASUREMENTS	82
3.3.1	<i>The measurement sessions</i>	83
3.3.2	<i>The measurement tools</i>	83
3.3.3	<i>The distribution of measurement points</i>	87
3.4	URBAN MORPHOLOGICAL PARAMETER (UMP)	90
3.4.1	<i>The buffer zone</i>	91
3.4.2	<i>Floor Area Ratio (FAR)</i>	93
3.4.3	<i>Site Coverage Ratio (SCR)</i>	95
3.4.4	<i>Compactness Index (CI)</i>	96
3.4.5	<i>Sky View Factor (SVF)</i>	98
3.4.6	<i>Degree of Compactness (Dc)</i>	101
3.4.7	<i>Facade to site ratio (FSR)</i>	103
3.4.8	<i>Shape Factor (SF)</i>	104
3.5	STATISTICAL APPROACH	108
3.5.1	<i>Data sorting</i>	110
3.5.2	<i>The statistical framework</i>	112
3.6	CONCLUSION	115
CHAPTER FOUR		117
4	THE DEVELOPMENT OF NOVEL URBAN MORPHOLOGICAL PARAMETERS	119
4.1	INTRODUCTION	119
4.2	THE PARTIAL SKY VIEW FACTOR (SVFx)	121
4.2.1	<i>The basic concept of SVFx</i>	121
4.2.2	<i>The calculation of SVFx from the fisheye lens images</i>	123
4.2.3	<i>The calculation of SVFx from the three dimensional models</i>	128
4.3	THE FAÇADE VIEW FACTOR (FVFX)	133
4.3.1	<i>The basic concept of FVFX</i>	135
4.4	THE TOTAL FAÇADE VIEW FACTOR (FVF)	140
4.5	CONCLUSIONS	141
5	FIELD WORK (RESULTS AND DISCUSSION)	145

5.1	INTRODUCTION.....	145
5.2	THE SELECTED DAYS OF STUDY	145
5.3	THE HOT SEASON MEASUREMENTS	147
5.3.1	<i>The sunny days measurements</i>	147
5.3.2	<i>The partially cloudy days measurements</i>	158
5.3.3	<i>The cloudy days measurements</i>	167
5.4	THE COLD SEASON MEASUREMENTS (COLD).....	172
5.4.1	<i>The sunny days measurements</i>	172
5.4.2	<i>The partially cloudy days measurements</i>	175
5.4.3	<i>The cloudy days measurements</i>	175
5.5	THE URBAN MORPHOLOGICAL PARAMETERS MEASUREMENTS	179
5.5.1	<i>Floor Area Ratio (FAR)</i>	179
5.5.2	<i>Site Coverage Ratio (SCR)</i>	179
5.5.3	<i>Compactness Index (CI)</i>	180
5.5.4	<i>Degree of Compactness (Dc)</i>	181
5.5.5	<i>Facade to Site Ratio (FSR)</i>	181
5.5.6	<i>Shape Factor (SF)</i>	182
5.5.7	<i>Sky View Factor (SVF)</i>	182
5.5.8	<i>Partial Sky View Factor (SVFx)</i>	183
5.5.9	<i>Total Façade View Factor (FVF)</i>	185
5.5.10	<i>Façade View Factor (FVFX)</i>	185
5.6	THE CORRELATIONS OF URBAN MORPHOLOGICAL PARAMETERS (UMP)	187
5.7	CONCLUSION	190
CHAPTER SIX.....		193
6	RESULTS AND ANALYSES	195
6.1	INTRODUCTION.....	195
6.2	SUNNY DAYS ANALYSES (SU-HOT)	196
6.2.1	<i>Night period: midnight to 6.00 am (ni-su-hot)</i>	197
6.2.2	<i>Morning period: 6.00 am to 12.00 noon (mo-su-hot)</i>	200
6.2.3	<i>Afternoon period: 12.00 noon to 6.00 pm (no-su-hot)</i>	203
6.2.4	<i>Evening period: 6.00 pm to midnight (ev-su-hot)</i>	206
6.3	PARTIALLY CLOUDY DAYS ANALYSIS (PR-HOT)	209
6.3.1	<i>Night period: midnight to 6.00 am (ni-pr-hot)</i>	209
6.3.2	<i>Morning period: 6.00 am to 12.00 noon (mo-su-hot)</i>	212
6.3.3	<i>Afternoon period: 12.00 noon to 6.00 pm (no-pr-hot)</i>	215
6.3.4	<i>Evening period: 6.00 pm to midnight (ev-pr-hot)</i>	218
6.4	CLOUDY DAYS ANALYSIS (CL-HOT).....	220

6.4.1	<i>Night period: Midnight to 6.00am (ni-cl-hot)</i>	220
6.4.2	<i>Morning period: 6.00 am to 12.00 noon (mo-cl-hot)</i>	223
6.4.3	<i>Afternoon period: 12.00 noon to 6.00 pm (no-cl-hot)</i>	225
6.4.4	<i>Evening period: 6.00 pm to midnight (ev-cl-hot)</i>	228
6.5	CONCLUSIONS.....	230
CHAPTER SEVEN		233
7	THE DISCUSSION OF STATISTICAL APPROACH RESULTS.....	235
7.1	INTRODUCTION	235
7.2	THE CLIMATIC FACTORS	235
7.2.1	<i>The sunny days</i>	236
7.2.2	<i>The partial cloudy days</i>	238
7.2.3	<i>The cloudy days</i>	239
7.3	THE URBAN MORPHOLOGICAL PARAMETERS (UMP)	240
7.3.1	<i>Floor Area Ratio (FAR)</i>	242
7.3.2	<i>Site Coverage Ratio (SCR)</i>	245
7.3.3	<i>Compactness Index (CI)</i>	248
7.3.4	<i>Degree of Compactness (Dc)</i>	250
7.3.5	<i>Façade to Site Ratio (FSR)</i>	253
7.3.6	<i>Shape Factor (SF)</i>	257
7.3.7	<i>Sky View Factor (SVF)</i>	259
7.3.8	<i>Partial Sky View Factor (SVFx)</i>	263
7.3.9	<i>Façade View Factor (FVFX)</i>	269
7.3.10	<i>Total Façade View Factor (FVF)</i>	273
7.4	THE TOTAL EFFECT OF UMP.....	277
7.5	CONCLUSIONS.....	294
CHAPTER EIGHT		297
8	CONCLUSIONS	299
8.1	INTRODUCTION	299
8.2	ANSWERING THE RESEARCH QUESTIONS	299
8.3	AIM AND OBJECTIVES	302
8.4	FUTURE RESEARCH	305
8.5	LIMITATIONS OF THE RESEARCH	306
APPENDICES		309
APPENDIX A: THE MODIFIED MODELS (M.M) OF THE SUNNY DAYS.....		309
	<i>The Night Period</i>	309

<i>The Morning Period</i>	311
<i>The Afternoon Period</i>	313
<i>The Evening Period</i>	315
APPENDIX B: THE MODIFIED MODELS (M.M) OF THE PARTIALLY CLOUDY DAYS	317
<i>The Night Period</i>	317
<i>The Morning Period</i>	319
<i>The Afternoon Period</i>	321
<i>The Evening Period</i>	323
APPENDIX C: THE MODIFIED MODELS (M.M) OF THE CLOUDY DAYS	325
<i>The Night Period</i>	325
<i>The Morning Period</i>	327
<i>The Afternoon Period</i>	329
<i>The Evening Period</i>	331
REFERENCES	333

List of Figures

Figure 2.1 the urban fabric and the elements of urban form (Oliveira 2016)	38
Figure 2.2 the diversity of urban space configuration (Carmona et al. 2010)	40
Figure 2.3 the diversity of cross section of buildings around the urban space (Krier 1979).....	41
Figure 2.4 the parallelism and convergence of masses to form the directional spaces (Carmona et al. 2010).....	42
Figure 2.5 width-to-length ratios between static and dynamic space (Carmona et al. 2010).....	42
Figure 2.6 the spacemate diagram (Berghauser Pont & Haupt 2007)	46
Figure 2.7 the parameters of Local climate zones method (compact high-rise zone) (Stewart & Oke 2012).....	47
Figure 2.8 the analysis of space syntax by DepthmapX software (Al_Sayed 2018). 48	
Figure 2.9 the urban boundary layer (UBL) and its sub-layers (Erell et al. 2011) ...	49
Figure 2.10 the radiation system of urban area (Oke 1988).....	52
Figure 2.11 the energy balance of urban area (Erell et al. 2011).....	54
Figure 3.1 The research map.....	70
Figure 3.2 the North West of England and the Merseyside area – UK (Met Office 2016c)(Young & Sly 2010)	72
Figure 3.3 The Liverpool City Region and the Merseyside county (Sykes et al. 2013)	73
Figure 3.4 The old Minster Court compound (Edwards 2016).....	76
Figure 3.5 The removed part of minster Court (Edwards 2016).....	77
Figure 3.6 The current site plan of Minster Court compound (digimap.edina.ac.uk/os)	78
Figure 3.7 The dimensions of Minster Court compound	78
Figure 3.8 Three dimensional model of Minster Court.....	80
Figure 3.9 the brick wall are dominant in Minster Court.....	81
Figure 3.10 The ground materials (asphalt, grass and concrete paths).....	81
Figure 3.11 the location of Minster Court relative to the weather station of Liverpool university (www.google.co.uk)	82

Figure 3.12 HOBO U12 data logger (www.onsetcomp.com)	84
Figure 3.13 The testing of sensor validity at a one of Liverpool University's laboratories	84
Figure 3.14 the hours of data loggers validation process	85
Figure 3.15 The handmade protective shield for sensor	86
Figure 3.16 the weather station of University of Liverpool	86
Figure 3.17 The locations of the measurement points	87
Figure 3.18 The surroundings of measurement locations (H1, H2 and H3)	88
Figure 3.19 The surroundings of measurement locations (H5, H6 and H9)	88
Figure 3.20 The surroundings of measurement locations (H7, H8 and H10)	89
Figure 3.21 The surroundings of measurement locations (H3, H11 and H12)	90
Figure 3.22 The buffer zones of the measurement points	92
Figure 3.23 the names of urban space walls	93
Figure 3.24 The calculation method of FAR	94
Figure 3.25 The calculation method of SCR	95
Figure 3.26 The calculation method of CI	97
Figure 3.27 The supportive tools to capture the fish eye image	99
Figure 3.28 the editing of fisheye image	100
Figure 3.29 Use HemiView software to calculate SVF	100
Figure 3.30 The black-white fisheye images at the hot season	101
Figure 3.31 The calculation method of Dc	102
Figure 3.32 The calculation method of FSR	103
Figure 3.33 The comparison between buildings regarding to their shape factor values and some related aspects	106
Figure 3.34 The shape factor values without ground floor area	107
Figure 3.35 The comparison of SF values with and without ground floor area	107
Figure 3.36 The sorting of field measurement data	112
Figure 3.37 The sorting of weather station data	112
Figure 3.38 The first part of the statistical framework	114
Figure 3.39 The second part of the statistical framework	115
Figure 4.1 The concept of the Partial Sky View Factor (SVFx)	122

Figure 4.2 The concept of the Partial Sky View Factor (SVF _x) on the fisheye lens images	123
Figure 4.3 Determining the diameter and border of the fisheye lens image	124
Figure 4.4 Cropping and saving of the circular projection of the fisheye lens image	124
Figure 4.5 Establishment of the four sectors on the fisheye lens image	125
Figure 4.6 The selection process of visible sky.....	126
Figure 4.7 The production process of the black-white fisheye lens image.....	126
Figure 4.8 The calculation of SVF and SVF _x depending on the pixels number	127
Figure 4.9 The interface of the plugin	129
Figure 4.10 The false segments (sky) and the true segments (buildings) on the hemisphere.....	129
Figure 4.11 The workflow of the plugin algorithm in Grasshopper	130
Figure 4.12 The verification of the SVF _x plugin versus LSS Chronolux and HemiView	131
Figure 4.13 The graphical outputs of the SVF _x plugin.....	132
Figure 4.14 The graphical differences between the top view of hemisphere and the fish eye image for the measurement point H8.	132
Figure 4.15 The main variables of FVF _x	135
Figure 4.16 The variables of the On-Site formula to calculate FVF _x	136
Figure 4.17 The effect of overlapping facades on FVF _x calculations	137
Figure 4.18 The relationships between FVF _x and urban space sides	138
Figure 4.19 The effect of facade locations and orientations on the FVF _x value.....	138
Figure 4.20 The influential facades regarding to the twelve measurement points in Minster Court	139
Figure 4.21 Changing the compactness of urban space by changing the relationships between the facades and the monitoring point	140
Figure 5.1 The sunny days measurements for locations H1,H2 and H4 – hot season	148
Figure 5.2 The sunny days measurements for locations H7,H8 and H10 – hot season	149

Figure 5.3 The sunny days measurements for locations H3, H5, H9, H11 and H12 – hot season	150
Figure 5.4 The urban configurations of north-facing locations H1, H2 and H4	151
Figure 5.5 The urban configurations of east-facing locations H3, H11 and H12 ...	151
Figure 5.6 The urban configurations of open space locations H5 and H9	152
Figure 5.7 The urban configurations of west-facing locations H7, H8 and H10	152
Figure 5.8 The vegetation cover around locations H3 and H12	153
Figure 5.9 The shadow areas around locations H1, H2 and H4	155
Figure 5.10: The vegetation cover around locations H1, H2 and H4	156
Figure 5.11: The visual comparison of compactness between locations H7, H8 and H10	157
Figure 5.12 partially cloudy days measurements for locations H1, H2 and H4 – hot season (PART 1).....	161
Figure 5.13 partially cloudy days measurements for locations H1, H2 and H4 – hot season (PART 2).....	162
Figure 5.14 partially cloudy days measurements for locations H7, H8 and H10 – hot season (PART 1).....	163
Figure 5.15 partially cloudy days measurements for locations H7, H8 and H10 – hot season (PART 2).....	164
Figure 5.16 partially cloudy days measurements for locations H3, H5, H9, H11 and H12 – hot season (PART 1).....	165
Figure 5.17 partially cloudy days measurements for locations H3, H5, H9, H11 and H12 – hot season (PART 2).....	166
Figure 5.18 The cloudy days measurements for locations H1, H2 and H4 – hot season	169
Figure 5.19 The cloudy days measurements for locations H7, H8 and H10 – hot season	170
Figure 5.20 The cloudy days measurements for locations H3, H5, H9, H11 and H12 – hot season	171
Figure 5.21: The sunny days measurements – cold season.....	174
Figure 5.22: The partially cloudy days measurements – cold season.....	177
Figure 5.23: The cloudy days measurements – cold season.....	178

Figure 5.24 the values of floor area ratio (FAR)	179
Figure 5.25 the values of site coverage ratio (SCR).....	180
Figure 5.26 the values of compactness index (CI).....	180
Figure 5.27 the degree of compactness values.....	181
Figure 5.28 the values of façade to site ratio (FSR).....	182
Figure 5.29 the values of shape factor (SF)	182
Figure 5.30 the values of sky view factor	183
Figure 5.31 the values of partial sky view factor (SVFx).....	184
Figure 5.32 the values of total façade view factor (FVF).....	185
Figure 5.33 the values of façade view facto (FVFX).....	186
Figure 6.1 Percentages of R-Sq(adj) for the basic and modified air temperature models in (ni-su-hot)	197
Figure 6.2 Percentages of R-Sq(adj) for the basic and modified air temperature models in (mo-su-hot).....	201
Figure 6.3 Percentages of R-Sq(adj) for the basic and modified air temperature models in (no-su-hot).....	204
Figure 6.4 Percentages of R-Sq(adj) for the basic and modified air temperature models in (ev-su-hot)	207
Figure 6.5 Percentages of R-Sq(adj) for the basic and modified air temperature models in (ni-pr-hot)	210
Figure 6.6 Percentages of R-Sq(adj) for the basic and modified air temperature models in (mo-pr-hot).....	213
Figure 6.7 Percentages of R-Sq(adj) for the basic and modified air temperature models in (no-pr-hot)	216
Figure 6.8 Percentages of R-Sq(adj) for the basic and modified air temperature models in (ev-pr-hot)	218
Figure 6.9 Percentages of R-Sq(adj) for the basic and modified air temperature models in (ni-cl-hot)	221
Figure 6.10 Percentages of R-Sq(adj) for the basic and modified air temperature models in (mo-cl-hot).....	224
Figure 6.11 Percentages of R-Sq(adj) for the basic and modified air temperature models in (no-cl-hot).....	226

Figure 6.12 Percentages of R-Sq(adj) for the basic and modified air temperature models in (ev-cl-hot)	229
Figure 7.1 The symbols of improvement rates (%)	241
Figure 7.2 The total effect of UMP on Ta under the sunny sky	278
Figure 7.3 The total effect of UMP on Ta under the partially cloudy sky	279
Figure 7.4 The total effect of UMP on Ta under the cloudy sky	281
Figure 7.5 The total effect of the urban morphological parameters (UMP) on the air temperature (Ta) throughout the hot season	283
Figure 7.6 the correlation of SVFn with the differences of maximum air temperature between the site (Ta) and the reference weather station (a.Ta)	284
Figure 7.7 the correlation of SVFe with the differences of maximum air temperature between the site (Ta) and the reference weather station (a.Ta)	284
Figure 7.8 the correlation of SVFs with the differences of maximum air temperature between the site (Ta) and the reference weather station (a.Ta)	285
Figure 7.9 the correlation of SVFw with the differences of maximum air temperature between the site (Ta) and the reference weather station (a.Ta)	285
Figure 7.10 the correlation of FVFn with the differences of maximum air temperature between the site (Ta) and the reference weather station (a.Ta)	286
Figure 7.11 the correlation of FVFe with the differences of maximum air temperature between the site (Ta) and the reference weather station (a.Ta)	287
Figure 7.12 the correlation of FVFs with the differences of maximum air temperature between the site (Ta) and the reference weather station (a.Ta)	287
Figure 7.13 the correlation of FVFw with the differences of maximum air temperature between the site (Ta) and the reference weather station (a.Ta)	288
Figure 7.14 the correlation of SF with the differences of maximum air temperature between the site (Ta) and the reference weather station (a.Ta)	289
Figure 7.15 the correlation of SVF with the differences of maximum air temperature between the site (Ta) and the reference weather station (a.Ta)	290
Figure 7.16 the correlation of SCR with the differences of maximum air temperature between the site (Ta) and the reference weather station (a.Ta)	290
Figure 7.17 the correlation of FSR with the differences of maximum air temperature between the site (Ta) and the reference weather station (a.Ta)	291

Figure 7.18 the correlation of CI with the differences of maximum air temperature between the site (T_a) and the reference weather station ($a.T_a$)292

Figure 7.19 the correlation of Dc with the differences of maximum air temperature between the site (T_a) and the reference weather station ($a.T_a$)292

Figure 7.20 the correlation of FVF with the differences of maximum air temperature between the site (T_a) and the reference weather station ($a.T_a$)293

Figure 7.21 the correlation of FAR with the differences of maximum air temperature between the site (T_a) and the reference weather station ($a.T_a$)293

List of Tables

Table 3-1 The monthly averages from 1981 to 2010 – the city of Liverpool (Met Office 2018)	74
Table 5-1: The correlation coefficients (r) and significant levels (p-value) of UMP	187
Table 6-1 the values of standard error of the regression (S) for (ni-su-hot)	198
Table 6-2 The signs of modified models (M.M.) for (ni-su-hot).....	200
Table 6-3 The values of standard error of the regression (S) for (mo-su-hot)	202
Table 6-4 the signs of modified models (M.M.) for (mo-su-hot).....	203
Table 6-5 The values of standard error of the regression (S) for (no-su-hot)	205
Table 6-6 The signs of modified models (M.M.) for (no-su-hot)	206
Table 6-7 The values of standard error of the regression (S) for (ev-su-hot).....	207
Table 6-8 The signs of modified models (M.M.) for (ev-su-hot).....	209
Table 6-9 The values of standard error of the regression (S) for (ni-pr-hot).....	211
Table 6-10 The signs of modified models (M.M.) for (ni-pr-hot).....	212
Table 6-11 The values of standard error of the regression (S) for (mo-pr-hot)	213
Table 6-12 The signs of modified models (M.M.) for (mo-pr-hot)	215
Table 6-13 The values of standard error of the regression (S) for (no-pr-hot).....	216
Table 6-14 The signs of modified models (M.M.) for (no-pr-hot)	217
Table 6-15 The values of standard error of the regression (S) for (ev-pr-hot).....	219
Table 6-16 The signs of modified models (M.M.) for (ev-pr-hot).....	220
Table 6-17 The values of standard error of the regression (S) for (ni-cl-hot).....	222
Table 6-18 The signs of modified models (M.M.) for (ni-cl-hot).....	223
Table 6-19 Tthe values of standard error of the regression (S) for (mo-cl-hot)	224
Table 6-20 The signs of modified models (M.M.) for (mo-cl-hot)	225
Table 6-21 The values of standard error of the regression (S) for (no-cl-hot)	227
Table 6-22 The signs of modified models (M.M.) for (no-cl-hot)	228
Table 6-23 The values of standard error of the regression (S) for (ev-cl-hot).....	229
Table 6-24 The signs of modified models (M.M.) for (ev-cl-hot).....	230
Table 7-1 The signs of climatic factors for the basic models (B.M)	236
Table 7-2 The improvement rates of R-sq(adj) by FAR.....	242
Table 7-3 the behaviours of air temperature by the effect of FAR.....	243

Table 7-4	The improvement rates of R-sq(adj) by SCR	245
Table 7-5	The behaviours of air temperature by the effect of SCR	246
Table 7-6	The improvement rates of R-sq(adj) by CI	249
Table 7-7	The behaviour of air temperature by the effect of CI	250
Table 7-8	The improvement rates of R-sq(adj) by Dc	251
Table 7-9	the behaviours of air temperature by the effect of Dc	251
Table 7-10	The improvement rates of R-sq(adj) by FSR.....	254
Table 7-11	The behaviours of air temperature by the effect of FSR.....	255
Table 7-12	The improvement rates of R-sq(adj) by SF	257
Table 7-13	the behaviours of air temperature by the effect of SF	258
Table 7-14	The improvement rates of R-sq(adj) by SVF.....	260
Table 7-15	The behaviours of air temperature by the effect of SVF.....	261
Table 7-16	The improvement rates of R-sq(adj) by SVF _x	264
Table 7-17	The behaviours of air temperature by the effect of SVF _n	265
Table 7-18	The behaviours of air temperature by the effect of SVF _e	266
Table 7-19	The behaviours of air temperature by the effect of SVF _s	267
Table 7-20	The behaviours of air temperature by the effect of SVF _w	268
Table 7-21	The improvement rates of R-sq(adj) by FVF _x	269
Table 7-22	The behaviours of air temperature by the effect of FVF _n	271
Table 7-23	the behaviours of air temperature by the effect of FVF _e	272
Table 7-24	The behaviours of air temperature by the effect of FVF _s	273
Table 7-25	The behaviours of air temperature by the effect of FVF _w	273
Table 7-26	The improvement rates of R-sq(adj) by FVF.....	274
Table 7-27	the behaviours of air temperature by the effect of FVF	275
Table 7-28	The total effect of UMP on Ta under the sunny sky	278
Table 7-29	The total effect of UMP on Ta under the partially cloudy sky	280
Table 7-30	The total effect of UMP on Ta under the cloudy sky	281

List of Equations

Equations 6-1 Basic models (B.M.) of (ni-su-hot)	199
Equations 6-2 Basic models (B.M.) of (mo-su-hot)	202
Equations 6-3 Bbasic models (B.M.) of (no-su-hot)	204
Equations 6-4 Basic models (B.M.) of (ev-su-hot).....	208
Equations 6-5 Basic models (B.M.) of (ni-pr-hot).....	211
Equations 6-6 Bbasic models (B.M.) of (mo-pr-hot)	214
Equations 6-7 Basic models (B.M.) of (no-pr-hot)	217
Equations 6-8 Basic models (B.M.) of (ev-pr-hot).....	219
Equations 6-9 basic models (B.M.) of (ni-cl-hot)	221
Equations 6-10 Basic models (B.M.) of (mo-cl-hot)	225
Equations 6-11 Basic models (B.M.) of (no-cl-hot)	227
Equations 6-12 Tasic models (B.M.) of (ev-cl-hot).....	230

Abstract

One of the severest impacts of climate change is temperature increase, and this will be especially evident in urban areas. This study is investigating the influence of urban morphology on the thermal microclimate of urban spaces.

Air temperature measurements were conducted at twelve locations, for both hot and cold seasons under the temperate maritime climate, in a residential development in the city of Liverpool, UK. Detailed analyses were undertaken to investigate and establish possible links between the urban morphology and the observed variations in air temperature around the residential complex especially in hot season.

Seven well-known urban parameters were used to get the numerical description of morphology around unsymmetrical and non-directional urban spaces. Three novel parameters have been developed by this study. One of them is intended to measure the compactness of an urban space while the other two are introduced as a novel approach by embedding the cardinal directions in the urban parameters. The directions are used usually as independent parameters to classify the urban canyons (directional space) and compare their results in the urban environmental studies.

Linear regression has been utilized to develop statistical models between the solar radiation, ambient air temperature and each of the ten urban morphological parameters as independent variables, while the on-site measured air temperatures were used as a dependent variable. About 400 statistical models were produced. Comparisons between adjusted R^2 values were held to determine the effect size of each urban parameter on air temperature. The increasing or decreasing of air temperature under the effect of the urban parameter was deduced by the signs of coefficients of the parameters in the regression models.

Overall, the analyses showed the superiority of the developed novel parameters that were based on the idea of direction versus other parameters in relation to the interpretation of differences in air temperature on a spatial basis. The results of this study may support the development of urban planning regulations, and may help the

development process of numerical models to predict variations in air temperatures from the effect of urban morphology.

Acknowledgements

I would like to take the opportunity to thank all that have helped in one way or another, particularly the following individuals.

Firstly, I extend sincere gratitude to my supervisor, Prof. Steve Sharples. He has supported me from the very beginning of my studies particularly for his time and expertise within the field of study. I also thank my secondary supervisor, Dr. Fei Chen, for her friendly conversations and words of encouragement.

I dedicate a profound appreciation to all staff and faculty members at Liverpool University's School of Architecture for their help and support. As well as to my colleagues at the University, especially Mr. Zuhair Nasar and Mr. Hussein Essam for their generous hospitality.

I would like to express my deepest thanks to the Iraqi Government (The Higher Committee for Education Development in Iraq (HCED)), for their financial support, whom without its completion would not have been possible.

I am sincerely grateful to my wife for her support, understanding and patience during both the good and hard times throughout this journey. A big thank you to my children Yousif, Zainab and Ahmed for their patience and endurance throughout my absence.

A very special thank you to my parents, parents-in-law and all my family in Iraq.

Finally, I extend my appreciation to my brother and his family in Cardiff for their support and assistance during my time in the U.K. A particularly thank you to my niece Ms. Ayaat Al-Sudani for her time and invaluable help.

Conferences

Al-sudani, A. and Sharples, S. (2016) 'Analyzing urban microclimate air temperature measurements using a novel parameter - the partial sky view factor', in *PLEA 2016 - Proceedings of the 32nd International Conference on Passive and Low Energy Architecture*; Los Angeles, pp. 1239–1245



Al-Sudani, A., Hussein, H. and Sharples, S. (2017) 'Sky View Factor Calculation A computational-geometrical approach', in *Space Syntax and Ontologies-Volume 2-eCAADe 35*. Rome, Italy: Sapienza University of Rome, pp. 673–682. Available at: http://papers.cumincad.org/data/works/att/ecaade2017_240.pdf.

List of Abbreviations and Symbols

a.Ta	Ambient air temperature (°C)
AVG	Average air temperature (°C)
B.M	Basic Models
CI	Compactness Index (m^2/m^2)
cl	Cloudy sky
cold	Cold season
Dc	Degree of Compactness ($m^2*no.$)
ev	Evening period
FAR	Floor Area Ratio (m^2/m^2)
FSR	Façade to Site Ratio (m^2/m^2)
FVF	Total Façade View Factor
FVFX	Façade View Factor
hot	Hot season
M.M	Modified Models
MAX	Maximum air temperature (°C)
MIN	Minimum air temperature (°C)
mo	Morning period
ni	Night period
no	Afternoon period
p	Significant level
p.cl	Partially cloudy sky
R ²	Coefficient of determination (%)
R-Sq(adj)	Adjusted coefficient of determination (%)
S	Standard error of the regression
SCR	Site Coverage Ratio (m^2/m^2)
SF	Shape Factor (m^2/m^3)
su	Sunny sky
SVFX	Partial Sky View Factor
SVF	Sky View Factor
solar	Solar radiation energy (W/m^2)
Ta	On-site air temperature (°C)
UHI	Urban heat island
UBL	Urban Boundary Layer
UCL	Urban Canopy Layer
UMP	Urban morphological parameter

Chapter One

1 The Introduction of Research

1.1 Introduction

An investigation of urban areas will, without a shadow of a doubt, expand human's knowledge in several fields. More specifically, this includes the efficiency of morphological features in mitigating the negative impacts of the climatic factors within urban areas and supporting the positive features. Therefore, measuring, understanding and examining the relationships between them are a vibrant topic of research as a basic step towards developing strategies and mechanisms to be consistent with those factors or control them

This chapter is dedicated to delivering a concise review of the research background and to present the research statement, questions, aim, objectives and scope. The structure of the thesis will be outlines in the last section of this chapter.

1.2 Research Background

In 2010, the total urban area that is defined by administrative boundaries was about 3% of the global land area (excluding Greenland and Antarctica), however, the built-up area that is predominated by artificial surfaces was less than 1% (Liu et al. 2014). The latter contributes significantly in the frequency and intensity of heat waves (Tan et al. 2010), energy consumption (Wong et al. 2011) and daily variances of air temperature that reach more than 10 C degrees compared to the rural surroundings (Collier 2006). Such problem are going to be more aggressive in the coming years (Collier 2006; Roth et al. 2011) due to the increasing of the world population that is growing about 83 million people annually (United Nations 2015), whereby 54% of humans are currently living in urban areas (Population Reference Bureau 2016). Consequently, the continuity of urbanisation and its repercussions are inevitable and the pace of climate change is escalating and moving forward (Chen & Ng 2011; Collier 2006). Thus, there is a need to quantify and assess the adaptation measures that influence urban climate like urban morphology and vegetation types (Matzarakis 2015). The urban morphology encompasses a large set of parameters

that significantly contributes in altering the urban climate (Martins et al. 2014). Unfortunately, the thoughtful urban planning based on the climate has only been weakly explored (Taesler 1991), due to the knowledge of urban climate not being translated efficiently in the design and construction processes of more sustainable urban areas; as a result of, the lack of communication between those interested in this matter (planners, architects, climatologists ...) (Chen & Ng 2011; Arnfield 2003; Roth et al. 2011).

This gap is influenced by a range of difficulties such as the nonlinearities, complexities and heterogeneity of the urban-climate relationship on different spatial scale, where the energy balance for each urban morphological unit is distinctive at each spatial scale. It is likely the differences in energy exchange between two land-use zones are less than the differences among a one building facades due to the latter being expose to different time-varying airflow and solar radiation (Arnfield 2003). As a result, this helps to create different climatic conditions from site to site within walkable distance, this is known as microclimate. The diversity of climate types (Tropical, Dry, Temperate, Continental and Polar) also contribute to the complexity of urban morphology-microclimate relationship, where each of them show different patterns in terms of its climatic factors. A different type of difficulty, which hinder the bridging of the gap, is the scarcity of quantitative tools and methods that help in exploring the concepts of the climate-responsive design that may contribute to ameliorating the microclimate of urban area (Roth et al. 2011; Nakano, Bueno, Norford & C. F. Reinhart 2015; Maoh & Kanaroglou 2009; Chen et al. 2012).

It is therefore important to take into account the influence of the urban morphology on climate by understanding the effect of these parameters on climatic factors like air temperature, and employ such knowledge to achieving a more sustainable urban design practice.

1.3 Problem Statement

This study is devoted to utilizing and developing many parameters as a tool to measure the urban morphology for the purpose of investigating their influences on

air temperature variation that act as an indicator of thermal microclimate under the maritime temperate climate.

In general, the temperate climates are characterized by unpredictable conditions throughout the year and possibility to experience the four seasons in one day (Met Office 2012). By adding these characteristics to the reasons of the aforementioned gap, it can be seen the reason for the shortage of urban-climate studies in temperate climate in general (Taleghani et al. 2015) and, in particular, the United Kingdom (Hughes 2006).

At the UK, the temperature is now higher of about 1°C than it was in the 1960s, and the warmest 8 years in the UK have occurred in the last 12 years (GOV.UK 2014). Approximately 2000 people died during the UK's 2003 record-breaking heat wave where the air reached temperatures of 38.5°C in Kent on the 10th of August (Met Office 2015). Also a six-week of the summer of 2018 from end of June to the August will be remembered due to the daytime temperatures in many parts of UK consistently topped 30 °C (The guardian 2018).

As a step to minimize a repeat of such events, the 2008 Climate Change Act was introduced to reduce the emissions of CO₂ in the UK by 80% by 2050 compared to the base year at 1990 (GOV.UK 2014). Urban area is responsible for a large part of these emissions as an energy source for heating and cooling processes.

Finding and understanding the links between urban parameters and air temperature may help to reduce the negative climatic effects in urban area, although, there is no guaranteed formula to insure a good microclimate in the urban spaces (Cortese et al. 2009). Therefore, the necessity of urban-climate studies continues on the urban micro-scale especially under the temperate climate.

1.4 Research Questions, Aim and Objectives

In order to gain an in-depth understanding of why the urban morphology should to be linked to the thermal microclimate, urban morphological parameters and air temperature variation will be investigated together as well as highlighting the mutual

interplay between them will be unveiled. This research is intended to answer the following four questions:

- 1- To what extent does the urban morphology influences the thermal microclimate of an urban space under the hot season condition of a maritime temperate climate?
- 2- Does the role of an urban morphological parameter vary by changing the sky conditions and day intervals?
- 3- Is there a mechanism to improve the ability of urban morphological parameter in regard to the interpretation of air temperature variation?
- 4- Does the behaviour of air temperature in terms of increase and decrease subject to the method of express the urban morphology?

It is hoped that answering these research questions will deepen our knowledge regarding the urban microclimate, this being the research aim. To reach this aim, the following five objectives need to be achieved:

- 1- To explore briefly the basic knowledge that is related to the nature of this research.
- 2- Exploring the existing methods to measure the urban morphology.
- 3- Measuring the air temperatures within urban spaces of a case study under a maritime temperate climate.
- 4- Developing a statistical approach to assess and analyse the relationships between urban morphological parameters and air temperature.
- 5- Determining the size of effect of each parameter and its role in terms of increasing or decreasing the air temperature.

1.5 The scope of the study

According to the foregoing, the pursuits to develop novel methods to define and quantify urban morphology features are highly recommended especially, in respect of simplifying and understanding the complexity of urban climate relations.

Therefore, this research intends to deepen our knowledge about the urban microclimate by analysing the variation of air temperature indicators (AVG. MAX. and MIN.) under three sky conditions (sunny, partially cloudy, and cloudy) within the hot season of a maritime temperate climate. This versus the variety of urban morphology that is expressed by ten different parameters where three of them were developed by this study and one of the seven parameters was used for the first time against the variation of outside air temperature on a micro-scale under the maritime temperate climate, according to the researcher's best knowledge. The outcomes of this study can provide architects and urban planners with an essential knowledge to make decisions that contribute to improve the thermal environment of the urban spaces.

1.6 Overview of Thesis Structure

This thesis includes eight chapters as follows:

Chapter One: provides a research background as a step to announce the problem statement, followed by the research questions, aim and objectives. The end of this chapter is devoted to concisely showing the scope of this study and the structure of thesis.

Chapter two: presents a part of theoretical background of this study in regard to the urban morphology and urban climate, in addition to separate section to review some of the previous research efforts that may have common points with this study.

Chapter three: sets out the research methodology, in addition to reviewing the case study, field measurement and the urban morphological parameters. While the last section will show the statistical approach to examine the relationship between air temperature and urban parameters.

Chapter four: introduces the novel methods that will be developed by this study to describe the urban morphology in three sections where each one of them was devoted to explain one method.

Chapter five: reveals and discusses the field measurements, it comprises mainly of four sections. The first section aims to show the mechanism to determine the days of

study. The second and third sections show and discuss the measurements of hot and cold seasons respectively. The final part of this section reveals the correlations between the urban morphological parameters values that were calculated for twelve locations throughout the site of case study.

Chapter six: presents and analyses the results of statistical approach mainly in three sections. First section deals with the results of sunny days, whilst the second and third sections present the results of the partially cloudy and cloudy days respectively.

Chapter seven: introduces the discussion of the statistical approach results mainly in three sections. First, a discussion of the behaviours of the climatic factors. The second section reveals the size effect of urban morphological parameters and their roles in regard to the behaviours of air temperature. The third section present mechanism and comparison to determine the total effect of urban parameters.

Chapter eight: summarises the key findings of the study which link to the research questions and objectives, followed by the research limitations and future work.

Chapter Two

2 Literature Review

2.1 Introduction

This chapter provides an interdisciplinary and theoretical background in three parts. It starts with the urban morphology section followed by the urban microclimate section. These two sections represent a brief knowledge base for the research efforts about the urban morphology-microclimate relationships that will show in the third part of this chapter. This concise work is to expand our understanding of the research context by clarifying what is meant by the idioms of the study's title and the potential connections between them.

2.2 The Urban Morphology

The word 'morphology' denotes the knowledge of form (Pont & Haupt 1900). Thus, the urban morphology term was defined from the morphologists perspective as the study of urban forms, taking into account the factors that contribute to their transformation and growth processes. Thus the elements that shape and structure the urban fabric of a city such as buildings, urban plots and urban spaces (street and squares) can be pointed out by urban form (Oliveira 2016), as shown by [Figure 2.1](#). Therefore, urban areas are extremely complex objects due to the diversity of their elements that can be grouped together in unlimited number of configurational relationships (ibid).

In order to simplify the complexity of urban form various concepts have been suggested, one of which is the concept of spatial urban scales (Kropf 2014). From the standpoint of perception, there are both large and small scale spaces. If the space cannot be perceived from an observation point, then it is beyond the human perception and it is a large scale space. The small scale space can be perceived from an observation point, although it is apparently larger than the human body. Hence, the perception of small spaces can be a prerequisite for the large urban environment perception (Jiang et al. 2000) and, therefore, understanding the urban form. Essentially, there are two types of the building-space relationship. The first case

when the space surrounds the building and secondly when the buildings define the space (Carmona et al. 2010). This study concerns the urban spaces that are defined by buildings.

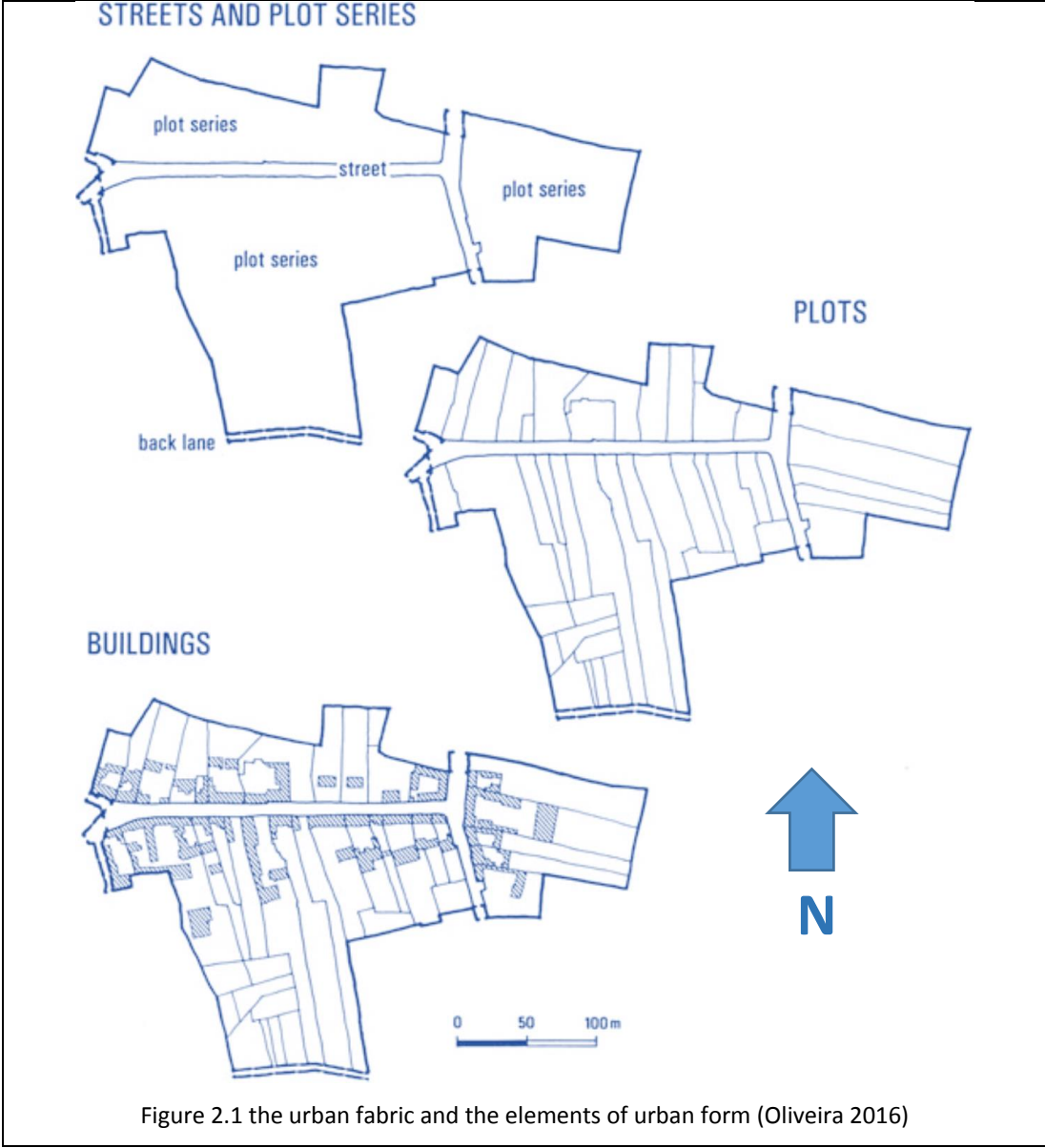
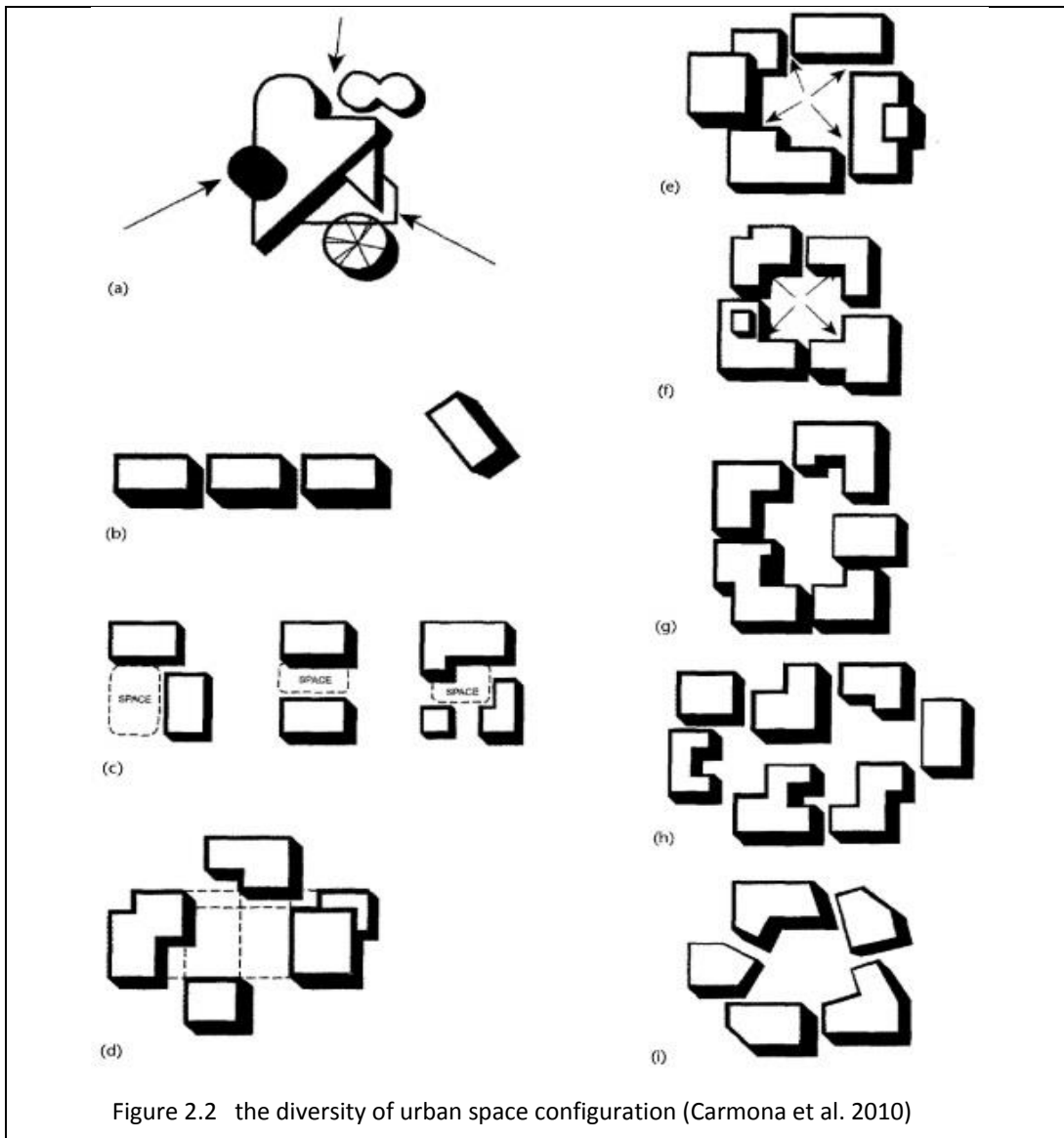


Figure 2.1 the urban fabric and the elements of urban form (Oliveira 2016)

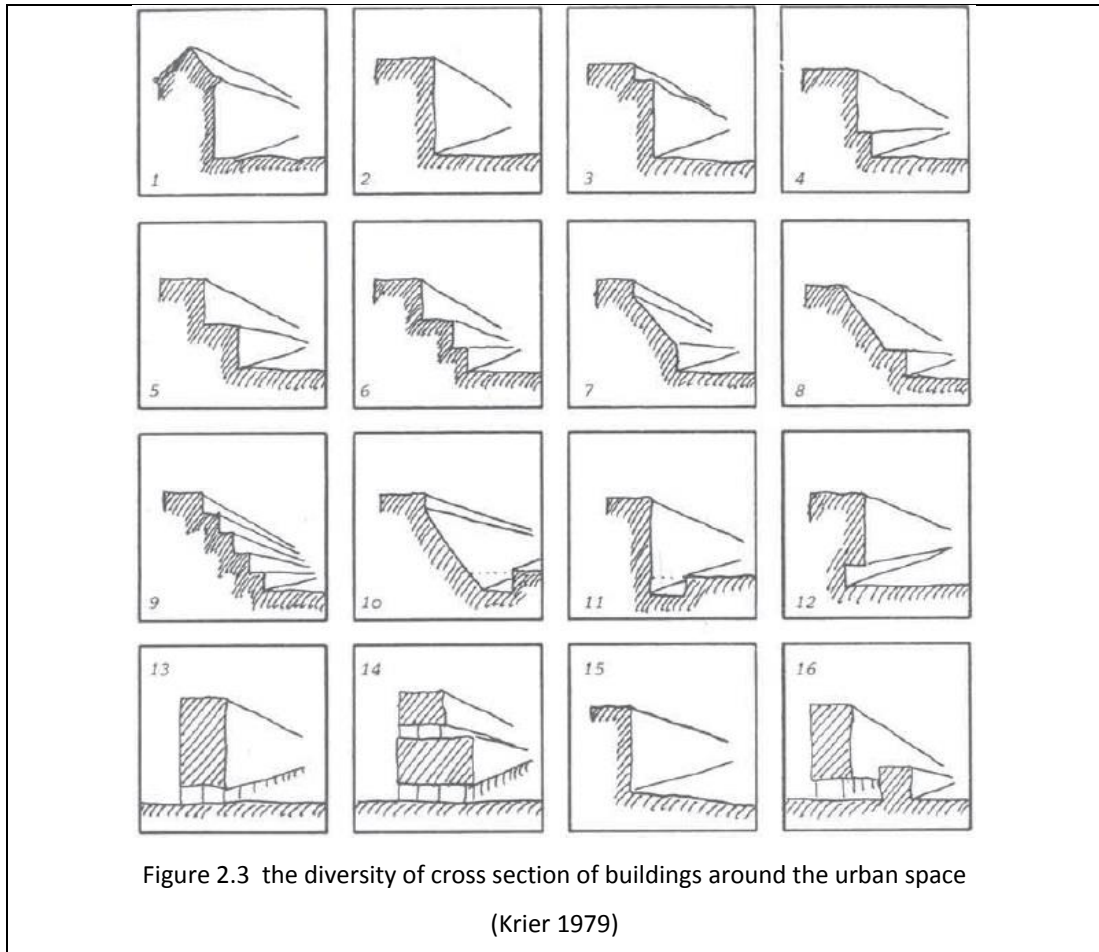
2.2.1 The configuration of urban space

According to the Cambridge Dictionary, an arrangement of elements or parts in a particular combination can be the simplest meaning of configuration (dictionary.cambridge.org). The general elements that define urban space are the floor, the surrounding structures and the overhead imaginary sphere of the sky (Carmona et al. 2010). More specifically, urban space is geometrically circumscribed

by a variety of facades which allow us to perceive it as an external space that can be public, semi public or private (Krier 1979). The containment degree or the perception of urban space enclosure partially relies on the arrangement of urban masses as illustrated by **Figure 2.2** that shows the simple imaginary scenarios of urban space configuration. A single building does not define a space, while a row of buildings may draw a weak definition of space illustrated by scenarios (a, b). The existence of a notable angle between two or more walls can achieve a degree of containment without the need for buildings to be connected to each other, as highlighted by case (c). The imaginary connections between the corners of buildings may strengthen the enclosure degree of space as can be seen in scenario (d). Combining several buildings together may create a clear urban space between them where this space can leak out through the open corners to form a gap or intersection between two buildings, although the sensation of enclosure can be stronger for the spaces with closed corners as shown by cases (e, f). Case (g) demonstrates a more complex and varied perimeter of the urban space with indentations in the facades of building and its ability to reduce the sense of monotony by forming a number of partially disguised or hidden subspaces. However, the increasing complexity may lead to a breakaway of the urban space into a series of disassembled spaces as shown by cases (x, h). Breaking the axis of sight or the movement axis between the urban space openings can increase the degree of containment as shown by scenario (i) (Carmona et al. 2010).

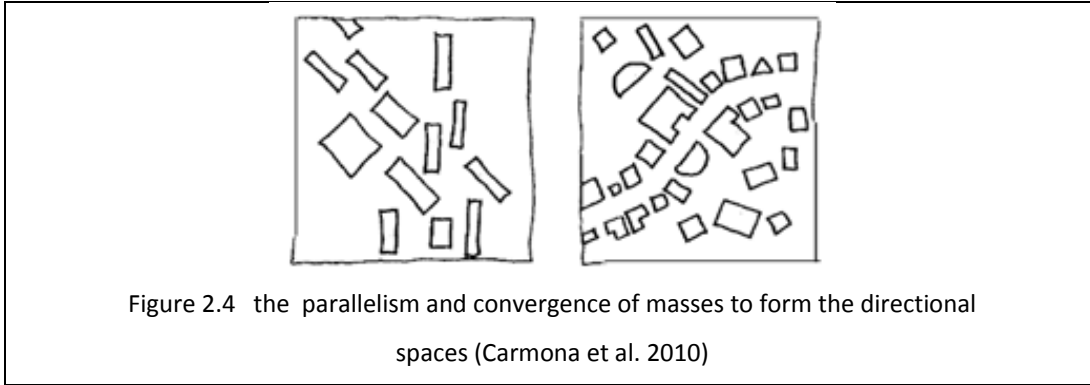


Diversity is not limited to the distribution of buildings around the urban space and the form of building itself but includes the diversity of heights and sections of buildings as shown by [Figure 2.3](#) and as a result increasing the complexity and diversity of urban space.



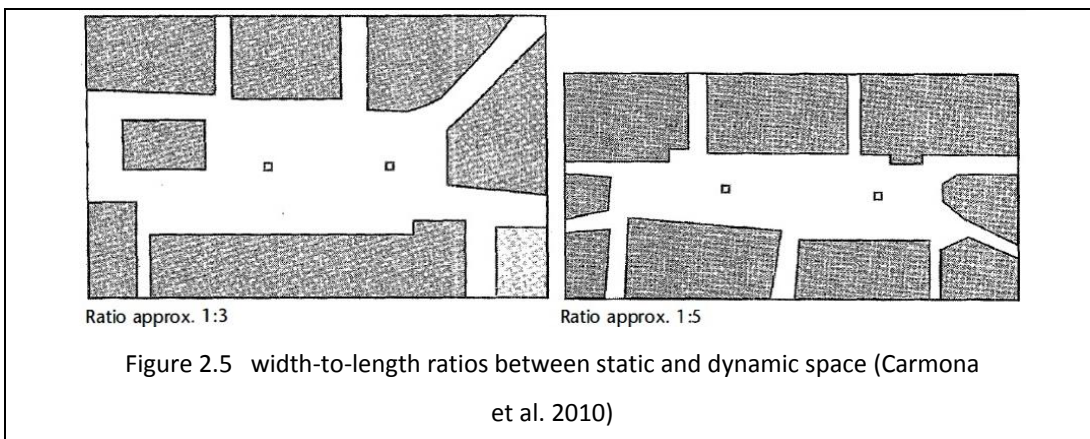
2.2.2 The types of urban space

Although urban morphology studies have distinguished between the spaces of urban area according to their functions or configurations, streets and squares are the most common names that were used to describe the urban spaces. Both of them are three-dimensional spaces, however, the street is a linear dynamic space enclosed by buildings on its opposite sides and gives a sense of movement (Carmona et al. 2010). It can be said that, street is a directional space that does not need to be straight such as the circular street, whereby buildings are grouped to form the common orientation of street, either through convergence or parallelism of these buildings around the space as shown by [Figure 2.4](#).



Square, plaza or piazza represent the first way, discovered by man, to use the urban space concept by arrangement of a group of houses around an outer space. This plan reduces the external surface area that being susceptible to attack by wild animals or enemies and makes this in-between space safe with high degree of control (Krier 1979). Square can act as a node that connects streets (Galloway & Kang 2009). The spatial pattern of square is still in-use particularly when designing the residential complexes and is known as courtyard (Krier 1979). Therefore, and according to the Oxford Dictionary, courtyard can be defined as an open-to-sky space that is surrounded completely or partially by building walls (en.oxforddictionaries.com).

Courtyard or square is a more static space generally with a less sense of movement. The dynamic sense of space starts to be felt through the dominance of one axis on urban space as a result of changing the ratio of space dimensions (width-to-length) to 1: 3 or more as shown by Figure 2.5, where the length is usually dominant compared to width in the street space (Carmona et al. 2010).



All in all, urban form is a complex system linked together by both dynamic and static interactions (Salingaros 1999).

2.2.3 The analysis of urban space

Urban spaces, such as courtyards, have been used for a long time as passive architectural design solutions across the world to provide shading and ventilation in both hot and humid climates as well as to break the cold winds in the cold climate. Courtyards have also appeared in temperate climates, however, the potential of courtyards as a passive solutions is unclear due to the rare researches in regard to the thermal performance of them in temperate climates (Taleghani 2014). ***“Microclimate is often neglected in urban design”*** (Carmona et al. 2010), along with the huge variety of these spaces in regard to their shapes, sizes, details and so on. Therefore, the analysis of urban form can be an essential approach to understanding the mutual relationships between urban form and microclimate.

In accordance to the Oxford Dictionary, analysis means methodological examination of something, in detail, with a view to discover more about it and its interpretation, such as the quantitative analysis which includes the measurement of quantities and the use of mathematical and statistical models (en.oxforddictionaries.com). Although the urban space is intricate mathematically more than we think (Salingaros 1999), the quantitative analysis of the urban form has not yet been explored rigorously enough (Pont & Haupt 1900). It has therefore not been applied thoroughly to urban space analysis, as the latter is an advanced state of urban form (Carmona et al. 2010). The explanatory power of urban morphology in regard to interpretation of urban phenomena can be promoted by quantitative analysis (Pont & Haupt 1900).

Relevant literature reviews reveal that there is no one accurate and agreed method to analysing urban form (Venerandi et al. 2017). However, the spatial urban scales may be one of the first and basic analytical techniques regarding urban form. In accordance to the perspective of spatial analysis, urban areas are considered organised complicated entities, however, the analysis of their spatial structure may contribute to solving their complexities and understanding them (Kropf 2009). The

spatial resolution of urban environment ranges from city scale to detailed scale of building components, so the urban form descriptions are scale dependent (Irger 2014). Urban areas can be classified spatially into the region (meso) scale that deal with whole city and beyond, the local scale (neighbourhood) express urban sectors and micro-scale for the individual buildings, urban spaces, urban trees and so on (Grimmond et al. 2010; Nichol & Wong 2005). However, the concern of urban designers and architects focus on the human scale that is considered as a measure of appropriate size for the built environment, where the dimensions of urban spaces and buildings are compared with the human figure proportions (Moughtin 2003). Dealing and decision on the smaller scale is responsible for geometrical coherence of urban area compared to the bigger scale therefore the larger scales need to be defined after the smaller scales as the coherence of elements that assemble geometrically lead to identifiable and definite urban morphology (Salingaros 2000).

Furthermore, the analysis on small scale can be pertinent for many fields such as the relationships between urban form on the one hand and thermal comfort, energy consumption and urban scale passive techniques on the other hand (Y.Nakamura & T.R.Oke 1988; Bottyan & Unger 2003; Zhang et al. 2012; Giovannini et al. 2013; Taleghani et al. 2015).

Despite the diversity of urban form on different scales, it is helpful to describe it by quantifiable measures that express its physical properties such as density (Pont & Haupt 1900). These quantifiable measures can be known as morphological parameters that represent the features or aspects of the three-dimensional urban form (Nikolopoulou 2004). The Oxford Dictionary defines parameter as ***“A numerical or other measurable factor forming one of a set that defines a system or sets the conditions of its operation”*** (en.oxforddictionaries.com). Decision makers and planners need urban morphological parameters to understand and control the intensity of urban development and consequently control the growth and change of urban form (Martins et al. 2014).

2.2.4 The description of urban form

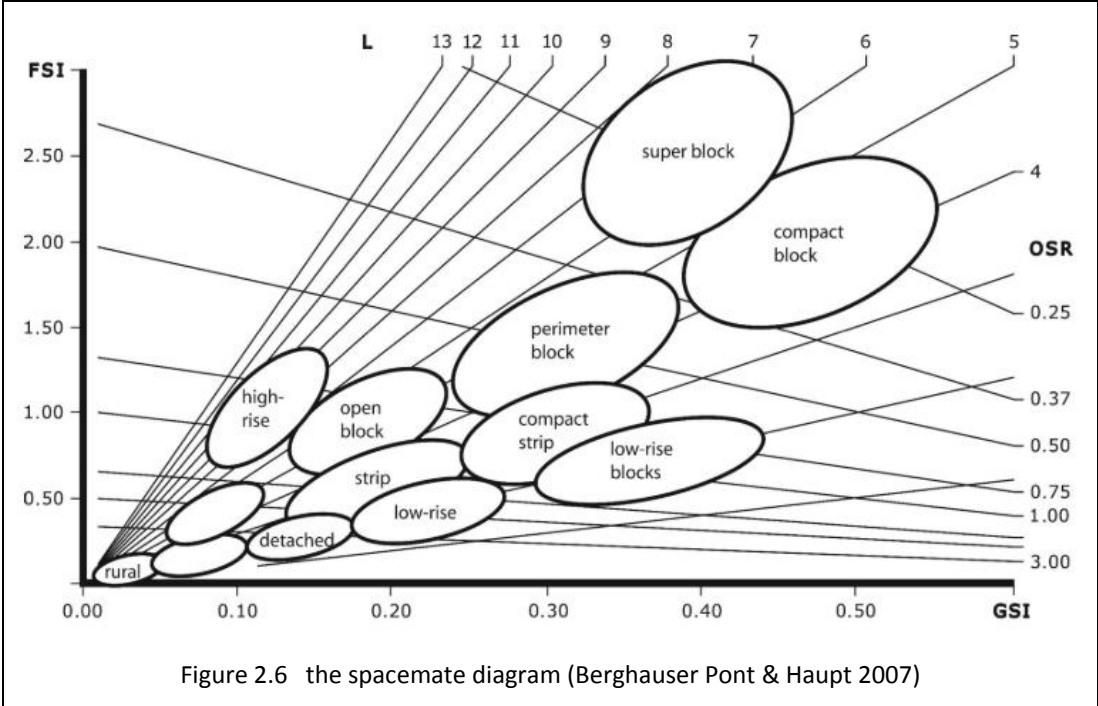
Urban form is a multidisciplinary topic. In general, the quantitative approaches to analyse this form can be classified into five main fields, including: economy, ecology, transportation, urban design and community design whereby each field has its specificity and at the same time affects and is affected by the other fields (Clifton et al. 2008). Therefore, the diversity and overlapping of parameters that describe urban form is very much likely.

The current study classifies the urban morphological parameters (UMP), according to their calculation methods, into three levels: simple, average and complicated. The simple parameters represent the values that can be extracted directly from urban area such as distances like distance from sea or distance from city centre and areas like built-up area, open space area or walls area (Eliasson & Svensson 2003; Maciel et al. 2013; Tong et al. 2018). Average parameters refer to values that can be calculated from unpretentious mathematical relationships of two or more simple parameters such as densities like floor area ratio and building coverage ratio (Berghauer Pont & Haupt 2007; Pont & Haupt 1900). Complex parameters mostly show complicated mathematical relationships of two or more simple parameters to be calculated such as sky view factor and viewsphere index (Watson & Johnson 1988; Yang et al. 2007).

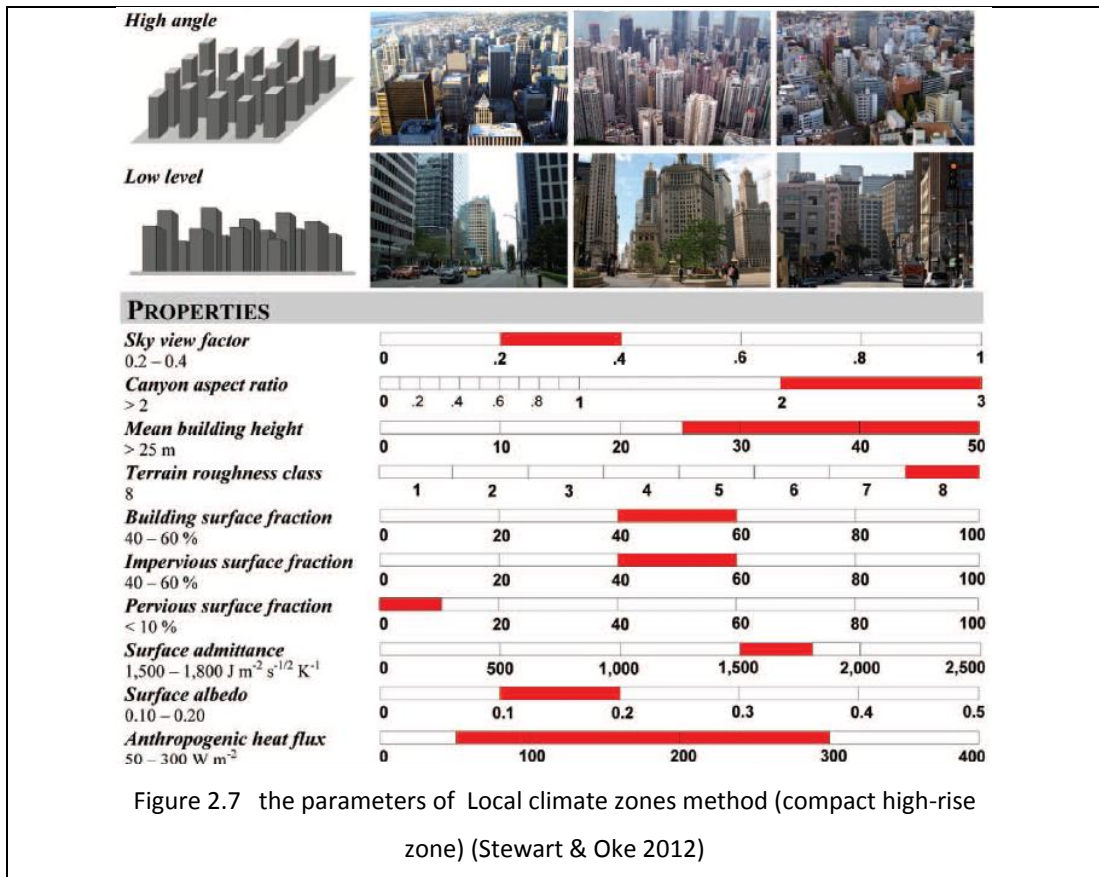
The ability of parameters to describe the urban form is limited, hence, many scholars have developed composite methods to give a more comprehensive look on the urban form and its role in relation to many matters like air temperature behaviours. These methods involve two or more of the simple, average or complex parameters in a relationship that is non-mandatory to be in mathematical formula.

Spacemate is a one of these methods that describe the urban form depending on graphical relationship between the numerical values of four urban morphological parameters: floor space index (FSI) to express the density, ground space index (GSI) to express the ground coverage ratio or compactness, spaciousness indicated as open space ratio (OSR) and the fourth parameter is the number of storeys (L). Each urban form, regardless of the spatial scale, can result in a unique combination of parameter

values and occupied a unique position on the graphical diagram of Spacemate as shown by **Figure 2.6** (Berghauser Pont & Haupt 2007; Pont & Haupt 1900).



Local climate zones' (LCZs) is a method that was developed to study the urban heat islands according to the group of parameters that mostly describe the urban form in a spatial scale ranging between hundreds of meters and several kilometres. The main parameters are Aspect ratio, Sky view Factor, Building surface fraction, impervious surface fraction, Height of roughness elements, anthropogenic heat flux density. This method classifies the urban and rural areas systematically into 17 standard classes and each class represents a local climate zone that can affect the air temperature behaviours in different way compared to other zones as a result to the differences in the values of urban forms parameters and other parameters. **Figure 2.7** shows that three different urban areas were classified or described as compact high-rise zones, representing one of the seventeen zones in this method where the three urban areas recorded convergent values of the parameters (Stewart & Oke 2012; Stewart et al. 2014).



Some computer tools were developed to explore the environmental performance of urban form on different spatial scales such as STEVE. This tool is used to predict the air temperature that results from the surrounding environment around a particular point in the urban space by using statistical models that were developed depending on long term field measurements. The urban morphological parameters and the climate parameters represent the predictors of these models. The morphological parameters, as a function to urban form, include surface area, average height to building area ratio, total wall surface area, green Plot ratio, sky view factor and average surface albedo, while the climate parameters include air temperature and solar energy. STEVE is a plug-in to support the graphical urban analysis by using the ArcGIS software to produce the maps of urban temperature (Wong et al. 2011; Hien et al. 2012).

Space syntax is a method that tries to interpret human behaviours and social activities from a spatial configuration perspective by providing a group of parameters that describe the urban form in relation to the movement and linkages between

urban spaces. The main parameters of this method are connectivity, control value and integration (Hillier 2007). The urban analysis on different scales by using space syntax has been made easier to understand the social processes throughout the built environment, by developing DepthmapX software that perform graph analysis of the spaces network as shown by **Figure 2.8** to derive parameters that may have social or experiential importance (Al_Sayed 2018). This method provides a quantitative tool in regard to social behaviour matters, many plug-ins on separated software such as ArcGIS and Rhino were developed to explore the potentials of parameters of this method more deeply (Jiang et al. 2000; Nourian et al. 2013).

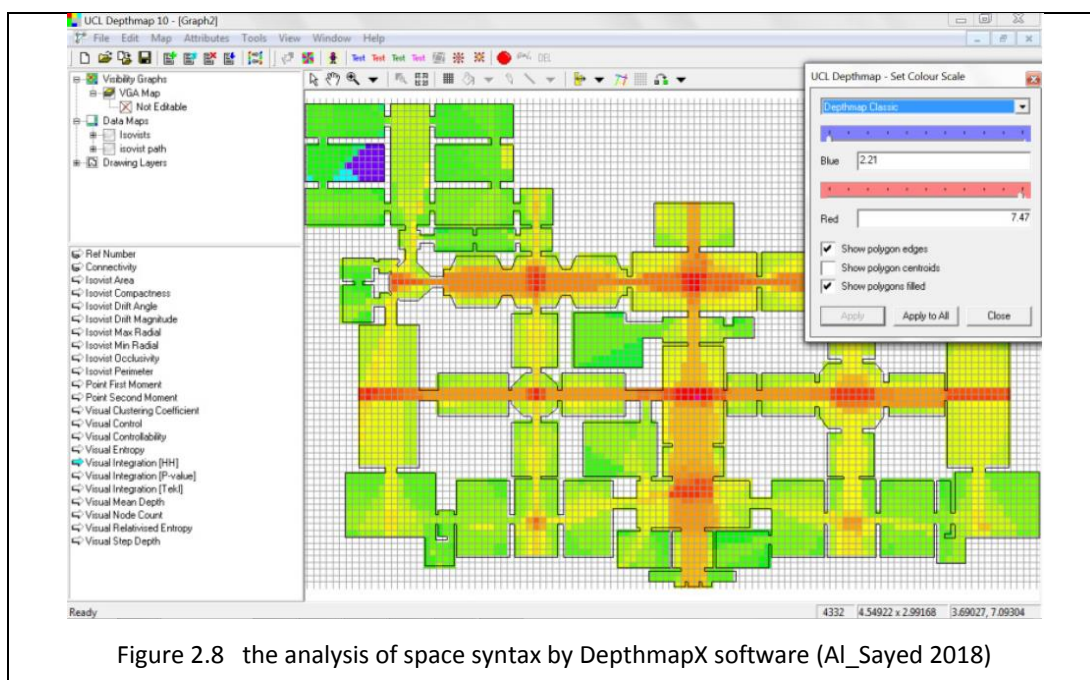


Figure 2.8 the analysis of space syntax by DepthmapX software (Al_Sayed 2018)

All in all, regarding the description of urban form, most of urban morphological parameters can be classified into three groups. Firstly, some parameters can describe limited properties of an urban area irrespective of the spatial scale like floor space index and ground space index that are used in Spacmate method. Another group of parameters can describe the configuration of surroundings around the measurement point like sky view factor that represent the openness of the urban space to the sky in the Local climate zones method. The third group of parameters that describe the urban form in regard to connectivity of urban spaces like the parameters of Space syntax method.

2.3 The Urban Climate

The Urban climatology is a multidisciplinary topic that focus on the study of urban area influences on climate and the implementation of the knowledge acquired with a view to improving the design and planning of cities (Mills 2014). Cities alter the overlying atmosphere considerably in almost every aspects (ibid), however the influences of terrestrial surfaces does not extend vertically more than 10 km to form the troposphere layer. The lowest part of this layer in an urban area is known as the urban boundary layer (UBL) that represent the entire air volume above city, where this layer is affected by the activities and characteristics of the built-up area. In general, UBL extend vertically to be around ten times the height of the urban area buildings and horizontally beyond the urban area edges and it can be divided into sub-layers as shown by Figure 3.9 where the knowledge about these layers is fundamental to the urban climate (Erell et al. 2011).

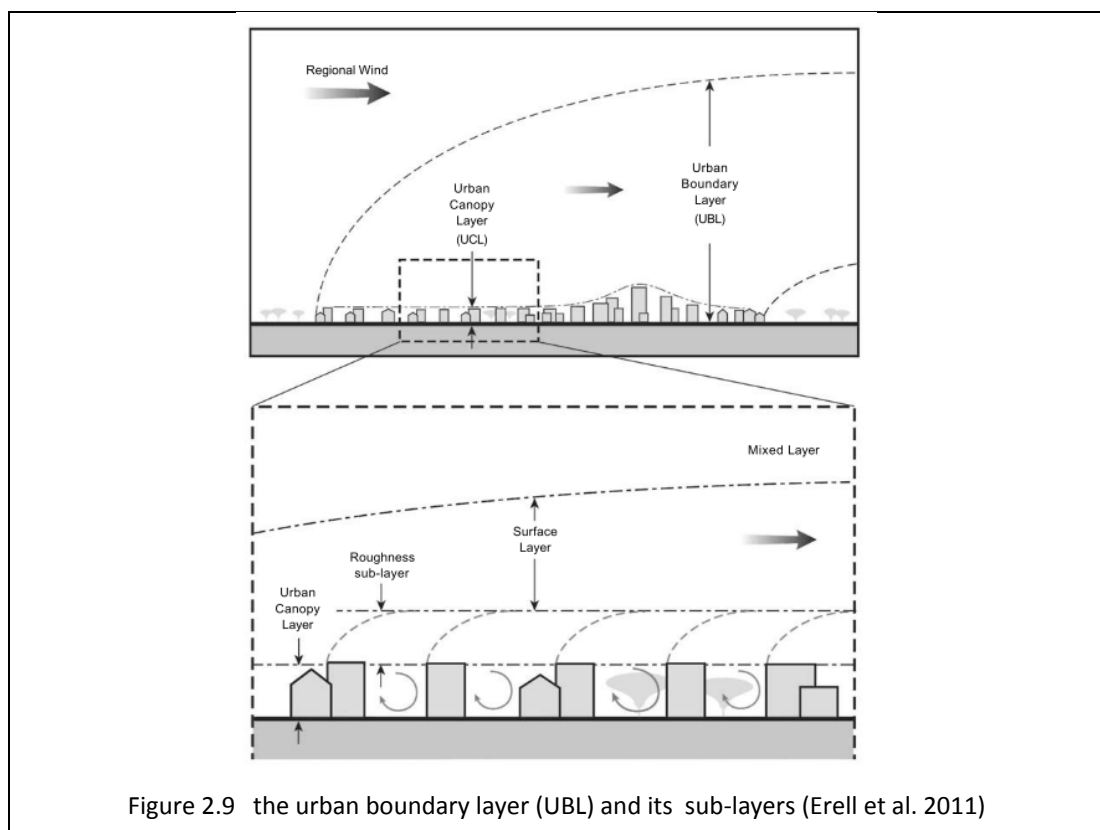


Figure 2.9 the urban boundary layer (UBL) and its sub-layers (Erell et al. 2011)

The mixed layer is the upper part that represents the bulk of UBL volume. The atmosphere within this sub-layer is not fully modified by the urban surfaces where

the influences of non-urban upwind terrain are existent as well. The Surface layer settles under the mix layer and it extends to be about five times the height of the average buildings of urban area. It is formed by passing the air over a sufficient length of urban fabric, where it is conditioned entirely by the ground cover and 3D geometry of urban surface as whole without subject to the influences of individual urban elements such as streets and single buildings. Therefore, the homogeneity of energy exchange between the urban surface and the atmosphere and the systematic curve of wind speed profile are features of this layer that is also known as the constant flux layer (Erell et al. 2011).

The mixture of influences from individual urban elements that characterizes the surface layer does not happen instantaneously above the buildings roofs, where these highly variable status extends from the roofs of buildings to at least twice the average buildings height to form the Roughness sub-layer that represents a transition phase between the homogeneity of the surface layer above and the highly variegated urban fabric that comprised of different heights buildings and vegetation in addition to different dimensions open spaces. The last part of atmosphere that extends from ground to the height of buildings and trees is the urban canopy-layer (UCL) that witnesses a high level of heterogeneity due to the variation of conditions from location to location within the canopy volume (ibid).

Within the UCL, the behaviours of temperature, radiation, wind and other climatic factors are determined by physical features of surroundings. The dimensions of urban spaces, the heights of buildings, the distribution and densities of vegetation and materials of buildings and ground surfaces represent samples of these features that contribute to creating a unique climate that may affect the thermal comfort and energy consumption. This unique climate that dominates on micro-scale urban area may extend horizontally from 1cm to 1km and known as the Microclimate (T.R.OKE n.d.). In other words, the microclimate of house garden may differ from the microclimate of the next street which, in turn, may show different behaviours in terms of air temperature and other factors compared to another open space in the same area. Therefore, the urban thermal environment may change distinctly from one location to another and the knowledge about temperature especially surface

temperature and air temperature is crucial to understanding this environment (Grimmond et al. 2010).

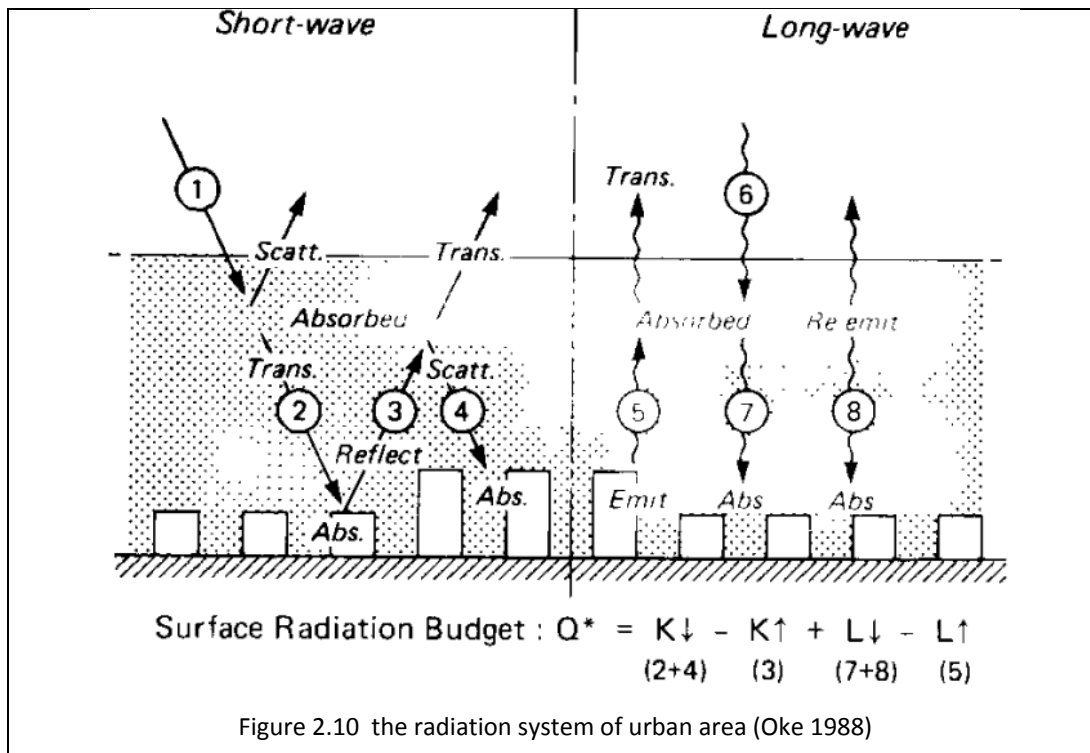
2.3.1 Surface temperature

The temperature of external surfaces and air within the urban space is governed by the exchanging mechanism of energy. Accordingly, the energy balance of surfaces is in charge of the understanding of the microclimate of any location (Oke 1988).

The solar radiation is the main source of energy and faces many behaviours as it passes through the atmosphere. A part of this solar is reflected (short-wave) to the sky again by the clouds and the constituents of the atmosphere that also absorb a portion of it. The rest of solar radiation reaches the earth and suffers absorption and reflection as well. The absorbent radiation will be emitted back by the earth surfaces as long-waves (heat) into sky. Most of the radiative energy that were absorbed by clouds and atmosphere constituents from sun as short waves and from the earth surfaces as short and long waves will be emitted back to earth as long waves. The net all-wave radiation flux (Q^*) can be expressed by the following formula for daytime (ibid), where its components can be understood from the [Figure 2.10](#).

$$Q^* = K \downarrow - K \uparrow + L \downarrow - L \uparrow \quad (2.1)$$

$K \downarrow$: incoming short-wave radiation, $K \uparrow$: reflected short-wave radiation, $L \downarrow$: incoming long-wave radiation, $L \uparrow$: outgoing long-wave radiation



The net all-wave radiation flux (Q^*) is the basic input of the energy exchange model that takes place at the urban surface. The balance between incoming and outgoing energy of urban area is not required to be equal at all times due to the transformation of energy from one form to another according to the first law of thermodynamics. The transformation processes include storing and releasing energy that are affected by the materials properties of surface such as albedo and emissivity, where the material absorption of radiation reduces by increasing the albedo value especially for light colour materials and this keeps the surfaces cooler, whilst the materials with high emissivity are good emitters and they release the heat as long waves readily. Other variables may affect the transformation processes of energy such as the duration of exposure, the diversity of shape, size, arrangement and compositions of urban surfaces and elements (Erell et al. 2011).

Another factor that can affect the energy balance in urban area is the heat that is released to the atmosphere due to human activities that mostly involves fuels combustion, known as anthropogenic heat (Q_F) (ibid).

Therefore the urban energy balance can be expressed by the following formula (Oke 1988).

$$Q^* + Q_F = Q_H + Q_E + \Delta Q_S + \Delta Q_A \quad (2.2)$$

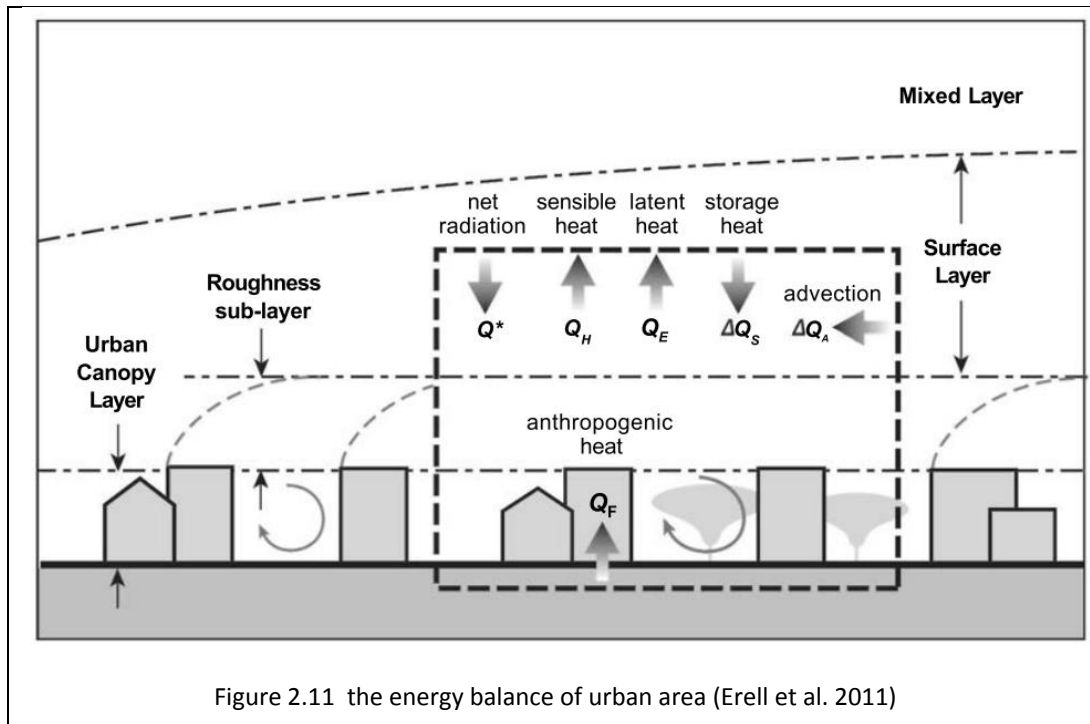
In addition to the net all-wave radiation flux (Q^*) and the anthropogenic heat (Q_F), the other inputs of this formula are shown by [Figure 2.11](#) that reveals the following terms:

Sensible heat flux (Q_H), is heat exchanged by convection between urban surfaces and adjacent air as a result of temperature differences between them. Although, the size of Q_H depending on the magnitude of the difference of temperature and the heat transfer resistance between the two mediums, it can be affected by geometry that may cause different air velocity for different surfaces especially with the diversity of solar exposure and orientation.

The evaporation and transpiration processes represent the turning of water of vegetation, wet surfaces and water bodies into a gaseous state by absorbing a specific amount of heat that is extracted from the air or surface and is known as the Latent heat flux (Q_E). The sensible heat and latent heat are related to each other in a negative relationship. Therefore, without enough moisture rate, the incoming energy increases the sensible heat that often leads to substantial rise in air temperature especially in urban areas compared to rural areas due to the lack of vegetation, permeable materials and water bounds.

The storage heat flux (ΔQ_S) is the change of heat stored in the urban area. The radiant energy from different sources like the sun, the atmosphere or the other terrestrial surfaces will be absorbed by the urban area surfaces. The microclimate, particularly temperature, is affected by the surface ability to absorb, store and emit the energy, where this ability is subjected to optical and thermal properties of surfaces, their size and their spatial arrangements. The heat storage in the air is much smaller compared to structures and ground of urban area.

Advection (ΔQ_A), is the transmission of heat and moisture from location to another that often settle on short distance as a result to the heterogamous of urban fabric that affect the surface energy balance and create hot and cool spots, often in close proximity. For the purpose of simplifying the energy balance model, many studies in urban climate have neglected this process.



The surface temperature is mostly higher than the air and it reaches its maximum value within the daytime whilst the lowest value at night time. A study in the city of Kyoto, Japan for the east-west oriented urban canyon showed that the differences between surface and air temperature reached 12-14 °C at midday and 3-4°C at night (Y.Nakamura & T.R.Oke 1988). In general, the temperature of urban surfaces is higher compared to the surrounding natural surfaces at rural areas and this phenomenon is known as surface heat island (SHI), however in desert environments the sands and rocks can be warmer than many of man-made surfaces at urban area (Erell et al. 2011). Thermal infrared techniques are used usually to document the surface temperature on different spatial scale on ground and from sky or space (Grimmond et al. 2010).

2.3.2 Air temperature

Air temperature can be considered as a measurement of how cold or hot the air is. After sunrise the sensible heat flux from the urban surfaces increases in response to increase their energy budget, consequently the air temperature within urban canopy layer (UCL) will change positively (T.R.OKE n.d.). The diurnal air temperature variation

relies on the condition of sky. The differences between incoming and outgoing radiation on clear days produces a wide range of daily air temperature range that is less under the overcast sky (Olgyay et al. 2015). On a seasonal base, it can be noticed that clear summer days are hotter due to receiving more solar radiation. This is in contrast to winter clear days that are usually cooler compared to the cloudy day as a result to easy release of heat through the clear sky especially with long interval of nocturnal outgoing radiation (ibid).

Air temperature is affected by many factors such as urban features, solar radiation, vegetation and wind speed (Erell et al. 2011). It affects many aspects such as energy consumption and human health especially in terms of the influences of heat waves (Mavrogianni et al. 2009).

The outside air temperature is more complicated to be estimated from simple functions compared to wind speed and solar radiation due to the multitude of variables (radiative, convective, evaporative and conductive) (Erell et al. 2011). For this reason, air temperature is measured on site or using statistical models to estimate it depending on observations over field (Oke 2004). However, the air temperature measurements are relatively simple by using direct techniques (thermistors, thermocouples), there is no general and simple scheme to extrapolating the air temperatures horizontally within the urban space (Grimmond et al. 2010; Oke 2004).

Usually, the air temperature of UCL is higher than its outskirts rural area although the warm-up of UCL after sunrise is slower because of many factors like mutual shading between buildings. The difference of air temperature between them can be insignificant at daytime, however, it reaches the maximum after sunset to form the canopy-layer heat island phenomenon (CLHI) that being pronounced with clear and calm atmospheric conditions (Erell et al. 2011).

2.3.3 Urban – Orientation – Climate relationship

Urban canyon is the element of urban form that has been investigated intensively in regard to the climate-responsive urban design (Krüger et al. 2010; Ali-Toudert &

Mayer 2007; Andreou 2014; Nunez & Oke 1977; Ali-Toudert & Mayer 2006; Chatzidimitriou & Yannas 2017; Johnson & Watson 1984; Y.Nakamura & T.R.Oke 1988; De & Mukherjee 2017; Strømman-Andersen & Sattrup 2011). It is likely that the reason behind this attention is that the urban canyon as a three-dimensional arrangement is defined and limited by its long axis direction. Therefore it is characterized by the simplification of the geometric relationships of a part of urban form by proposing a two-dimensional cross-sections to describe the urban area along the main axis of the directional urban space (Erell et al. 2011). Only one of the two parallel canyon walls will cast a shadow at a given moment in daytime, so the north-south oriented streets for example will witness a shadow area in the morning by the eastern wall that faces the west, while the shadow from the western wall can be noticed in the afternoon. In return, the east-west streets experience more distortion where the northern walls that face the south receive the solar radiation most of the daytime in contrary with the southern wall that cast the shadow in the urban canyon space most of the daytime (Erell et al. 2011; Oke 2004).

Hence, the orientation of canyons is the technique that has been utilized to understanding the relationship between urban morphology and climate factors, the directional urban spaces represent the recommended choice to exam this relationship due to the systematic solar radiation-shade patterns throughout the year, in addition to the urban air-flow, that playing a pivotal role in dispersion of urban heat, is mainly subjected to the configuration of urban obstacles and their directions in terms of wind speed and its direction. Consequently, the geometry and orientation of the canyon influence the energy balance and the thermal environment within the urban space (Nunez & Oke 1977).

Although, the importance of orientation in understanding the urban-climate relationship in regard to the directional urban spaces, it is not easy to utilize the orientation concept with non-directional urban spaces that usually show more complicated geometry with partially or completely absence of physical axes, parallel walls and systematic shapes.

Different methods were used to describe the urban morphology in regard to urban-climate studies not only with non-directional spaces but also with directional spaces

as a way to get more understanding for this relationship as what will be revealed in the next section. However, it was difficult to find a way to describe the urban form of non-directional and directional spaces in relation to the orientation concept and apply it to investigate the urban-climate relationship on micro urban scale.

2.4 The researches of urban-climate relationship

The interaction between urban morphology and climate factors creates the urban thermal environment which is a complex concept because of the diversity and interference of its variables. However, it can be expressed mainly by two outputs, air temperature and thermal comfort, (Park et al. 2018), that may represent the most simple and fundamental output of the urban thermal environment. The thermal structure of urban space is dominated by the micro-scale effects within the urban canopy layer (UCL) that extend from ground surface to the roof of building (Y.Nakamura & T.R.Oke 1988; Giovannini et al. 2013). There is a vast amount of literature concerning the urban-climate relationship. However, there is a scarcity of research related to analysis of urban form and its environmental influences in the intermediate scale that includes the elementary components of urban fabric like urban spaces and buildings (Zhang et al. 2012). Hot climates have received most attention whilst a limited number of studies appear to exist in regards to micro scale for temperate climates (Taleghani et al. 2015). This scarcity is particularly notable in the United Kingdom, which were not limited to micro-scale but extended to include larger scales (Hughes 2006). This section will, therefore, try to adhere to its boundaries that were drawn by the title of thesis i.e. to cover some studies that have been conducted on urban micro-scale under the temperate climates by submission dense summary of some studies as a first level. Following this, as a second level, analysis to explore the context around the urban-climate relationship In regard to the impact of urban form and its parameters on air temperature as a function of the thermal microclimate and extract some concept that may support the different stages of this study.

The description of urban form can be considered as a way to distribute the selected studies into many groups. As a first group, urban space can be described or measured depending on the relationship between the measurement point and the surrounding buildings. This kind of parameter is rare, with sky view factor (SVF) being a sample of them. Many studies have investigated SVF-microclimate relationships regarding variables such as air temperature and solar radiation.

Krüger and Emmanuel, (2013) studied the differences of seasonal ambient temperature between urban and rural weather stations i.e. the effect of the Urban Heat Island (UHI). The differences of intra-urban temperature at day/night times between stations in Glasgow, UK were evaluated for the period between March and August 2011. The influence of atmospheric stability that was classified according to sky conditions and wind speed into six grades for UHI and intra-urban air temperatures. The utilization of this classification can make the influence of urban morphology expressed by the sky view factor (SVF) on the microclimate clearer to understand. This study found that the relationship between SVF and intra-urban air temperature variability and warming trends was more pronounced by analysis of field measurements. The evidence of a relationship between canopy urban heat island and urban morphology was not significantly affected by the choice of more stable conditions for analysis (Krüger & Emmanuel 2013).

A study in the city of Montreal, Canada (Wang & Akbari 2014) investigated the variation of urban microclimate regarding air temperature and wind speed as a result of urban morphology variations for four urban districts that differed in terms of layout, function and building volume within boundaries covering (300m x 300m) each area. SVF was calculated for different points within some of urban canyons and intersections inside each area. ENVI-met software was used to calculate SVF and simulate the microclimate factors for a 24h period in winter and summer. Simplified 3D models and weather data from a rural weather station where a part of the results for trying to validate against the field measurements data for some points. The result of statistical analysis for the outputs of one hour after 4 hours of sunset in both summer and winter days in addition to the outputs of summer day at mid noon against SVF pointed out the high importance of SVF in terms of affecting the

microclimate of urban environment. In general, the coefficient of determination (R^2) in summer was lower than in winter, maybe because of the vegetation effects in the summer. SVF was inversely correlated with air temperature at night for both seasons, winter ($R^2= 0.53$) and summer ($R^2= 0.25$), while a weak positive correlation was observed in the summer daytime ($R^2= 0.04$). Regarding the wind speed, it was observed to increase with an increase in SVF for summer night time ($R^2= 0.25$) and winter night time ($R^2= 0.32$) and the same behaviour was noticed in the summer daytime ($R^2= 0.35$).

In a third study (Drach et al. 2018), the joint effect of urban morphology and stability of atmospheric conditions on the variability of daytime intra-urban air temperature for Glasgow-UK, was investigated. Sky view factor (SVF) was taken as the urban morphology indicator and measured for 32 locations including urban parks, neighbourhood green spaces, East-West axis orientation street canyons, narrow streets and public squares. Similarities, in terms of wind speed and solar energy intensity, were utilized to classify the measurement period into many levels of stability regarding the atmospheric conditions. The readings of reference weather stations for 23 days in spring and summer 2013 were compared with the field measurements at these locations. For each of these days, the field data were recorded from half past two in the afternoon and continued for more than one hour, whilst air temperature at each location was measured for two minutes. The findings showed that the differences of maximum intra-urban temperature correlated strongly with the stability of atmospheric conditions. Moreover, the air temperature differences were remarkable in the urban canyons, with a direct correlation to the SVF values and with an inverse trend for locations with higher values of SVF.

Another study (Unger 2009), supported the quantitative approach of urban morphology description by developing a software-based method to estimate SVF from the database of 3D urban model by using ArcGIS software. 35 urban areas within the city of Szeged, Hungary, with dimensions (500mx500m), whereby each area was selected to exam the effect of SVF on intra-urban air temperature variation. The data was collected for one year (2002-2003). The measurement session began approximately 4 hours after sunset and lasted in accordance with the length of the

street and the speed of the vehicle holding the air temperature sensor, which was recording every 10 seconds at a height of about 1.4m above ground level. Each urban area was covered with 15-20 measurement points, where SVF was simulated in each point for two heights (ground level and 1.4m height). The regression analysis was done for the data for whole year, non-heating season and heating season. The results showed that the variation of air temperature for the whole year could be explained by SVF variations in accordance with the values of coefficients of determination (R^2) as 44.1% above ground level and 42.6% at ground level. The non-heating and heating seasons saw no significant difference from previous R^2 values. However, the increase of SVF caused a decrease in the air temperature in all models.

On the same path, but with different tools, a more accurate method was developed by MATLAB software to calculate sky view factor (SVF) using high resolution JPEG format fisheye images. Later, the improved values of SVF for 59 sites across the city of Manchester-UK were input in to statistical relationships against the air temperature measurements for these sites in both the winter and summer seasons of 2010, to reveal the effect of improved urban morphology indicator on the urban heat island (UHI) under the clear and calm climatic circumstances. The results showed that an increase of openness to the sky led to a general decrease in the air temperatures. The relationship between SVF and UHI intensity was weak for SVF values bigger than 0.65 for summer nights ($R^2=0.3217$) and winter nights ($R^2 = 0.3625$), while these percentages turned out to be better, as 63% and 53%, respectively, for the deep canyons with SVF values smaller than 0.65. The role of SVF was not affected significantly by the orientations of canyons that affected the entrance of solar radiation into the canyon space (Cheung et al. 2016).

Densities and compactness are terms that are well known in the practice of urban design. According to the Oxford Dictionary, density means the quantity of people, mass or things per unit of a given area, space or volume. Compactness refers to the state of being dense, when the parts gather closely together (en.oxforddictionaries.com). Many urban parameters are related to these terms and some of them represent the core of municipal planning regulations. Unlike SVF, these parameters describe all the specific urban area and are not associated with the

measurement point in regard to their calculation methods, such as floor area ratio (FAR).

(Maciel et al. 2013) utilized the parameters that describe the urban form with regard to compactness or density on micro scale. Influences of urban surface characteristics, such as built, green and open area ratios, were investigated. This study concerned the variation of ambient air temperature at the urban micro-scale with radius lower than 1km in two university campuses under the two different climates of Uxbridge-UK and Cuiaba-Brazil (temperate and tropical climates). The regression analyses for the measurement of three summer days showed that the effect of surface characteristics within a 50m radius around the measurements points considerably impacted on temperature in both climates. However, the locations with a higher built cover ratio had a higher air temperature compared to locations with a higher green cover ratio in addition to the distribution of small green area within the urban fabric could work effectively to reduce the air temperature. A different set of urban planning indicators were investigated by bivariate linear regression against long-term field measurement data (2006–2010) to evaluate the variation of intra-urban maximum (MAX) and minimum (MIN) summer temperatures in 25 locations within the city of Florence-Italy (Petralli et al. 2014). These indicators were calculated around each of the measurement points on nine different size circles with radius expanding from 10m to 500m. The linear regression coefficient (β) of the urban indicator was used to determine its effect on air temperature according to the size of effected area. Vegetation indicators and urban form indicators were used individually in this study, the latter includes Street Cover Ratio (SCR), Building Cover Ratio (BCR) and Building Volume Density (BVD) that represented the ratio of total volume of buildings to the total area of effect zone. The results showed that the effect of indicators on MIN temperature was stronger with an increasing radius of influential area. MIN was positively related to SCR for all areas whilst it was positively related to BCR and BVD for all circles except for radius =10m. The identical behaviours were noticed with MAX temperatures; however, the relationship with MIN was stronger than MAX, both for smaller and bigger circles because of the storage of incoming solar radiation during the daytime and then re-radiated thermal radiation at night

time at different speeds according to the characteristics of each location. As a third study, the surface air temperature was studied to reveal the roles of urban and meteorological factors in developing the urban heat island (UHI) in Szeged city (Hungary) for the period between March and August 1999 (J. Unger et al. 2001). Field measurements focused on the inner part of the administration district that was divided into a grid of squares with dimensions 500x500 metre each with an average distance between measuring points of approximately 110 m. The urban parameters include the percentage of built-up area and the distance from the city centre while the environmental measurements (wind speed, temperature) were averaged by grid cells. The general results of the statistical analyses suggested that the built-up density significantly influences air temperature levels, also affected by the distance from the city centre.

Compactness influences the accessibility of solar radiation in the built environment, and so various parameters that measure the compactness of urban form were involved in statistical analysis to explore their influences on the solar energy potentials on roofs and facades of buildings within 16 neighbourhoods in the city of Geneva, Switzerland (Mohajeri et al. 2016). The simulation approach was used to calculate the hourly solar irradiation on the urban surfaces for one year using CitySim software, whereas the weather data for the simulation processes were extracted from Meteonorm software. The urban form parameters included volume-area ratio, plot ratio, site coverage, building density, nearest-neighbour ratio and population density, each one reveals different aspect of urban configuration. The regression was used to seek the relationships between the variables (radiation levels and urban parameters), while the coefficient of determination (R^2) was used as a measure of how well the variation of radiation levels can be explained by the compactness parameters. The results showed that there were strong negative linear correlations between the annual solar irradiation, on the one hand, and the parameters volume-area ratio, building density, plot ratio and site coverage, on the other hand. The values of R^2 were 0.74, 0.73, 0.72 and 0.59 respectively. The neighbourhood's distance from the city centre showed a strong positive linear correlation with the annual solar radiation ($R^2 = 0.61$). The increase of other

parameters (population density and nearest neighbour ratio) led to a decrease in the annual solar radiation. However, the correlations were weak compared to the previously mentioned parameters. In general, the compact urban forms received lower levels of solar radiation and, therefore, the solar potential of roofs was less affected by compactness than façades. In the same topic, but within different areas, seven urban morphology indicators were chosen to examine their effects on the solar availability on the facades (S_f) of 14 urban areas of Rome, Italy and Barcelona, Spain (Morganti et al. 2017). These indicators include Gross Space Index (GSI), Floor Space Index (FSI), Façade-to-site ratio (VH_{urb}), average building height (H_{bid}), volume-area ratio (V/A), Building aspect ratio (S/V) and sky factor of façades (SF). The typological characterization of the real urban areas were represented by simplified 3D models that were each comprised of 9 regular and identical urban blocks. Heliodon2 software was used to calculate the solar radiation on the facades of the central block for one year, considering the other blocks as urban obstructions. The results of regression analysis suggested negative correlations between solar radiation and each of GSI (R²=0.6), FSI (R²=0.31), VH_{urb} (R²=0.59) and V/A (R²=0.53) and positive correlation with SF (R²=0.79), while other indicators (H_{bid} and S/V) had no effect on the availability of solar radiation, with values of R² < 0.005. Multiple linear regression analysis was applied to get the most accurate model to predict the solar radiation in Mediterranean cities, where the compensation of GSI, VH_{urb} and SF showed the most accurate model, with R² = 0,91.

The third group contains studies that deal with the types of urban form. A pilot study, spanning three days in July 2010, was carried out at the city of Leipzig-Germany based on field measurements and questionnaires (Franck et al. 2013). As part of the study, the effect of four types of urban form, such as residential areas, on the relationship between outside and inside air temperatures were investigated. These types included detached and semi-detached houses, linear developments such as terrace houses, multi-storey residential courtyard block with closed perimeter and open perimeter multi-storey courtyard block. Although the results showed a poor relationship between indoor and outdoor temperature, the Pearson correlation coefficient was about 50% for the courtyard with open perimeter compared to the other forms that

had lower effects. Besides the vegetation, other influential factors included distance to city centre and materials, the outdoor air temperatures depending on urban form types. The air temperatures between morning and evening periods were convergent for both types of courtyard forms in comparison to terrace, detached and semi-detached houses that witnessed sensible reduction of air temperature at evening time. A reason for this may be due to the blocking of wind movement inside the courtyards, whilst the smooth movement of wind is likely to cool the surface of other urban forms.

The last group of studies from the urban form perspective can be considered as a mixed group. Some studies utilized different types of urban morphology parameters with each other, such as sky view factor, with the compactness parameters or urban form types and so on.

Air temperature data were measured at 18 locations for 18 months between 1998 and 1999 within one of the Swedish cities- Gothenburg (Svensson & Eliasson 2002). The analysis of variance test was done as a statistical approach to explore the air temperature differences under the effect of three categories of urban form (dense urban area, multi-family and single houses) within day and night times. Data from a permanent meteorological station on the outskirts of the city were used to classify the measurement period into different weather groups. The characteristics of these urban forms were distinguished from each other by the values of sky view factor (SVF), buildings or impervious surface density and vegetated surface density. All these urban parameters were calculated from fish eye images that were captured in the cold season, when the seasonal change in density of greenery was not considered. For statistical analysis, the field data was distributed into four groups according to the seasons whereby each group in accordance to cloud cover was divided into three sub-groups which were in turn divided into two smaller groups depending on wind speed. For each day in these groups the temperature data of two hours were selected, at 12pm as day-time data and after three hours of sunset as night time data as the deviation of temperature occurred in this interval. The results of this study focused on the roles of the urban forms without focusing on the detailed parameters. The cool island phenomenon was observed as the air temperatures

within the three urban forms during daytime accompanied by clear circumstance were always colder than the outskirts reference station by up to 4°C and these differences may be bigger, particularly if the wind speed was less than 3.3 m/s. Conversely, on cloudy days, the urban environments are always warmer of about 2.5°C. The built-up areas were always warmer at night time, the dense forms during clear conditions were warmer with the highest deviation of temperature (8 °C). However, the other urban forms (i.e. multi-family and single houses) showed very convergent differences of temperature against the outskirts station of about 4°C.

The degree of urban thermal environment exacerbation was investigated versus changes of urban form and density regarding air temperature and thermal comfort in the city of Seoul, South Korea (Park et al. 2018). Three existing urban areas were selected and altered to produce one alternative for each area. The urban forms of these areas were altered as follows: area (A) from multi-family housing complex to be tower type apartment complex, area (B) from flat type apartment complex to be tower type multi-purpose apartment while area (C) was not changed significantly as commercial and office area. The development of urban forms was measured depending on two parameters - floor area ratio (FAR) and building coverage ratio (BCR). The air temperature and thermal comfort were simulated by ENVI-met software for a summer day of June 2015 for the six models. The results of simulated air temperature revealed that the increase of FAR by 124% and the decrease of BCR by 29% led to a reduction in the maximum and average temperatures of the urban area A by 1.81°C and 0.87°C respectively. The maximum and average temperatures of the urban area B increased by 0.28°C and 0.38°C as a response to increasing FAR and BCR by 111.9% and 8.5%, respectively. Urban area C witnessed a decrease of 0.42°C and 0.2°C for maximum and average values as a result of increasing FAR by 131% and decrease BCR by 14%. The increasing of FAR does not necessarily exacerbate the air temperature, while the decreasing of BCR leads to a reduction in the air temperature and improve the thermal comfort a result of the disposition of the buildings and change in their sizes and forms that may contribute to improving the role of wind movement and shadows. Therefore, in general, BCR has a significant effect on the thermal environment of urban areas, certainly more than FAR.

In short, the results of these studies showed clear variation in the influence of urban form on microclimate despite the convergence of the climatic characteristics of the case studies. The behaviours of climatic factors witnessed positive or negative trends that ranged from weak to strong in regard to the influences of the urban morphological parameters. This diversity of results is expected due to the detailed diversity of convergent climates, urban form and the ability of parameters in description that form. In addition, the variation and details of research processes such as the time scale of study, the method of data acquisition, the method of data analyses and so on.

Consequently, all this diversity represents a motivation for more studies with different aims, the most important of which is to submit novel concepts in measure and description the urban form to contribute in understanding the urban-climate relationships on micro scale.

2.5 Conclusions

Our cities are big and complicated entities that need to be measurable, describable and understandable in regard to themselves or their influences on different matters like climate that affect human health, energy consumption and so on.

The changing of our urban area form alters mainly the energy balance of urban surfaces that contribute to creating a microclimate with unique thermal environment, especially within the vertical space from ground surface till roof level that represents the vital atmosphere in which the human being interacts with the urban environment. Urban morphological parameters are the quantitative methods that were used to make the urban form measurable, consequently the urban-microclimate relationship can be tested and analysed as a fundamental step to understanding the effect of urban form on microclimate, especially air temperatures in terms of behaviours and intensity of influence, which has clearly diversified in previous studies, leaving the door wide open for further research in this field. The next chapter provides comprehensive demonstration of the methods and tools that were used to achieve the aim of this study by understanding a side of urban-microclimate relationship.

Chapter Three

3 Chapter Three: Research methodology

3.1 Introduction

This chapter considers the methods and tools that were applied to extract and process the data of the selected case study to answer the research questions and to achieve the aim of this study. The research map shown by **Figure 3.1** can be a brief guide to the general methodology of current research.

Firstly, this study displayed theoretical background about the urban morphology, the microclimate and their interplay in the first and second chapters. Accordingly, the third and fourth chapters were devoted to revealing the methods and tools that were applied to the specific case study data to investigate the linkages between thermal microclimate and urban morphology using a quantitative approach. This approach includes the following stages (the field measurements, the calculation of urban parameters and the development of novel urban parameters), in addition to developing a statistical framework that used the outputs of these stages (Chapter Five) as inputs to be processed statistically.

The statistical analyses results are revealed in Chapter Six with the findings of the field work providing a basis for a comprehensive discussion (Chapter Seven), The results of this study were compared against the findings of previous studies. After that, the conclusions of the study will be delivered in Chapter Eight about the relationship between the air temperature as a function of thermal microclimate and the urban morphological parameters as a function of urban morphology under the influence of one of the marine climates, specifically the moderate ones as shown in the city of Liverpool at United Kingdom (UK).

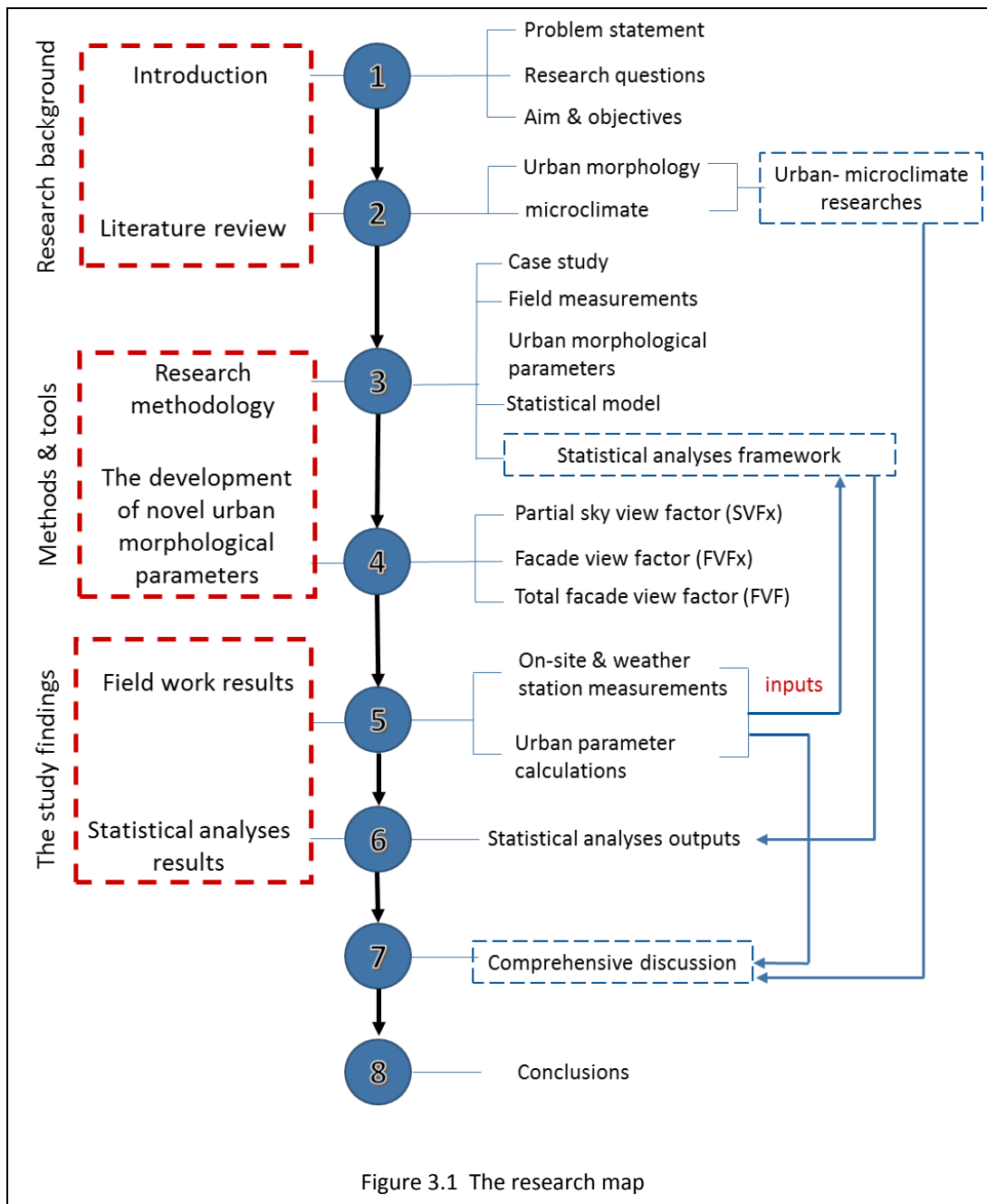


Figure 3.1 The research map

3.2 The study area context

According to the methodology, the case study and its urban and climatic context needed to be uncovered first. According to the Köppen climate zones, the United Kingdom (UK) is affected by the temperate climate zone (Met Office 2012). The temperate climate zone includes a range of climates: the Mediterranean climates that usually witness a dry warm or hot summer, the humid-subtropical climates that in general witness humid summer with plentiful rain while its winter is dry and the

maritime climates that are affected by the oceans, like in UK, that may experience cold winter nights and hot summer days although the usual temperatures are quite moderate and the summer is warm (ibid).

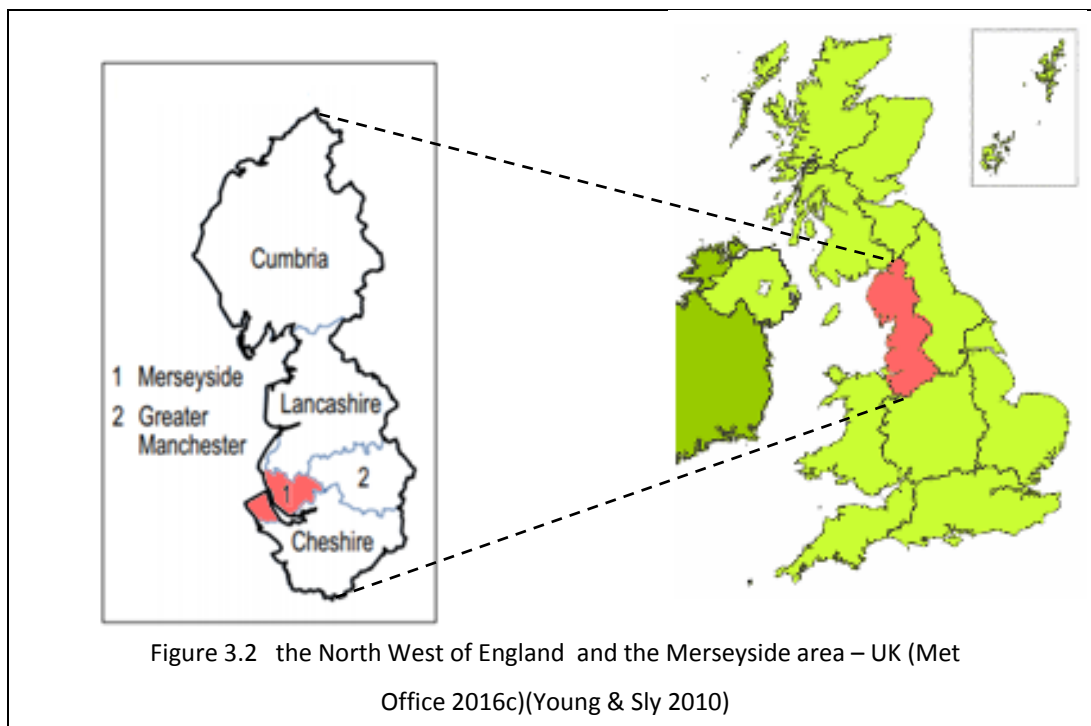
All these climates experience four distinct seasons; however, unpredictable weather is likely to happen throughout the year, like in UK the four seasons can be seen in one day (ibid). Therefore, the variability of UK weather from location to location and from day to day is well known as a result of "***Its position in the mid-latitude westerly wind belt on the edge of the Atlantic Ocean with its relatively warm waters, yet close to the continental influences of mainland Europe***" (Met Office 2016c). The changes of topography, altitude and some other factors contribute to customize the temperate maritime climate into eleven regional climates throughout the UK, The west and north parts of the UK tend to be wetter, cooler, cloudier and windier than that further south and east (ibid).

One of these regional climates affects North West England, which consists of five main areas, where Merseyside is one of them, as shown by [Figure3.2](#). Usually, the highest values of mean annual temperatures for the North West England were recorded along the coasts of the Isle of Man and Merseyside. However, the increase of altitude leads to a decrease in the mean annual temperatures that reach their lowest values in the Lake District area. The air temperatures experience both a diurnal and a seasonal variation, where in winter the mean daily minimum temperatures is fluctuating from 2°C along the coasts and in Merseyside to 0°C or below in the highland areas. The minimum values of air temperature usually occur before the sunrise and the extreme minima is recorded often in January or February. Air frost occurs when the air temperature falls below 0°C at 1.25m above the ground. The average number of air frost days range from around 20 in Merseyside to more than 75 a year in the Lake District. The warmest month in North West England is July; however, the extreme maximum air temperatures can happen in both July and August. For instance, the heat wave of 2006 witnessed the extreme maximum air temperature on 19th July at Crosby, Merseyside. In general, maximum temperatures occur about 2 or 3 hours after midday (Met Office 2016b).

Regarding sunshine hours, they are affected by clouds and daytime length, which gradually decreases from the longest interval at June to the shortest interval at December.

North West England has some of the wettest places in the UK, but Merseyside is a dry area compared to other areas. It witnesses about 30 days with rainfall 1 mm or more in summer and about 40 days in winter, while spring is the driest season compared to autumn/winter (ibid).

North West England is one of the more exposed areas of the UK, being close to the Atlantic Ocean and having some large upland areas. The winter season and especially from December to February, witnesses the strongest winds of the year. The south-westerly winds prevail through the year, but the north to north-east winds occur frequently in spring (ibid).



The city of Liverpool (latitude: 53.411°N, longitude: -2.989°, elevation: 19.0 m above mean sea level), occupies the eastern side of the Mersey River. It covers a land area of 111.8 km² with a population 487,600 people in 2016 (Liverpool City Council 2018) and it is a one of six sectors that form the Liverpool City Region (723.97 km²) -

Knowsley, St Helens, Sefton, Liverpool and Wirral) in addition to Halton (Sykes et al. 2013) as shown by Figure 3.3.

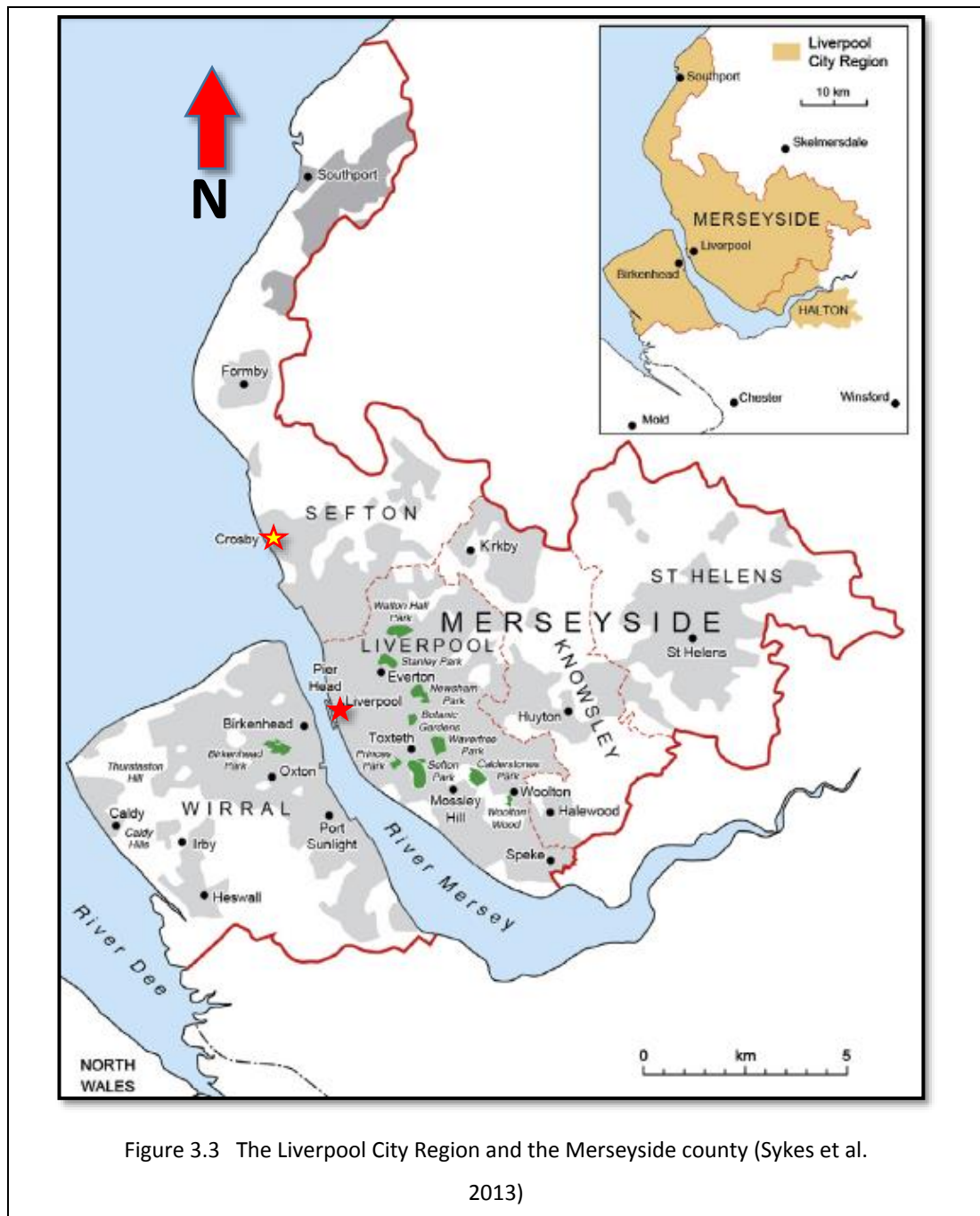


Figure 3.3 The Liverpool City Region and the Merseyside county (Sykes et al. 2013)

According to the 30 year climatic averages between 1981 and 2010 at the nearest weather station to the city of Liverpool (Crosby), located about 10.5 km to the north of the city (Met Office 2018), the lowest monthly average of maximum air temperatures were recorded at January and February respectively while July and August recorded the highest monthly average of maximum air temperatures

respectively, as shown by [Table 3-1](#). In terms of the monthly average of minimum air temperatures the same months witnessed the same behaviour.

The monthly averages of air frost days are zero for July and August while January and February witness the bigger numbers of these day throughout the year.

February is one of the driest month of the year in terms of the monthly average of rainfall, while October is the wettest month with rainfall rate 97.3 mm/month.

Regarding monthly average of wind speeds, January and February represent the windiest months with monthly mean wind speed of 6.5 m/s. August is the calmest month due to its monthly mean wind speed of 4.5 m/s.

Table 3-1 The monthly averages from 1981 to 2010 – the city of Liverpool (Met Office 2018)

Month	Max. temp (°C)	Min. temp (°C)	Days of air frost (days)	Sunshine (hours)	Rainfall (mm)	Days of rainfall >= 1 mm (days)	Monthly mean wind speed at 10m (knots)
Jan	7.2	2.4	7.8	n/a	74.9	13.8	13.5
Feb	7.3	2.1	7.9	n/a	54.4	10.7	13.3
Mar	9.4	3.8	3.4	n/a	63.6	12.5	12.7
Apr	12.2	5.1	1.5	n/a	54.3	10.4	11.1
May	15.6	7.9	0.4	n/a	54.9	10.6	10.6
Jun	17.9	11.1	0.0	n/a	66.2	10.5	11.1
Jul	19.7	13.3	0.0	n/a	59.0	10.1	11.7
Aug	19.4	13.2	0.0	n/a	68.9	11.2	8.6
Sep	17.3	11.0	0.1	n/a	71.7	11.5	11.5
Oct	13.9	8.2	1.2	n/a	97.3	14.8	12.0
Nov	10.2	5.2	3.1	n/a	82.6	14.6	12.6
Dec	7.5	2.5	7.5	n/a	88.8	13.9	12.4
Annual	13.2	7.2	32.8	n/a	836.6	144.3	11.8

The city of Liverpool contributes to the global climate change by producing 2.8 million tonnes per year of CO₂ emissions, with households responsible for more than 37% of these emissions (Liverpool City Council 2009).

Possibly as a result of climate change, heavy precipitation events decrease relative to the summer rainfall rates in most regions of the UK and Liverpool City is among them; however, marginal increases of heavy precipitation events were recorded over the North West England in the winter over the past 45 years (CAG Consultants 2009).

It is expected that the average annual temperature of Liverpool will rise about 0.9°C by 2040 and 3.8°C by 2100, while the maximum summer temperature for the same years is expected to be 1.2°C and 4.9°C higher respectively (ibid). To understand the importance of these numbers it should be mentioned that an increase of 1°C likely leads to the loss of many mountain glaciers and the disappearance of large part of coral reefs (ibid).

3.2.1 The case study

The configuration of the case study characterized by diversity of urban spaces in terms of shapes, sizes and heights in one site where all these spaces were open to each other with minimum variety of external wall materials of walls and ground materials. These characteristics minimize the effects of other factors that affect air temperature like variety of albedo or stagnation of the air movement due to the isolation of a part of the whole open space of the site. Therefore, the role of urban morphology will be clearer regarding the variation of air temperatures.

The historical background of the case study belongs to the post-war housing programme in Liverpool. Many large blocks of flats were built in Liverpool during 1930s, under the direction of city architect Sir Lancelot Keay (1883-1974), and one of the well-known surviving example in the Edge Hill area (L7) is Minster Court, or what was known as Myrtle Gardens. It was built between 1936 and 1937 according to the layout shown in [Figure 3.4](#) (Municipal Dreams 2015; Edwards 2016).

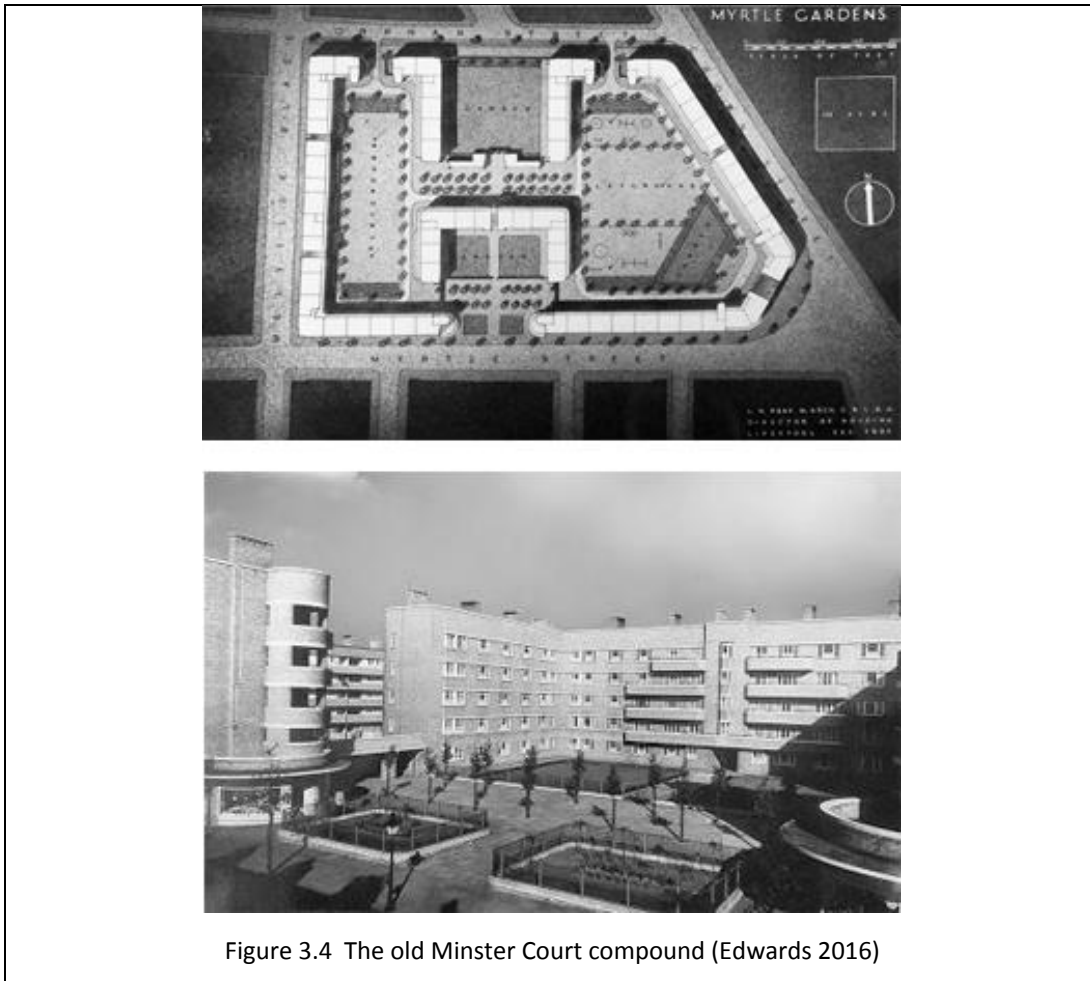


Figure 3.4 The old Minster Court compound (Edwards 2016)

The residential complex was subjected to major refurbishments, which resulted in the completely removal of the huge block on the southern-eastern corner of the site [see [Figures 3.5](#)] and removal of the upper floor of the block that defined the western and southern sides of the site.



The new addition, which replaced the removed block, and the final layout of the residential compound is shown in [Figure 3.6](#), which dates back to the 1980s. The total area of the current site is 21,300 m² and the description of current spaces in terms of shapes, areas and dimensions are shown by [Figure 3.7](#) which reveals the complexity and diversity of these urban spaces.



Figure 3.6 The current site plan of Minster Court compound
(digimap.edina.ac.uk/os)

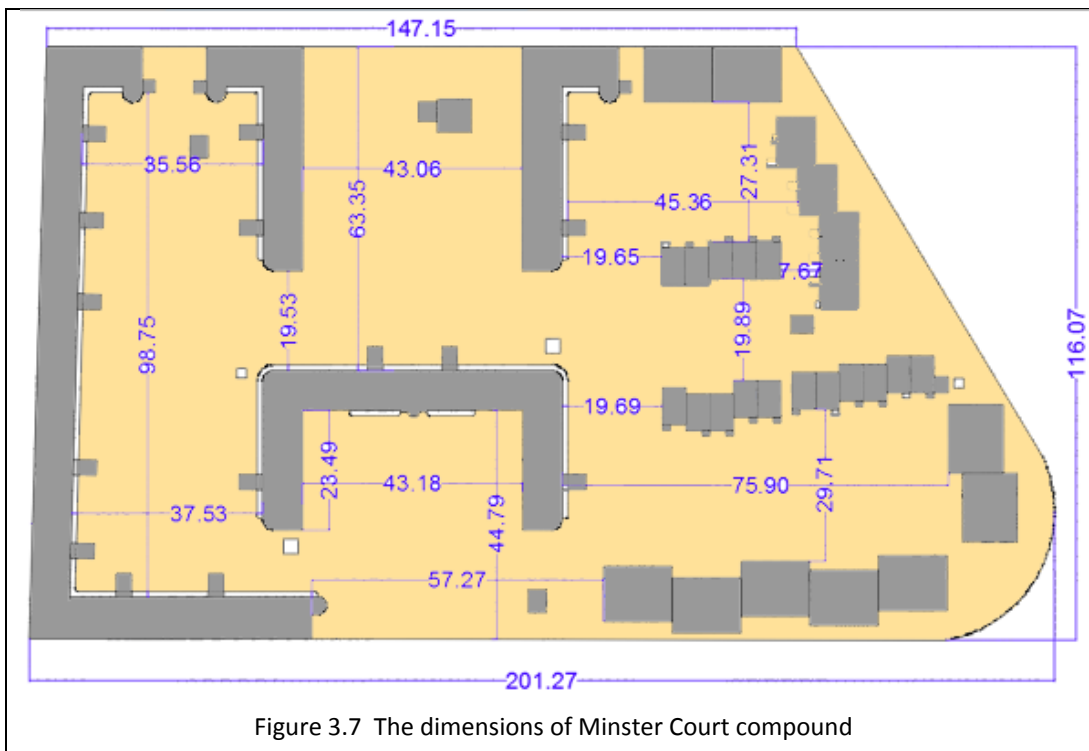


Figure 3.7 The dimensions of Minster Court compound

The current layout contains five different types of blocks as shown by the three dimensions model in Figure 3.8. The first type is the four-story building that represent

one huge mass occupies the western side of the site and extends to block the southern western and northern western corners of the site. The approximate height of this block is about 11m. The second type is the five-storey buildings that settle on middle part of the compound, they are three buildings with the same height (15m). The third type is the two-storey terraced houses with pitched roofs situated in the middle of the eastern half of the site as three separate masses. The uniform height of these blocks is around 7.5m. The fourth type is the three-storey buildings with pitched roofs that occupy the southern eastern and northern eastern corners as three individual blocks with a uniform height (10m). The last type is the service buildings, which include the management building of the complex located near the middle of the north side of the site, as an independent building of two floors with a height of 7.5 m and other small buildings of one floor distributed on the site.

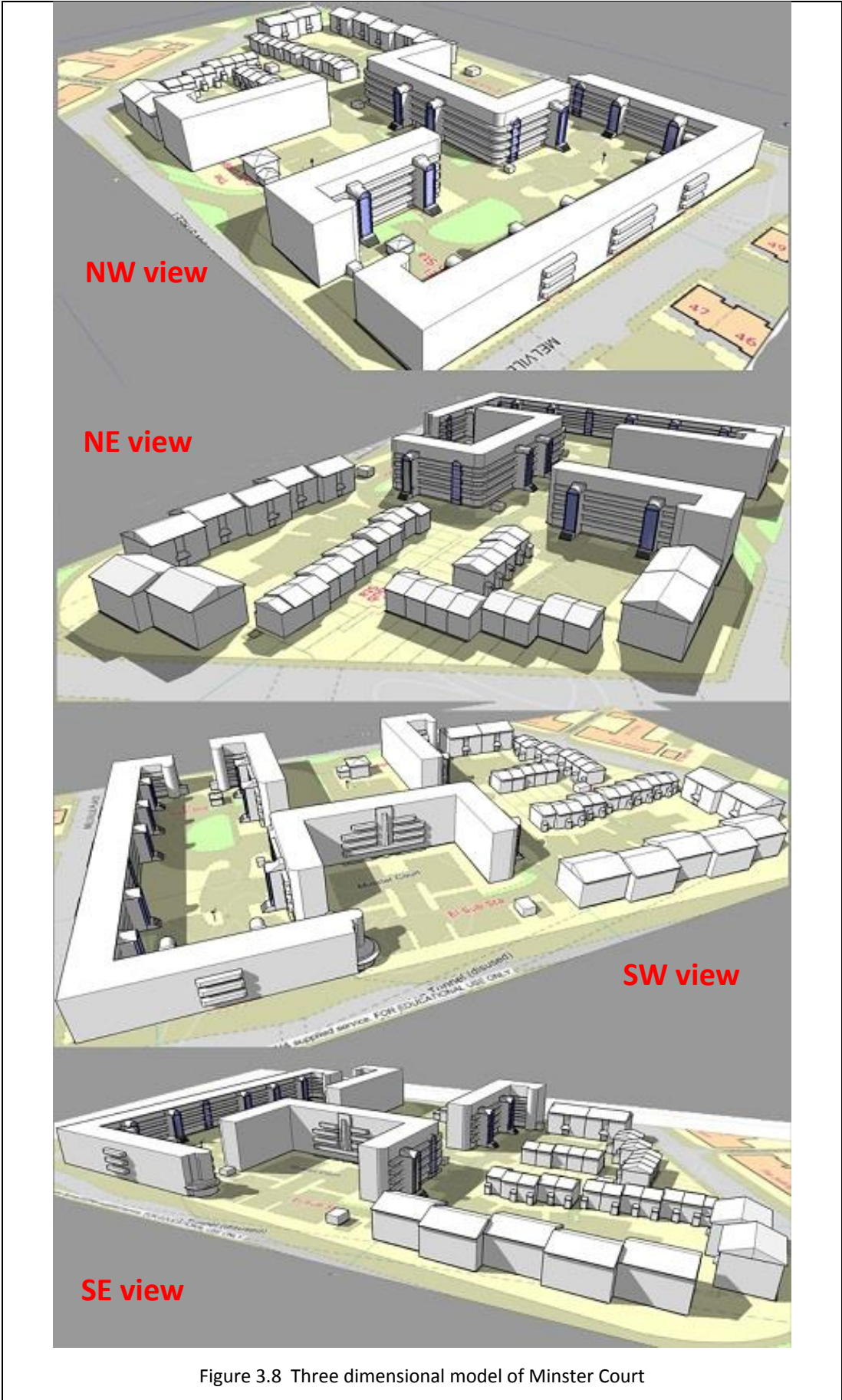


Figure 3.8 Three dimensional model of Minster Court

In terms of walls materials, brick is the dominant material while the glass of windows and doors in addition to the concrete strips of balconies floors and slabs break the monotony of the brick surfaces, as shown by **Figure 3.9**.



In terms of the ground materials, the dominant materials are asphalt and grass in addition to the existence of narrow concrete strips used as pedestrian paths, as shown by **Figure 3.10**, while trees are seen in different places on the site.



The Minster Court complex is located just a short distance from the University of Liverpool and its own weather station that located about 700 m in the North West direction of the residential compound as shown by **Figure 3.11**. The red circle represents the study site, the blue circle determines the position of the University weather station and the yellow circle refers to the location of the main square of the University (Abercromby Square) that is located in front of the School of Architecture.



3.3 Field measurements

The on-site measured air temperature is the basic indicator of the thermal microclimates of an urban space. Therefore, the measurement of variables that create these microclimates is the first step to understanding the interdependency between the physical features of urban space and air temperature. Therefore, this section is devoted to show the basic steps to measure the air temperature on field.

3.3.1 The measurement sessions

The field measurements of air temperature were conducted for the hot season 2014 and for the cold season 2015. Although July and August may represent the hottest time in the year at the city of Liverpool according to [Table 3-1](#), August was selected to represent the hot season due to it being the calmest month in terms of wind speed and there is no big differences in terms of air temperature compared to July. The hot season measurement session extended from 30th July till 4th September 2014. February was selected to represent the cold season (1st -28th February 2015). The rain rate and wind speed in this month are lower in general compared to January with no real differences in air temperatures. These two months represent the coldest period in the Liverpool.

For the same sessions the weather data for the climatic factors (ambient air temperature, solar radiation, wind speed and rain rates) were collected from the weather station of the University of Liverpool. The on-site measured air temperature and a part of these climatic factors represent inputs to the statistical approach that will be revealed at the end of this chapter. The advantage of using these variables is that it is relatively easy to define relationships between them and urban configuration (Ng 2010).

3.3.2 The measurement tools

A Hobo data logger U-12, [Figure 3.12](#), is one of Onset Computer Corporation products (www.onsetcomp.com). This logger is mainly designed to measure air temperature in indoor environments and it may be able to measure other variables besides to the temperature according to its version. According to the manufacturer, the measurement range of air temperature is between -20° and 70°C with accuracy about $\pm 0.35^{\circ}\text{C}$ from 0° to 50°C and the sample rate ranges from 1 second to 18 hours according to user preferences. The drift rate of this sensor is 0.1°C/year and so the investigation of sensitivity of loggers before distributing them in the field was necessary as a matter of results validity.



Figure 3.12 HOBO U12 data logger (www.onsetcomp.com)

The testing of sensor validity was done by putting the data loggers inside an old version of scientific cooler incubator with accuracy ($\pm 0.5^{\circ}\text{C}$) in one of Liverpool University laboratories as show by **Figure 3.13**. The air temperature inside the refrigerator was 10°C while the sample rate of sensors was 10 minutes to be corresponding to the sample rate in the field measurements. The results of the two continuous days of the validation process showed that the thirteen sensors kept their accuracy ranges according to the limits of manufacturer specifications as shown by **Figure 3.14** that show the first hours of these validation process. These twelve data loggers were used in the field measurements; however, one of them lost a large part of its data due to undefined technical problem and so it was ruled out. The field measurements data extracted from eleven sensors were used this study.



Figure 3.13 The testing of sensor validity at a one of Liverpool University's laboratories

These data loggers are designed to work in indoor environments; therefore, they should be protected from direct solar radiation and rain before when using them in outdoor environments. Twelve shields were made by the researcher from recycled materials as shown by [Figure 3.15](#). The main plastic shield was recycled from broken lighting fixtures that were cut into square units about 200 x 200 mm in the School of Architecture’s workshop. Then this plastic shell was isolated with 0.5 cm of cork to protect the logger from the thermal stock of the shell and from the direct sun rays due to the transparency of shell. This cork was recycled from the packaging box after the end of its original function regarding to protect against shocks. The side wings were recycled from strip blinds to protect the sensor from the low angle sun rays and the rain that come from sides. Wooden blocks (about 50 x 50 mm) were used to support the shield and to bind it easily to the mast by the tie-cables. The total cost of each shield did not exceed £2. This shield did not experience any problems in its function throughout the measurement sessions.

Readings from the data loggers were extracted and processed by software from the same manufacturer (HOBOWare for Windows) before using them in the analyses process.

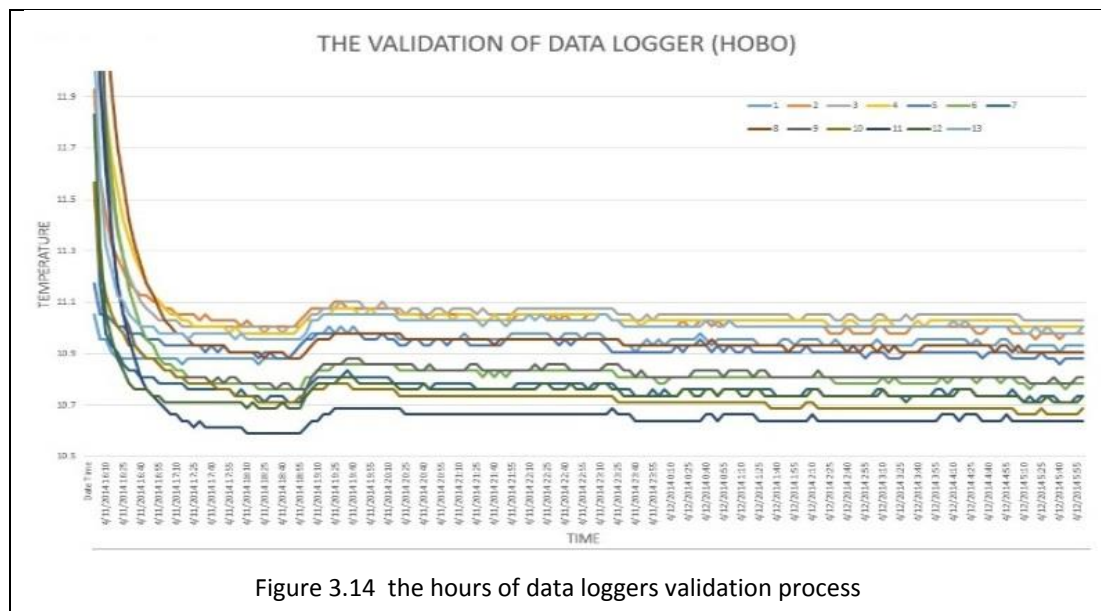


Figure 3.14 the hours of data loggers validation process

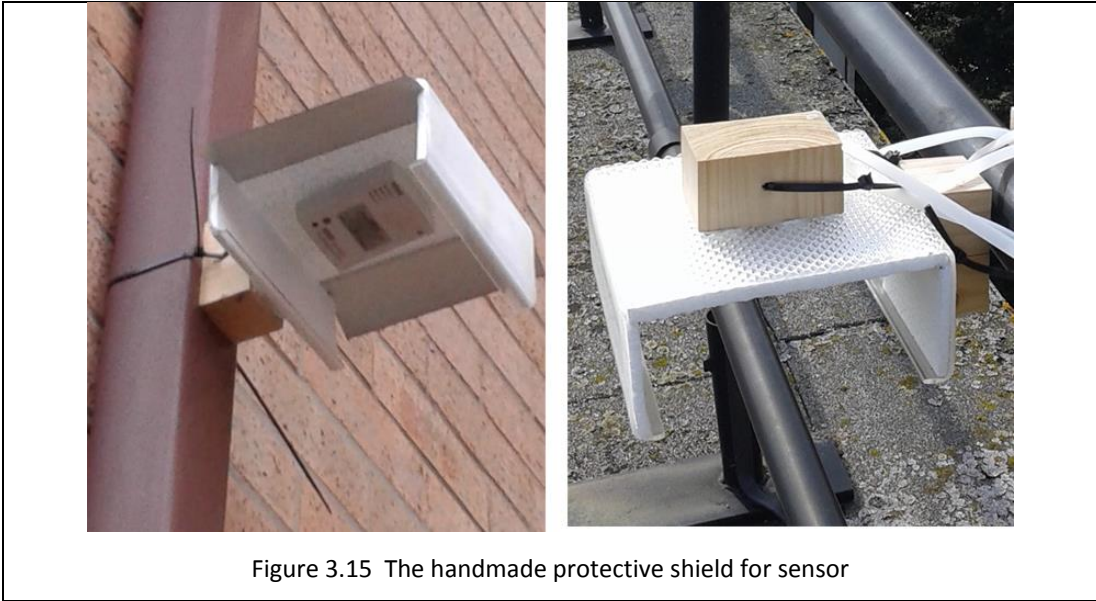


Figure 3.15 The handmade protective shield for sensor

In terms of the reference weather station, it is owned by the University of Liverpool [see Figure 3.11] and it occupies the roof of the Mathematics school on a height of around 20 m from the ground surface. It consist of many devices [see Figure 3.16] to measure different climate factors such as solar radiation, air temperature, and wind speed and so on.

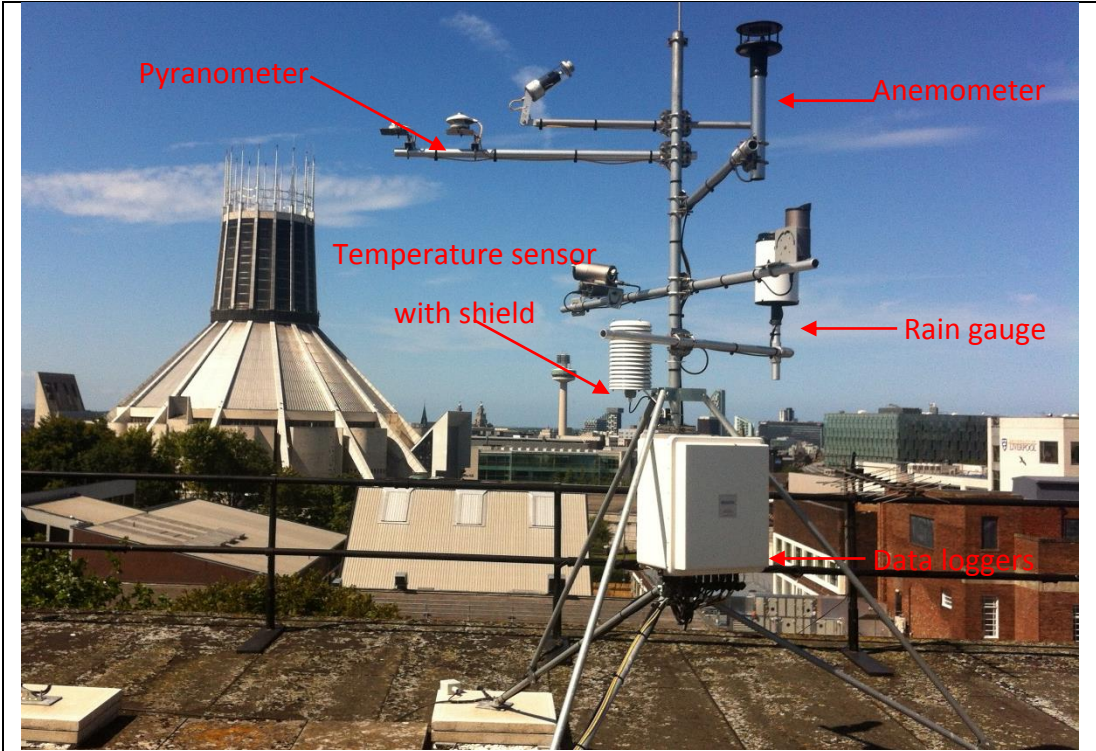
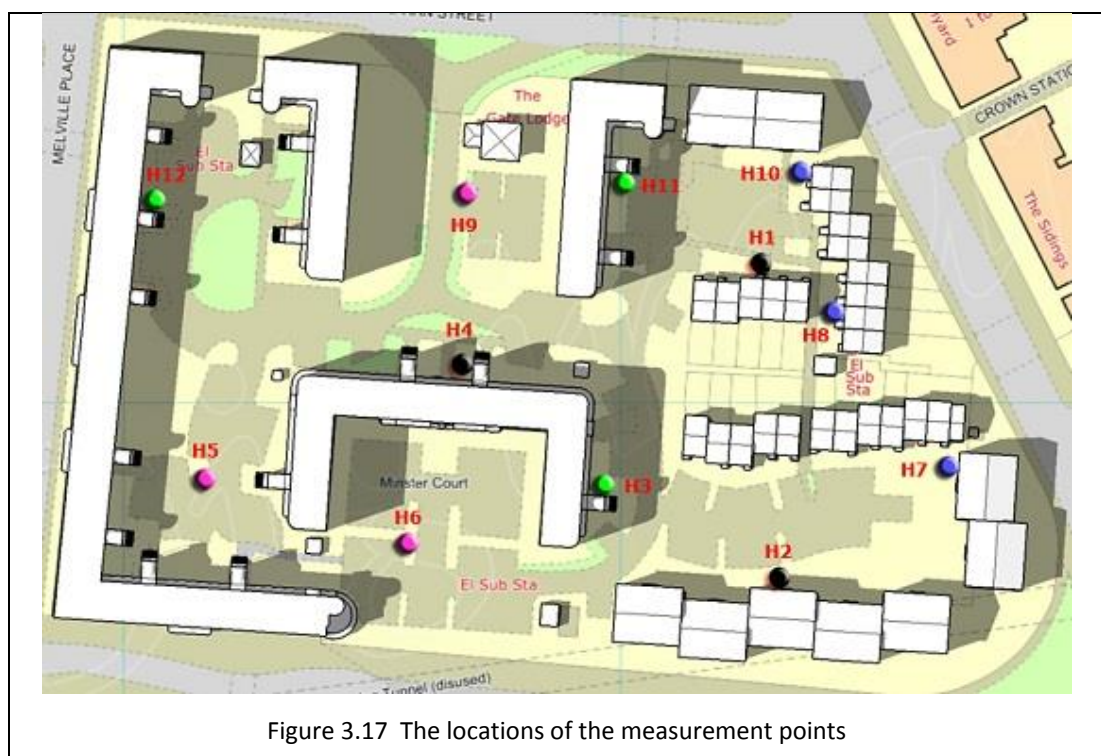


Figure 3.16 the weather station of University of Liverpool

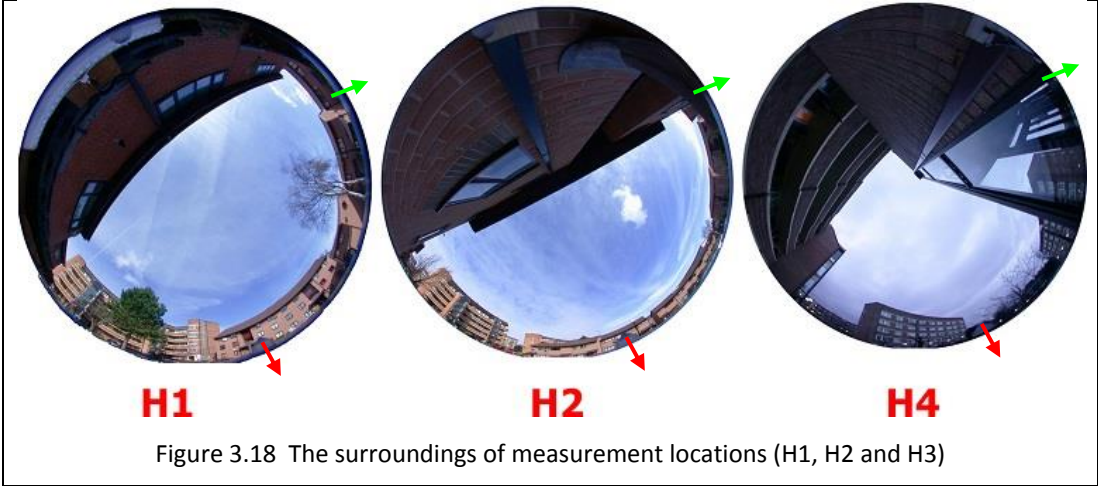
3.3.3 The distribution of measurement points

The Onset Hobo data loggers were distributed at twelve locations around Minster Court. Each location was named as (Hx) where (x) represents the number of that location, and so the names of locations ranged from H1 to H12. These locations were divided into four groups. Each group contained three locations that shared some features in terms of the urban configuration around the measurement point, as shown by Figure 3.17. Data loggers were mounted at heights of 2.5 - 3 m above ground level (relying on available access and security issues). They were fixed about 250 mm away from any wall to reduce the effect of wall convection that may affect readings. There is no clear instructions about air temperature measurements (Grimmond et al. 2010), although some studies refer to 300 mm (Sinou 2007) and 500 mm (Nakamura & Oke, 1988) as appropriate distances from the walls.

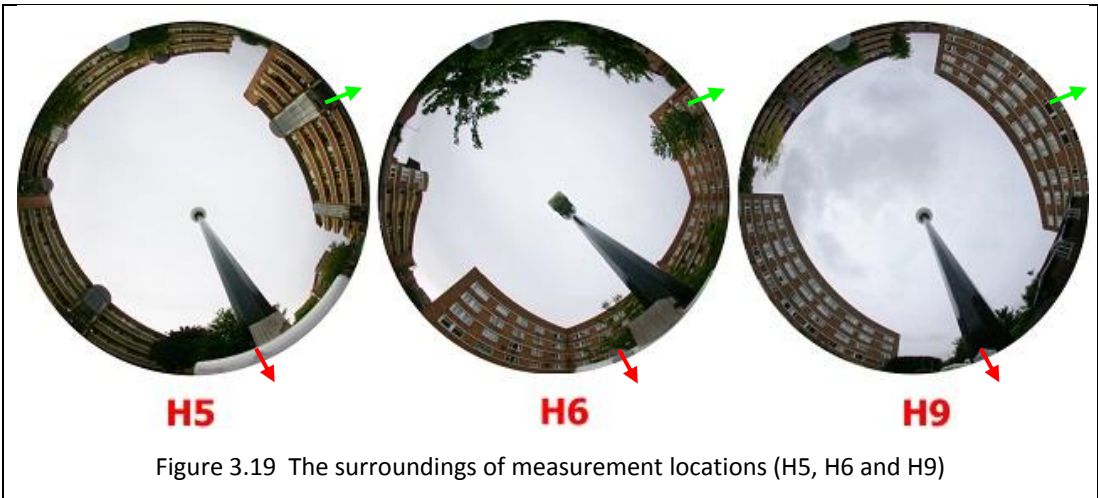


The data loggers at locations (H1, H2 and H4), as illustrated by the black dots, were fixed near the southern sides of the urban spaces. The southern facades, that may affect these measurement points, are least affected by direct solar radiation compared to other surfaces and so the measurement points are in the shade area

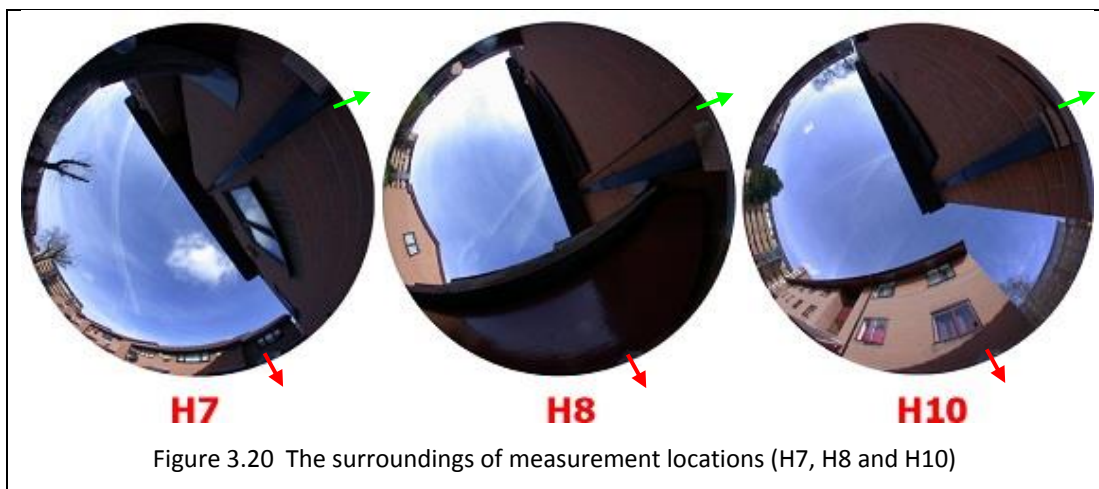
about all the daytime. The height of these sides and their surrounding differs between the three places as illustrated by images from a fish eye lens that was targeted to the sky to show all surroundings of the measurement points as shown by **Figure 3.18**. These images were taken at the same height as each data logger, about (2.5-3 m) from the ground, and the red arrows on them point to the northern direction while the green arrows point to the eastern direction.



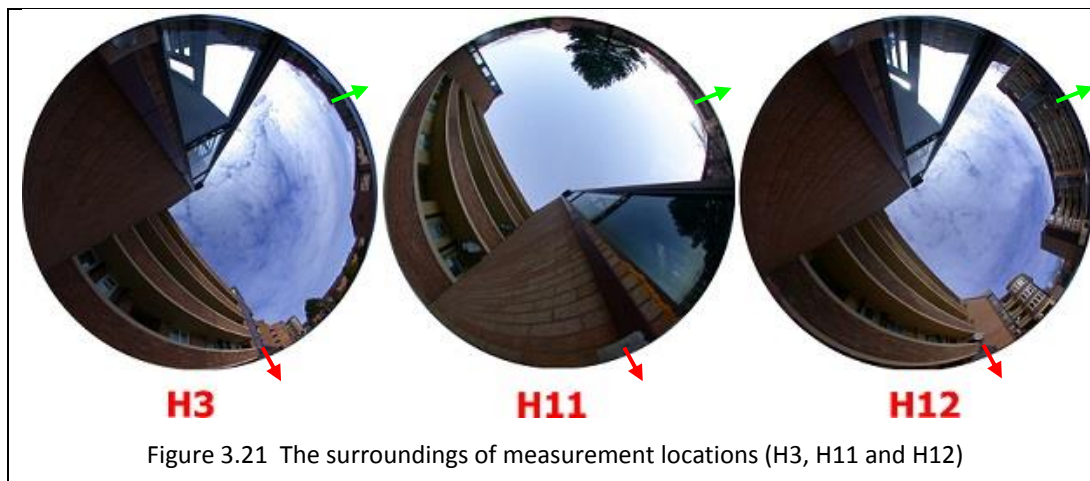
The data loggers of H5, H6 and H9 were settled in the middle of the urban spaces as indicated by the purple colour dots in **Figure 3.19**. The height of buildings that surrounded these locations ranged from 4 to 5 floors. The ground surface around the measurement point received direct solar radiation about most of daytime.



The data loggers at locations H7, H8 and H10 were illustrated by the blue dots. These sensors were mounted near the eastern walls of the urban spaces in confronting the Western hemisphere. The eastern sides are not illuminated by the direct sun rays before the midday, so the measurement points stay under the shade at the first half of the daytime. The height of these sides and their surroundings ranges between 2 and 3 floors in general especially for the Northern walls that may affect the measurements. These walls receive the direct solar radiation most of the daytime especially at H7 and H10. **Figure 3.20** shows the diversity of urban configuration around the measurement points.



The green dots show the measurement points locations at H3, H11 and H12. The western walls of the urban spaces are the dominant on these locations with height ranges from 4 to 5 floors in addition to the Northern wall at H11 and Southern walls at H3 and H12 as shown by **Figure 3.21**. The Western walls receive the direct solar radiation till about midday owing to their facing to the Eastern hemisphere. Although the data loggers were mounted about 3m from these walls, they could be affected by the reflected solar radiation and the emitted heat from these surfaces. Especially the locations H3 and H12, because of their southern walls that block the direct radiation from reach the measurement points and their adjacent surfaces in contrary to the Northern wall at H11 that receive the direct solar radiation throughout the first half of the day time.



3.4 Urban Morphological Parameter (UMP)

Urban morphology can be defined as the three dimensional form which results from a group of buildings and their in-between spaces (Nikolopoulou 2004). The urban morphological parameter represent tools that can describe or measure some configuration features of that three dimensional environment (like shapes, porosity, compactness) qualitatively or quantitatively, so that the urban form can be categorized and compared partially in terms of the specific parameters with its peers from another sites according to a convergent urban scale.

The disaggregation of urban form scale, that ranging from building scale to the city scale, affects how the form is measured, analysed and understood, and as a result different methodologies, development mechanisms and solutions will be adopted following to the determined scale (Kotharkar et al. 2014). Therefore, the selection of suitable parameter is an important matter in urban environment studies to understand the connections between the morphological features and the complex behaviour of air temperature variation across the urban fabric (Salvati, Palme, et al. 2017).

According to what was mentioned above, many urban morphological parameters were developed. Each of them shows a part of the qualitative aspects of urban form, like buildings shapes and street patterns (Morganti et al. 2017), while some of these aspect can be described numerically, like compactness, that represent a one principles of sustainable urban form to save energy and increase the quality of life

(Kotharkar et al. 2014). Therefore, many quantitative morphological parameters were adopted by the planning regulation of municipal authorities to watch and control the development of urban areas (Salvati et al. 2015; Ng 2010). However, there is no parameter that can describe the urban form adequately, and very different three dimensional urban forms can record similar values for the same parameter (Salvati et al. 2015).

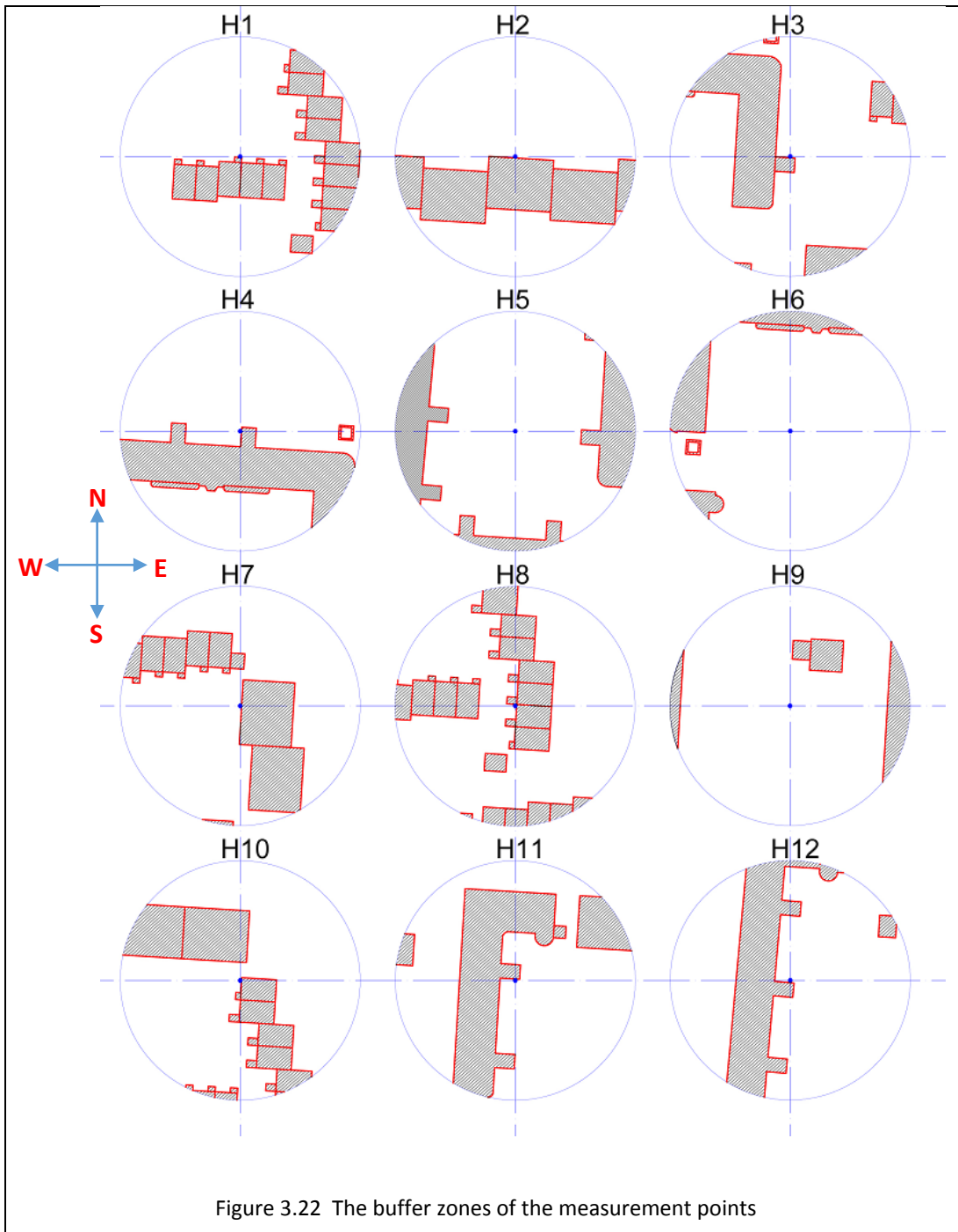
Therefore, this study adopted seven different parameters that have been used by large number of previous studies. In addition, this study developed three novel parameters that will be revealed in a separate chapter.

3.4.1 The buffer zone

The buffer zone is an imaginary border to define the influential urban domain around the data logger. It is a widespread approach in urban environmental studies to explore the relationships between specific surroundings and the related microclimates; however, there are no basic principles to determine the suitable radius of the zone (Unger 2009). The radius of the influential area has ranged from 500m to 10m according to many studies (Yan, Fan, Guo, Hu, et al. 2014; Hien et al. 2012; Petralli et al. 2014)(Sun 2011). A pilot study has shown that ranging of radius from 15 to 17.5 m for a green area in Hong Kong was not suitable to explore linkages with air temperature differences (Giridharan et al. 2007). Likewise, wider areas with radii of 565m and 125m do not have a real effect on the correlation coefficients for maximum, minimum and average air temperature models of the sites in Curitiba-Brazil, while the effect of urban features within a radius 56m was taken into account for the same models (Krüger & Givoni 2007). The influence of radiation transfer can be neglected if the radius of effect area is 200 m or more (Unger 2009). Thus, determining an appropriate scale of an urban study area may affect the role of urban geometry regarding to air temperature changes (ibid).

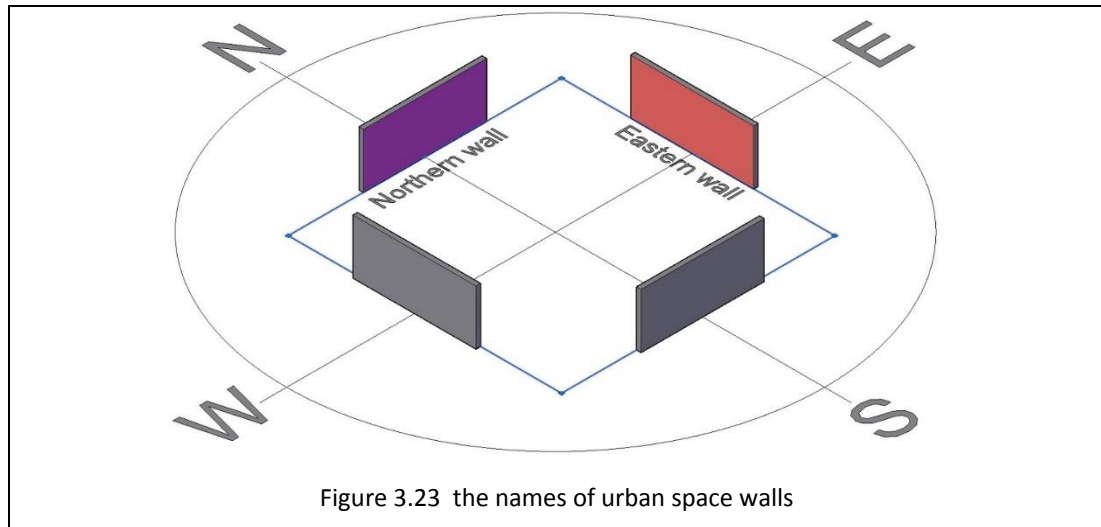
Because of the relatively small scale of the Minster Court compound, this study, as an initial attempt, adopted 25 metres as a radius for the influential zone. By using the AutoCAD software and after drawing the site plan of the compound, the buffer zones

around the measurement points were drawn by using the CIRCLE command, The position of a data logger represents the centre of the circle as shown by Figure 3.22.



It should be noted that this study named the facades, the vertical surfaces or the walls that surrounded the urban space depending on their locations in connection with the cardinal directions of the urban space, as shown by Figure 3.23. For instance,

the wall on the eastern side of the urban space was defined as the eastern wall that face the western horizon of that space, and the same thing for the rest walls.



The following sections were devoted to display the urban parameters and their calculation methods that have been applied to the urban fabric inside the buffer zones.

3.4.2 Floor Area Ratio (FAR)

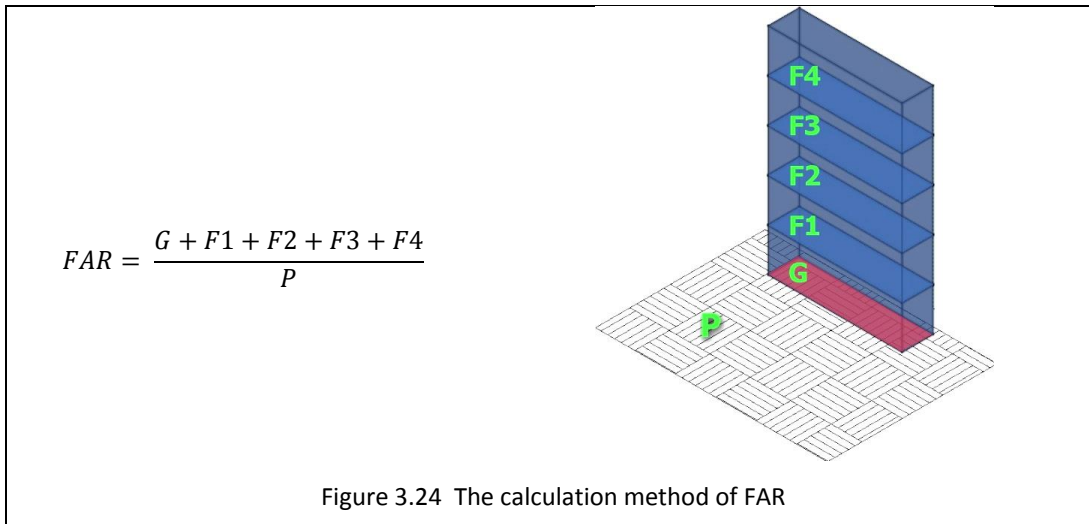
It is an urban physical indicator that express the built floor area in relation to the land area and it is also known as floor space index (Berghauser Pont & Haupt 2007) or plot ratio. FAR is widely used in the urban planning regulations as a standard measure to control the construction densities of urban area zonings (Ng 2010).

The initial concept of this parameter was adopted firstly by the Building Ordinance of Berlin at 1925 then an international conference in Zurich referred it as a common urban planning standard in Europe at 1948 (Pont & Haupt 2009). It looks like the British planning standards adopted this parameter as it has been mentioned by many planning policy reports for different city councils in the UK like Glasgow (Glasgow city council 2014), London Borough of Ealing (Ealing Council 2004) and London Borough of Hammersmith & Fulham (Hammersmith & Fulham Council 2013) .

FAR can be calculated as a ratio according to the following formula:

$$FAR = \frac{\text{the gross floor area of the building (m}^2\text{)}}{\text{the plot area (m}^2\text{)}} \quad (3.1)$$

The gross floor area takes into account the overall area of the building on each floor below or above ground as shown by Figure 3.24 without exclude anything like stairs, thickness of walls, circulation spaces and lift shafts, while the plot area represents the site area that defined precisely by official documents (Ng 2010).



In general, the changing of FAR values refers to change the floors areas and the height of the building. These variables may block the direct solar radiation and wind movement and affect the building surface area that act as thermal reservoir. Consequently, the variation of FAR values may affect the microclimate of an urban area. Therefore, many studies have been conducted in relation to this parameter to investigate its effect on the urban heat island (Jin et al. 2018), renewable energy potential regarding to solar energy in London (Sarralde et al. 2015) and Geneva (Mohajeri et al. 2016), outdoor thermal comfort and urban ventilation in tropics (Ignatius et al. 2015). All the above are indicative of the importance of this parameter and its potential that can be used to understand the effect of urban morphology on air temperature under the maritime temperate climate in the city of Liverpool.

3.4.3 Site Coverage Ratio (SCR)

SCR is a well-known urban morphological parameter, especially regarding to the planning regulations of municipality departments in many countries; it is known also as the building coverage ratio. The measurement of coverage became a part of the Building Ordinance of Berlin, Germany at 1925 and before that in 1916 the Zoning Resolution of New York City determined the amount of ground that can be built (Pont & Haupt 2009). These may be the oldest use of the coverage concept in an official planning policy.

The concept of coverage represents the relationship between the solid and the void in urban context or between built and non-built land. Therefore, SCR is used to preserve areas for landscaping and to prevent over-build (Ng 2010). Consequently, controlling the population density and its related infrastructure. SCR measures the proportion of the site area covered by the built mass according to the following formula that connects between the ground floor area of the building (G) and the area of the lot (P) (Pan et al. 2008), as shown by [Figure 3.25](#).

$$SCR = \frac{\text{the ground floor area of the building (m}^2\text{)}}{\text{the plot area (m}^2\text{)}} \quad (3.2)$$

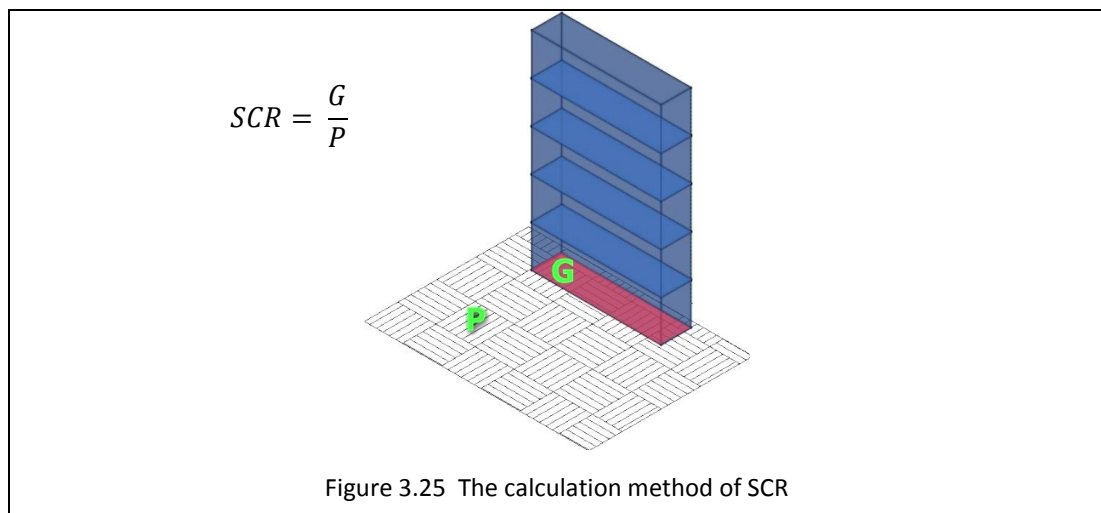


Figure 3.25 The calculation method of SCR

The high values of SCR refer to more urban blocks and less intra-spaces and this binary activity leads to obscuring more sky and reducing the solar radiation from reaching the space in addition to disruption of wind movement between urban spaces. It is not unlikely to get analogous values of SCR for different locations that

show a diversity in their configurations in terms of sky line, permeability, layout of buildings and their distribution on site (Pont & Haupt 2009). This represent a weak point against SCR regarding to the urban environmental researches. However, it has been used frequently to investigate the influence of urban morphology on thermal comfort (Park et al. 2018), energy consumption (Salvati, Coch, et al. 2017)(Yunitsyna & Shtepani 2017), solar energy (Mohajeri et al. 2016), urban heat island (Yuan & Chen 2011) and air temperature (Ignatius et al. 2015).

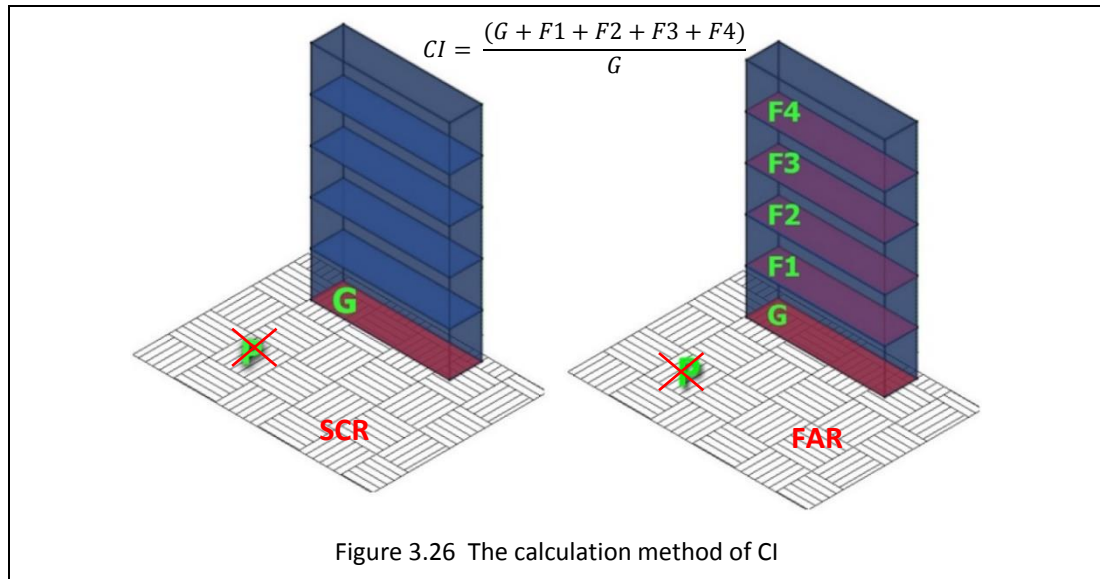
SCR looks like familiar to the planning policy in the UK to express the density of urban area (FAREHAM Council 2009; Ealing Council 2004), however a limited number of studies utilized it for case studies in the UK to investigate the renewable energy potential of neighbourhoods (Sarralde et al. 2015), the noise of urban areas (Margaritis & Kang 2016; Wang & Kang 2011) and the correlation between the heat wave vulnerability index and the heat demand of urban domestic (Mavrogianni et al. 2009). Therefore, its influence on the air temperature behaviour under the maritime temperate climate still needs more investigation.

3.4.4 Compactness Index (CI)

Although CI is defined as a ratio of FAR to SCR for the same building or urban site, it is not as well-known as them in terms of the urban planning regulations. However, it has been mentioned frequently by the urban morphological researchers (Berghauser Pont & Haupt 2007; Steadman 2014; NES et al. 2012; Berghauser Pont et al. 2015; Kickert et al. 2014) where all these studies described it by the layer or L. CI may indicate the average number of floors in an urban area if each floor in the building shows the same area as the ground floor of the same building as shown by [Figure 3.26](#). Therefore, and depending on the calculation method demonstrated by the following formula, CI will equal the number of floors of a building.

$$CI = \frac{FAR}{SCR} = \frac{\text{the gross floor area of the building (m}^2\text{)}}{\text{the ground floor area of the building (m}^2\text{)}} \quad (3.3)$$

The denominator of the both parameters (FAR and SCR) is the same (the plot area P).



The compactness index is the name that was used in the first study (Cheng et al. 2006) that mentioned this parameter according to the best knowledge of the researcher. This study did not reveal the source of this parameter that was used as a morphological indicator to investigate its correlation with daylight factor and photovoltaic cells potentials in urban context. The compactness index was utilized later in a limited number of urban environmental studies regarding different aspects, like the ambient temperature, external heat gain, outdoor thermal comfort and urban ventilation as a comprehensive approach that affected urban features in tropic climates (Ignatius et al. 2015); to reveal the connections between the index of heatwave vulnerability and urban domestic heat demand in London (Mavrogianni et al. 2009); to introduce recommendations for planners and government agencies regarding to the relationship between urban morphology and microclimate (Wei et al. 2016) and to understand the interferences between geometric-analytical parameters, solar radiation and energy consumption of a residential block under a Mediterranean climate (Morganti et al. 2012).

Its effect on air temperature variation is not clear, especially with the variation of climates on the Earth; therefore, it was adopted as a measure of urban morphology to investigate its influence on air temperature in the city of Liverpool – UK.

3.4.5 Sky View Factor (SVF)

The sky view factor is a one of the most well-known parameters in urban environmental studies regarding to solar radiation (Rehman & Uzair 2017; Polo et al. 2016; Yousuf et al. 2018), urban heat island (Unger 2009; Shaker & Drezner 2010; Cheung et al. 2016), thermal comfort (Krüger et al. 2011) and other fields like daylight (Nasrollahi & Shokri 2016). However, some studies have referred to the limited discussion about its relationships to daytime urban temperatures (Chen et al. 2012).

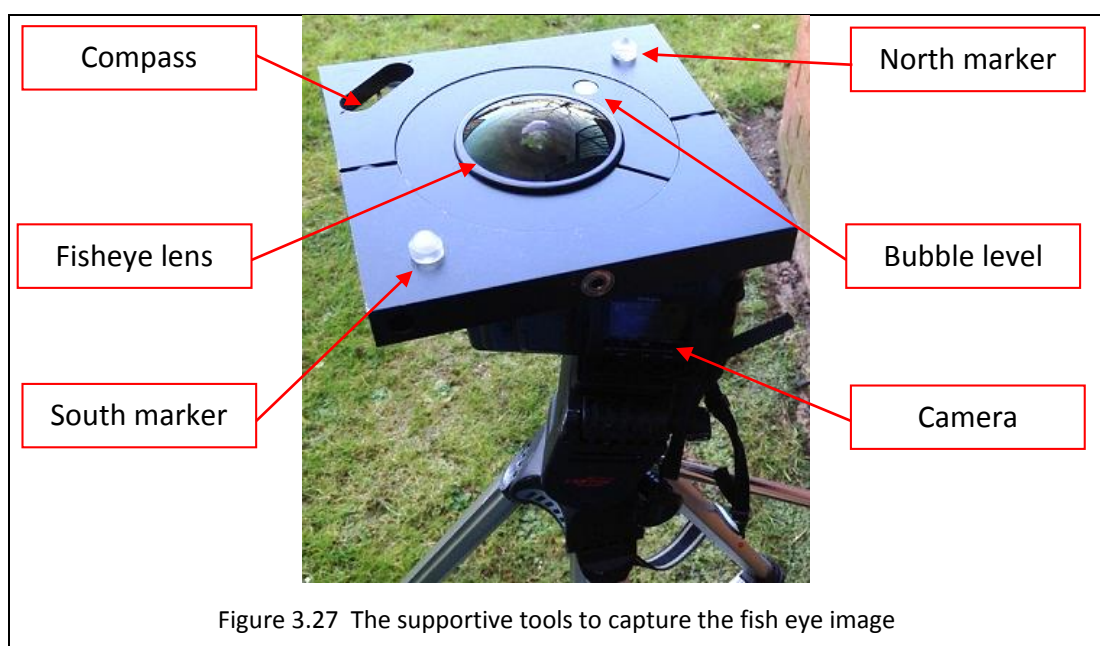
As a simple description, SVF represents the proportion of sky dome or the exposure degree to the sky that can be seen from the measurement point near the surface of ground; furthermore, it is a dimensionless parameter with values ranging from completely open to the sky (SVF=1) to completely blocked from the sky (SVF=0) (Zhang et al. 2012; Nikolopoulou 2004; Erell et al. 2011). However, a more complicated description is the ratio between the radiation that is received by a planar surface to the entire radiating environment of the hemisphere and, therefore, it affects the radiant heat exchange between the sky and the urban canopy (Svensson 2004). Although there are differences between the two descriptions and their applications, it can be concluded that SVF in general is a geometrical parameter that is determined according to the configuration of the surroundings around the measurement point and, therefore, many methods were developed to calculate SVF depending on this concept.

The analytical method or geometrical method is intended to calculate SVF by analysing the radiation flux that reaches the visible sky from the studied surface (Johnson & Watson 1984), where this radiation flux is affected by the geometrical characteristics of neighbouring vertical surfaces that define the skyline around the measurement position.

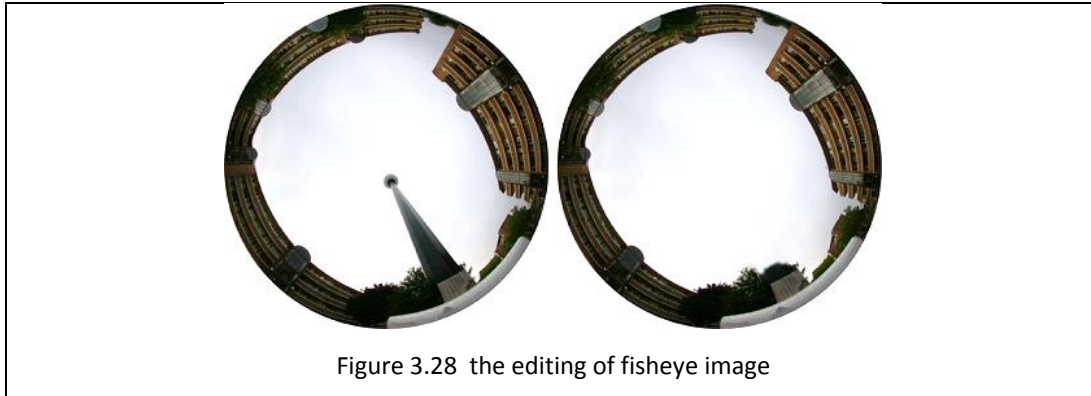
The hemispherical photography method was devoted to project the real three-dimensional environment on a two-dimensional image by using a fisheye lens that provides an upward-looking view to show which parts of the sky are visible and which parts are blocked by man-made structures, trees and landscape features. These obstacles draw the skyline around the observation point. Although the numerical

models of this method witnessed many levels (Johnson & Watson 1984; Steyn 1980), currently many software or plugins have been developed to process this kind of images and calculate SVF like HemiView (www.delta-t.co.uk), BMSky-view (Rzepa 2009), RayMan (<http://www.urbanclimate.net/rayman/>) and CCL on MATLAB (Cheung et al. 2016).

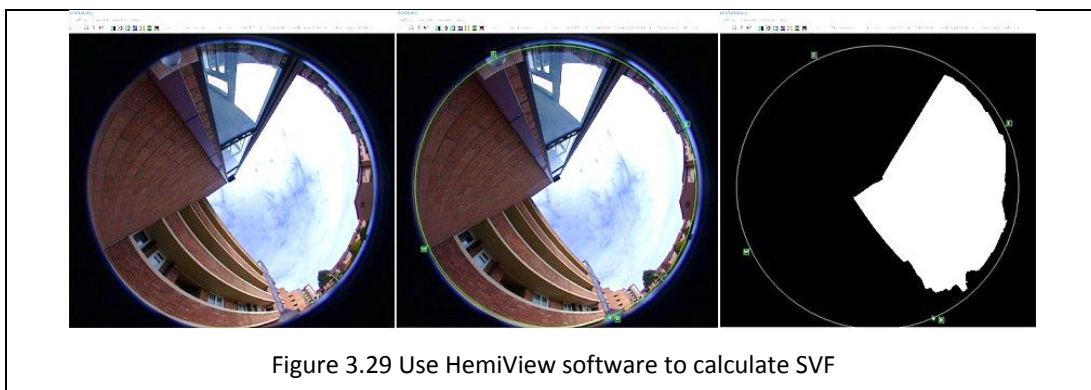
This study used fisheye images and HemiView software to calculate SVF. The photographic method is suitable to analyse the geometry of real urban context on a small scale (Chen et al. 2012) like the Minster Court compound. The field work tools used to capture these images were Nikon Fisheye Converter FC-E8 and a Nikon Coolpix 995 camera in addition to the self-levelling mount that help to keep the fisheye lens and the camera aligned to the horizon depending on the bubble level while the North direction of site is defined by the compass. The northern and the southern directions can be recognised by existence two markers on the two sides of lens, as shown by Figure 3.27, These markers appear on the image itself. These settings are necessary to use HemiView software to calculate SVF. The photos were taken one by one at the same heights of data loggers. The horizon of image was settled by the bubble level and the compass during the imaging process to ensure the correct orientation and correct level of the image.



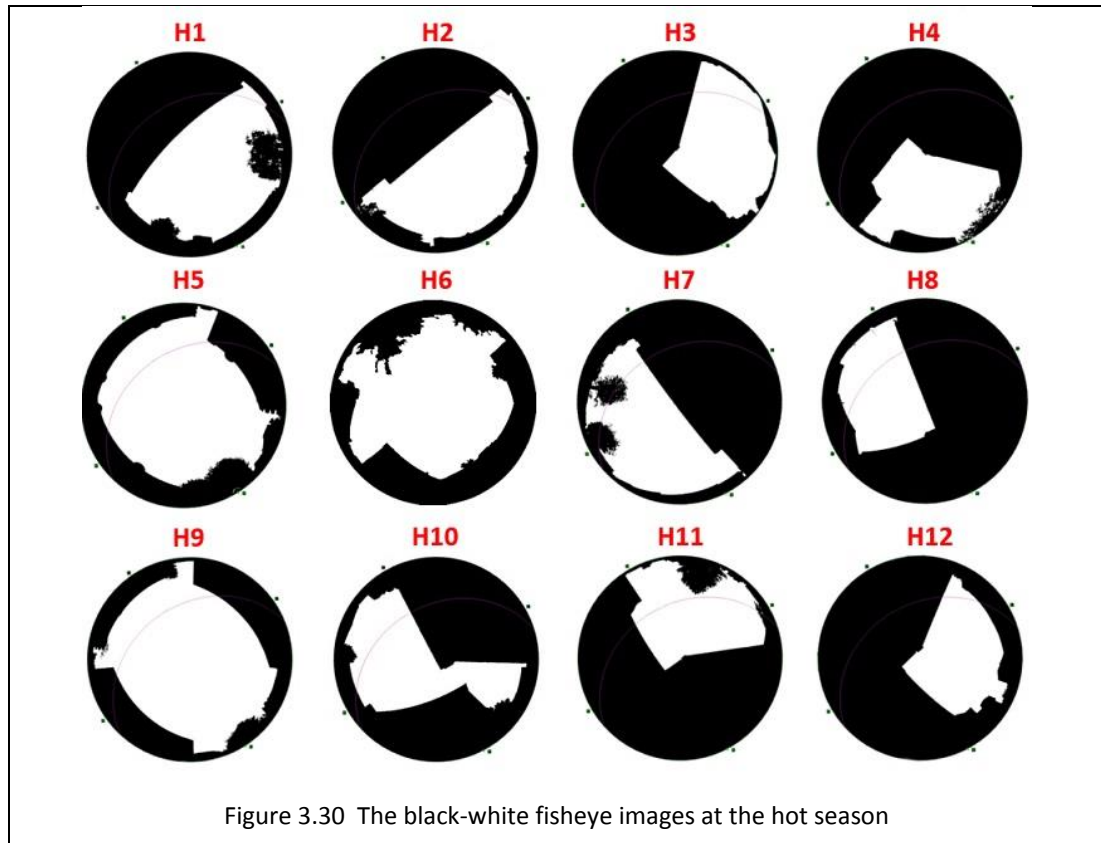
Before sending images to HemiView software, some images were edited by Photoshop to remove some obstacles that have no real effect on air temperature, like lamp posts that occupy effective parts of images as shown in [Figure 3.28](#).



The HemiView software is a Windows-based program that was used to analyse the hemispherical photography image (fisheye image). It supports many image file formats and the JPEG (*.jpg) produced by the Nikon Coolpix 995 camera is a one of them. The image is imported by HemiView and before turning it in to a black-white image, it should be matched with the hemispherical co-ordinate system of the software by defining the general location of the image site, the kind of lens and the outer border of the image by a horizon circle that can be aligned precisely between the markers of the image as shown by [Figure 3.29](#). This circle also helps to remove the excess from the image. The lens has the ability to shoot more than 180 degrees and therefore this circle keeps the effective area of image inside it as equal as possible between different images because the distance between the two markers is equal between different images.



Finally, the sky view factor values can be calculated automatically from the black-white images. Figure 3.30 shows the black-white fisheye images at the hot season for all locations throughout the Minster Court compound.



3.4.6 Degree of Compactness (Dc)

The degree of compactness is a simple geometrical parameter of urban fabric that can control the heat exchange regime in a particular zone of city. The motivation to develop Dc is that the usual urban parameters like SVF, H/W ratio and SCR have not considered the differentiated heights of entire urban zones and therefore the role of urban fabric volume that affect the microclimate of site is absent (Fahmy & Sharples 2009a; Fahmy 2012).

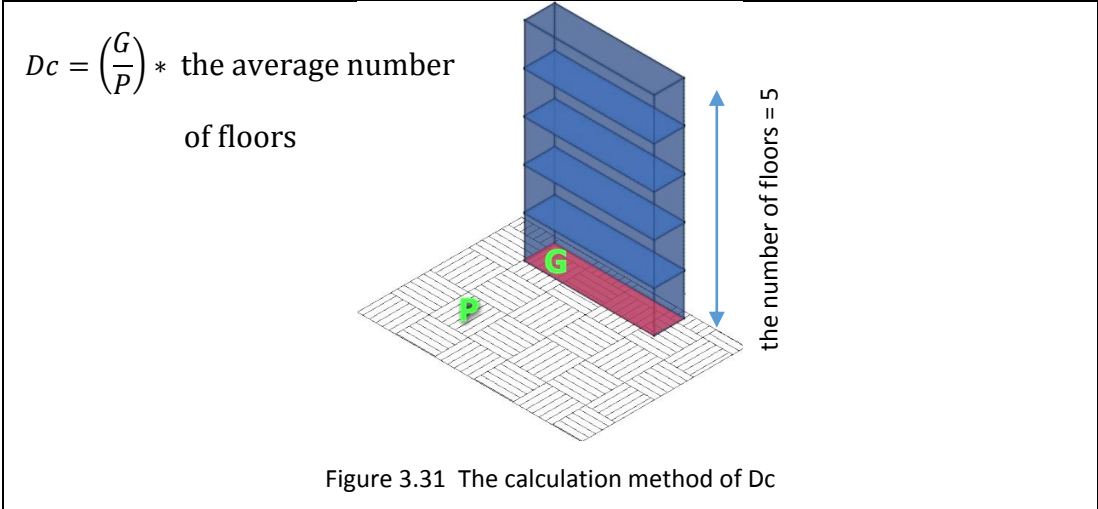
The compactness degree can be calculated depending on the following formula:

$$Dc = \text{the site construction percentage} * \text{the average number of floors}$$

The site construction percentage represents the ratio of the total ground floor area of the buildings on the site to the total area of the site (Fahmy, Mohamad & Sharples

2008; Fahmy & Sharples 2011); in other words, this ratio represents the site coverage ratio (SCR). Therefore, Dc can be calculated according to the following formula as shown by Figure 3.231.

$$Dc = SCR * \text{the average number of floors} \quad (3.4)$$



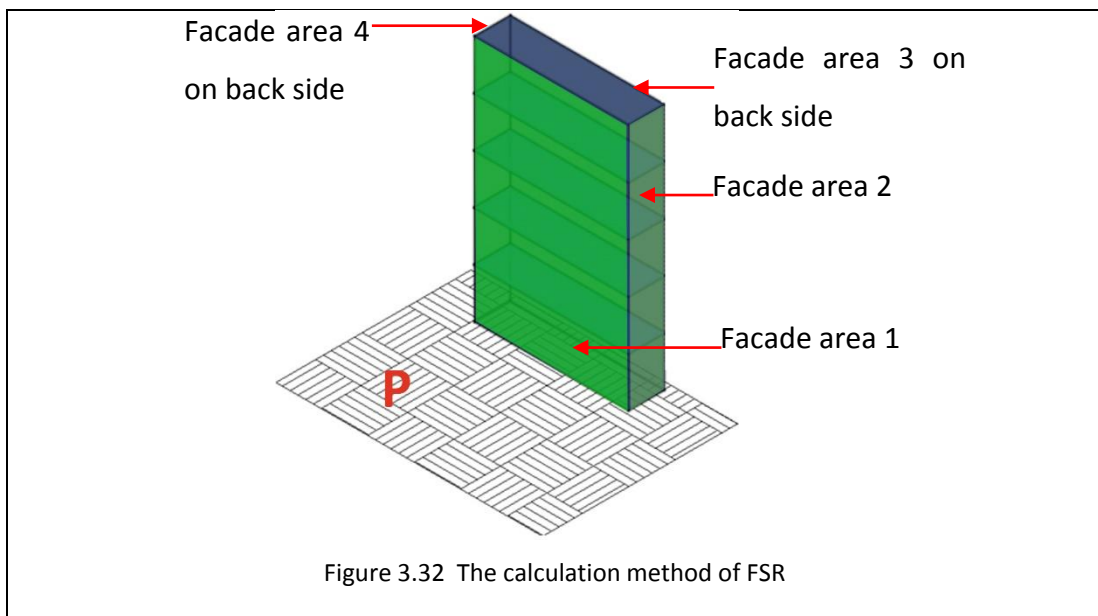
Dc is a climate-based urban planning parameter that can affect three factors: first, the population that inhabits the certain urban area; second, the height of built-up area in terms of the total building floors to accommodate the population and, third, the climate reaction to the height of urban canopy (Fahmy & Sharples 2011). In this way, and from the view point of Dc, it can classify the city zones in to five categories (city centre = very compact, central urban = compact, general urban = medium, sub urban = open and rural urban = very open) regardless the network type, therefore the built-up area will be under control in terms of solar access and population by controlling Dc (Fahmy & Sharples 2009a). An adequate degree of compactness can provide enough shelter according to planning laws and allow the wind movement to cool the urban space or provide more shade depending on the orientation of canyons, vegetation, configuration of urban fabric units and the urban spaces. This combination can optimize the urban passive activity as a hybrid urban form (Fahmy, Mohamad & Sharples 2008). It can be customized this form to increase the compactness within each fabric group and lowered between the groups and this technique will support both wind movement and shading effects (Fahmy 2012).

According to the above-mentioned allegations, this study is going to investigate the potential of the degree of compactness (Dc) in terms of its effect on air temperature by using its calculation method to describe the urban morphology inside the buffer zone for each the measurement points.

3.4.7 Facade to site ratio (FSR)

Facade to site ratio is an urban morphological parameter that represent the ratio between the total facades area (vertical surface area) to the urban site area (horizontal surface area) (Bueno et al. 2013). Therefore, it can be described as a vertical density index for the urban site (Morganti et al. 2017). The FSR can be calculated by the following formula as shown by Figure 3.32.

$$FSR = \frac{\text{the total facade area of builing (m}^2\text{)}}{\text{the plot area (m}^2\text{)}} \quad (3.5)$$



This parameter may have different names, like degree of diversity (Dv), where it measures the diversity of vertical morphology for the urban location (Fahmy & Sharples 2009b). Urban designers may be more familiar with the term vertical-to-

horizontal ratio (VH) (Mao et al. 2017; Bueno et al. 2014; Nakano, Bueno, Norford & C. F. C. F. Reinhart 2015). Vertical surface density is another description for FSR where it quantifies the density of façades in urban area (Salvati, Coch, et al. 2017).

In general, and according to what mentioned before, an increasing of FSR can increase the absorption of solar radiation due to the multiple reflections between the vertical surfaces and reduce the speed of wind and thermal loss because of reducing exposure to the sky. All this will impact the thermal storage capacity of vertical urban surfaces, surface temperature, air temperature and, consequently, energy consumption. Therefore, many studies have utilized FSR to investigate the relationships between urban morphology and temperature (Salvati et al. 2015), solar energy (Morganti et al. 2017) and urban energy needs (Street et al. 2013). However, there is a lack in understanding the abilities of this parameter due to the scarcity of studies that investigate it compared to other parameters like sky view factor (SVF), while most of the existing studies relied on simulation. FSR is one of the parameters to predict the urban air temperature depending on the data of weather stations outside the cities by using the urban weather generator model (UWG)(MIT 2018).

Therefore, a part of this study is determined to explore the potential of FSR in terms of the air temperature variation in the moderate maritime climate by using field measurements data; then its result will be compared with the previous studies results.

3.4.8 Shape Factor (SF)

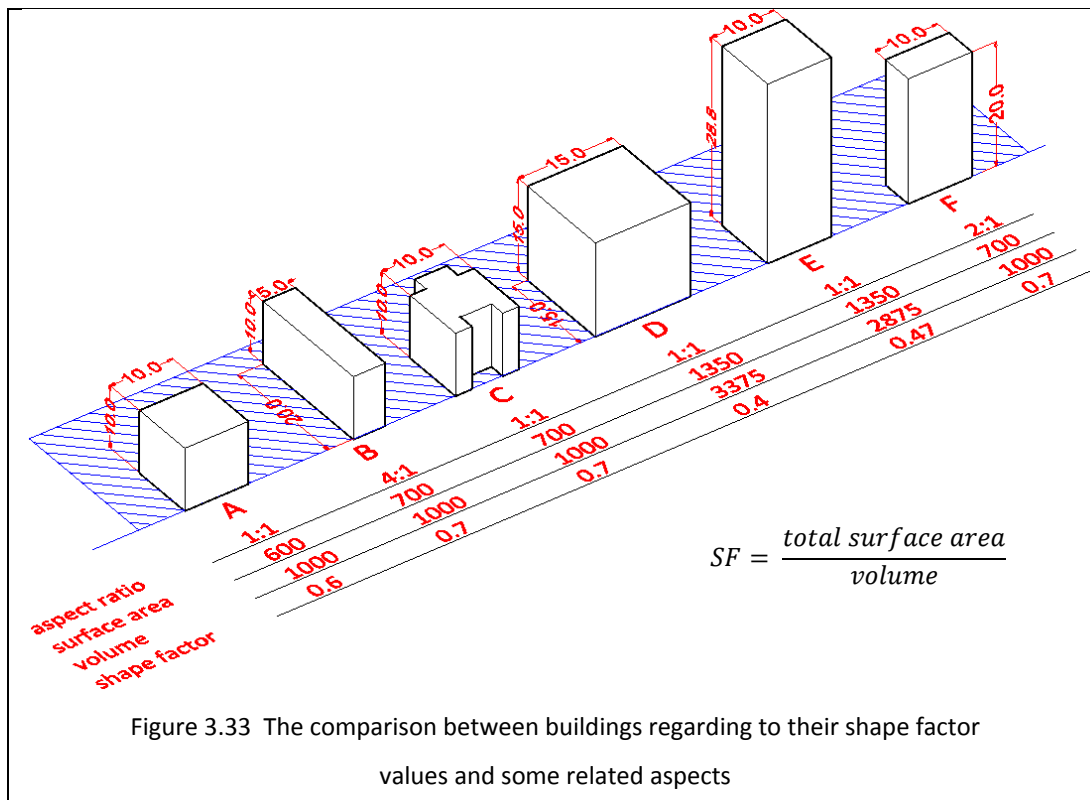
The shape factor parameter follows the allometric rules that describe the change of organisms shape as they grow in size during their life (Steadman et al. 2009); therefore, it is used in many fields like biology and architecture (Carneiro et al. 2010). SF is a well-known simple indicator to evaluate whether or not the building envelope to its volume supports heating or cooling energy-efficiency under the influence of the external environment (Alsabry et al. 2017). The importance of the relationships between the shape factor and the primary energy demand of the buildings have contributed to setting SF as a requirement by the German Building Code for the

energy performance of the buildings since 2002 and many countries in Europe have followed this (Lylykangas 2009).

The shape factor is the ratio of total surface area of the building envelope to volume of the building and therefore it represents the measure of building compactness. Therefore, the buildings with smaller SF values are more compact and they have the lower surface area for a given volume. Consequently, a lower thermal loss can happen from the indoor to the outdoor environment, in this regard the sphere and the cube are perfect forms (Geletka & Sedláková 2012; Mumovic & Santamouris 2009).

According to **Figure 3.33**, changing the aspect ratio (L/W) produces a different surface area for an equivalent height and floor area (like A & B), while for the same aspect ratio and the same form the object with bigger volume has the smaller surface area. The change in surface area is smaller than to be equivalent to a change in volume (Danielski et al. 2012). Therefore, the shape factor for bigger objects is smaller (like A & D). Also, SF is relying on the building form configuration, as shown by cases A and C. The latter shows a bigger surface area and bigger shape factor, although both have the same aspect ratio and same volume. Another change of building form can be done by increasing the height for the same shape with the same aspect ratio (like A & E). In general, the small value of SF belongs to the tall building due to the small volumes versus the relatively big surface area in shorter building (Carneiro et al. 2010). It is not unlikely that buildings with different forms, dimensions and ratios show similar values of SF (like B, C and F).

The importance of SF can be inferred generally if the shape factor may interpret more than 10% of building energy consumption in cold climates, while this percentage reduces in warmer climates (Danielski et al. 2012).

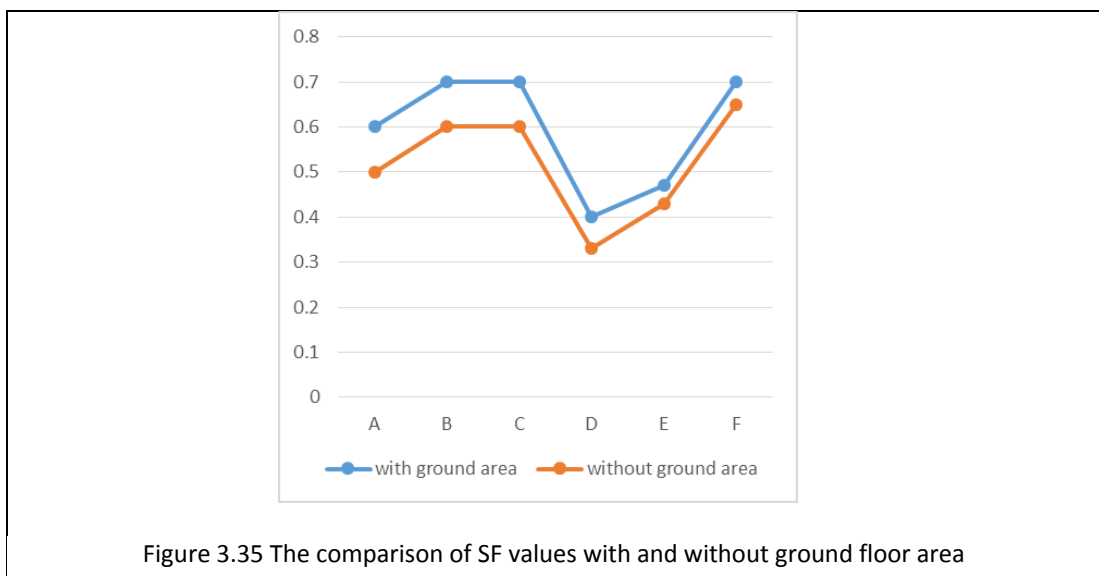
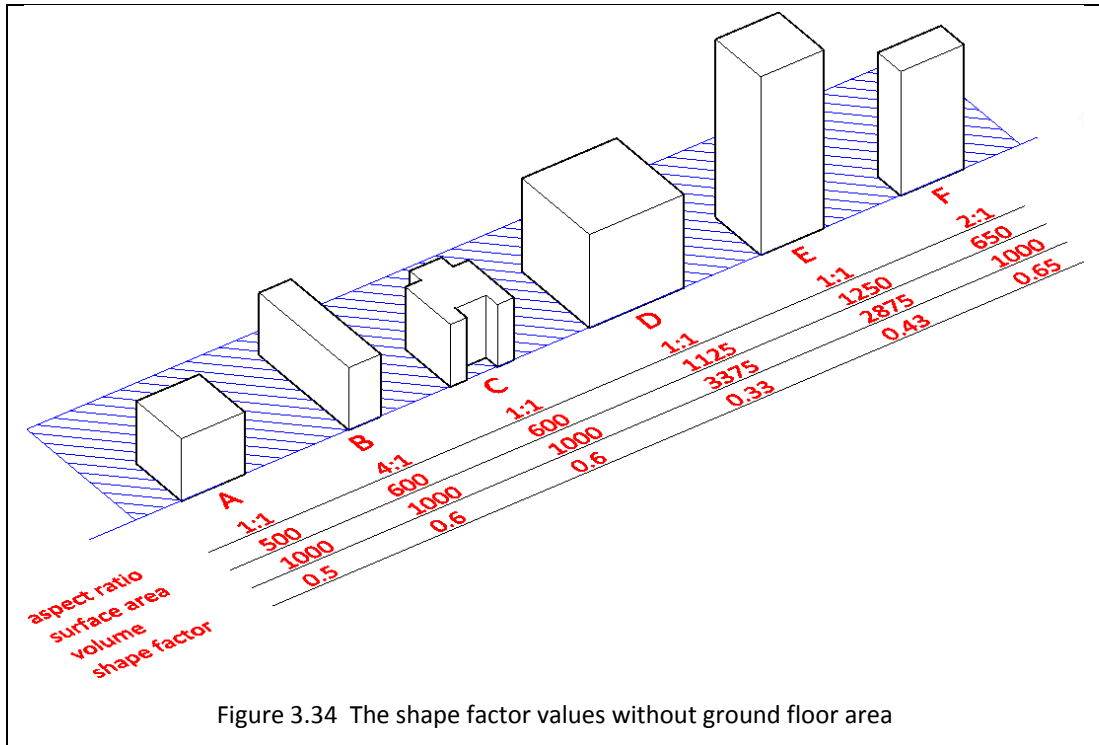


The external surfaces of buildings act as a barrier between the indoor and the outdoor environments, thus they represent a part of the urban space envelope. Therefore, a more compact shape of a building (low SF values) results in lowering exposure to the outside environment and consequently low thermal stocks of the building surfaces by the solar energy. According to the researcher's best knowledge, the studies on the effect of the SF on air temperature in urban space are almost non-existent. Therefore, this study will be a leader in uncovering this relationship and employing SF as an urban morphological parameter in urban microclimate studies.

The surfaces that affect the thermal microclimate directly are roofs (RO) and walls (WA); therefore, the ground area of a building will be excluded as it is not a part of the thermal envelope of urban space. The shape factor will be calculated individually for each building or block within the urban site and the total summation of all SF values represents the shape factor value of the site according to the following formula.

$$SF = \sum_{x=1}^{x=n} \frac{(RO_x + WA_x)}{V_x} \quad (3.6)$$

where (n) is the total number of building on site. Figure 3.34 shows the new values of the surface area and shape factor after excluding the ground floor area of a building. Figure 3.35 reveals the comparison between the old and new values of SF, where it can be noticed that the exclusion of building ground area did not affect SF value as a rate between old and new values like A, B and C, while other cases (D, E and F) were affected



3.5 Statistical approach

A statistical approach to the measured data permits estimation of the influence of an urban area on the microclimate (Grimmond et al. 2010). Therefore, such an approach has been used extensively, especially linear regression analysis, in urban environment studies (Morganti et al. 2017; Svensson 2004; Salvati, Coch, et al. 2017; Mohajeri et al. 2016; Grimmond et al. 2010; Jin et al. 2018). The need to describe the relationships between some independent variables and responsive or dependent variables mathematically is the motivation to use the linear regression; it will not simplify the complexity of the world but it may help to understand its processes (Jim Frost 2015). The independent variables of regression can be just one variable and the regression model will know as simple linear regression, while the regression model with more than one independent variable is called multiple linear regression.

This study will use multiple linear regression owing to the existence of many variables that affect the air temperature. In addition, multiple regression affords a method to understand the bonds of a group of independent variables versus a dependent variable, and it enables prediction or explanation of the dependent variable (Orme & Orme 2009).

Many software can be utilized to develop regression models, such as Microsoft Excel, MATLAB and SPSS. Minitab software versions 16 - 17 was used to analyse the main influences of urban morphological parameters on the variation of air temperatures. The data files from the University's weather station were processed firstly by Microsoft Excel to change their extension and to extract and categorize the final data set that will be utilized in the statistical analyses. The data from sensors were processed firstly by HOBOWare then they sent to Microsoft Excel to be categorized before sending them to Minitab.

The outputs of regression process can be useful to analyse and judge the relationships between urban morphological parameters (UMP) and the indicators of thermal microclimate.

R-square (R^2 %) is a one of these outputs, and it is known as the coefficient of multiple determination or the coefficient of determination. It represents the explanatory

power of a regression model as a percentage of how the changes of dependent variable fit the changes of independent variables. Therefore, R-squared measures how well the model fits the data. R-squared is between 0 and 1 or 0% and 100%, and in general the higher value the better (Minitab 2013b). However, it has problem, where an increase in the number of independent variables leads to an increase in the value of R^2 in general. For this reason, the adjusted R squared (R-Sq(adj) %) was developed to solve this problem, whereby it will change only if the extra independent variable improves the model or makes it worse more than would be anticipated by chance (Minitab 2013a). (R-Sq(adj)%) will be the main value to evaluate the effect of urban morphology on thermal microclimate.

The standard error of the regression (S) will be referred as another statistic to validity the changing of the (R-Sq(adj)%) value under the effect of urban parameters, where both of them do not change unless the new independent variable has a real impact on the statistical model (Jim Frost 2014). S shows how wrong the multiple regression model is on average utilizing the units of the dependent variable. In other words, it demonstrates the average distance of the observed values from the regression line. Therefore, it assesses the accuracy of the model and the lower the value of S then the higher the accuracy of the model (Minitab 2014b). Consequently, the influential urban parameter leads to an increased (R-Sq(adj)%) value and a decreased S value.

Both of these statistics may be worthless without a significance level (p-value) that represents the first line of defence of the statistical model. It determines whether there is a statistically significant relationship between the variables of the model. A p-value that is equal or lower than 0.05 indicates that the statistical model is significant (Minitab 2014a), and it will be utilized in analyses while the model with a p-value more than 0.05 will be ignored. Each independent variable of the statistical model can be insignificant. Therefore, a multiple regression model can be simplified to analyse by removing those insignificant independent variables depending on the stepwise method that can identify useful variables by adding or removing them as a one step at a time based on their p-value (Minitab 2014c). Stepwise regression in the

statistical software is an automated procedure can be chosen to yield one model that can be simpler.

The coefficients of regression describe the relationship between an independent variable and the dependent variable. The coefficient sign shows the direction of the relationship between the influential variable and the responsive variable. The positive sign shows that as the independent variable increases, the dependent variable also increase. While the negative sign shows that the increase of influential variable leads to decrease the dependent variable (Frost 2017). So, the regression coefficient sign can reveal the effect of an urban parameter in terms of it increasing or decreasing air temperature.

3.5.1 Data sorting

The sorting of data is a crucial matter in any study. In urban morphology research diverse methodologies have been adopted by researchers regarding this matter. Some studies categorized their data depending on the seasons or sky conditions in terms of sunny sky or cloudy sky (Giovannini et al. 2013; Taleghani, Tenpierik, van den Dobbelen, et al. 2014), while the selection of data of a limited number of days according to some characteristics from a longer measurement duration and dividing them into daytimes and night-times or into more than two periods are different approaches (Yan, Fan, Guo, Wu, et al. 2014; Hien & Jusuf 2010). Some researchers focused on calm climatic conditions and a specific part of the day, such as calm nights (Svensson 2004) and afternoon periods (Middel et al. 2014; Chen et al. 2012); other studies sorted their environmental measurements into maximum, minimum and average values (Wong et al. 2011; Hien et al. 2012).

An architect or planner will usually care about the daytime duration regarding to design of urban spaces as it is the normal time for human activities in these spaces, while the climatologists may focus more on the night time because of the big differences of temperatures between the urban areas and their outskirts in a phenomenon known as urban heat island (UHI) (Eliasson & Svensson 2003). The UHI

may bring real problems regarding thermal comfort, public health, economics and pollution.

The data of this study can be distributed into two kinds - effective data and supportive data. The data that are used directly by models of statistical analyses as dependent variable (on-site measured air temperature (T_a)) and as independent variables (ambient air temperature ($a.T_a$), solar radiation (solar) and the urban morphological parameters (UMP)) represent the first kind. The second kind (wind speed (W_s), rain rates and sunny hours) are devoted to support the discussion about the statistical analyses results. According to [Figure 3.36](#) and [Figure 3.37](#), the data from on-site measurements and the data of a weather station represent the two wings of field measurements and they follow the same steps. The data from the both sources were split into hot season dataset and cold season dataset. Each dataset were then subdivided into three groups of days according to the sky conditions (sunny days, partially cloudy days and cloudy days). Each group of days were next distributed into four periods, each one of them representing six hours of the day - the night period (12am-6am), the morning period (6am-12pm), the afternoon period (12pm-6pm), the evening period (6pm-12am)). The dataset of each period were separated into three smaller datasets as hourly average (AVG), hourly maximum (MAX) and hourly minimum (MIN). This approach will reduce the disparities of readings that happen because of differences in seasons, sky conditions and daily periods. The statistical model traces and compares the patterns of change between dependent and independent variables. Therefore, the effect of the urban morphological parameter (UMP) on air temperature can be clearer with lower disparities of other independent variables throughout the measurement period. The change of T_a might follow the change of UMP depending on climatic conditions prevailing in that period.

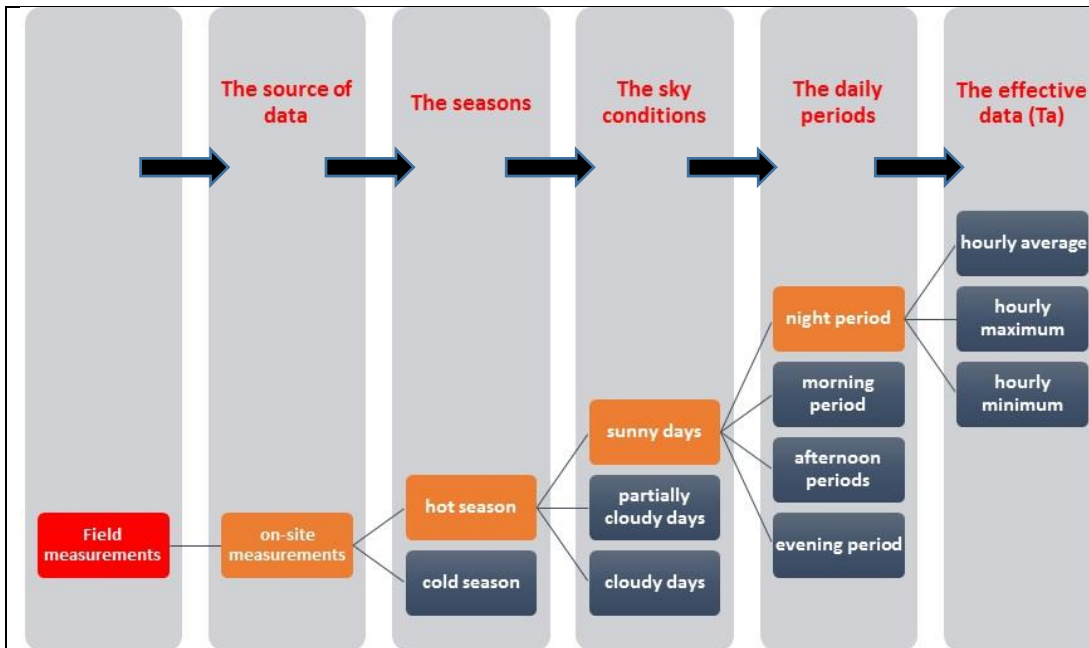


Figure 3.36 The sorting of field measurement data

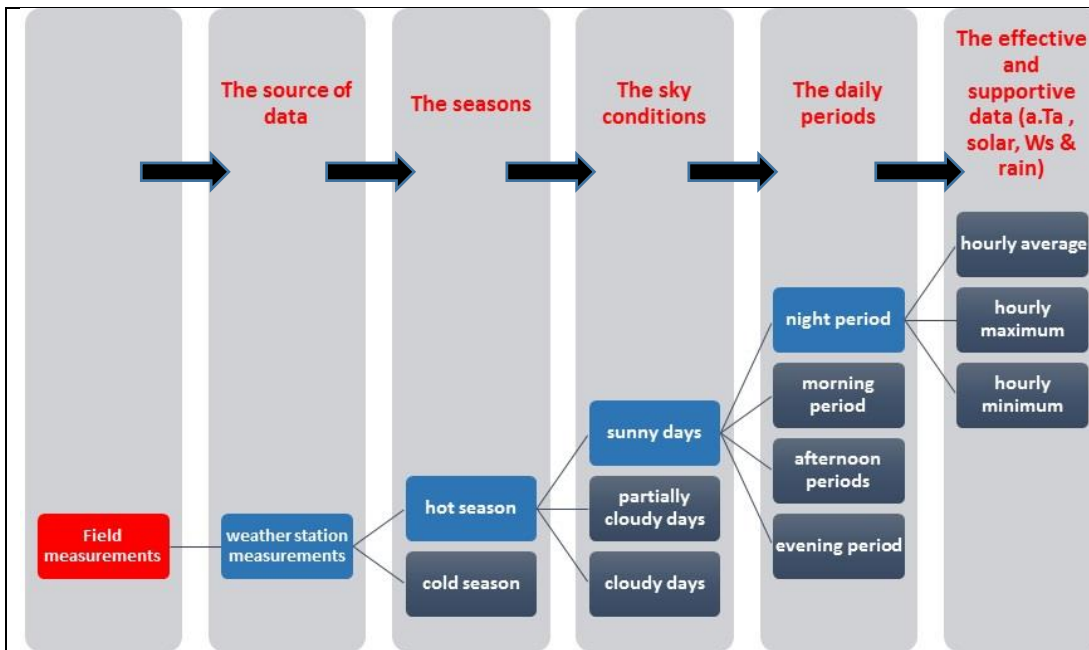


Figure 3.37 The sorting of weather station data

3.5.2 The statistical framework

This framework was designed to investigate the relationships between on-site air temperatures (T_a) as dependent variables and the urban morphological parameters

(UMP) and the climatic factors as independent variables. The climatic factors that will be inserted to the statistical models are the ambient air temperature (a.Ta) and the solar radiation (solar) These two factors represent the most important factors that affect air temperature (Erell et al. 2011; Olgyay et al. 2015).

The first part of the framework is shown by [Figure 3.38](#). Where a sample of the data was treated here as an example for the rest of the effective data.

The hourly datasets as (avg, max and min) for Ta as dependent variable and both a.Ta and solar as independent variables were used as inputs for the statistical analyses to produce the indicators of thermal microclimate as regression models that will be referred as Basic Models (B.M). These models (AVG, MAX and MIN) represent the relationship between on-site measured air temperature (Ta) and the climatic factors (a.Ta and solar) without the contribution of the urban morphological parameters (UMP).

These B.M were modified by adding one UMP each time as a third independent variable to produce the Modified Models (M.M). Therefore, the behaviour of air temperature (Ta) at the night period, as a sample, was expressed by three basics models (AVG, MAX and MIN). Each one of these models was modified ten times by add a one of the ten UMP. Consequently, the total number of statistical models for each period was thirty-three.

[Figure 3.39](#), as the second part of the statistical framework, shows the Basic Model of AVG and their related Modified Models as a sample. Three outputs of B.M were selected and compared with the same outputs from each one of the ten M.M. The outputs were R-Sq(adj), S and the regression coefficient signs of climatic factors (a.Ta and solar). R-Sq(adj), which represent the explanatory power of the statistical model and any increasing or decreasing trend after adding one of the UMP refers to its contribution in explain the air temperature differences throughout the specific daily period. In other words, the size effect of UMP on Ta can be deduced by the improvement rate that represents the difference between the two values of R-Sq(adj) in B.M and M.M $((R-Sq(adj) \text{ of M.M}) - (R-Sq(adj) \text{ of B.M}))$.

S is another gauge to verify the effect of UMP on Ta. The decreasing of S refers to an increase in the accuracy of the model after adding a UMP; S does not change unless the UMP causes a real effect on Ta behaviour. Therefore, the comparison between B.M and M.M regarding to S values was referred to support the result of R-Sq(adj).

The signs of the regression coefficients show the roles of (a.Ta, solar and UMP) in terms of increasing or decreasing the on-site air temperature (Ta) throughout the specific daily period.

The effect sizes and the roles of all UMP will be compared regarding the periods, sky condition and season to explore the most important UMP that effect the thermal microclimate of urban space.

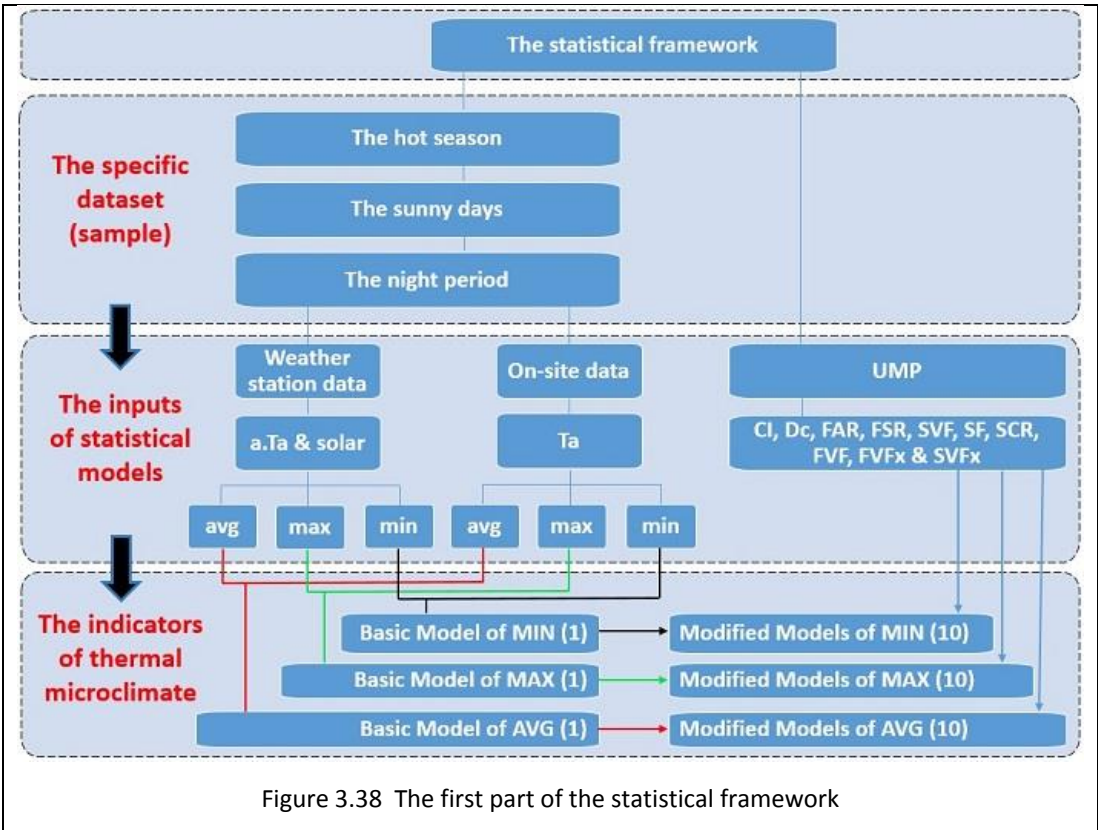


Figure 3.38 The first part of the statistical framework

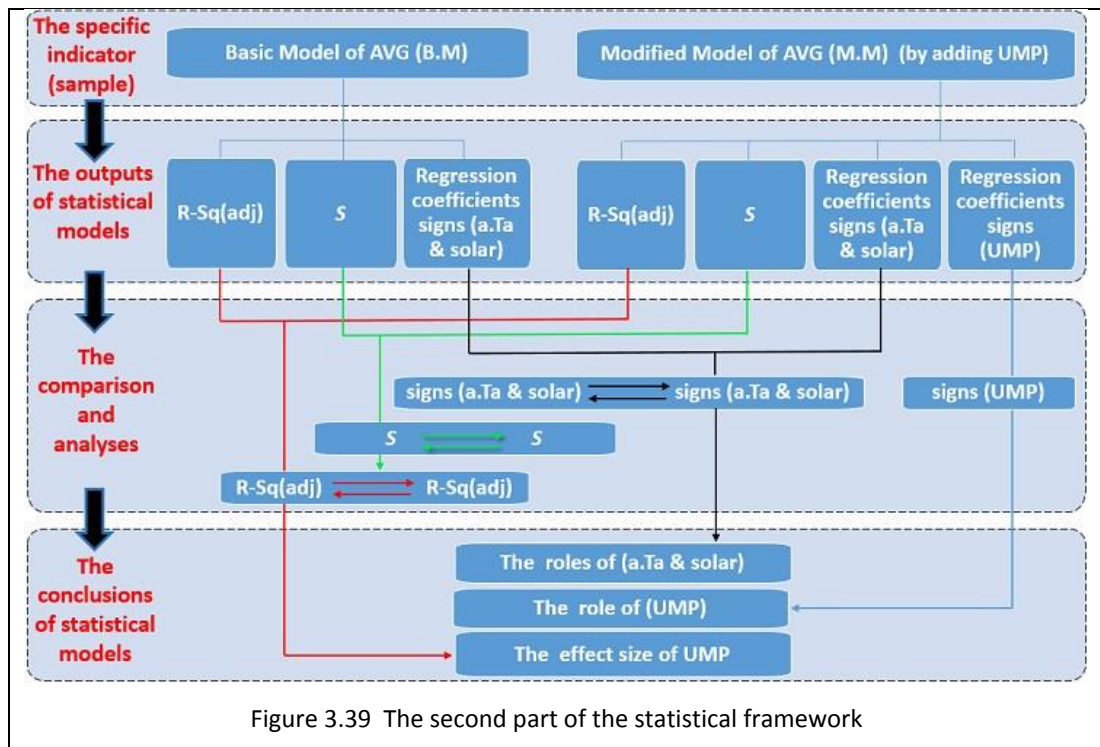


Figure 3.39 The second part of the statistical framework

3.6 Conclusion

The methodology of this research was described in detail throughout this chapter. To answer the research questions, a case study site was selected and analysed in terms of its ambient climatic circumstances and urban features to prepare the essential background for the comprehensive discussion at the end of the study and to determine the measurement periods.

Field measurements and urban morphological parameters are the twin key features of this methodology. The linkages between them represent the main motivation of this research. The field measurement tools in terms of their abilities, validity and protection were discussed before revealing their locations on the site. The measurement points were distributed around twelve locations that can be classified into four groups, and each one of these groups has properties that may differ from the other groups.

The influential urban area around the measurement points were determined according to the buffer zone concept that has been used frequently by other studies. Seven of the best-known urban morphological parameters were defined and their

calculation methods were illustrated for quantifying the morphology features that may affect the microclimate air temperature.

The strategy of data sorting for the field measurements and weather station data represents the first part of the statistical framework that was developed to understand the Interrelationships between air temperature and urban morphology features under the temperate maritime climate. The technical details of using multiple liner regression models and their outputs represent the second part of this frame.

This chapter can be considered as describing the first part of the methodology and tools that were utilized in this study. The next chapter represents the second part of the methodology, which involved the development of some novel urban morphology parameters which were developed exclusively for this research.

Chapter Four

4 The development of novel urban morphological parameters

4.1 Introduction

This chapter represents the second part of describing the methods and tools used for this study. It is devoted to presenting the methods that were developed by this research to measure the geometry of urban morphology to describe it numerically.

Much effort has been made in analysing and explaining the effects of urban areas on climate (Collier 2006). However, the knowledge gap about their relationship is still present and influenced by several difficulties such as: lack of long term observations, the variety of measurement types, climates, locations etc. (Arnfield 2003; Bottyan & Unger 2003; Unger 2009). Moreover, the nonlinearity, complexity and heterogeneity of urban climate systems (Arnfield 2003) may result in the scarcity of quantitative tools, methods and simulation models that help in climate sensitive design (Roth et al. 2011; Nakano 2015; Maoh & Kanaroglou 2009; Chen & Ng 2011). The aforementioned factors lead to the lack of communication between those interested in this field (planners, architects, climatologists ...) and therefore the knowledge of urban climate is not being translated efficiently into the design and construction processes of urban areas (Arnfield 2003; Chen & Ng 2011; Roth et al. 2011).

As a result, the thoughtful urban planning based on the climate has been explored weakly (Taesler 1991). Therefore, the necessity to quantify and assess the influential variables like urban morphology parameters by developing concepts, methods or tools is pivotal to revealing the governing inter-relationships of climatology and urban planning (Matzarakis 2015; Roth et al. 2011; Taesler 1991). Consequently, developing novel urban morphological parameters is a motivation and a part of the aim of this study. The methods to describe the urban morphology numerically can be a base to develop models that predict the effect of urban morphology on urban climate especially for imaginary scenarios by simulation or to analyse this relationship for real cases.

The development methodology of the novel parameters in this study depends on considering the cardinal directions (N, E, S & W) as a part of the parameter itself rather than dealing with the direction concept as an independent variable for the urban morphology. The directions and the orientations have attracted much attention at the urban scale and the individual building scale (Taleghani et al. 2015; Silva 2017; Shishegar 2013; Lau et al. 2014; Krüger et al. 2010; De & Mukherjee 2017; Chatzidimitriou & Yannas 2017; Cao et al. 2015; Andreou 2014; Ali-Toudert & Mayer 2006; Ali-Toudert & Mayer 2007).

Most of above mentioned studies have referred to the effective role of the direction concept in understanding the relationship between the urban morphology and different matters like microclimate factors, mutual shading, thermal comfort, solar energy and energy consumption. However, they focused mainly on urban canyons, where directivity is the main feature of the streets, but not for the node spaces such as intersections, squares and urban courtyards. Even the few studies that tried to study these non-directional spaces in relation to the concept of cardinal direction have dealt with them like urban canyons through a number of rectangular alternatives in varying proportions (Rodríguez-Algeciras et al. 2018; Taleghani, Tenpierik & van den Dobbelsteen 2014; Taleghani, Tenpierik, van den Dobbelsteen, et al. 2014).

Based on what was previously mentioned, this research assumes that the concept of directions can be a cornerstone to the development of novel urban morphological parameters. This can be effective in understanding the urban morphology – urban microclimate relationships by explaining the variation of microclimatic factors under the effect of urban morphology in relation to the cardinal directions.

The next sections will show some urban parameters that were developed by this study and depending on this methodology.

4.2 The Partial Sky View Factor (SVF_x)

The sky view factor (SVF) and orientation of urban spaces have been investigated extensively but separately from each other in many studies. However, some researches have discussed these relationships regarding urban canyons. Based on field measurements at different periods of the year in Curitiba city, Brazil, it has been suggested that the thermal conditions at a site cannot be predicted accurately by the SVF alone - a combined analysis of the SVF, the solar trajectory and canyons orientations can yield more precise relationships with air temperature, especially for streets with asymmetrical sides (Krüger et al. 2011). Another study has been conducted by utilizing the hot season data of Lisbon, Spain (Mediterranean climate) to identify and evaluate the design priorities of thermal-sensitive urban space by simulation of some bioclimatic variables for theoretical alternatives of urban canyons. The variation of these variables against the morphological features of these canyons were analysed depending on five alternatives of aspect ratios, two orientations of each canyon (N-S and E-W) and SVF that measured in the middle and on the two sides of each alternative for each orientation. This combination can submit creative design solutions to take in to account the connections between the urban structure and the urban bio-climate (Nouri et al. 2017).

These studies have revealed the potential of relationships between SVF and orientations in terms of understanding and analysing the urban microclimate. However, there is no clear mechanism to apply this vision in non-directional spaces like squares or urban courtyards. Therefore, the partial sky view factor (SVF_x) was developed by this study as an initial step to filling this gap.

4.2.1 The basic concept of SVF_x

The concept of SVF_x can be illustrated by [Figure 4.1](#). The domed form represents the sky hemisphere where the centre of dome is the location of measurement point, the black areas represent the projection of the neighbouring buildings around that point whilst the blue area of the dome is the visible sky from that location. The sky hemisphere is subdivided diagonally into four quadrants that follow the four cardinal

directions (N, E, S and W) as shown by the partitions on the dome, where each subdivision represents the openness degree to the sky on that direction. Therefore, there are four values of SVF_x. SVF_n represent the openness degree on the North direction and so on for SVF_e, SVF_s and SVF_w. Each subdivision can be calculated as a ratio between the area of open sky on the quadrant and the total area of the sky hemisphere according to Equation (4.1).

$$SVF_x = \frac{\text{the area of sky on the selected quadrant}}{\text{the total area of hemisphere}} \tag{4.1}$$

Hence, the sky view factor can be calculated as the summation of the four values of SVF_x or it can be calculated as a ratio between the total area of visible sky to the total area of the sky hemisphere according to the following formula (Al-Sudani et al. 2017).

$$SVF = \frac{\text{the total area of visible sky}}{\text{the total area of hemisphere}} \tag{4.2}$$

The concept of SVF_x can be applied on fisheye lens images as shown in Figure 4.2. The red dotted circle represents the area of the plain projection so the SVF can be calculated according the following formula (Debbage, 2013; Al-sudani and Sharples, 2016).

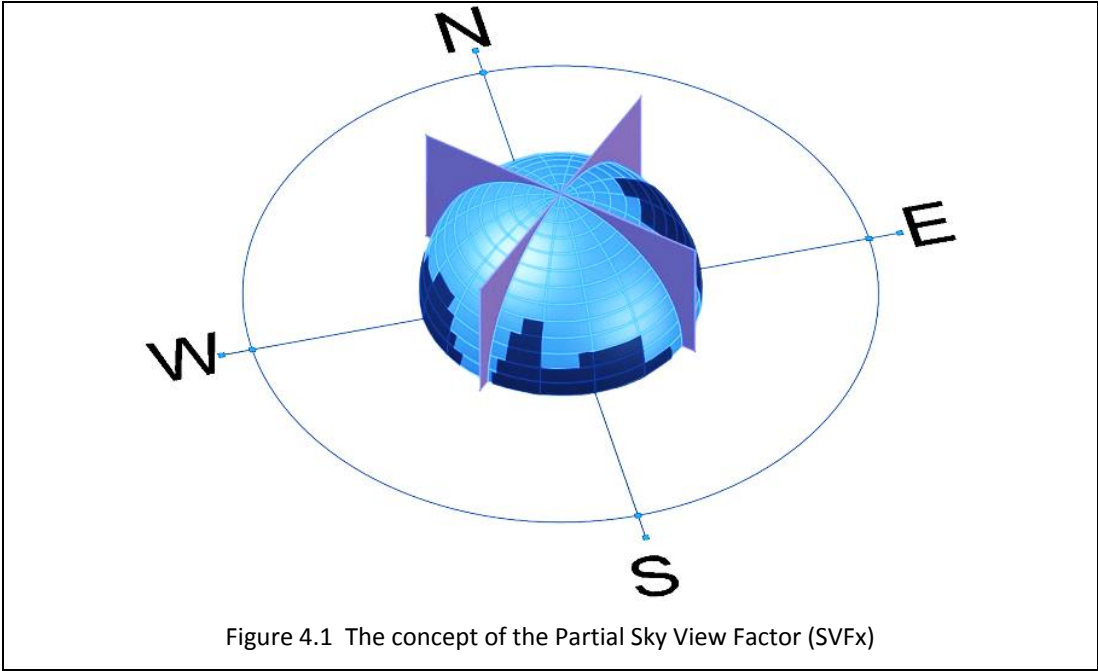
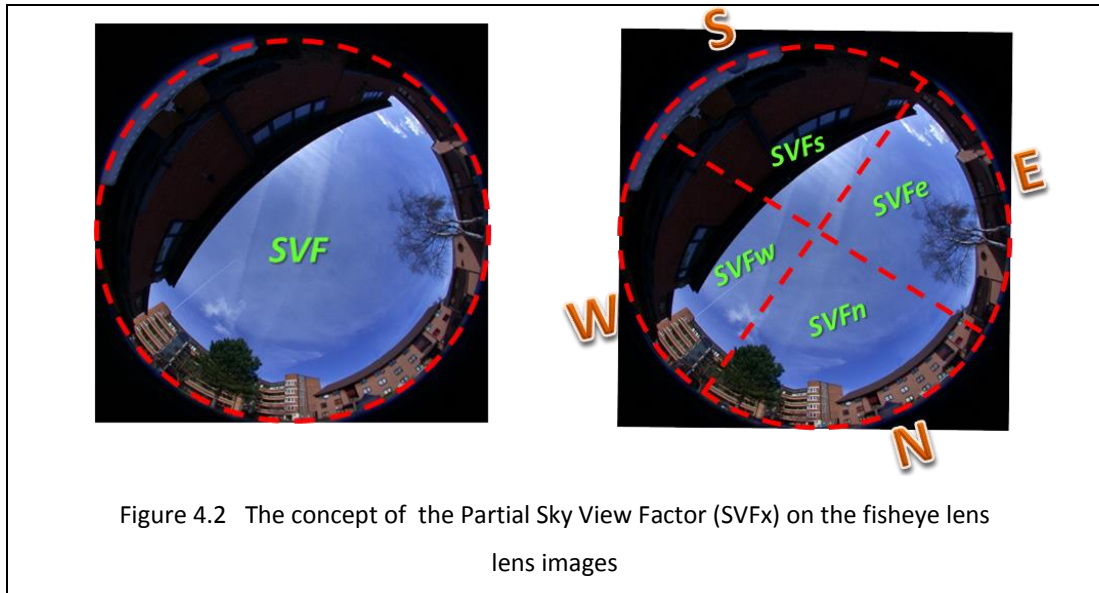


Figure 4.1 The concept of the Partial Sky View Factor (SVF_x)



What has been mentioned above illustrated the calculation method of SVF_x but did not explain how to apply this method and extract the results from both fisheye lens lens images and 3D models. This will be the task of the following two sections.

4.2.2 The calculation of SVF_x from the fisheye lens lens images

Although Photoshop software has been used extensively regarding imaging processes to measure the area of leafs or plant canopies in the plant sciences (Liu et al. 2013; Macfarlane et al. 2007) and to measure the tissue areas of biopsy in the biological sciences (Dahab et al. 2004), the usage of this software for analysis of fisheye lens images and calculate SVF in urban studies is rare. Therefore, this study is going to reveal its abilities to calculate SVF and SVF_x from fisheye lens images.

After inserting the fisheye lens image into Photoshop CS5, the ruler tool can be used to measure the diameter of image that should be uniformed for all other images. The diameter is necessary to define the circular border of fisheye lens image by paths option from ellipse tool. This border should be edited by a right click on the computer mouse and then choosing option (make selection) to determine the area inside the border as an active area as shown by [Figure 4.3](#).

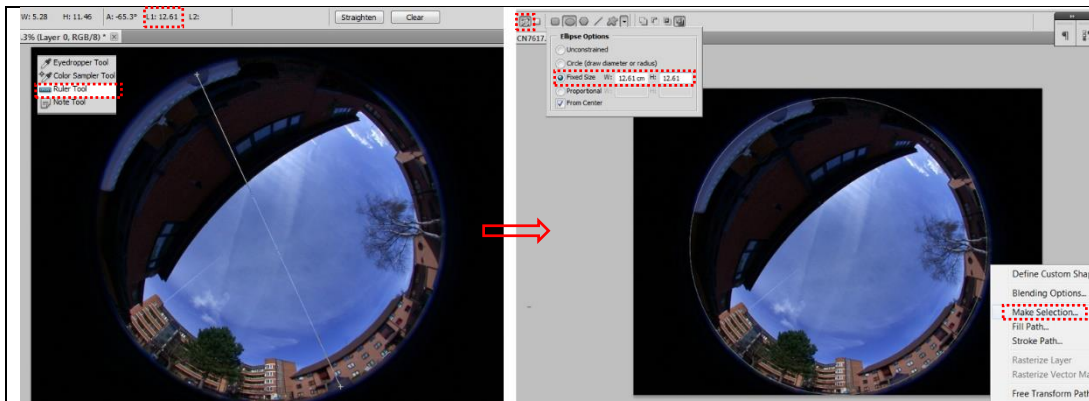


Figure 4.3 Determining the diameter and border of the fisheye lens image

Later, the rest of the image out of circular selection area must be deleted to prepare to trim the image by choosing the crop option from the Image list as shown in **Figure 4.4**. The circular selection area should be saved by choosing the Save selection option from the Select list. This area represents the total area of circular plain projection of the fisheye lens image.

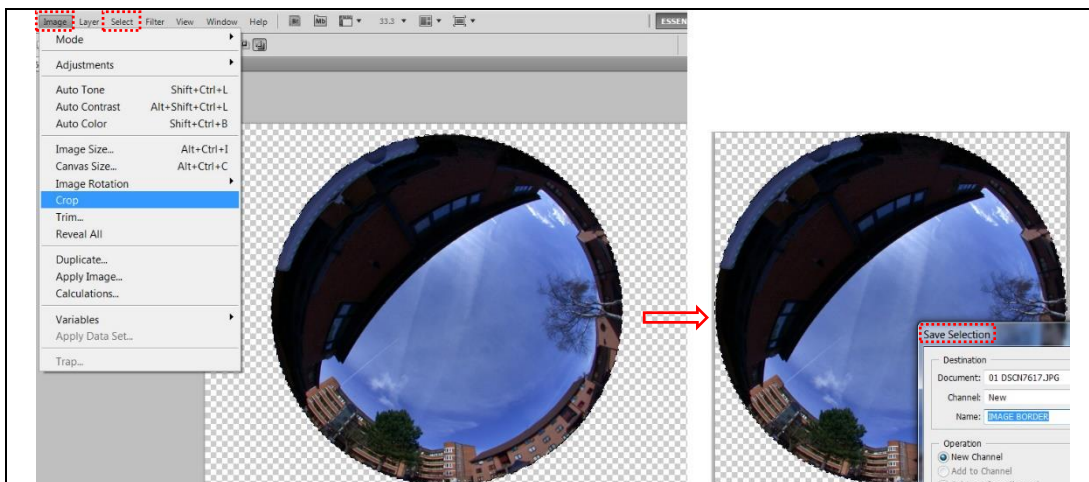
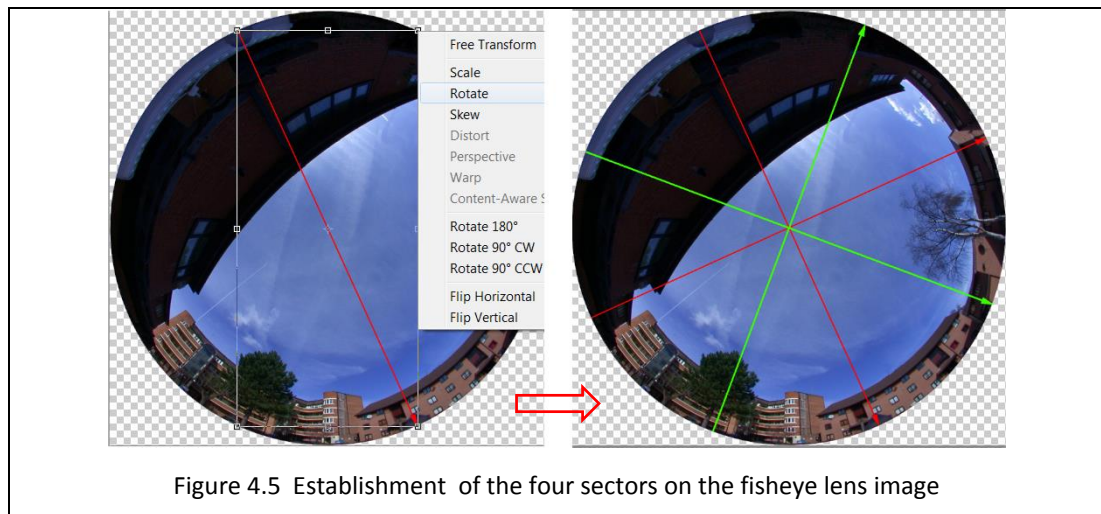


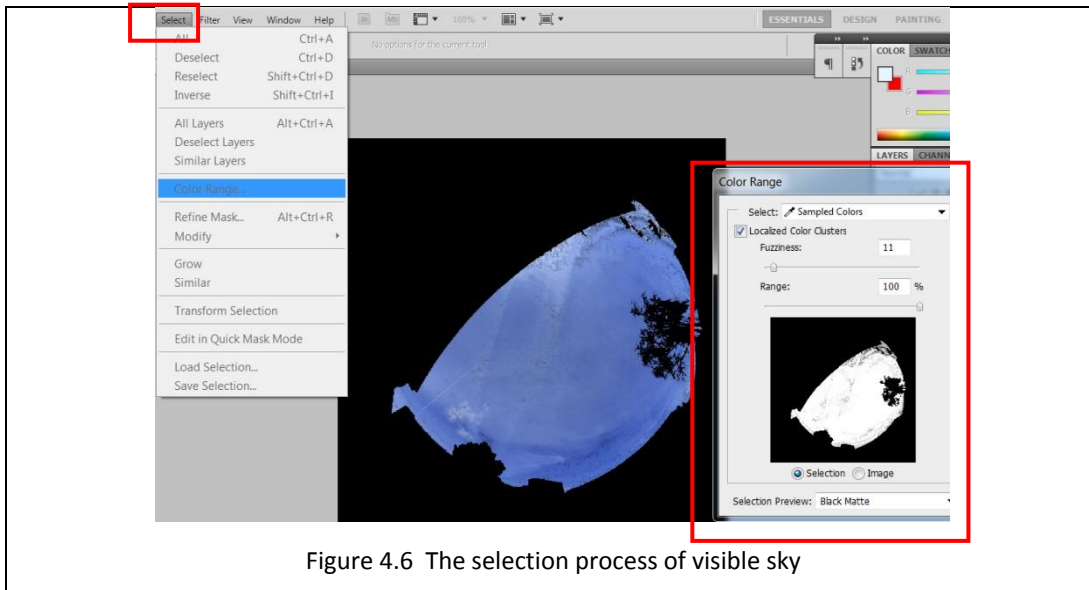
Figure 4.4 Cropping and saving of the circular projection of the fisheye lens image

By using the Line tool, the N-S direction can be determined depending on the markers in the image, while the E-W direction can be created by copy and rotate for the arrow of N-S direction. To define the four quadrants on the image (green lines), it can be copied and rotated by 45° for the red arrows that represent the cardinal directions as shown by **Figure 4.5**. The appearance of the red and green diameters can be

controlled by activation or deactivation of their layers and for the next step these diameters should be deactivated.



The next step is devoted to determining the border of visible sky on the image where many difficulties can be faced due to the presence of clouds, trees and the reflection of the sky on the building windows. Colour range option from the Select list was utilized according to the settings shown by [Figure 4.6](#). The Eyedropper tool from the colour range box was used to select an area based on the colour value, where the same value will be selected automatically in all images. To add more colour values, the shift key on the keyboard must be held continuously through the selection process. Some areas may need to be selected or deselected manually by different tools such as the magic wand windows. The increasing of image resolution can solve a part of this problem, especially for tree selection. After finishing the selection process of the sky, the selection area should be saved by using the Save selection option from the Select list to be used later.

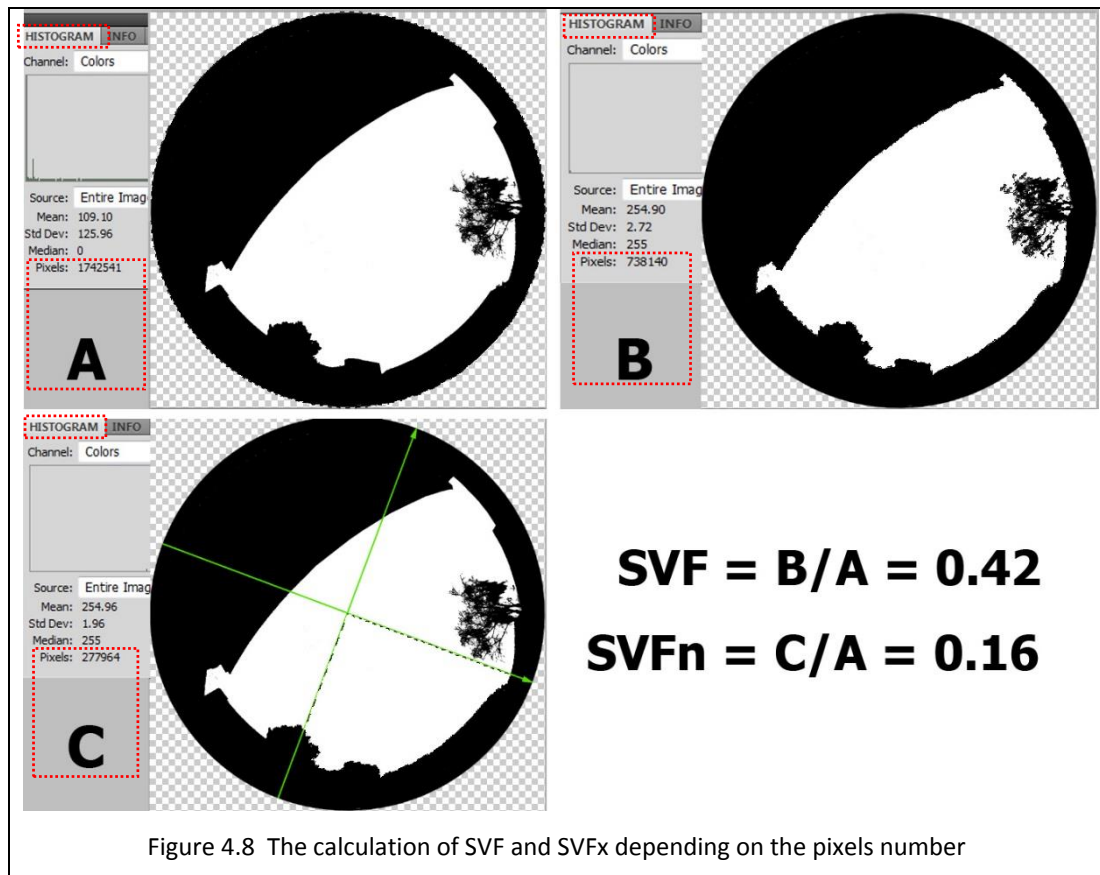


Both selection areas that were saved before can be loaded by the Load Selection option at Select list and then their intersection can be used to produce the black-white fisheye lens image by using the paint bucket tool, as shown by Figure 4.7.



All pixels in the fisheye lens image are equal in size, so the number of pixels can represent the area of selected part versus the area of other parts. The number of pixels inside the selection area can be calculated by the histogram option at the Window list. Figure 4.8 shows the pixels number for the circular selection area (A), visible sky area (B) and, in addition to that, the visible sky area on the Northern quadrant (C) can be selected by the magic wand tool after activation the layer of green diameters. The sky view factor can be calculated as the ratio of B to A. while

the partial sky view factor for the Northern quadrant (SVF_n) as a sample for the other sectors can be calculated as a ratio of C to A.



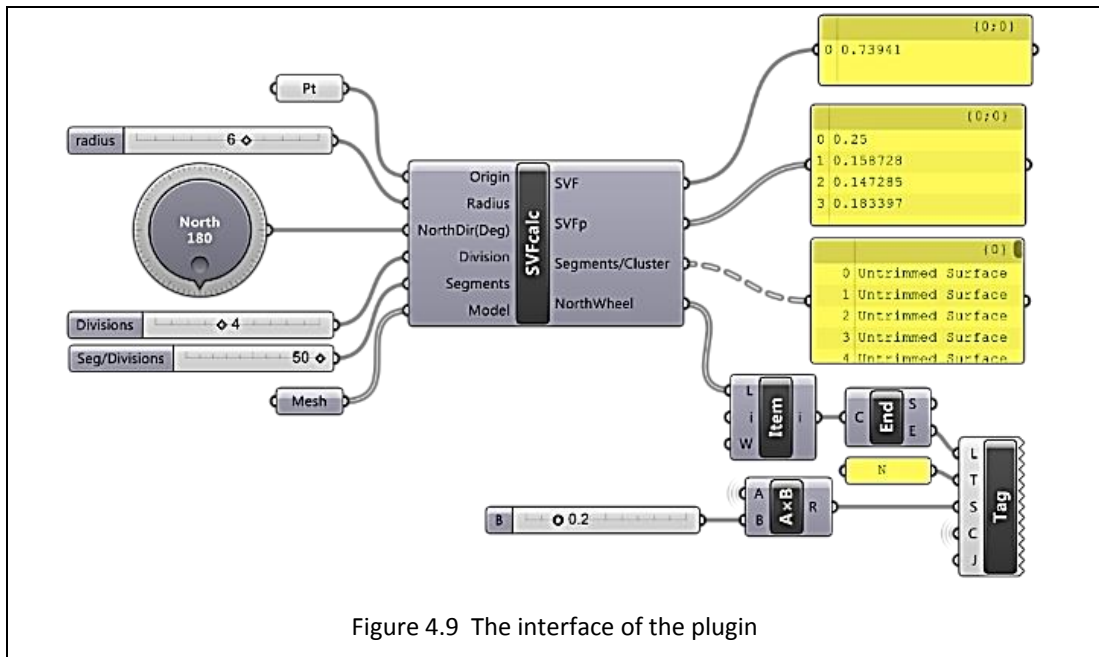
This method to calculate SVF_n depends on the fisheye lens images that can be applied for the real urban fabric, especially with existing trees. The accuracy of calculating SVF and SVF_n by using Photoshop software depends on the resolution of the fisheye lens image, the condition of sky, the existence of trees and the density of leaves as well as the professionalism of the Photoshop user. Also, AutoCAD software can be used to calculate SVF_n from the fisheye lens image. For more information refer to Al-sudani and Sharples, (2016). Although this technique by AutoCAD is not affected by sky condition and does not need high professionalism in using the software, it needs to deal in detail and completely manually with the skyline of buildings and trees. It is thus a time-consuming technique in comparison to the Photoshop technique.

4.2.3 The calculation of SVFx from the three dimensional models

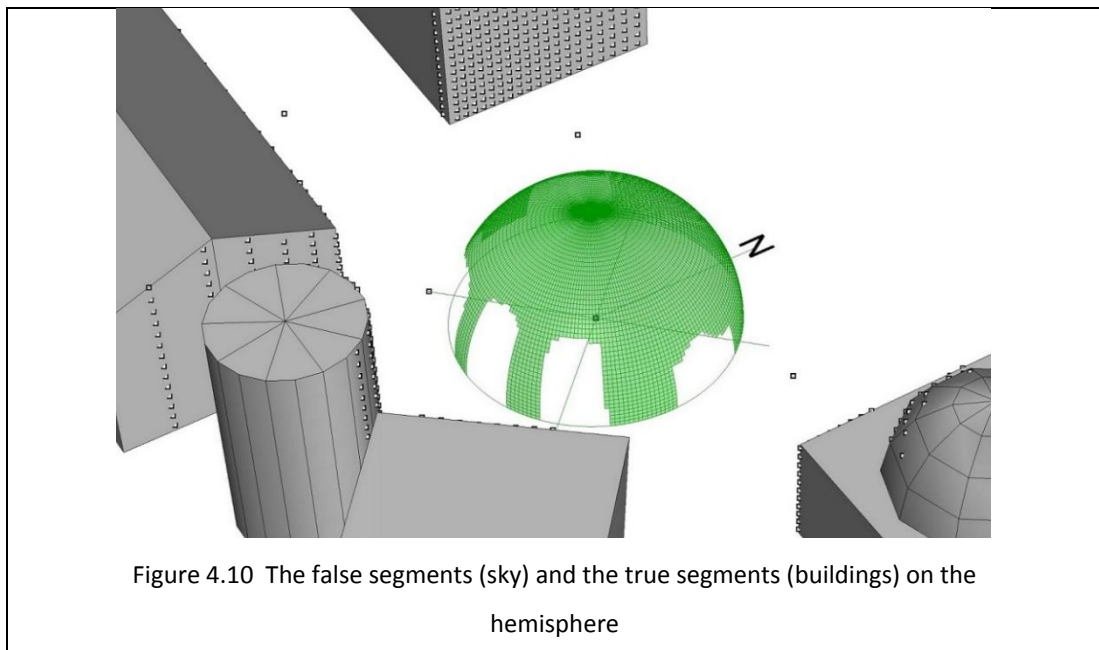
The 3D computer model is widespread to represent the imaginary or realistic urban fabric in the urban environmental studies. For that reason, this study developed a computer software plugin to quantify the partial sky view factor (SVFx) relying on the hemispheric projection of 3D model by using the graphical algorithm editor (Grasshopper) that integrates with the Rhino 5 modelling tool. This plugin can calculate more than four sectors on the sky hemisphere and it can deal with an unlimited number of measurement points simultaneously within a simulated urban fabric. Therefore, it can save time compared to the Photoshop - fisheye lens image method. However, the latter approach can deal with trees in a more convincing way compared to this plugin.

Although two different approaches have been used to develop this plugin, one of them was used to calculate SVFx in this study and will be revealed soon. The other approach, and more details about the current approach, were displayed in a separate study for the researcher (Al-Sudani et al. 2017).

This plugin needs six inputs according to [Figure 4.9](#). These inputs are the measurement point(s) (Pt), the radius of sky hemisphere (radius), the Northern direction of the urban site that determined in degrees clockwise from Y axis of the world coordinate system in Rhino 5 (North), the number of sky sectors that can be more or less than four (Divisions), the number of vertical and horizontal segments in a one quadrant of sky hemisphere (Seg/ Divisions) and the 3D model of the urban site (Mesh). The increasing of (Seg/ Divisions) will increase the accuracy of results but also the process time. The latter will also be longer by processing many points instead of one measurement point. The outputs of this plugin are SVF, SVFx and a 3D model of hemispheric projection that show the diameters that define visually the number of sectors and their locations in addition the north sign.



This plugin calculates the value of SVF by an algorithm that generate rays from the measurement point at the centre of the segmented hemisphere where each beam penetrates the centre of one segment on the hemisphere. Once the beam hits any surface of the three-dimensional model then the segment of the hemisphere that was penetrated by the beam will have a (true) value. SVF represents the ratio between the total area of false segments that are open to the sky and the total area of the hemisphere, as shown by [Figure 4.10](#).



The accuracy is affected by the number of segments per sector, where the number of vertical segments equals the number of horizontal segments for each quadrant. The values of SVF_x is ordered clockwise from the north direction then then can be taken and processed by other softwares like Minitab or excel. **Figure 4.11** shows the algorithm workflow of the SVF_x plugin in five phases. Phase 1 is devoted to drawing a sphere with its centre at the measuring point while its radius and north direction are determined on the interface screen. The second phase processes the sphere to divide it horizontally to get the hemisphere that can be divided into quadrants and segments according to the inputs. In the third phase, the rays are generated from the centre of the hemisphere and the kind of segments (true or false) will be determined. SVF and SVF_x are calculated and listed according to phase four while the graphical representation of the hemisphere with quadrants and north direction sign is the results of phase five.

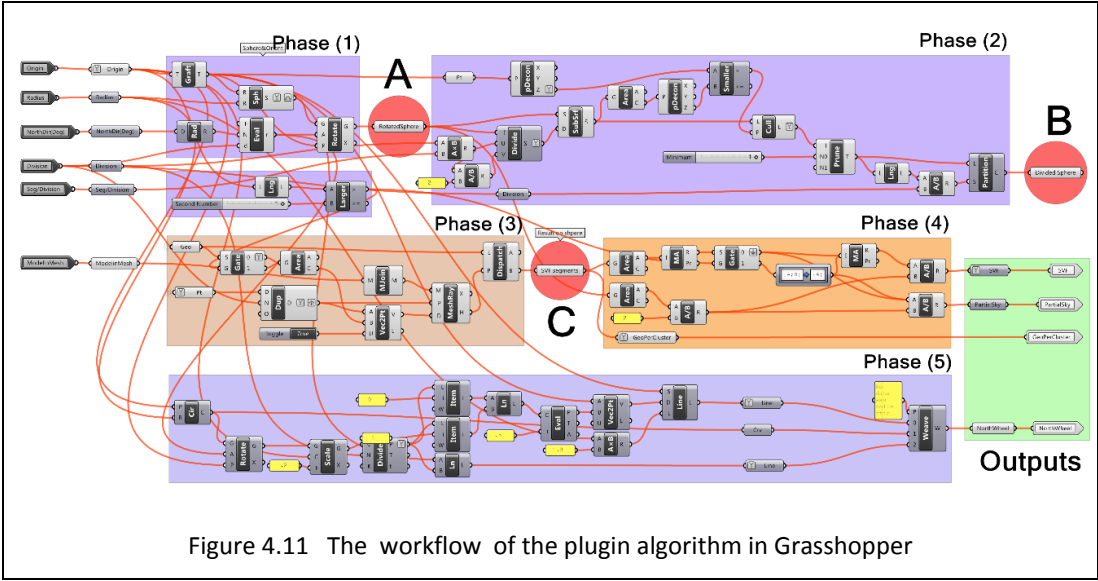
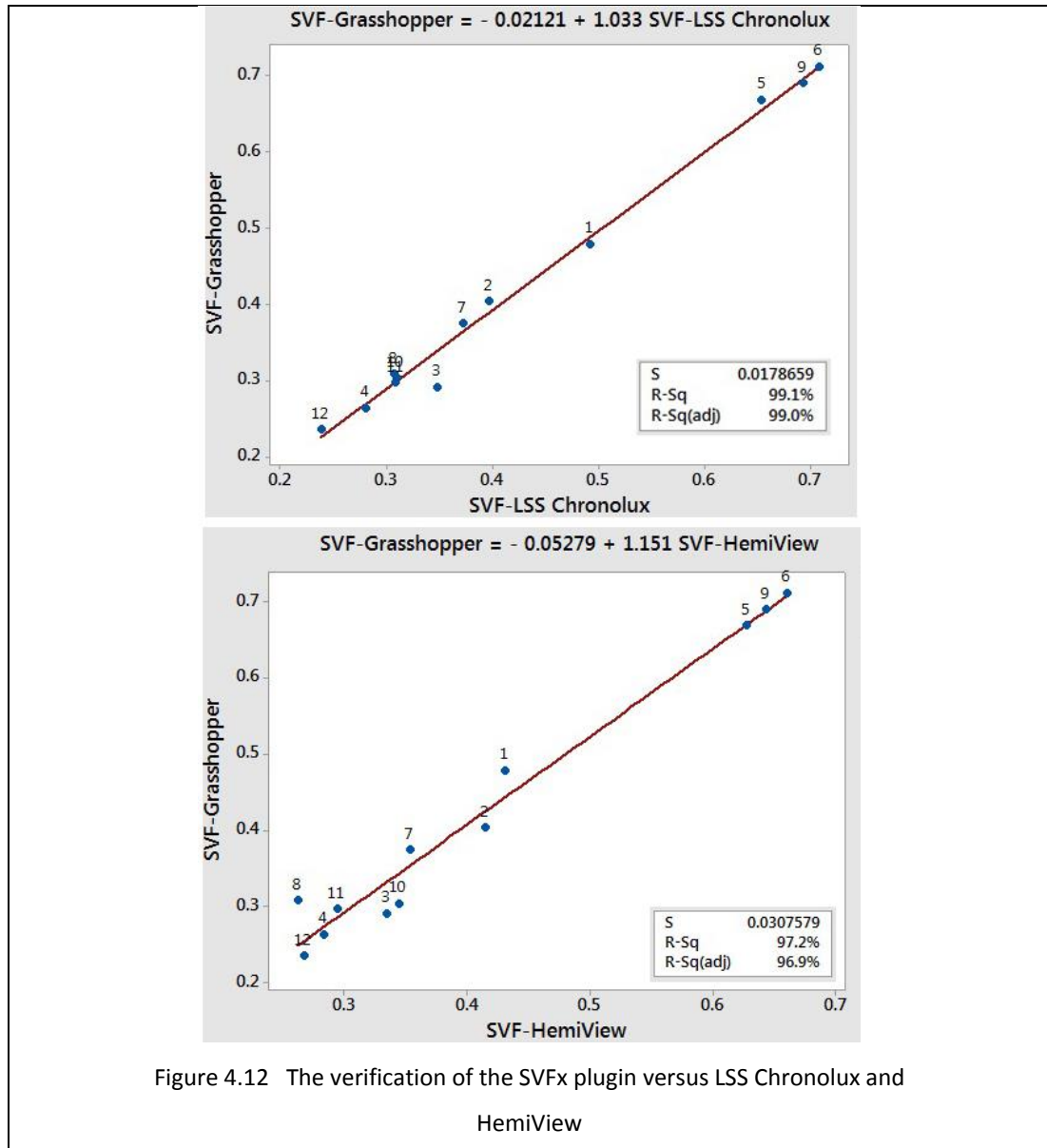


Figure 4.11 The workflow of the plugin algorithm in Grasshopper

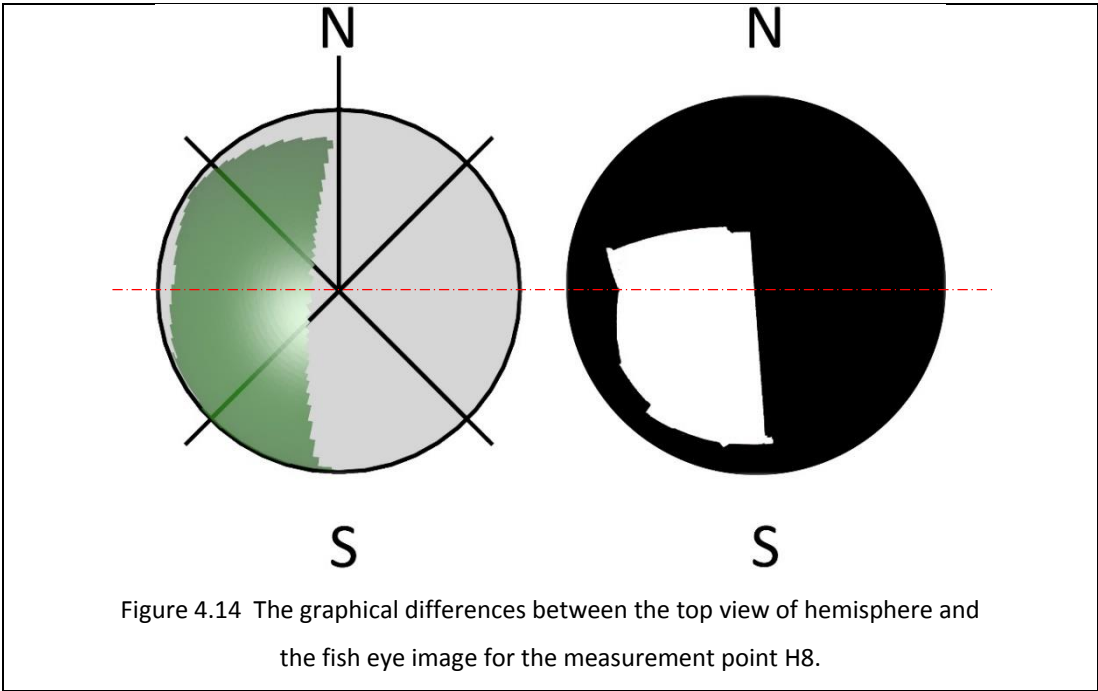
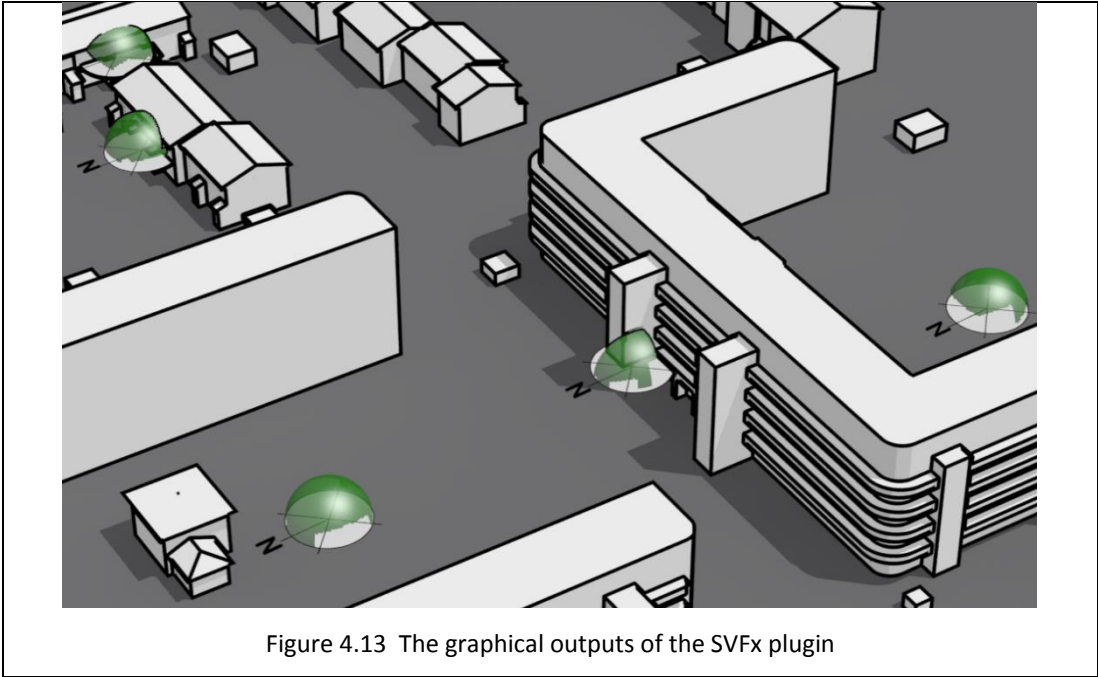
The validity of the developed SVF_x plugin were verified versus LSS Chronolux regarding SVF values for the twelve measurement points of the case study. LSS Chronolux is a plugin that compatible with Sketch Up 2013 and it has been utilized previously to calculate SVF from 3D models (Paramita et al. 2016; Zwolinski & Jarzowski 2015). In addition, the SVF_x plugin was verified against the results from HemiView that were used to calculate SVF from the fisheye lens images as shown in **Figure 4.12**. The Coefficient of Determination (R^2) between LSS Chronolux and SVF_x

plugin was 99.1%. However, this ratio fell to 97.2% with HemiView due to the differences in the accuracy of the 3D model compared to the real case besides the effect of trees existence in the fisheye lens images.



The graphical outputs of the plugin are revealed in [Figure 4.13](#), where the hemispheres located at the same height as the sensors and the green shell represents the visible sky. However, the graphical comparison cannot be held for the same location between the outputs of the plugin versus the outputs of the Photoshop method or the HemiView software, as shown by [Figure 4.14](#) which reveals different area for the visible sky in location H8 because of the area that is represent by the

fisheye lens image is reduced. The fisheye lens image displays the real sky hemisphere as a 2D circular image and this transformation entails changing the surface area from $(2\pi r^2)$ for the hemisphere into (πr^2) for the 2D image, where r is the radius. Consequently, each pixel in the image represents an area bigger than what is visible in the image due to the ratio of image and hemisphere areas being 2 (Cheung et al. 2016).



4.3 The Façade View Factor (FV_{Fx})

The façade as a conductive cortex between two environments simultaneously (building space and an urban space) has been studied extensively in relation to the envelope of building in terms of thermal comfort (Hwang & Shu 2011), daylighting (Vanhoutteghem et al. 2015), solar radiation levels (Flores et al. 2015), energy consumption, heat transfer and renewable energy (Agathokleous & Kalogirou 2016). In return, façade as the envelope of the urban space has not had the same focus. The main reason behind this may be the lack of computational resources that can help to explain climatic processes such as radiation exchange in urban areas (Robinson 2006).

However, some attempts are worthy of attention, especially in developing the computer models; for example, ENVI-met for the simulation of surface-plant-air interactions in urban environments (Ozkeresteci et al. 2003). On the same line, the potential of façades regarding the utilization of renewable energy technics on urban scale has been revealed through investigating the availability of solar and daylight for hypothetical urban forms in Switzerland by developing a computer tool, based on the RADIANCE software base, that deals accurately with variables like luminance distribution and multiple reflections between buildings (Compagnon 2004). Also, STEVE is an assessment tool to reveal the effect of urban planning on air temperature, under the climate of Singapore that depends on statistical models, including climatic and morphological predictors. Where the total wall surface area of the buildings around a measure point within the radius of influence area 50m is a one of these predictors (Jusuf & Hien 2009; Hien et al. 2012).

Instead of utilizing the area of façade directly, the Urban Weather Generator (UWG) model, that represent a plugin for Rhino software, uses a different approach of calculating the ratio of façade area to site area as a variable to calculate the air temperatures of an urban space depending on data from outside a city weather station to estimate the urban heat island influence on building energy (Nakano, Bueno, Norford & C. F. Reinhart 2015), Complexity is the other name of this ratio (Chatzipoulka et al. 2016). The approach of using ratio instead of pure façade area does appear in other studies, like the ratio of wall area-to-volume (Steadman et al. 2009) and the envelope area to volume ratio (Ferrante 2016) that can be mentioned

as form factor (Fernández de Trocóniz y Revuelta and Gálvez Huerta, 2012) or Compactness (Chatzipoulka et al. 2016). These tools explore the comprehensive influence of all urban components which interact simultaneously with the climatic factors. Therefore, the role of a determined urban component, like a building's façade, may need more study to evaluate it. As a result, further research is required to fill this gap and make the matter more calculable.

Furthermore, the concept of improving the microclimate of urban spaces by using façades has been discussed from several perspectives. For example, using a low cost strategy that is represented by coloured facades to create and accelerate the air flow in urban settings to reduce the impact of hot days and their low wind speeds on Netherlands urban areas in climate change era as a new climate adaptation measure (Kleerekoper et al. 2015). Green façades have been utilized as a countermeasure against the urban heat stress in German by testing the mean radiant temperature (T_{mrt}) in front of a façade that had two halves (vegetated and bare); the results in this case showed a limited reduction of (T_{mrt}) near the green side (Jänicke et al. 2015). Façade materials have been investigated, and the results of a study of common façade materials in Malaysia revealed that the urban microclimate witnessed amelioration by using white concrete tiles and granite for external walls versus brick and concrete, which showed a higher capability to absorb and store heat (Din *et al.*, 2012). Modern materials have also been researched, such as the retro-reflective (RR) materials that reflect the solar radiation back to the incoming direction of the source instead of reflecting onto roads. This creates a mitigation of UHI phenomenon by reducing the absorption of solar radiation and increasing the albedo of urban canyons (Yuan et al. 2016).

Although the façade represents the envelope of the urban space, it is difficult to find a method or parameter for gathering its relative variables like areas, locations and directions in one relationship to express the morphology of that space, where the microclimate of the urban space is affected by these relationship in different ways.

4.3.1 The basic concept of FVFX

It is a novel method to express a visible urban scene in a 360° view around a monitoring point as a numerical value through calculating a morphological-spatial relationship between building facades and the watching point; this value may be considered as a parameter of urban space configuration.

The graphical blueprint of the calculation method of FVFX is illustrated by Figure 4.15, where the area of façade's surface (fa), the horizontal view angle (θ) and the perimeter length of an imaginary triangle (tp) between the façade and the observation point are the variables of the method. In general, the triangle layout adapts to any change in the façade's width, point location and façade's position through altering the horizontal view angle, the perimeter length or both. The façade area adapts to the changes of its dimensions.

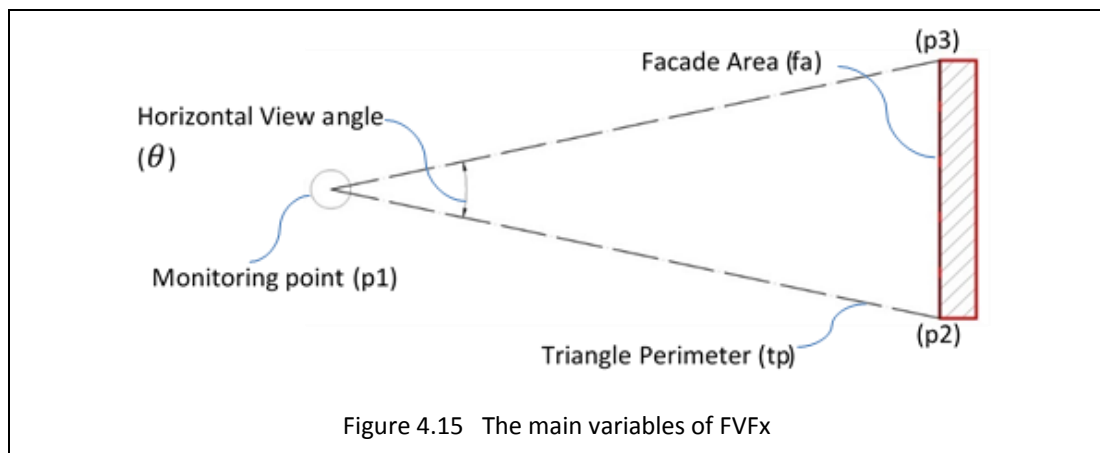


Figure 4.15 The main variables of FVFX

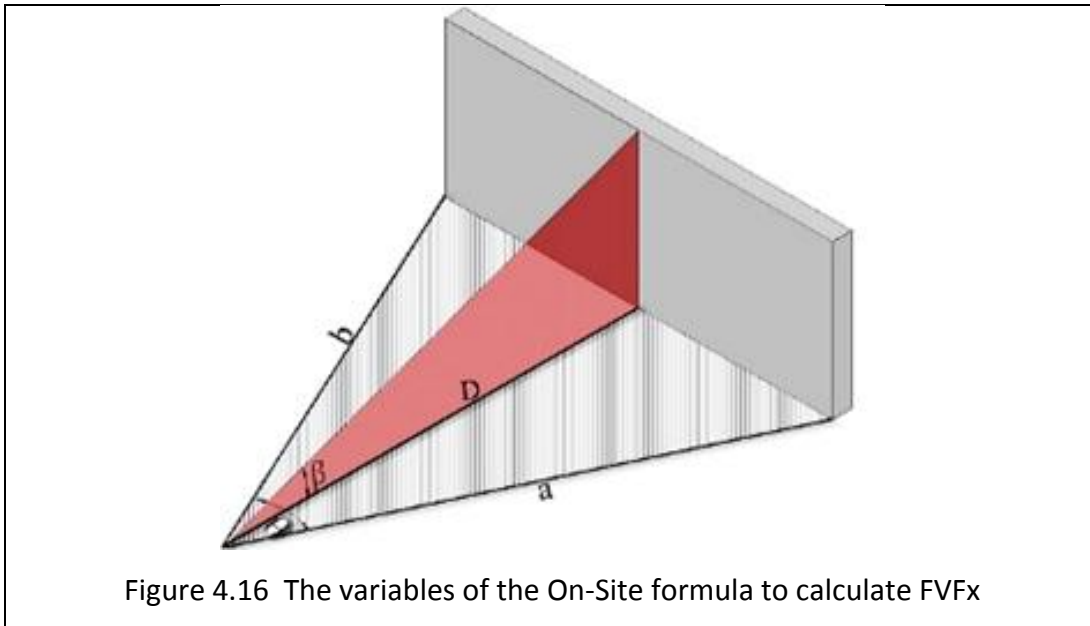
FVFX is a one value for a one facade's surface that can be seen from the measurement point. It can be calculated by two formulas. In-Design formula which is used if the variables are available or they can be extracted from documented drawings.

$$FVFX = \left(\frac{\text{Facade Area (fa)}}{\text{Triangle Perimeter (tp)}} \right) * \text{Horizontal view angle } (\theta) \quad (4.5)$$

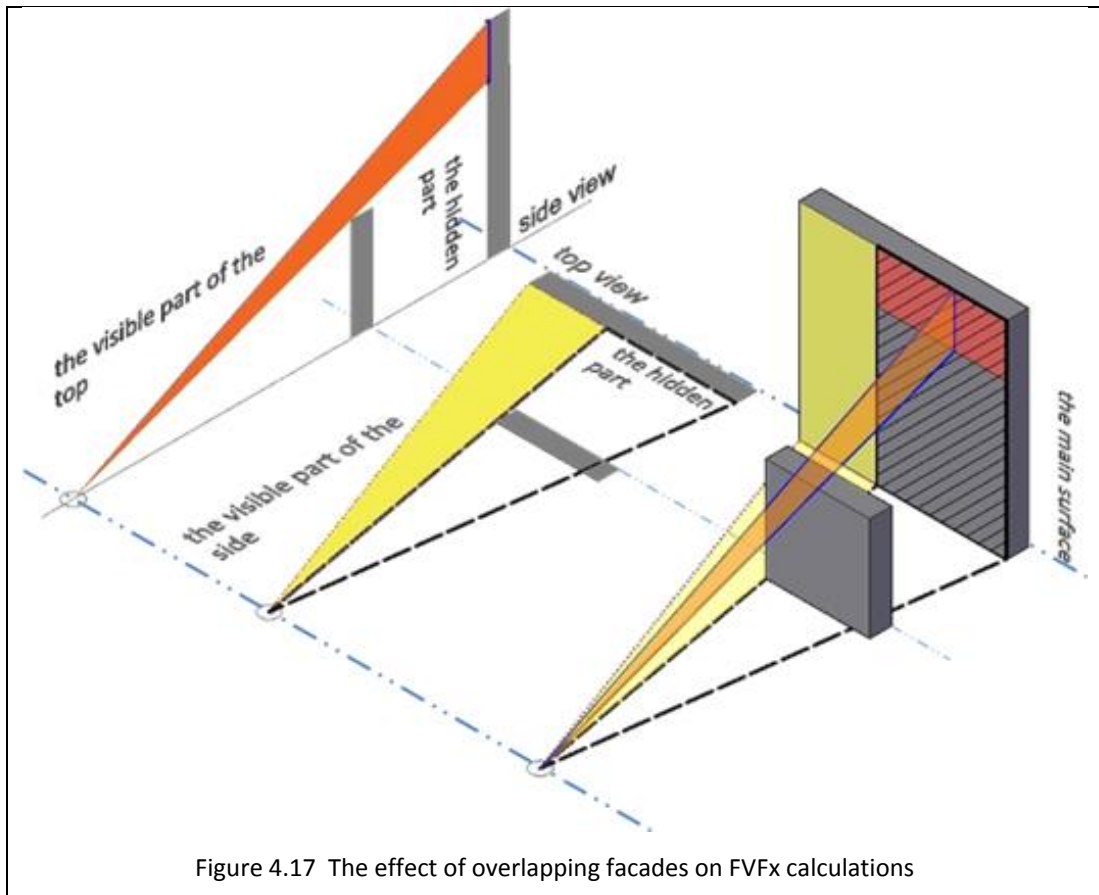
On the other hand, when the variables must be measured on site in the real urban area by surveying devices like total station, then On-Site formula can be used.

$$FVF_x = \left[\frac{(\tan \beta * D) * \sqrt{(a^2 + b^2 - 2ab\cos\theta)}}{(a + b + \sqrt{(a^2 + b^2 - 2ab\cos\theta)})} \right] * \theta \quad (4.6)$$

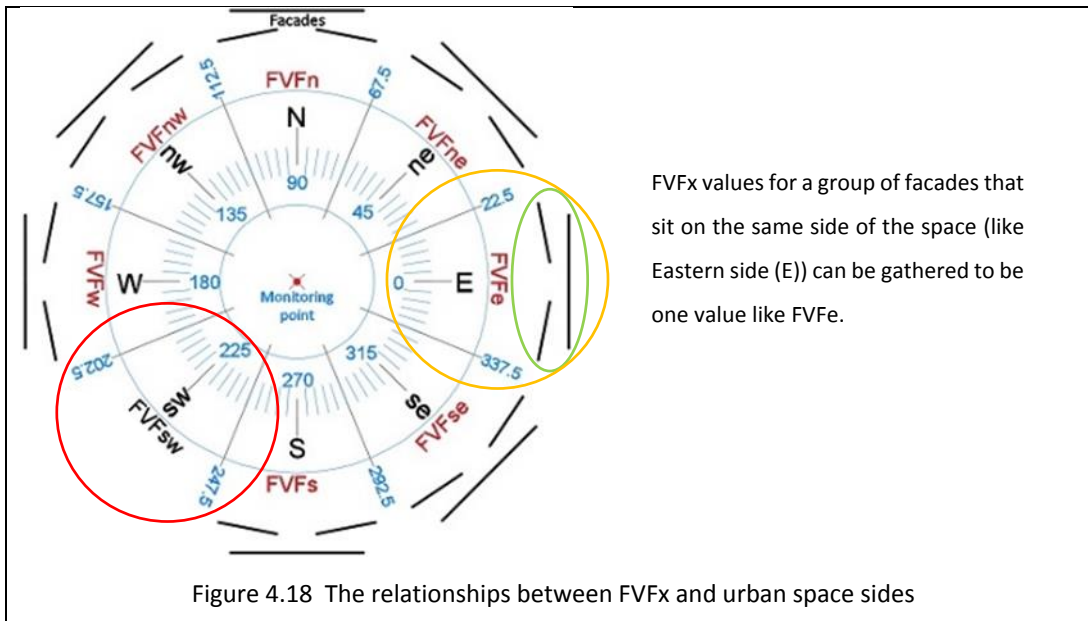
Where (a, b) represent the lengths of triangle segments, (D) is the distance between the monitoring point and the middle of the façade width. It is not necessary to make D vertically on the façade. (θ) is the horizontal view angle and (β) is the vertical exposure angle as shown by [Figure 4.16](#).



There are many complexities that may be raised against this method, like how to calculate FVFx for the overlapping facades. FVFx is calculated for the façades or their parts that have eye contact with the vantage point. Some façades or their parts may stay out of the view field as a result of their locations relative to the measurement point location. FVFx can be calculated for the visible top parts of buildings by subtracting the value FVFx for hidden surface from the value FVFx of the main surface. As for the visible side parts of buildings, FVFx is calculated separately as an independent façade as shown by [Figure 4.17](#).

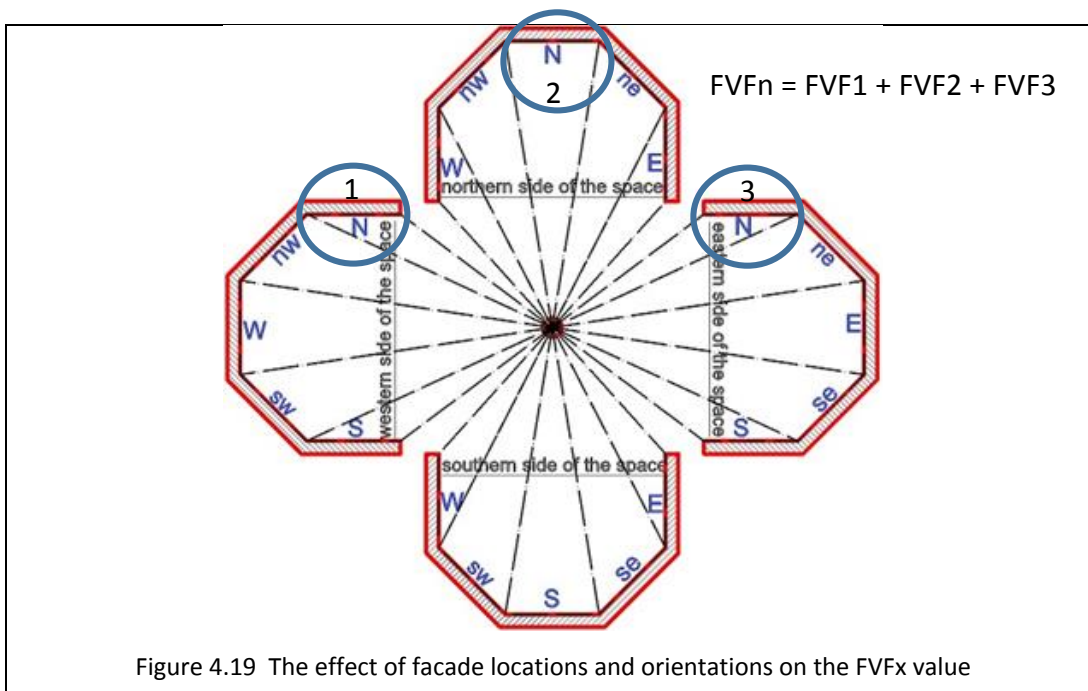


Another matter is how to deal with many façades surrounding the same measurement point, as shown in [Figure 4.18](#). Essentially, there are eight directions around the measurement point: four cardinal directions (N, E, S & W) and four secondary directions (NE, SE, SW & NW). Each group of façades that faces the same direction, and which do not rotate more than 22.5° on each side of this direction, are aggregated into a one value by summation of the values of FVx for all facades of that group. Therefore, there are eight values of FVx for each measurement point. These values can be symbolized according to the eight sides of the urban space around the measurement point. FVFe for the Eastern faces of urban space, north-east faces (FVFne), Northern faces (FVF_n), north-west faces (FVF_{nw}), Western faces (FVF_w), south-west faces (FVF_{sw}), Southern faces (FVF_s) and south-east faces (FVF_{se}). With no facades on a specific side of urban space the value of FVx will be zero on that side like FVF_{sw} on the same figure.

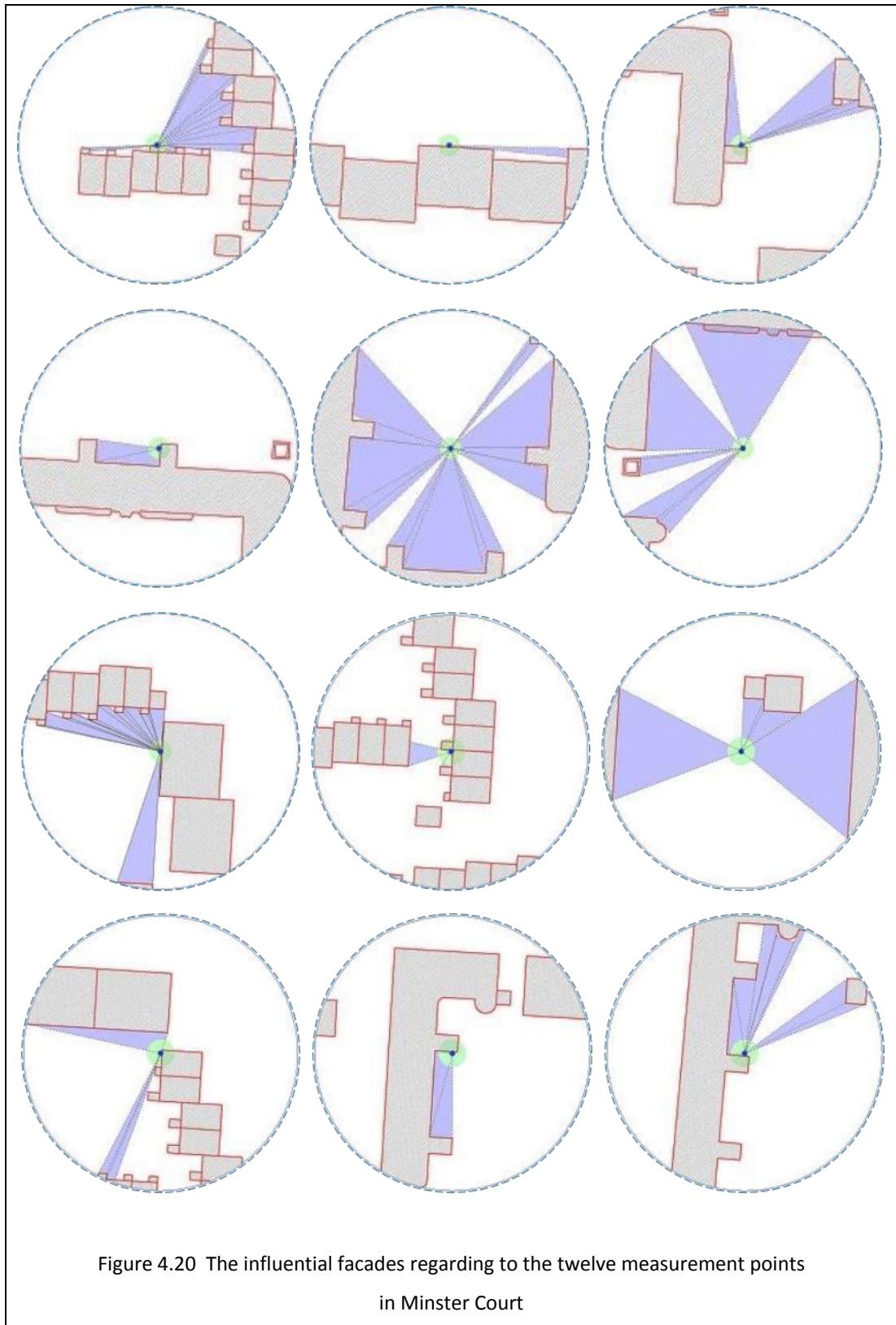


FVx values for a group of facades that sit on the same side of the space (like Eastern side (E)) can be gathered to be one value like FVFe.

It should be mentioned that the configuration of buildings on each side of the urban space may generate five different values of FVx according to the position and rotating angle of building façades. Figure 4.19 shows that four buildings on the four sides of the urban space, where each side of the space has the range of five facades. For example, FVFn for the measurement point is equal the summation of FVx for each façade sit on the northern side of the measurement point and face the south direction.

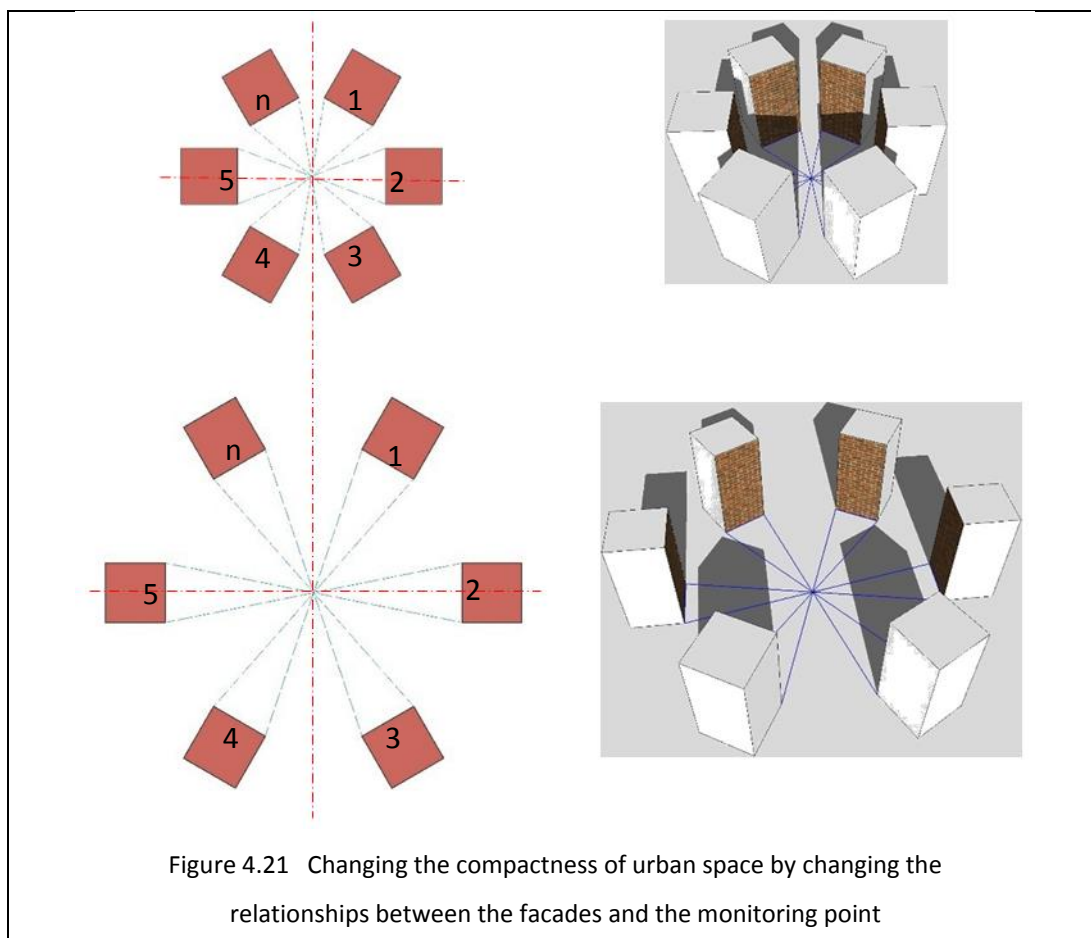


FVfx is calculated and categorized for all visible facades inside the buffer zone regarding the case study, as demonstrated in [Figure 4.20](#).



4.4 The Total Façade View Factor (FVF)

Increasing the façade area leads to a growth in the value of FVF_x , and more sky will be blocked and the permeability of the urban space will be reduced in response to the façade area. Changing the location of the measurement point may cause the same impacts, especially if the point is moved to be nearer to the façade, due to increasing the horizontal view angle and decreasing the perimeter of the imaginary triangle between the point and the façade. Therefore, the FVF_x concept may have extra merit in expressing the compactness of urban space, as shown by [Figure 4.21](#).



The total summation of FVF_x values for all visible façades around the monitoring point produces the Total Façade View Factor (FVF), which can be considered as a directory of compactness of the urban space around the monitoring point. Therefore, FVF will be considered as an urban morphological parameter in this study and it can be calculated according to the following formula:

$$FVF = FVF_{x1} + FVF_{x2} + \dots + FVF_{xn} = \sum_{x=0}^{x=2\pi} FVF_x \quad (4.7)$$

According to the structure of this formula, FVF has a positive relationship with FVF_x which, in turn, changes positively by elevating the horizontal view angle, the façade area or both, while increasing the length of the triangle perimeter is accompanied by a reduction in the FVF_x value.

The relationship between these three inputs adapts automatically to accommodate wide range of possibilities, therefore FVF has promising potential to describe the configuration of urban space in more accuracy due to it taking into consider many variables that affect the urban morphology.

4.5 Conclusions

The methods and tools that were developed by this study to describe the morphology of urban space numerically were revealed in this chapter. The adopted methodology of development depends on recruitment of the cardinal directions (N, E, S & W) as a part of the calculation methods of the urban parameter itself to establish a novel approach that takes into account the concepts of directions and orientations to deal with the configuration of non-directional urban spaces regarding many aspects, such as environmental effects. Three novel urban morphological parameters were developed in this chapter.

The Partial Sky View Factor (SVF_x) is a development of the well-known parameter the sky view factor (SVF), and is based on dividing the sky hemisphere into four quadrants according to the cardinal directions (N, E, S and W). SVF_x is the ratio between the area of visible sky in one quadrant and the total area of sky hemisphere. Attempts to calculate this variable may be difficult and time-consuming. Therefore, a number of techniques have been developed to calculate it from fisheye lens images and three-dimensional models.

The Façade View Factor (FVF_x) is the second novel parameter that was developed to define a mathematical relationship between the area, the position and the direction

of a façade with the measurement point as an approach to describing the morphology of an urban space, where the microclimate of the urban space may be affected by this relationship.

The total façade view factor (FVF) is the third parameter that represent an indicator of urban space compactness. It expresses the visible urban scene in a 360° view around the measurement point as one numerical value by the combination of FVFX values for all visible façades from the point.

These parameters are affected by many variables, such as area, position and direction of the façade as an envelope of urban space, in addition to the measurement point location.

Due to the diversity of variables that were covered by the novel parameters, the potential of these parameters is good regarding the description of the morphology of urban space. Therefore, the expectations about their roles in terms of explaining the air temperatures variations around an urban site are high.

Chapter Five

5 Field Work (Results and Discussion)

5.1 Introduction

As an introduction to the statistical analysis, to be discussed in the next chapter, this chapter is devoted to a review and discussion of the field measurements. This includes on-site air temperatures (aT), climatic factors (the ambient air temperature (a.Ta) and solar radiation) and measurements of urban morphological parameters (UMP). These variables represent the numerical inputs of this analysis.

The field measurements of air temperature (aT) and the weather station measurements of climatic factors will be elucidated as an average of each hour (AVG) to provide a general idea about the variety of the thermal microclimate. Although the hourly maximum (MAX) and hourly minimum (MIN) dataset represent, with AVG, the indicators of thermal microclimate in the statistical analysis, they will not be reviewed here. Too much detail may result in confusion and difficulty in capturing the meanings and the interrelationships between the variables (Szokolay 2014). Although the wind speed and rain precipitation are not inputs to the statistical analysis, their measurements will be mentioned to draw the whole image of the circumstances accompanying the field measurements and due to the likely effects of these two factors on air temperature.

The relationships between the ten urban morphological parameters (UMP) that were calculated in the previous two chapters will also be investigated. The reason for this is to facilitate further ideas that may help to explain the roles of UMP in the statistical analysis. The values of UMP relate to the field data that describe the change of urban configuration around the measurement points, numerically, from one location to another.

5.2 The selected days of study

The on-site air temperatures (Ta) were measured for the twelve locations in a residential compound (Minister Court) in the city of Liverpool (England, UK) for the

hot season at 2014 and for the cold season at 2015. These measurements covered two intervals: 29th July – 3rd September and 1st February – 28th February, respectively. However, not all of the days were used in the study. To understand the effect of urban morphology on air temperature the unstable days (i.e. windy, rainy or both) were removed. Air speed and wet surfaces can have a noticeable effect, notably on the energy balance of urban areas. According to the Beaufort wind force scale, a calm wind speed is (1-2 m/s) (Met Office 2016a); however, it was not easy to find calm dry days. Less stable days were therefore also selected when these days presented a gentle breeze with wind speeds of about 5 m/s and rain rates lower than 2 mm/hour. It should be noted that the vast majority of study days were below these limits.

It was also not easy to find days with a 100% sunny or cloudy sky and subject to the limits mentioned above. Consequently, the selected days were categorised into three groups according to the length of the sunny periods throughout the daytime, which were obtained from the University of Liverpool's rooftop weather station. The days that witnessed sunshine hours of more than 60% of the length of daytime were considered as a 'sunny day' whilst the days that were between 30% and 60% were a 'partially cloudy day'. Any day with sunshine hours lower than 30% of its daytime length were described as a 'cloudy day'.

To better understand the effect of UMP on the behaviour of on-site measured air temperature, and how this role is affected by the diversity of climatic factors during the day, the day (24 hours) was divided into four periods, each of them extending for six hours. The night, as the first period, lasted from midnight to 06.00 am; the morning, as the second period, from 06.00 to 12.00 noon; the afternoon period ran from 12.00 noon to 18.00; and finally the evening period from 18.00 to midnight.

Although it has passed the validation test without problem, sensor data at location H6 has been ignored having not recorded many parts of the study time due to undefined technical problems.

5.3 The hot season measurements

The hot season included 19 days categorised into three groups: the 'sunny days', the 'partially cloudy days' and the 'cloudy days'.

5.3.1 The sunny days measurements

The field measurements of the selected sunny days (4th, 7th, 9th, 15th August and 2nd September) are shown below in [Figure 5.1](#), [5.2](#) and [5.3](#). The lines indicate the hourly average of near ground surface air temperatures (2.5-3.0m height) of eleven locations in the residential compound. It also shows the weather station's measurements as a reference guide to distinguish the hotter and colder locations versus the ambient air temperature, solar, wind speed and rain rates depending on the four periods of day as mentioned above.

The daytime length decreased about one hour by shifting the sunrise time from 05:32 to 06:22 between the first and last days, whilst another hour was cut by changing the sunset time from 21:02 to 19:59. The hourly average of solar energy had reached the highest value on the 4th August (822 Ww/m²) while 2nd September recorded 751 W/m² as the lowest maximum average of solar energy between all days. However, the highest value of a.Ta was recorded at the shortest day 2nd September (as 21.2°C) while the lowest value of a.Ta was recorded at the longest day 4th August (as 13.0°C). This may be the result of the effect of wind speed that was lower on the 2nd September compared to 4th August. The average wind speed reached 4.5 m/s on the 9th August while 7th August value was 0.54 m/s as the lowest value throughout the sunny days. The hourly rate of rain was 1.4 mm/h on 7th August as the highest rate compared to other days. The longest sunny interval throughout the daytime was about 13 hours on 4th August while the shortest interval was 9 hours on 15th August.

Generally speaking, the similar periods showed convergent behaviours of on-site air temperature, where the morning and afternoon periods represented the least stable periods compared to others because of increasing solar radiation levels that may have changed the thermal storage in the urban surfaces which, in turn, affected the air temperatures. The night period was the most stable period due to the absence of solar radiation and the dissipation of the stored heat in the urban surfaces.

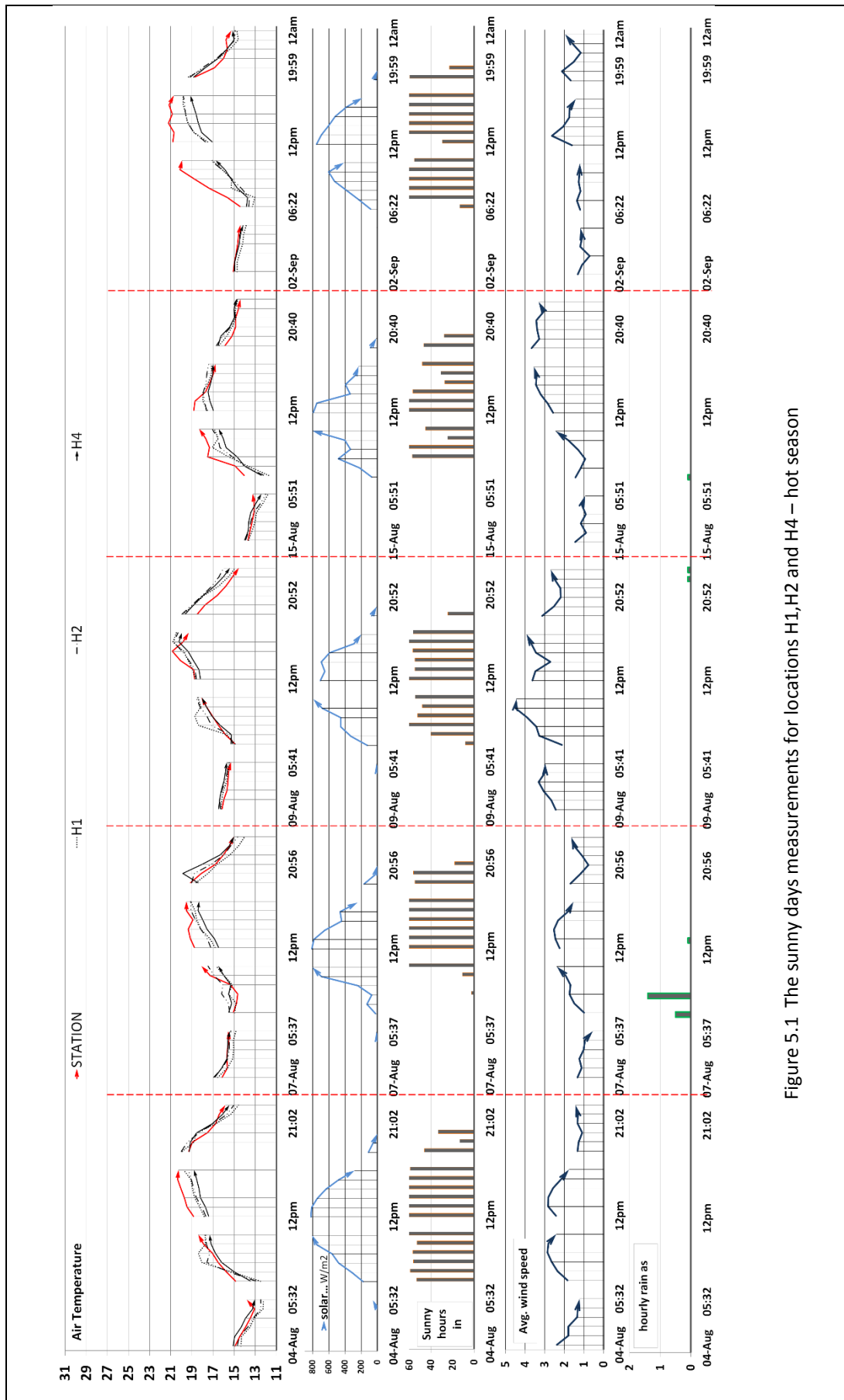


Figure 5.1 The sunny days measurements for locations H1, H2 and H4 – hot season

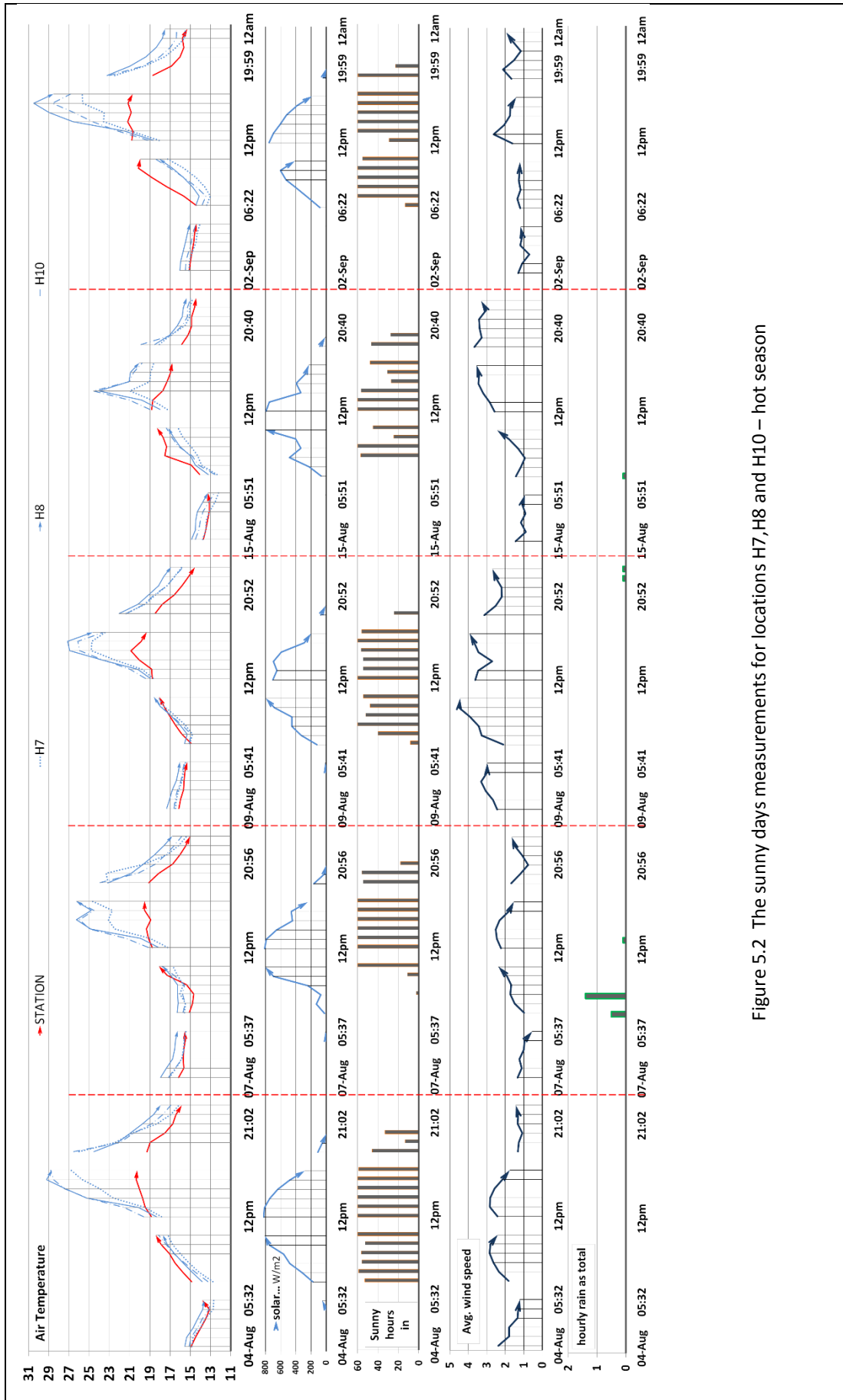


Figure 5.2 The sunny days measurements for locations H7, H8 and H10 – hot season

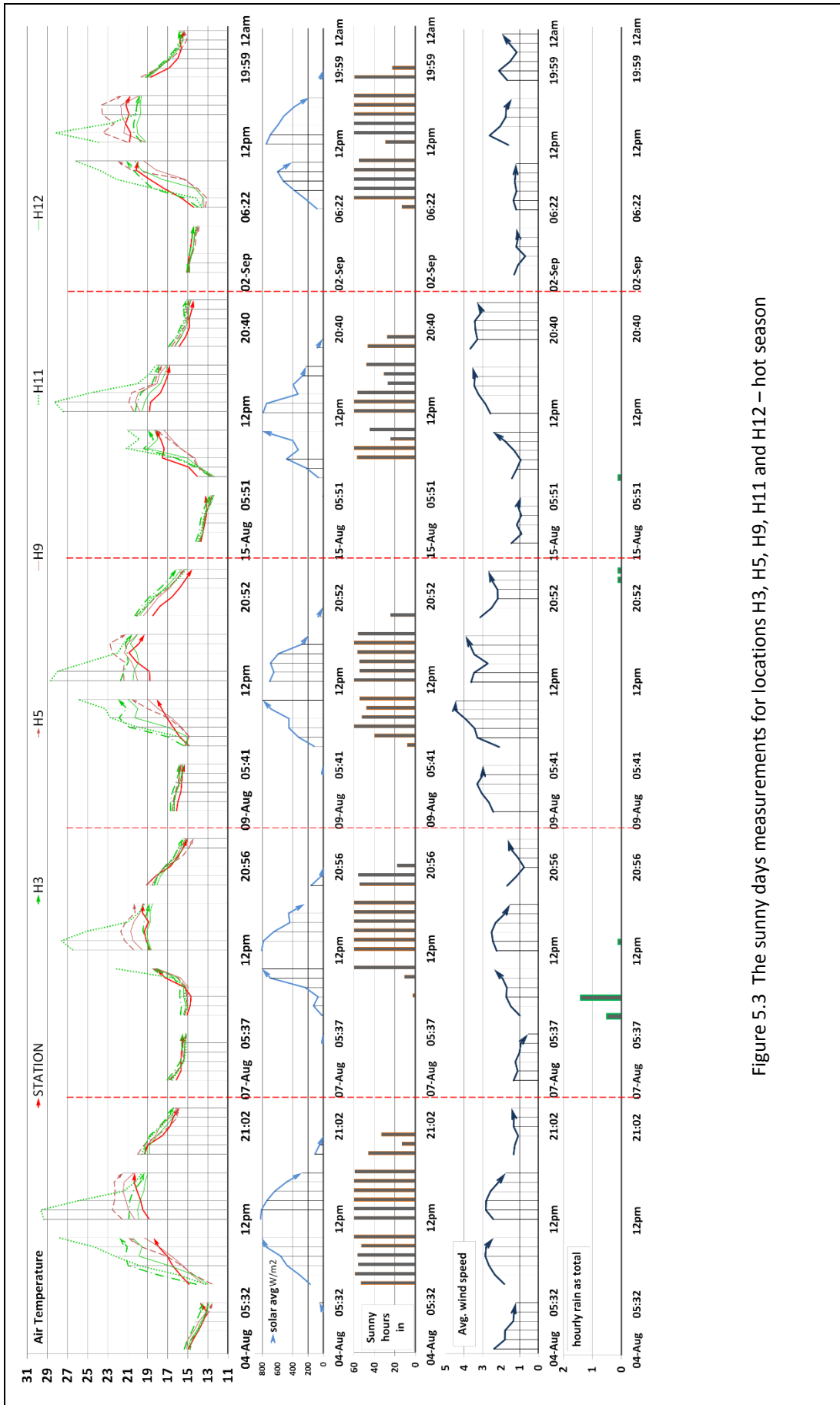
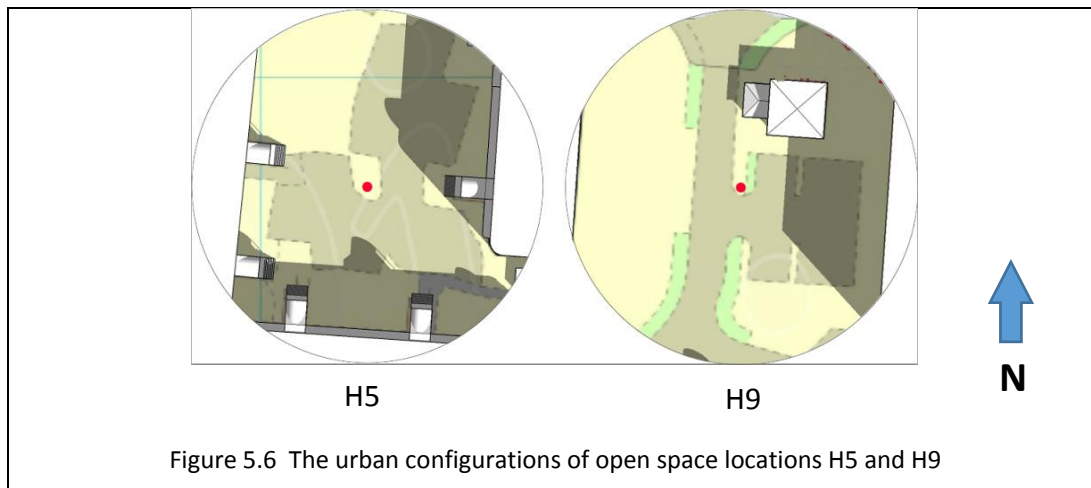
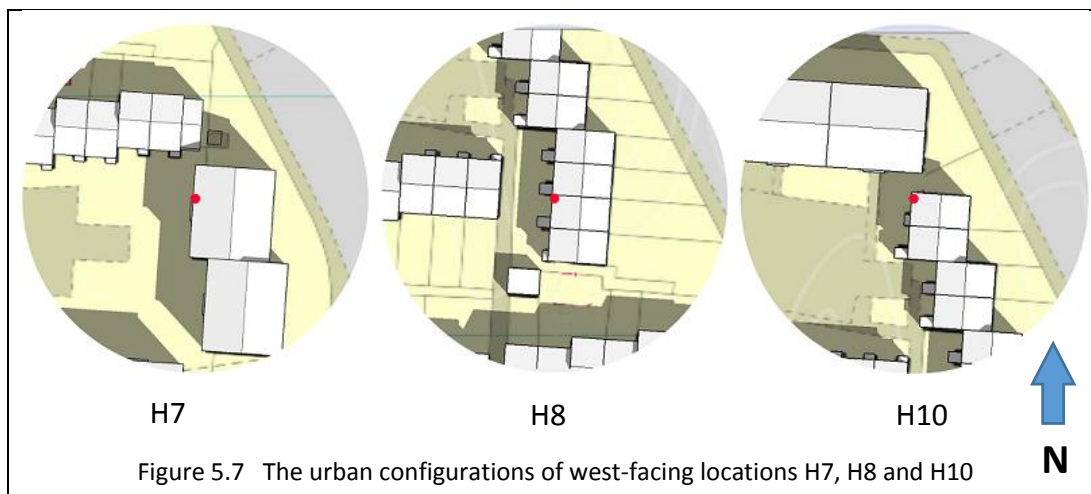


Figure 5.3 The sunny days measurements for locations H3, H5, H9, H11 and H12 – hot season

- The purple colour set included H5 and H9. The measurement points were in the middle of the urban spaces that were defined, mainly, by the buildings on the eastern, southern and western sides, as shown by [Figure 5.6](#).



- The blue colour set is the last and included H7, H8 and H10. The influential masses surround the northern and eastern sides and the space was more open to the west. H8 is more defined and compact than the other locations, as shown by [Figure 5.7](#).



Although all locations saw increasing air temperatures in the morning period, some locations, such as H3, H11 and H12, observed the higher increases due to the potential impact of large vertical east and north facing surfaces being warmed by the morning sun in the east and south east, especially for H11. These neighbouring

surfaces received high levels of direct and indirect solar radiation that caused an increase in the air temperature (aT) during the morning periods. However, they lost this benefit in the afternoon periods by virtue of the solar radiation that irradiated the south and west-facing vertical faces from around midday and beyond, especially at H7, H8 and H10. These locations recorded higher air temperatures than others because of the influential contribution of thermal storage.

The measurement point at H11 received direct solar radiation from early morning until about 13:00 whilst the points of H3 and H12 did not receive any direct solar radiation. This is the reason for the significant disparity of air temperature between H11 and H3/H12. In comparison to H3, H12 produced the lowest air temperature during the daytime due to the effect of the five storey building located on the eastern side of H12 that stopped the morning sun from reaching H12 earlier as did happen with H3. In addition, there are likely to be effects from the grass areas and the trees around H12 compared to the solid surfaces around H3, as shown by [Figure 5.8](#).



On some days location H1 witnessed an increase in temperature at about 9.00 am where this solo behaviour for a measurement point in the black colour group may be attributed to increasing thermal storage by a direct solar gain or by the effect of the ground around the sensor. The low heights of the obstructions on the southern side of H1 compared to H2 and H4 will generate short shadows and so the asphalt that represents the predominant material around H1 was exposed to the direct sun

throughout this period and this may have affected T_a . The days that witnessed this phenomenon also witnessed higher wind speeds, especially in the morning period. The last factor may have contributed in some way to this behaviour under the effect of the urban configuration.

H8 has some shared features with H3 and H12, such as the vertical surfaces that block the western view and the equality of distances between these surfaces and the sensors. However, H8 showed a simple increase of air temperature compared to H3 and H12 in the morning period. The continuous surface that define H8's west-facing side and receive the direct solar energy till midday had no big effect on air temperature, although the space of H8 is much smaller than the spaces of H3 and H12. The difference in height of the blocks may explain the height of western masses of H3, H12 and H8 (15, 11 and 6 metres), respectively. Therefore, the low heights around H8 may lead to a dispersion of the warm air near the ground surface to the sky, swiftly to be replaced by cold air and so the increasing of air temperature will gradually get as long as the eastern faces under shade, the intensity of solar radiation. The thermal storage of urban surfaces in the morning period are not enough to make a substantial change in air temperature.

Regarding the afternoon period (12:00 to 18:00), unstable air temperature behaviours were observed. Some points recorded an increasing of air temperatures versus other locations that witnessed a decreasing of T_a . This contrast in behaviour is due to the appearance of shadow areas on urban surfaces in some locations along with the general increase of wind speed in this period whilst other locations were still under the direct solar radiation as a natural result of the movement of the sun. However, the locations that were not influenced by direct radiation, such as H1, H2 and H4, were more consistent with the ambient air temperature ($a.T_a$), while the locations of the blue colour set (H7, H8 and H10) kept their ascent for most of this period due to the impact of the direct solar energy that has started to lose its intensity after midday.

Although H1, H2 and H4 have convergent forms, H4 may be the coolest location compared to all measurement points, especially throughout the afternoon period. This behaviour of H4 can be explained by the differences of shade areas around the

measurement points due to the differences of building heights, whereby these shaded areas reduced the effects of the ground near surface on the air temperature. **Figure 5.9** compares H1, H2 and H3 for the three times in terms of shade areas. H4 witnesses the biggest shade area for all times, by virtue of its five story building. In comparison, the two story mass at H1 produced the smallest shade areas between the three locations. Conversely, H1 primarily recorded the highest air temperatures compared to the other two locations.

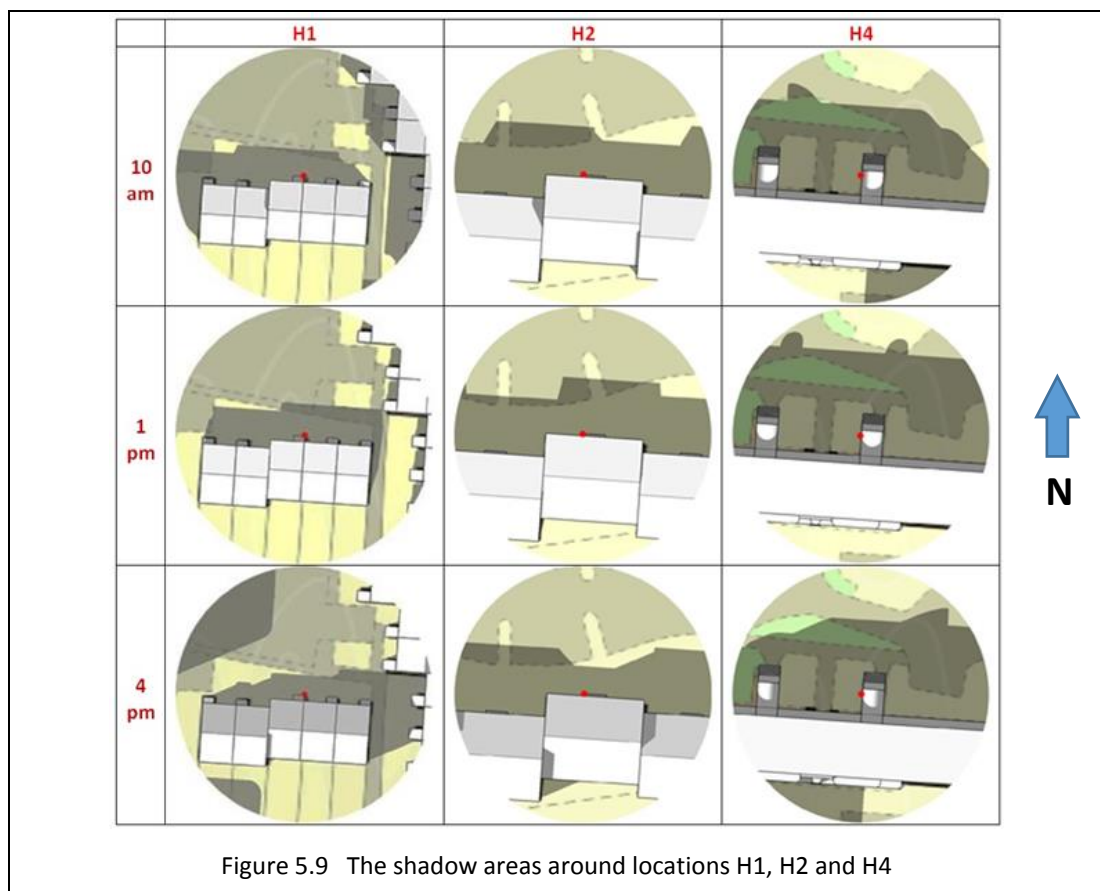
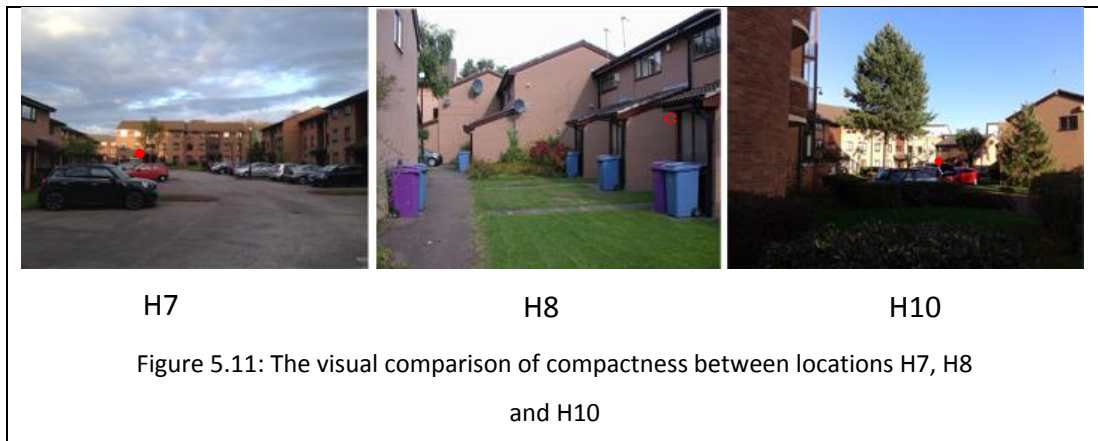


Figure 5.9 The shadow areas around locations H1, H2 and H4

Conversely, from midnight to sunrise H4 was the warmest point in the black colour set in general. H4 is a little more surrounded than the other two locations and, as a result, the radiative long wave cooling to the sky will be less efficient as the sky was obstructed by the building. In general, these cool air temperatures in H1, H2 and H4, due to the absence of direct solar for most of the daytime, do not have enough stored heat in the nearby vertical surfaces to be released as high levels of long wave radiation at night. In addition, the grassy cover with trees may contribute to the cooling down of air temperatures, as seen in **Figure 5.10**.

may be down to the contrast between the locations that started to lose their heat earlier compared to other locations that were receiving the solar energy until the end of the afternoon period. However, the dropping of air temperature looks faster in the locations that have higher thermal stocks.

The area of urban surfaces affected by the direct solar energy after midday around H8 was smaller compared to H7 and H10 whilst H8 stayed on the top within the morning and the evening periods. This was because of the ratio between the vertical surfaces and the dimension of space around H8 that is considered more compact in comparison with others, as shown by [Figure 5.11](#).



H1 and H2 were the coolest locations in this period, possibly due to their nearest vertical surfaces not receiving any direct radiation during the day. In addition to the wind speed effect that increases lightly, particularly before the midnight in the sunny days group.

The in-situ measured air temperatures in all locations maintained their downward trends during the night period, but at a slower pace and with less differences between them compared to the evening period. Subsequently, the air temperatures graph dropped smoothly as a result to the dissipation of stored heat in the urban surfaces. However, H8 and H10 recorded higher air temperatures compared to others.

5.3.2 The partially cloudy days measurements

The partially cloudy days group includes ten days of the hot season (31st July, 3rd 5th, 12th, 14th, 20th, 22nd, 23rd, 24th and 31st August). The hourly average of on-site measurements in the eleven points are shown in [Figures 5.12, 5.13, 5.14, 5.15, 5.16 and 5.17](#), which also show the weather station measurements. The number of sunny hours represents about 60% to 30% of the daytime duration because of the effect of clouds. The day length itself lost about two hours between the first day (15:43 hours) and the last day (13:44 hours) in this group.

The hourly average of solar energy had reached the peak at 3rd August (as 765 W/m²) while the longest day (31st July) witnessed 455 W/m² as the lowest maximum average of energy between all the partially cloudy days. The highest average value of daytime ambient air temperature was recorded on 31 July (as 21.2°C) while the lowest value of night time a.Ta was recorded on 24th August (as 10.5°C). Noticeably, the longest day recorded the highest average value of a.Ta, although it witnessed a low level of solar energy and this may be due to its wind speed (3.6 m/s) compared to 5.6 m/s that was recorded on 3rd August, that saw the highest hourly averages of wind speed and solar energy in this group. The highest hourly rate of rain in this group was 1.7 mm/h and it was recorded on 23rd August.

Although the differences of general circumstances compared to the sunny days in terms of decreased solar energy intensity, increased wind speed and increased rain rate, convergent behaviours can be seen for locations that shared configuration features. The active behaviours of H3, H11 and H12 can be seen mainly in the morning period for some days while the demeanour of the green colour graphics (H7, H8 and H10) were more recognisable in the afternoon periods as the hottest locations from 6.00pm to 6.00am. This activity was subject to the change of sun location as mentioned above with the sunny days in addition to the sunny intervals within these periods.

Both periods (morning and evening) kept their conflicted behaviours that was noticed in the sunny days measurements however there are some differences in the in-situ temperature behaviours that was affected by the climatic factors. It is worth noting

that the night period witnessed steady ambient air temperatures and air temperatures from midnight to 06:00 am for some days, like 3rd, 22nd, 23rd and 31st August. This behaviour may be attributed to the wind speed that exceeded 3m/s for most of these days as well as the wet urban surfaces due to rain. These two factors may have helped to lose most of the thermal stored heat that affected the on-site measured air temperature that has become under the control of ambient temperature. Supporting this idea is the response of all locations to a suddenly decreasing ambient temperature on August 24th, whilst the day before, beside the high solar intensity, witnessed a great deal of rain compared to other days.

In general, the wind speed increased with increasing intensity of solar energy and decreased with increasing rain levels. This affected the air temperatures, especially at H5 and H9, where these sites witnessed a variety of behaviours that may be difficult to explain. H9 represented the coolest location throughout the afternoon period on July 31st versus H5 that represented the fourth warmest point for most of this period, where the intensity of solar energy was lower than 400 W/m², with one of lowest wind speeds in this period (lower than 2 m/s). The afternoon period on August 3rd exceeded the thresholds of 600 W/m² and 4 m/s regarding the solar energy and wind speed, respectively. However, H5 and H9 kept about the same previous ranks with differences that exceeded 2°C between them. Similar behaviours were observed regarding the climatic factors and on-site measured temperature on the 12th of August. Conversely, 5th and 14th August did not witness big differences between H5 and H9 in the afternoon period, although the climatic factors were like other days. On the 31st of August H5 was affected by an increasing ambient air temperature. Simultaneously, H9 was affected by a decrease in the solar intensity. The increasing of ambient air temperature on the last day may be attributed to a decreasing wind speed along with an absence of cloud cover and a direct solar radiation level of about 500W/m². Consequently, the compacted space around H5 under these circumstances will keep the heat longer than H9 and stay warmer, especially by the effect of thermal storage for the five storey building on the eastern side of H5.

In terms of the black colour set (H1, H2 and H4), they witnessed the more stable behaviours compared to others. In general, H2 was the hottest location, especially in the morning and afternoon periods, while H4 represented the coolest location for the same periods. It is not clear why H2 is warmer compared to H1; however, it should be remembered that the trees in the H1 space are nearest to the measurement point compared to H2. Furthermore, many days (3rd, 12th, 23th and 24th) witnessed very close values between H1 and H2 in the afternoon period. Regarding the night period, H4 recorded the warmest air temperature compared to other two locations on 31st July, 3rd, 5th, 12th, 20th and 23rd August. The location of H4 is more enclosed compared to H1 and H2 by the masses of building entrances on the eastern and western sides of the measurement point [see [Figure 5.4](#)]. These masses may slow the air movement around the measurement point while their vertical surfaces store the heat from the direct radiation that affect the air temperature by the radiant of the long waves after the sunset.

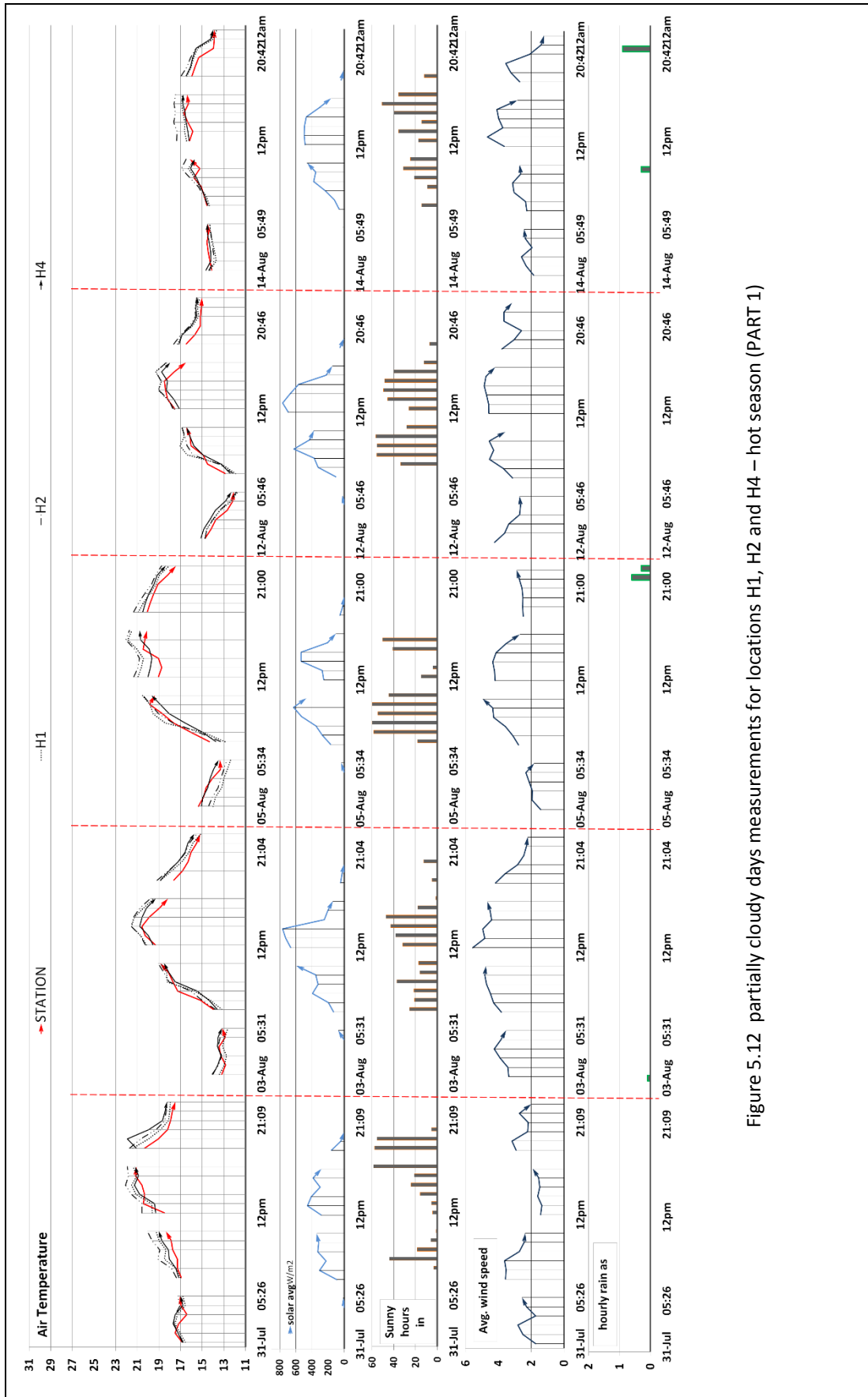


Figure 5.12 partially cloudy days measurements for locations H1, H2 and H4 – hot season (PART 1)

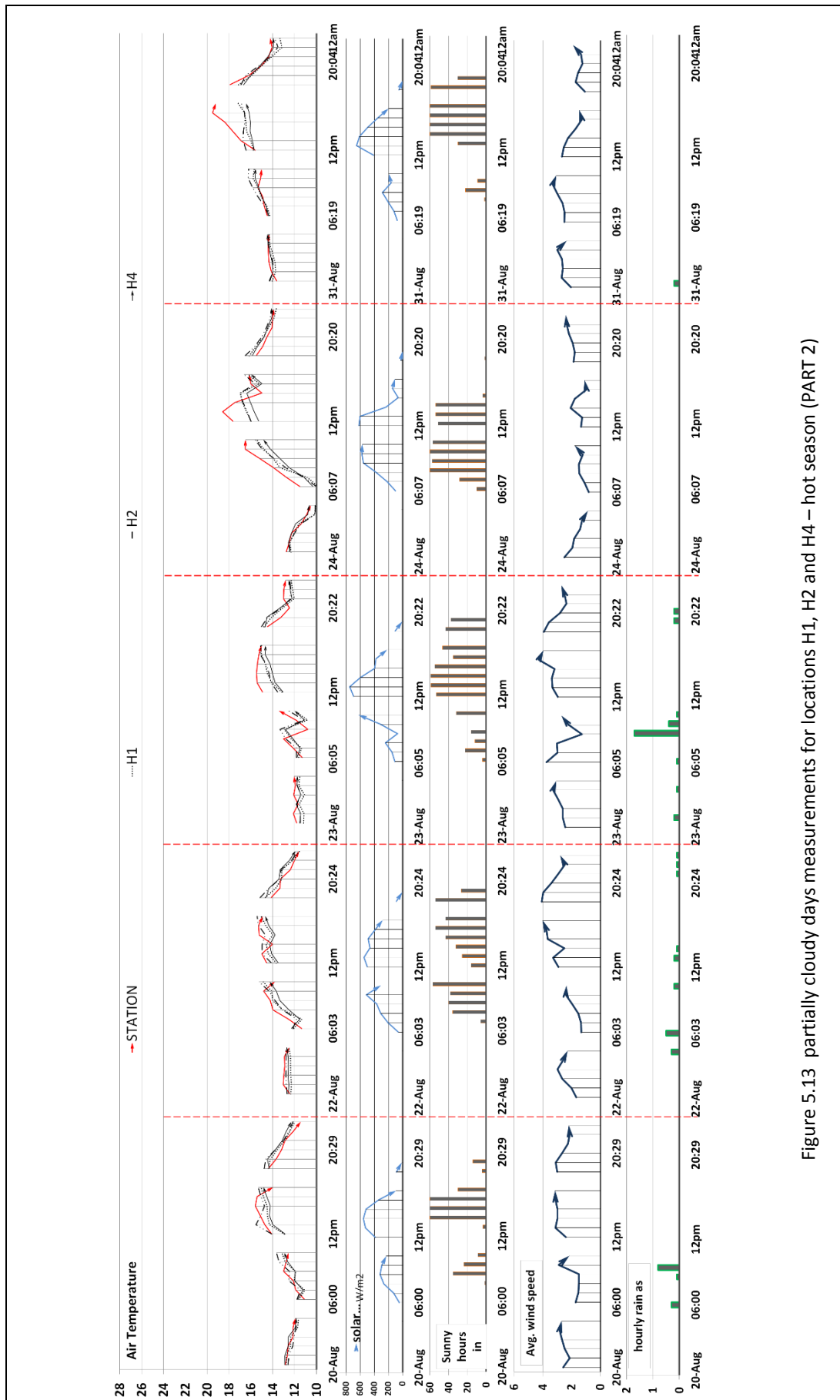


Figure 5.13 partially cloudy days measurements for locations H1, H2 and H4 – hot season (PART 2)

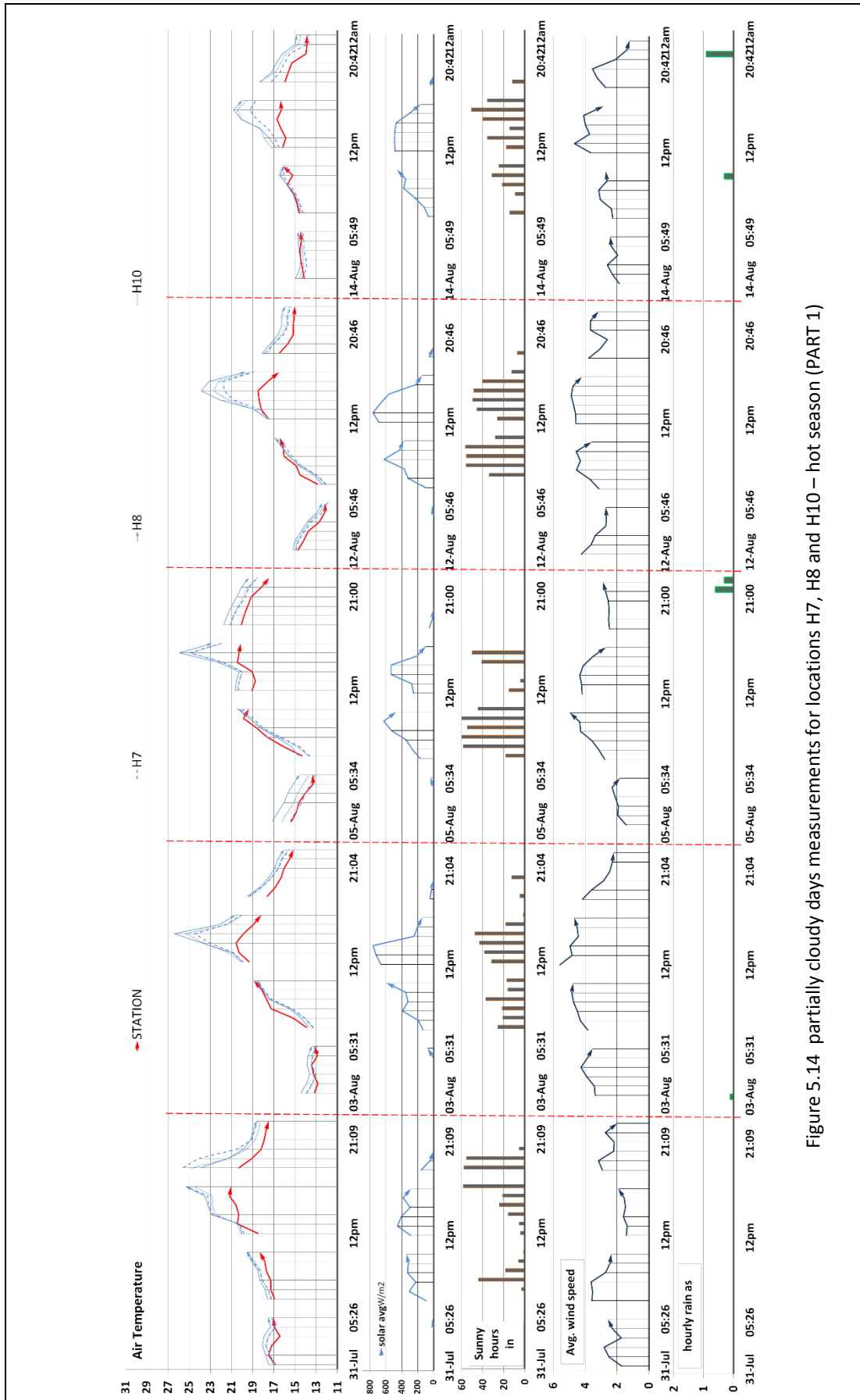


Figure 5.14 partially cloudy days measurements for locations H7, H8 and H10 – hot season (PART 1)

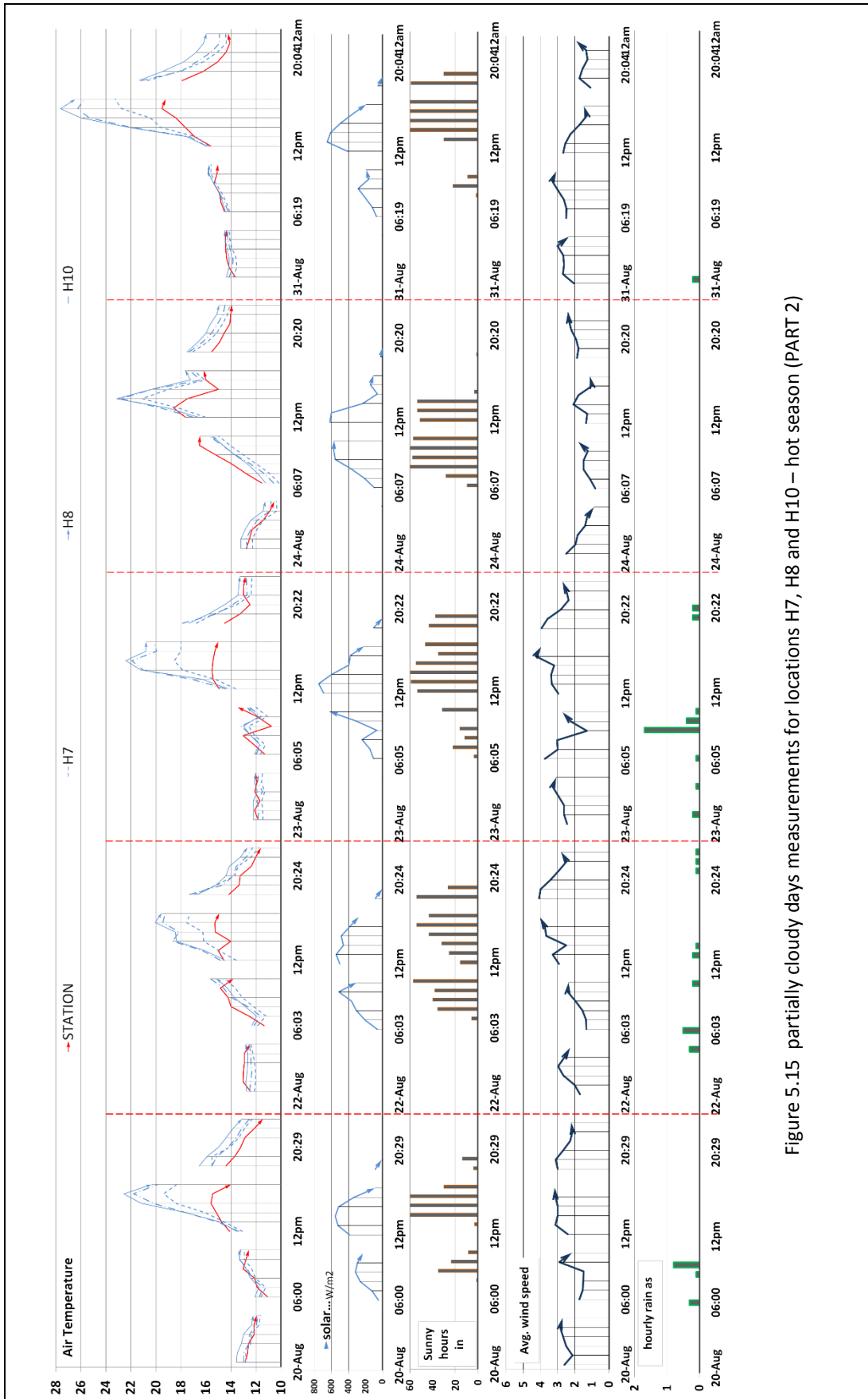


Figure 5.15 partially cloudy days measurements for locations H7, H8 and H10 – hot season (PART 2)

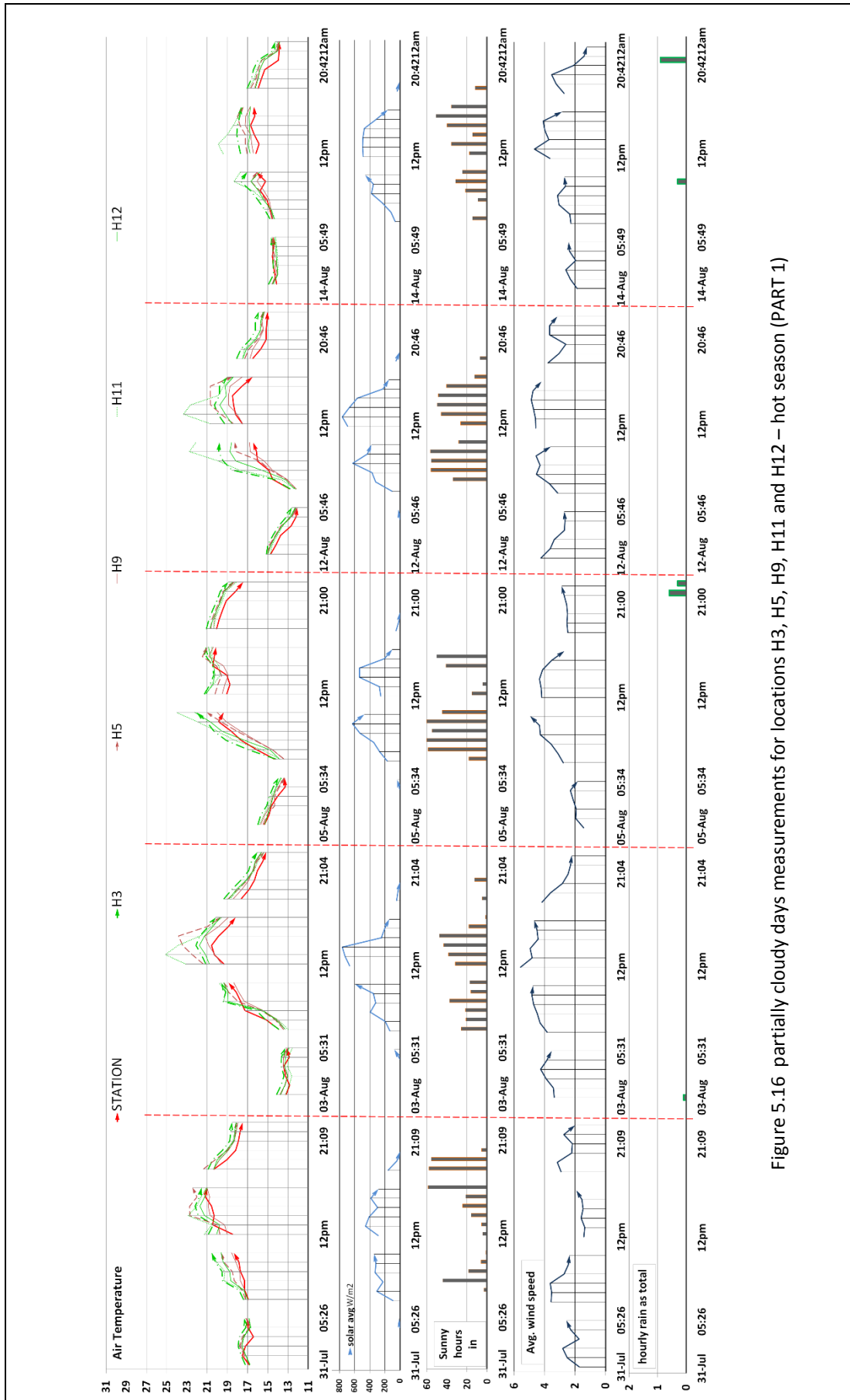


Figure 5.16 partially cloudy days measurements for locations H3, H5, H9, H11 and H12 – hot season (PART 1)

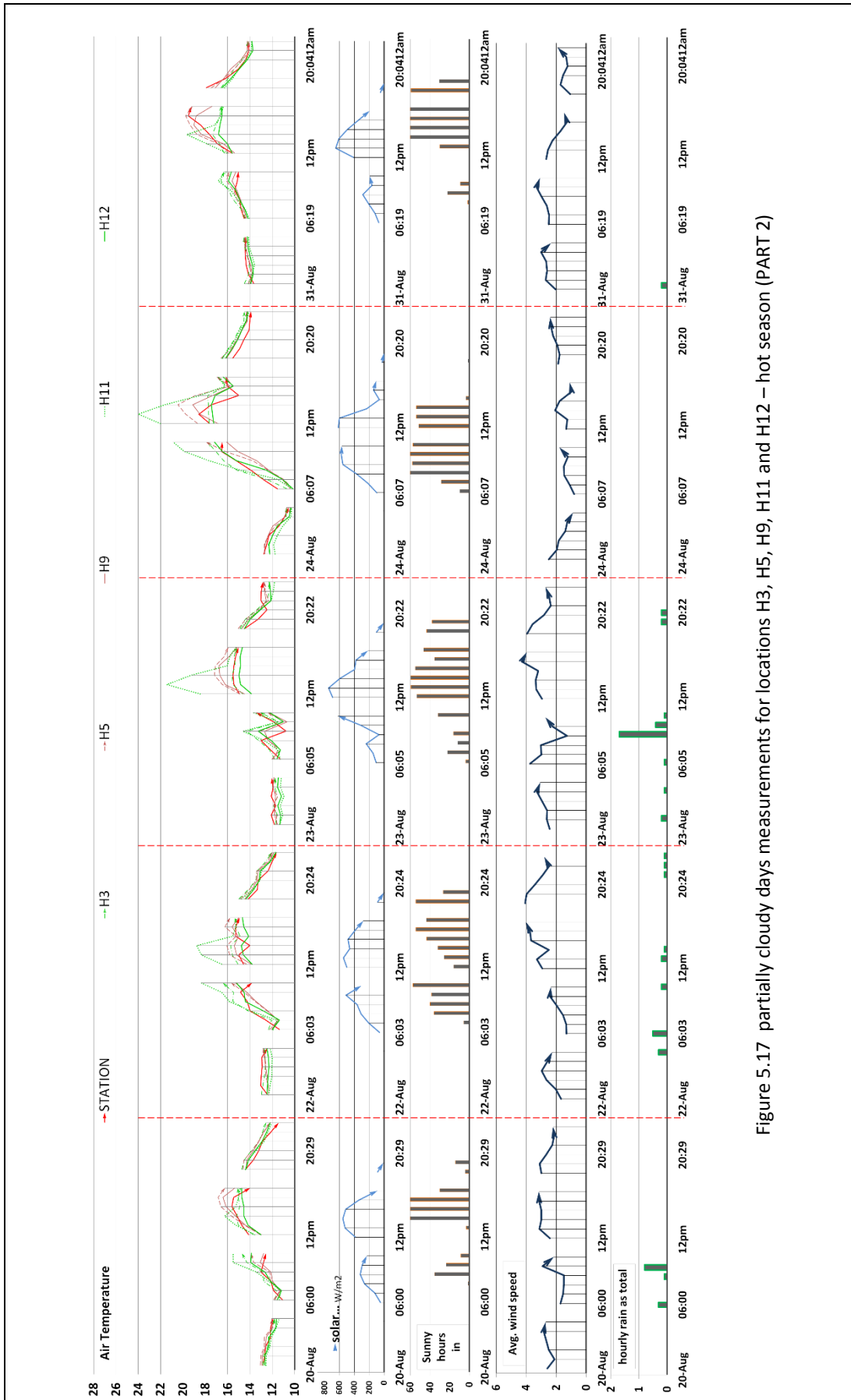


Figure 5.17 partially cloudy days measurements for locations H3, H5, H9, H11 and H12 – hot season (PART 2)

5.3.3 The cloudy days measurements

The cloudy days group comprises four days of the hot season (30th July, 8th August, 16th August and 3rd September). The total summation of the sunny intervals in each day is lower than 30% of the daytime duration because of the clouds. There is a difference of more than 2 hours between the longest daytime (15:45 hours) at the first day and the shortest daytime (13:30 hours) on the last day. The air temperature measurements of the 11 locations and the measurements from the University weather station are shown by [Figures 5.18, 5.19 and 5.20](#) as hourly averages except for the graphics of sunny hours and rain that were measured as hourly totals.

The greatest hourly average value of the ambient air temperature was recorded on 8th August (as 24.2°C) while the lowest value throughout the cloudy days was also recorded on 8th August (as 13.4°C). The maximum hourly average of solar energy between all cloudy days was recorded 8th of August (as 810 W/m²) while 16th August witnessed the minimum value (as 348 W/m²). 8th August also witnessed the lowest hourly average of wind speed (as 1.2 m/s) in contrary to 16th August which witnessed the highest hourly average of wind speed (as 5.4 m/s).

The first thing that can be noticed for the cloudy days is the air temperature of the measurement points being higher than the ambient air temperature in most days. This behaviour may attributed to the emitted heat that will be trapped and remitted back to the Earth by the clouds; consequently, the temperature will not decrease quickly, particularly at night (DAS 2010) and therefore the locations will stay warm, especially the ones that received direct solar radiation.

All sites experienced a decrease in temperature during the evening and night periods in contrast to the morning period that witnessed increasing temperatures from 6 am to 12 pm. In the afternoon period many locations maintained the escalating tendency of air temperatures for most of this period between 12 pm and 6 pm, although the decline of solar radiation levels started before midday.

In general, the differences of the air temperature between the measurement points are moderate compared to the sunny and partially cloudy days. However, there are shared behaviours with them in terms of the roles of the blue colour set (H7, H8 and

H10) at the afternoon period and the green colour set (H3, H11 and H12). This did not prevent the emergence of some different behaviours. For example, H9 recorded the lowest air temperatures, especially in the morning periods where the short intervals of the solar radiation and the wind speed were the reason for this behaviour. This may be the effect of the vertical surfaces that may slow the wind speed or keep some heat but is limited because of the big distance to the measurement point. Yet, H4 kept is usually ranked as the coolest location at the afternoon period.

With very low levels of solar radiation, accompanied by light rain and wind speeds over 5m/s, the afternoon period of 16th August showed unfamiliar behaviours where H3, H11 and H2 represented the warmest locations, respectively, while H8 came fourth. Furthermore, H3 was warmer than H8 in the night period where H2 came third, directly after H8. These behaviours are difficult to explain because of the combined effect of several factors without the dominance of a specific factor. Nonetheless, the big masses on the eastern sides of H3 and H11 and the continuous three stories mass on the southern side of H2 may have protected measurement points against the wind and rain, a possible cause for these results. Possibly, the western side of the H8 is protected but with a small thermal mass compared to other sites. H3 has extra protection from the mass of building entrance on its southern side and therefore it did record the highest air temperature from midday to midnight.

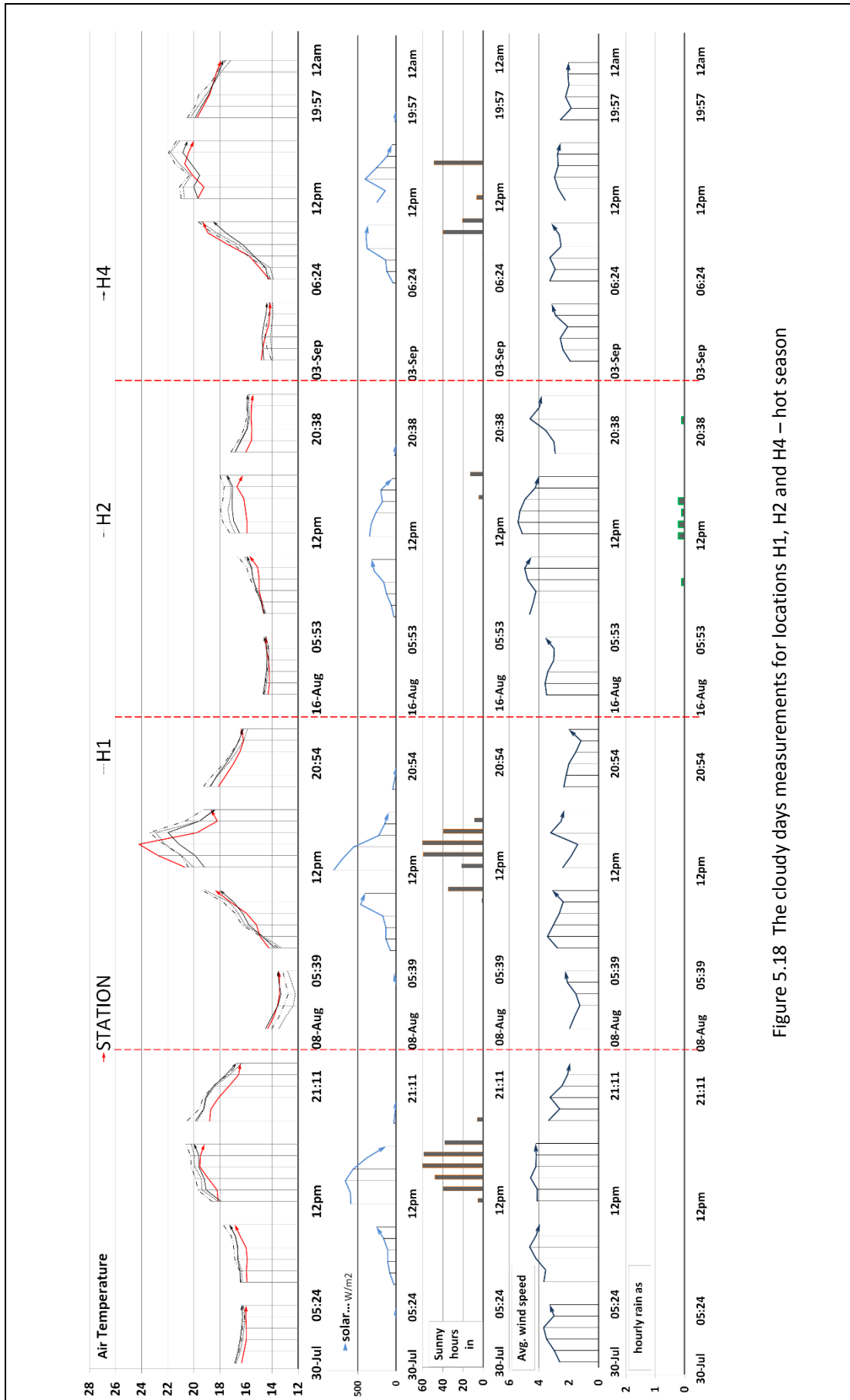


Figure 5.18 The cloudy days measurements for locations H1, H2 and H4 – hot season

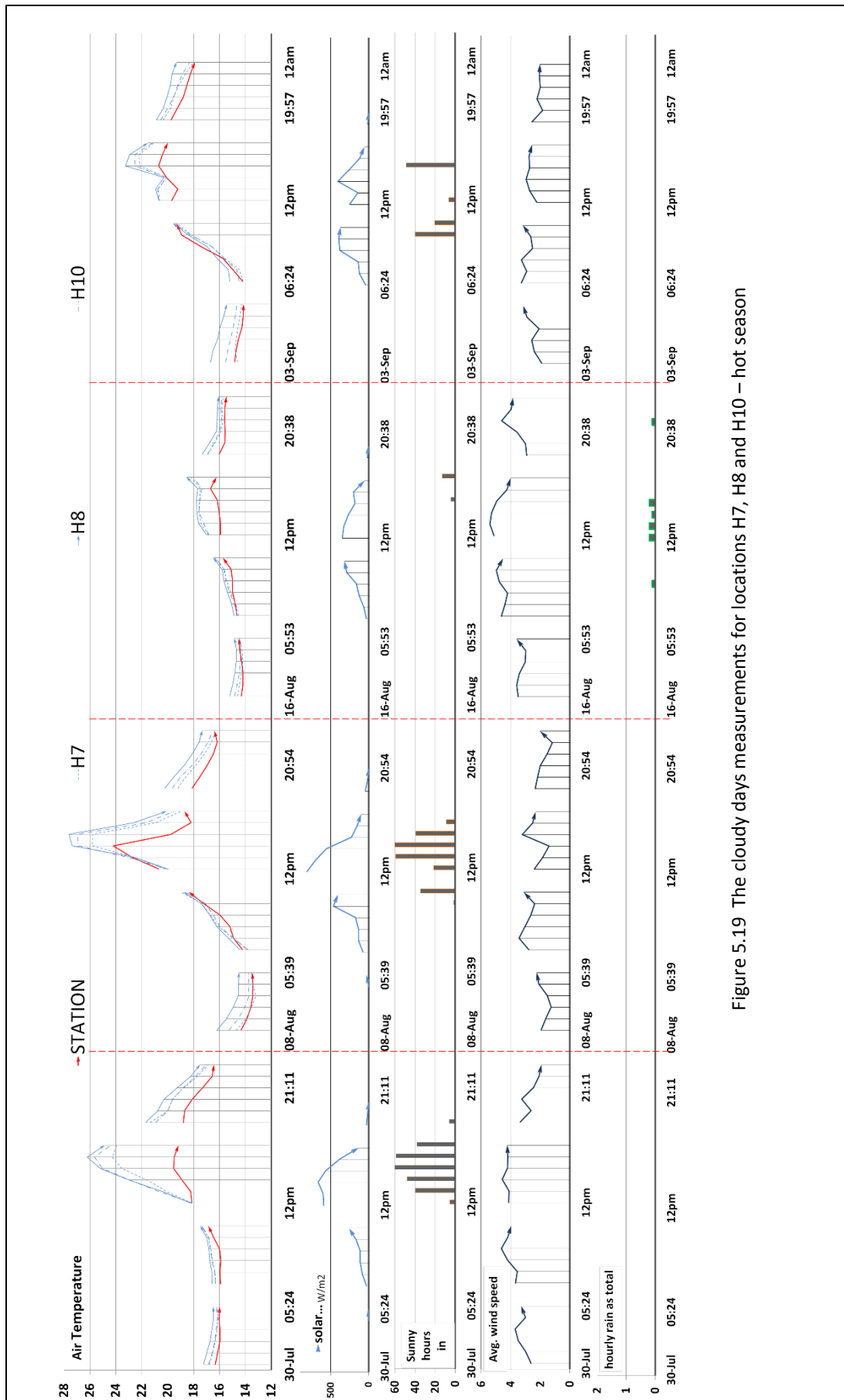


Figure 5.19 The cloudy days measurements for locations H7, H8 and H10 – hot season

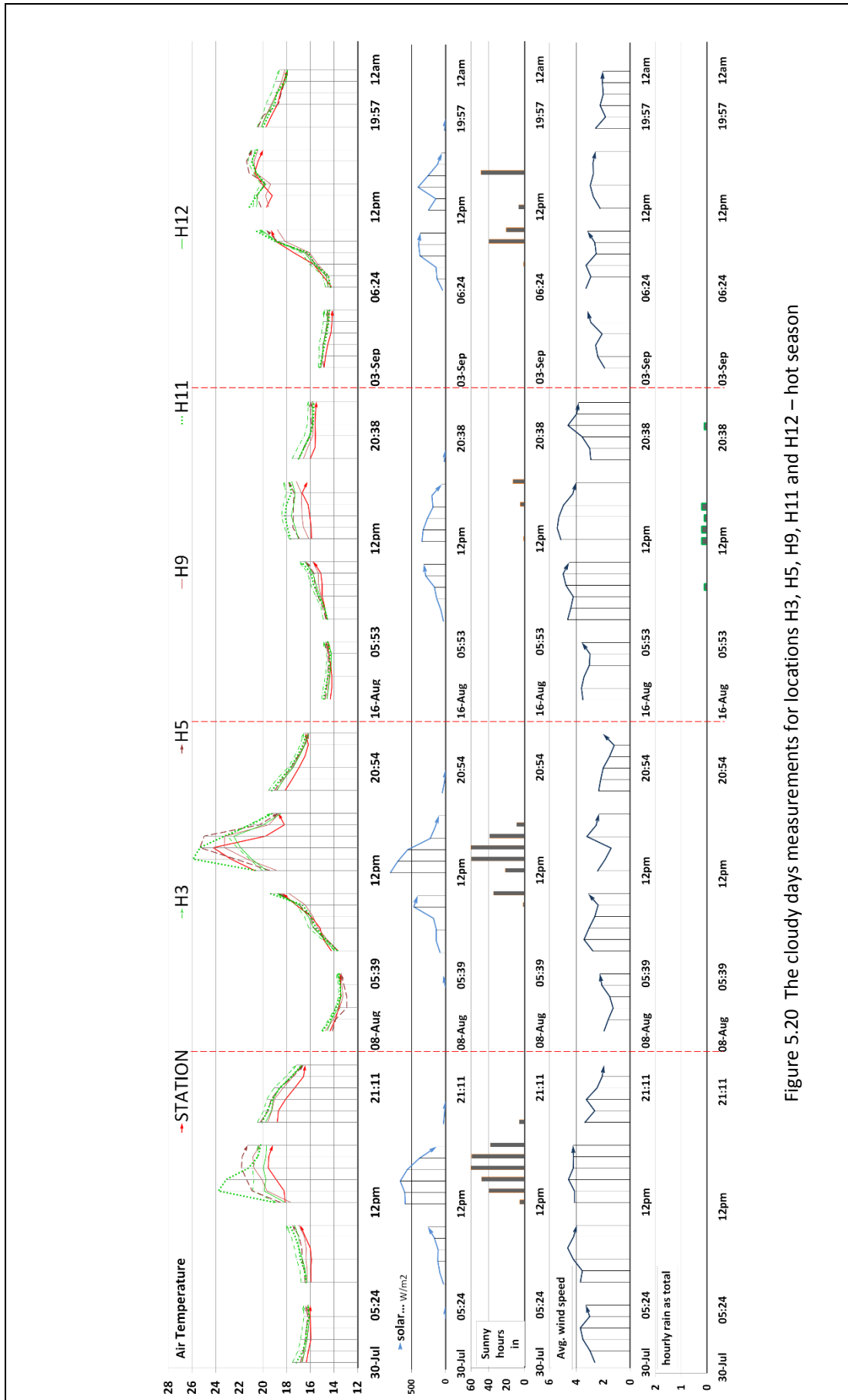


Figure 5.20 The cloudy days measurements for locations H3, H5, H9, H11 and H12 – hot season

5.4 The cold season measurements (cold)

The cold season includes 12 days categorised into three groups: the sunny days, the partially cloudy days and the cloudy days.

5.4.1 The sunny days measurements

The sunny days group of the cold season includes three days (3rd, 4th, 6th February). The hourly average of on-site measurements at the eleven points are shown in [Figures 5.21](#) that also reveals the measurements of the University weather station. The number of sunny hours represents about 60% of the daytime duration or more where the longest sunny interval in the sunny days was 8:42 hours on 6th February while the shortest one was recorded on the 3rd of February as 7:53 hours. The daytime was reduced by about eleven minutes between the first day (9:05 hours) and the last day (9:16 hours).

The hourly average of solar energy hit the peak on 6th February (as 336 W/m²) while the lowest maximum average was 328 W/m² on the 3rd February. The highest and the lowest average value of daytime ambient air temperature was recorded 6th (as 7.7 C) and 3rd February (as 0.6 C). The maximum hourly average of wind speed was 3.2 m/s at 4th February while the minimum value was recorded at 6th February as 0.9 m/s. There was no rain in these days according to the measurements of the weather station.

Compared to the sunny days of the hot season, similar behaviours of air temperature can be noticed. Where the evening and night periods experienced a dropping of temperatures, the morning period witnessed a consistent increasing of Ta, while most locations have started to lose their heat after the mid-afternoon period. H7, H8, H10 and H11 kept their reputation as the most active locations especially H8 that continued as the warmest location in different periods.

In general, the decline in the role of urban configuration in influencing the behaviour of air temperature was obvious regarding storage and thermal radiation of stored heat. This may be due to the weak intensity of solar radiation and the shortness of

daytime and the general lowering of ambient air temperatures. The superiority of the purple colour set locations (H5 and H9) compared to the green colour set locations (H3 and H12), especially in the morning period, may support this assumption. The neighbouring western walls that may affect H5 and H9 are distant from the measurement points, and the locations H3 and H12 were more active in the hot season because of the effect of these walls. Therefore, the superiority of H5 and H9 was likely because of the impact of non-porous ground materials like asphalt. This may support this justification that the air temperatures of H3 were higher compared to the H12 which may be affected by the vegetation cover around it.

Notably, the on-site measured air temperature reduced below the zero Celsius mark for most locations in the interval between the night and morning periods on the 3rd and 6th of February, although the ambient air temperature did not go down to the zero Celsius at all and the wind speed was mostly under 2m/s. This may support the previous claim about the limited impact of urban configuration regarding the behaviours of air temperature. The thermal storage of the vertical surfaces around these locations were not enough to change the temperature of the cold air that gathered near the ground surface to make tangible difference that could be captured by the sensors because of the weak solar intensity and shortness of daytime, whereas the University weather station at a height more than 20 m from the ground surface may measure the warmer air that rises to the sky.

The urban configuration may hinder the circulation of air, particularly at low wind speeds, and this effect can be important with the active thermal storage that may change the air temperature.

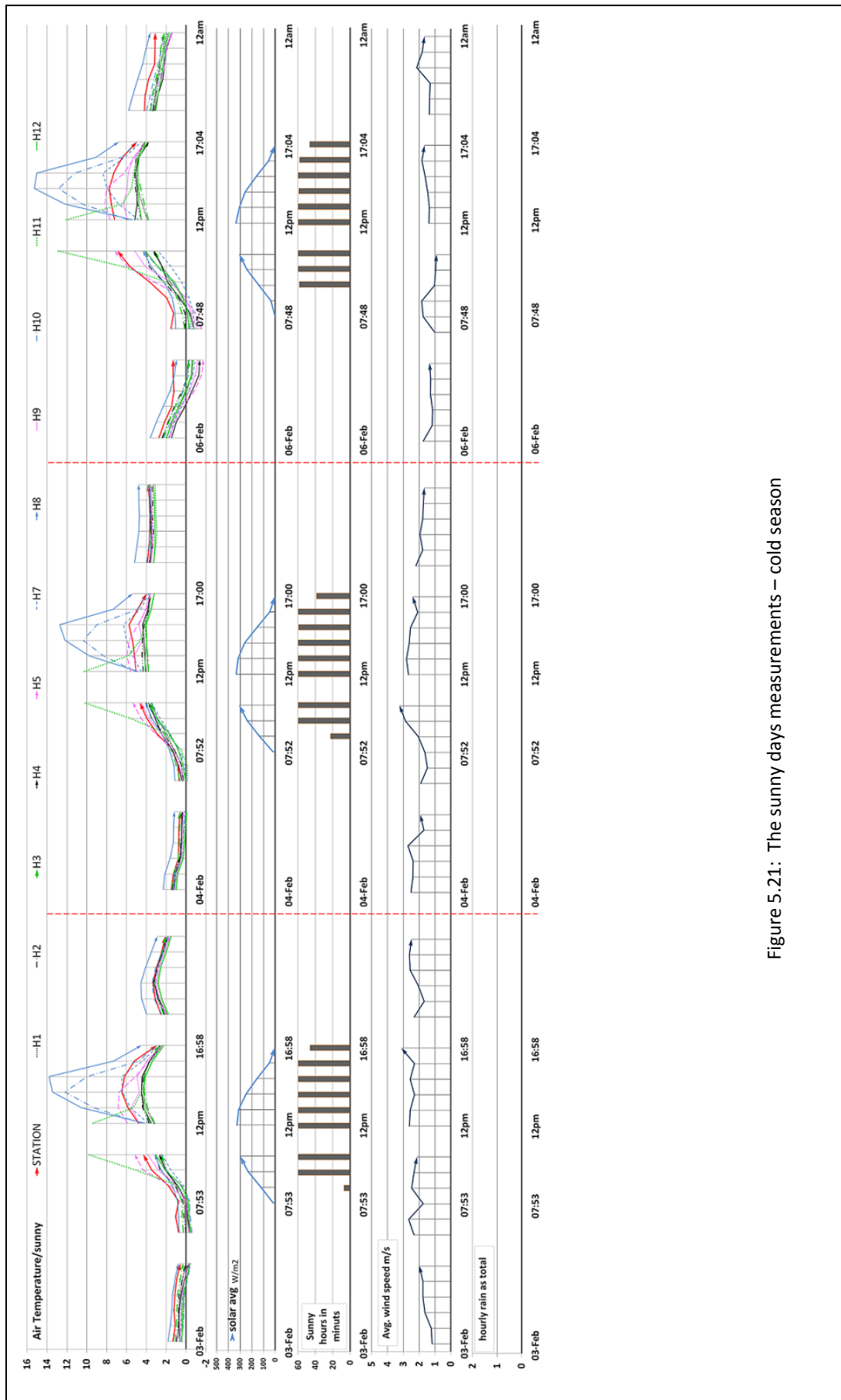


Figure 5.21: The sunny days measurements – cold season

5.4.2 The partially cloudy days measurements

The partially cloudy days group comprised three days of the cold season (7th February, 15th February, 21st February). The sunny intervals in each day ranged between 30% and 60% of the daytime length, where 21st February witnessed 5:24 hours as the longest sunny duration in this group versus 2:54 hours as the shortest sunny duration that was recorded on the first day of this group (7th February). The daytime increased by about one hour from the first day (9:20 hours) and last day (10:15 hours). The on-site measurements and the weather station measurements are showed by [Figure 5.22](#).

The highest hourly average value of the ambient air temperature was recorded at 15th February about 8°C while 3°C represents the lowest value in this group, recorded on 7th February. The greatest hourly average of the solar energy was 447 W/m² at 21st February, while the weakest average was recorded at 7th February as 279 W/m². 21st February witnessed the highest hourly average of wind speed (as 5.65 m/s) in contrary to 7th February that recorded 0.8 m/s as the lowest hourly average.

Although the locations of H7, H8, H10 and H11 witnessed some activity, especially in the afternoon period of 21st February, mostly, the in-situ measured air temperatures moved in a smooth parallel pattern to the change of ambient air temperature. This refers to the primary link the field measurements and the ambient air temperature while the role of urban configuration was secondary or significantly ineffective due to the weak effect of solar radiation compared to the hot season.

5.4.3 The cloudy days measurements

[Figure 5.23](#) shows the hourly average of the air temperature near ground surface (2.5-3m height) for the eleven locations throughout six cloudy days of the cold season (2nd, 5th, 10th, 11th, 20th, 25th of February) in addition to the weather station's measurements. 25th February witnessed the highest hourly average value of the ambient air temperature (as 10.8°C) while the lowest value in the cloudy day was recorded at 2nd February (as 1.2°C). The minimum hourly average of the solar energy was 64 W/m² 11th February, while the maximum average was recorded on 25th

February as 283 W/m^2 . The highest hourly average wind speed (3.8 m/s) was recorded on 11th February while the lowest hourly average (0.7 m/s) was recorded on the 2nd February.

In general, the differences of on-site air temperatures were convergent between most locations irrespective of the day period and there was a common tendency for these differences to follow the ambient air temperature changes. This behaviour refers to the limited impact of the urban environment on air temperature because weak intensity solar energy, absence the direct radiation and the short length of daytime compared to the hot season circumstances.

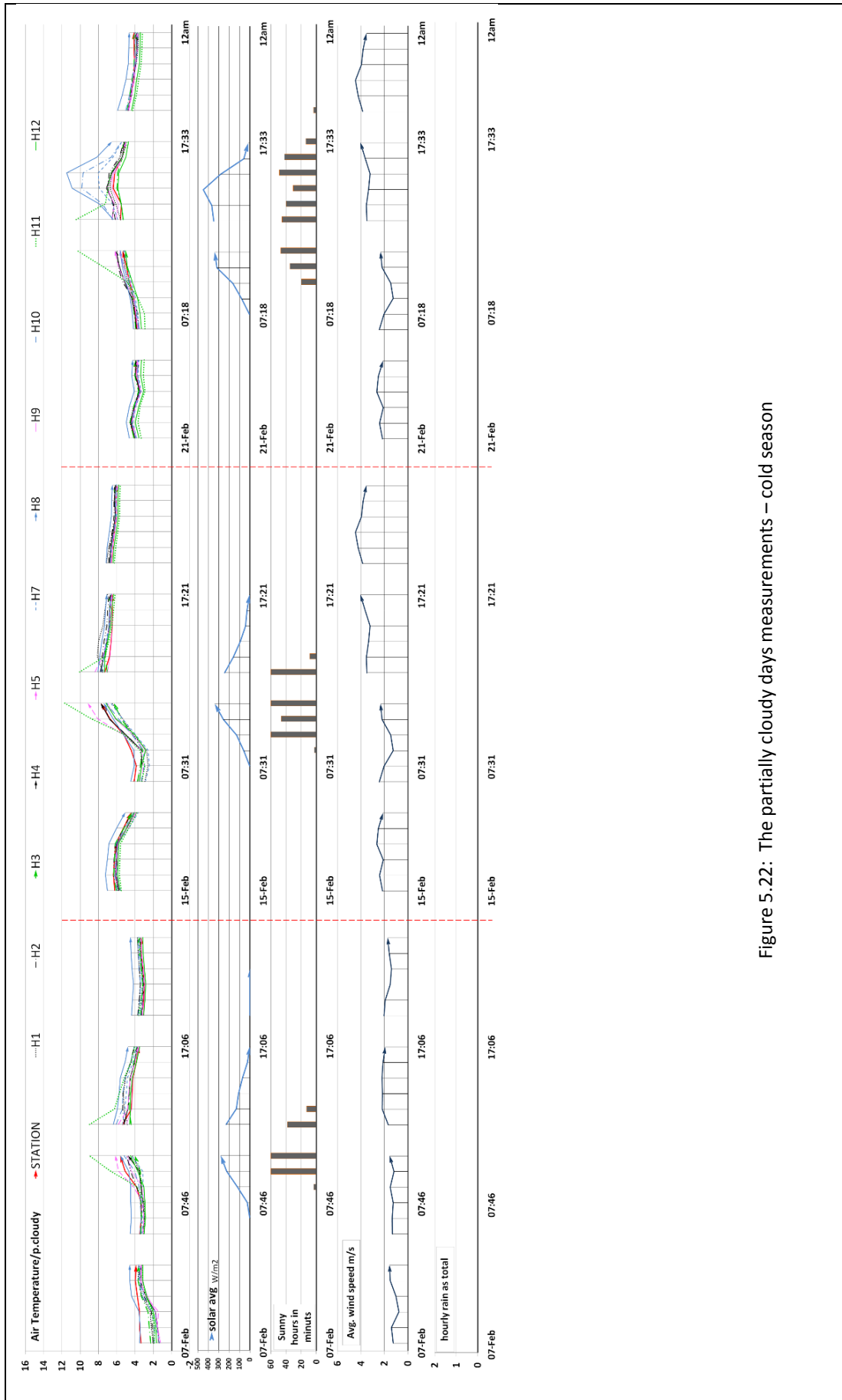


Figure 5.22: The partially cloudy days measurements – cold season

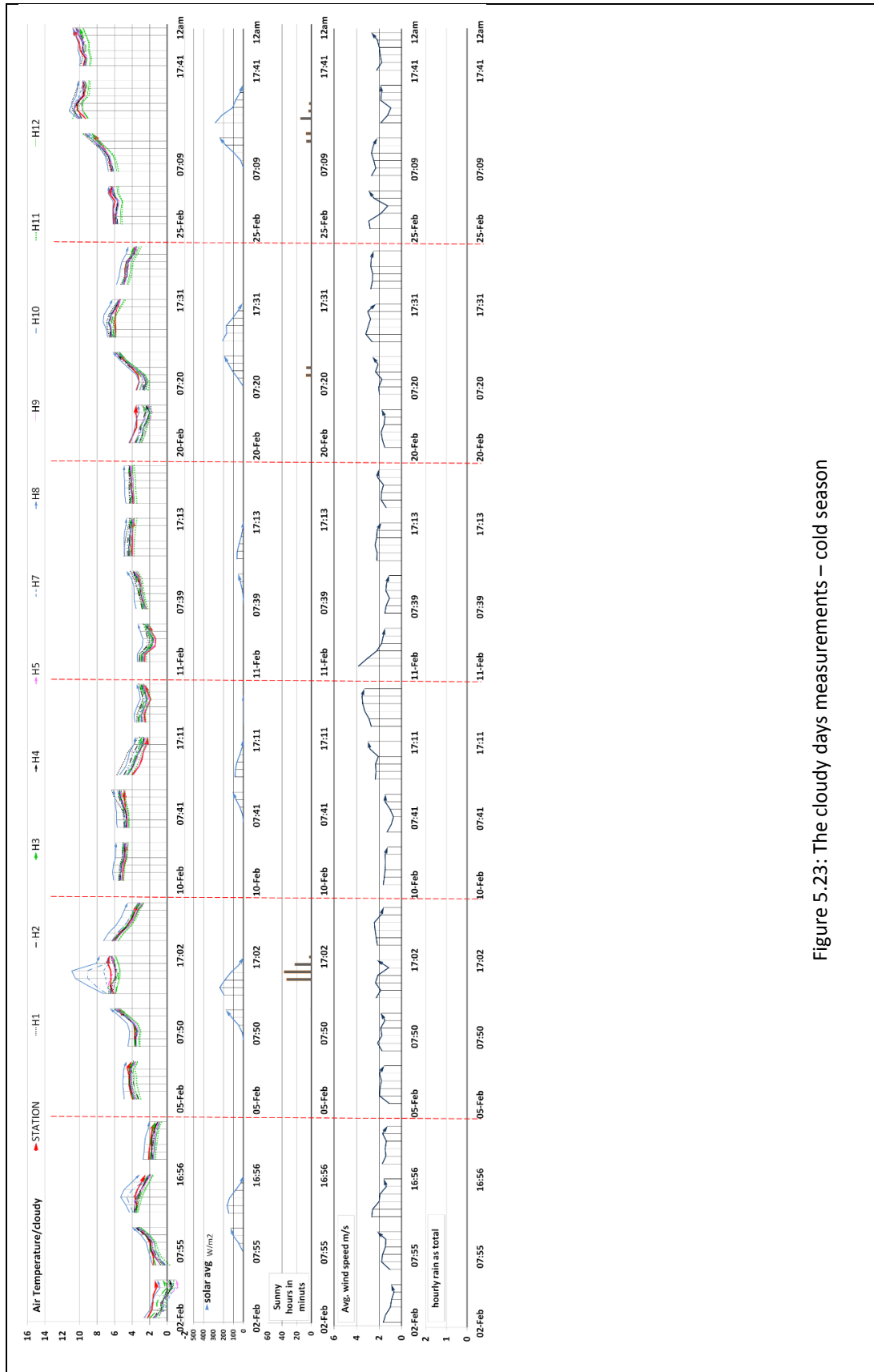


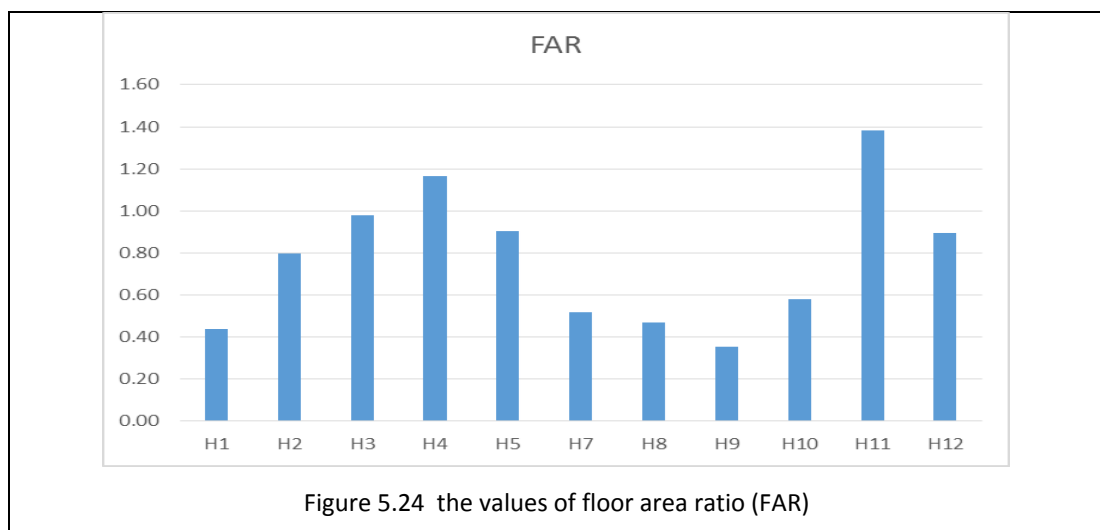
Figure 5.23: The cloudy days measurements – cold season

5.5 The urban morphological parameters measurements

The urban morphology of the all measurement locations (except H6) within the buffer zone was measured by the ten parameters. The results of each parameter will be explained briefly to be aware about the differences between them in terms of express the configuration of each location.

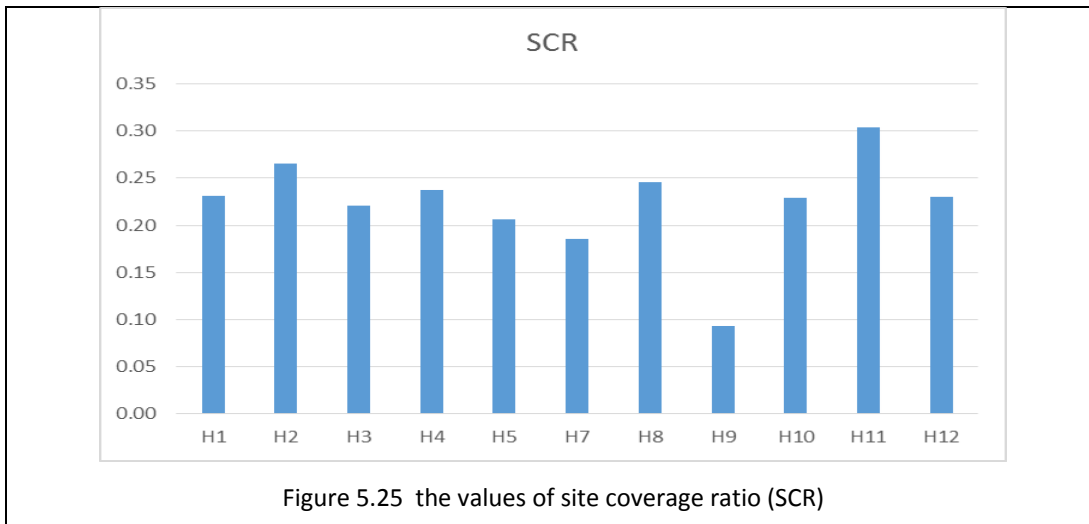
5.5.1 Floor Area Ratio (FAR)

Figure 5.24 shows obvious differences in terms of FAR values, where the locations with higher gross floor area of the buildings because the bigger number of floors and the bigger area of floor recorded the higher values of FAR such as H11, H4, H3, H5 and H12. In contrast the other locations like H9, H1, H8 and H7 showed the lower domination of buildings on the location compared to the first group.



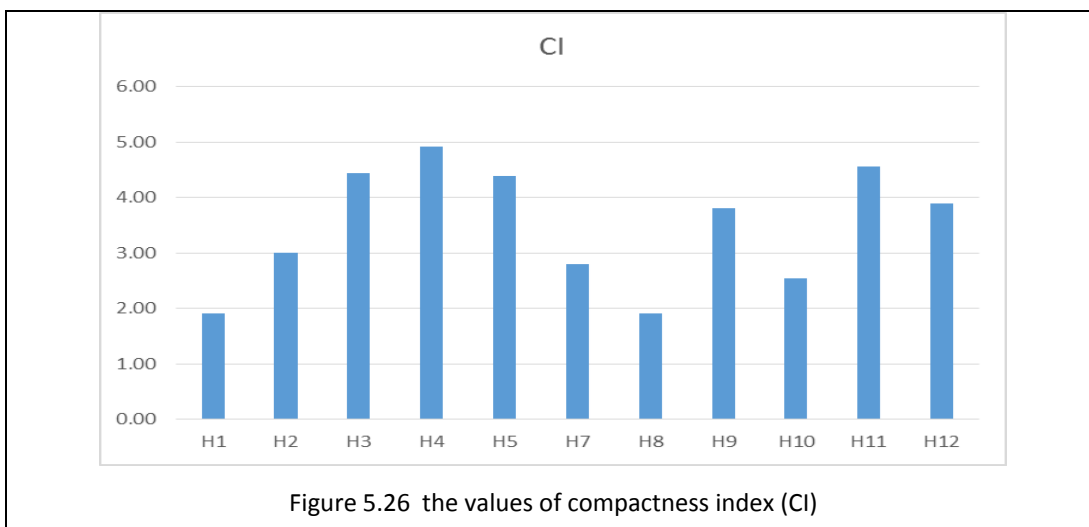
5.5.2 Site Coverage Ratio (SCR)

Figure 5.25 shows there is convergent between SCR values although the location H9 recorded for the second time the lowest value of a parameter in contrast with each of H8, H1 and H7 that recorded high values. This means the built ground floor area is convergent between the most of locations although the shapes of ground floor are different from location to another.



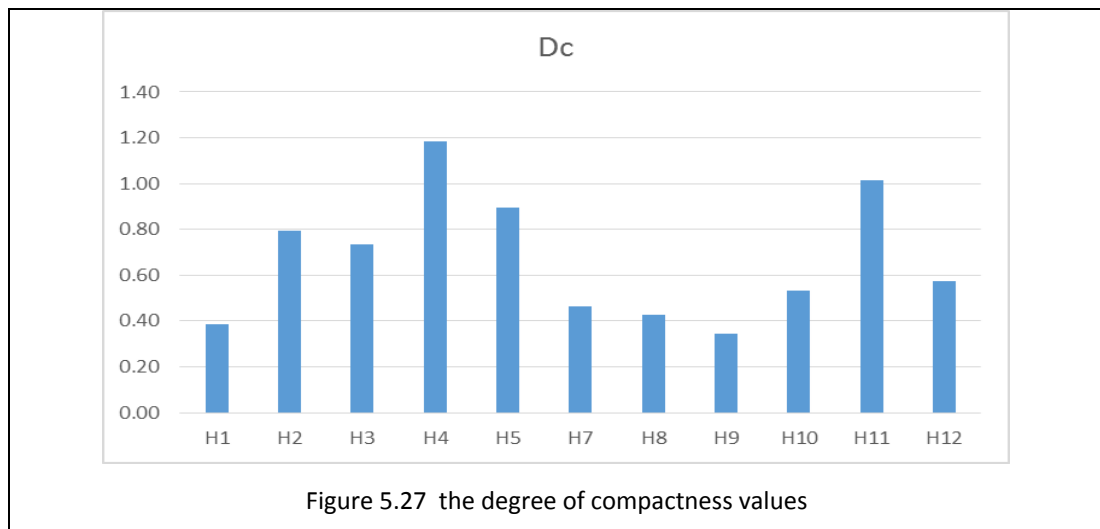
5.5.3 Compactness Index (CI)

Figure 5.26 shows the values of CI, where it can be noticed there is similarity with FAR in terms of spatial distribution of values although H9 recorded high value compared to some locations. The reason behind that is CI represents the ratio between FAR and SCR and because of the convergence between the SCR values, the pattern of FAR values is dominant.



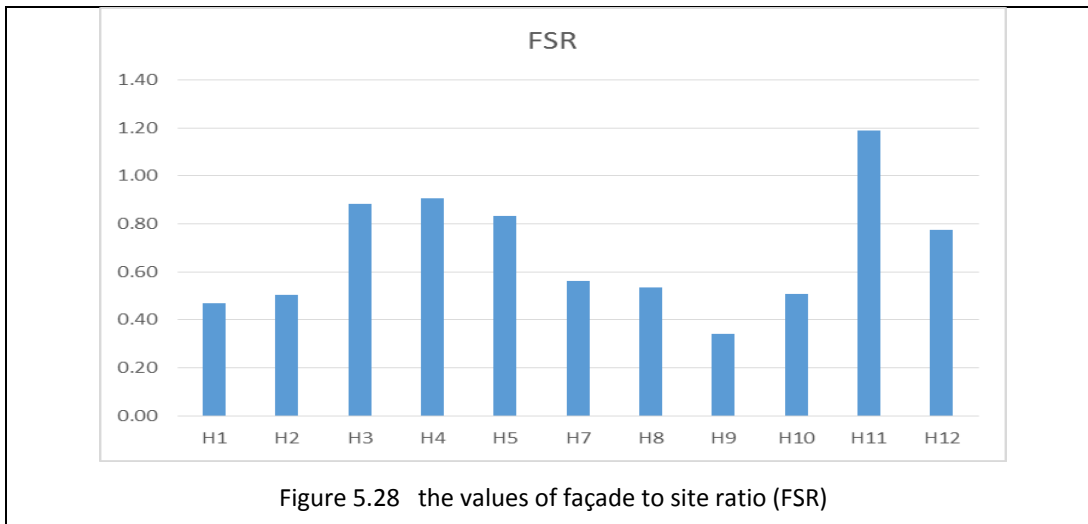
5.5.4 Degree of Compactness (Dc)

Figure 5.27 illustrates the values of Dc that follow the patterns of the FAR and CI values. The reason is belong to one factor. the area of location (buffer zone) is the same between all measuring points, therefore the results of calculation method of degree of compactness ($Dc = SCR * \text{the average number of floors}$) be more similarity to the values of gross floor area, especially the ground floor is similar to upper floors for most building types in the case study.



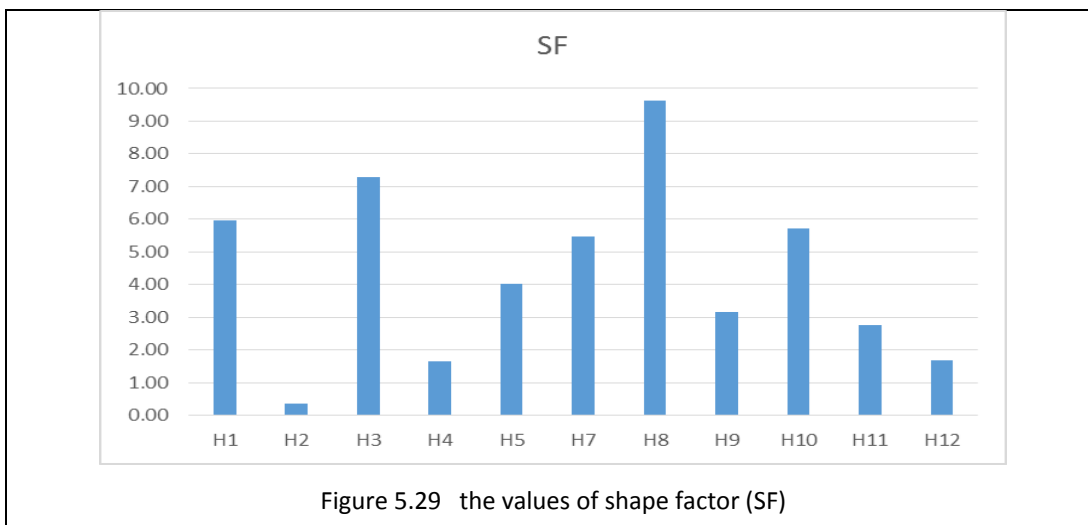
5.5.5 Facade to Site Ratio (FSR)

The spatial pattern of FSR values that shown by Figure 5.28 converge to the distribution of FAR values. Due to the total facade area of building in each location is a reflection of the value of gross floor area as a result to the similarity of areas and shapes between the ground floor and its upper floor for most buildings within the buffer zone that in turn it covers the same area for all measuring points.



5.5.6 Shape Factor (SF)

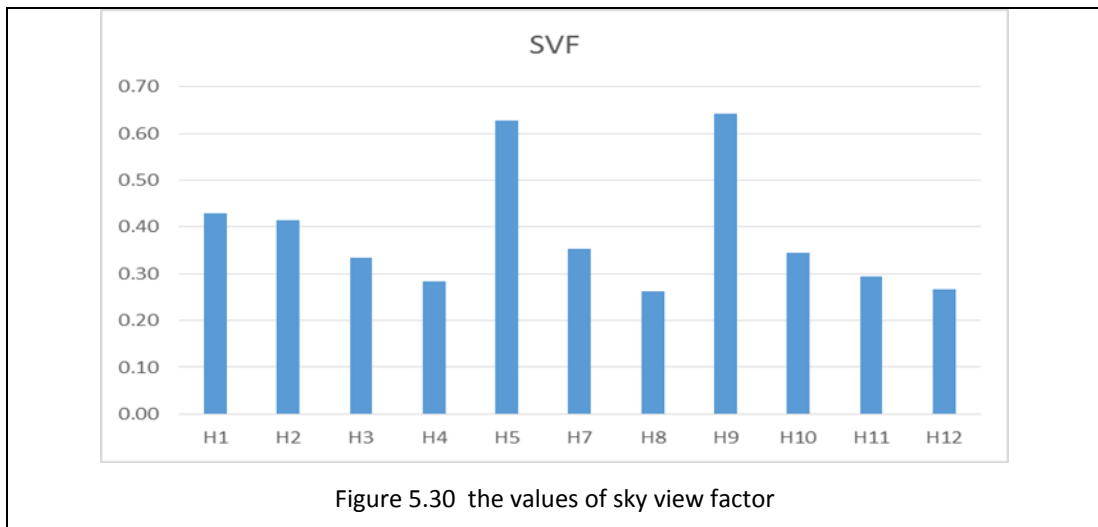
Figure 5.29 shows that the locations H2, H4 and H12 have the more compacted buildings that recorded lower ratio between the total surface area and volume. Contrary, the buildings within locations H8, H3, H1, H10 and H7 recorded the highest values of SF.



5.5.7 Sky View Factor (SVF)

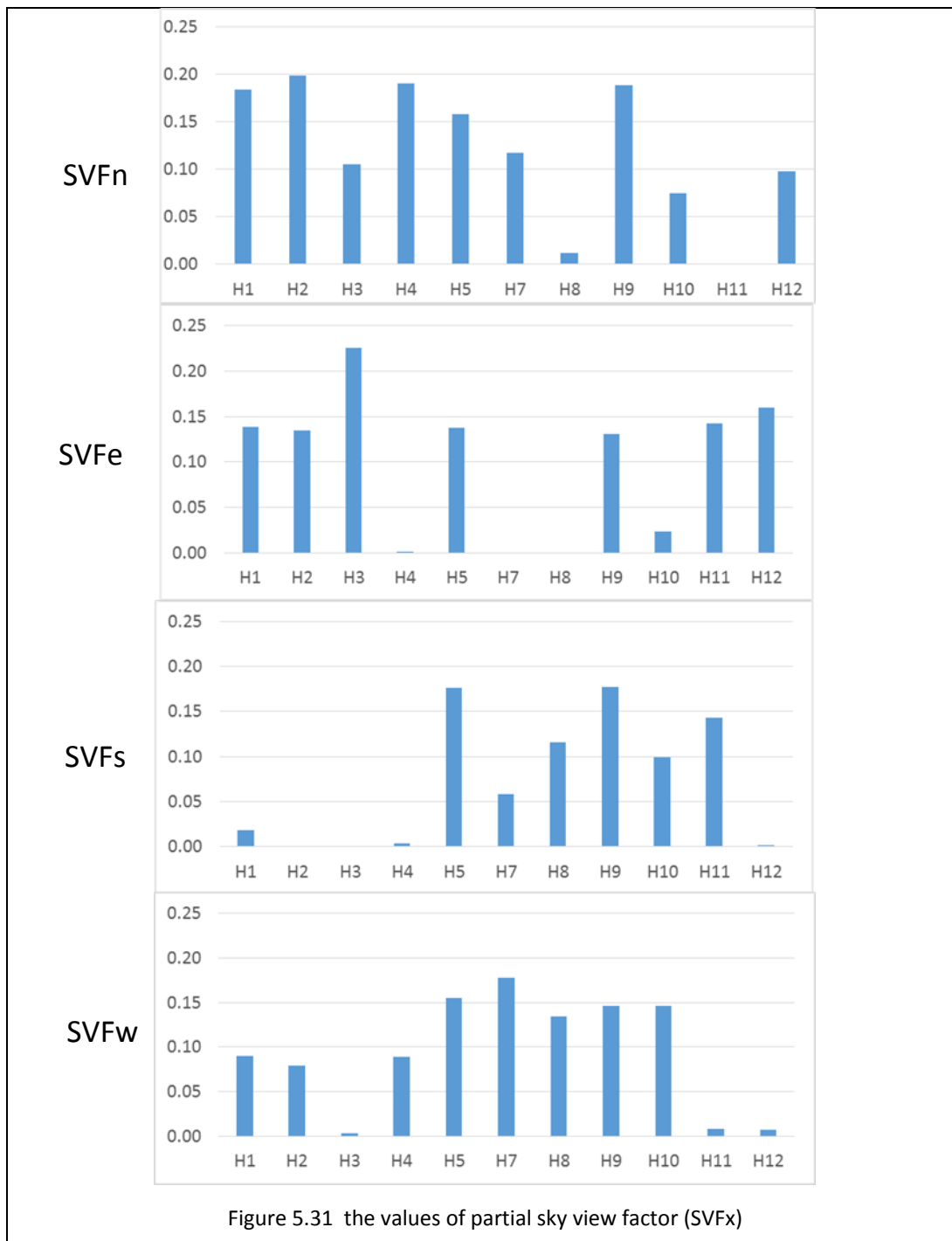
The openness degrees to the sky are convergent in H5 and H9, and they are bigger notably compared to other locations. H1 and H2 have about the same values of SVF that in turn are bigger than the convergent values of H3, H7 and H10. While H4, H8,

H11 and H12 recorded the lowest openness degrees to sky compared to other locations as shown by [Figure 5.30](#).



5.5.8 Partial Sky View Factor (SVF_x)

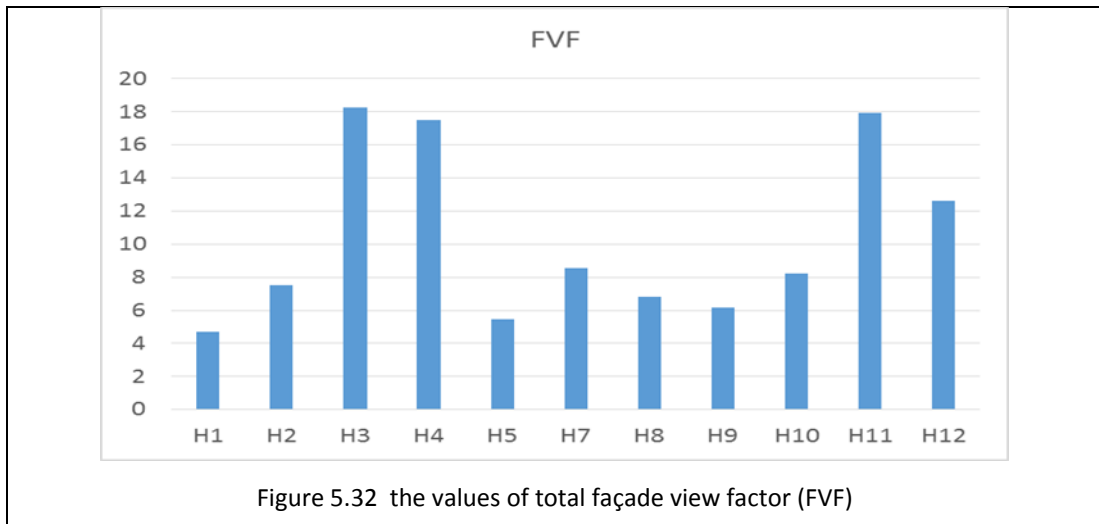
[Figure 5.31](#) shows that the morphology of each location can be described by four values of the openness degree to the sky according to the cardinal directions. It can be noticed that each subdivision shows different pattern in terms of the spatial distribution of values, and this gives a high peculiarity of the morphology of each location that cannot be expressed by the solo value of SVF.



Where some locations about completely open to the sky on one direction and about completely blocked on another direction such as H2 and H3. On the other hand, some location open widely to the sky on all directions such as H5 and H9

5.5.9 Total Façade View Factor (FVF)

Figure 5.32 shows that the locations that surrounded by the higher buildings recorded the higher values of FVF such as H3, H11, H4 and H12 because of the large façade areas around these locations compared to others that recorded more homogeneous values. It can be said FVF represent the compactness of urban space around the measurement point.



5.5.10 Façade View Factor (FVFX)

Figure 5.33 shows that there are just four subdivisions of FVFX instead of eight as mentioned before, because of the building facades block the same four directions around the all measuring point.

It is clear that morphology of space around the measuring point was represented more accurately by four values instead of the one value of FVF.

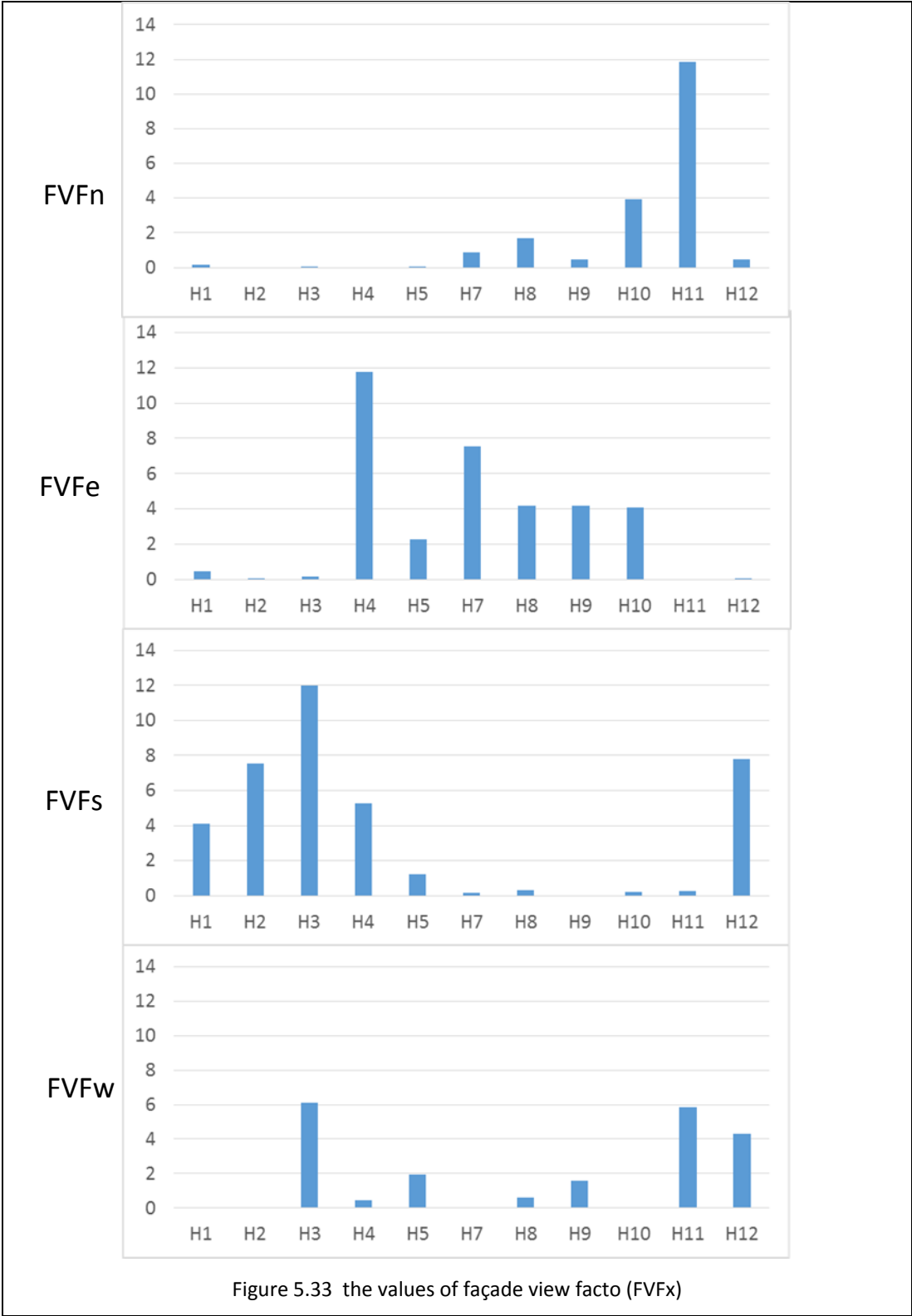


Figure 5.33 the values of façade view facto (FVFX)

5.6 The correlations of urban morphological parameters (UMP)

The urban morphological parameters (UMP) are utilized to describe the relationship between mass and spaces by measuring the configuration of a specific urban site, numerically, by using general inputs like dimensions, areas and sizes. The urban morphological parameters represent a part of the variables of the statistical analyses in the next chapter. Thus, uncovering the strength of these linkages may help in understanding the relationships between UMP and air temperature depending on the shared configuration features between the measurement locations on the one hand and the similarity degree of air temperature behaviours in these location on the other hand. This section is, therefore, devoted to exploration and discussion of linkages between UMP depending on the significant correlation, as shown by [Table 5-2](#). The red cells represent the significant linkages ($p \leq 0.05$) and the bold values represent the strength of these linkages.

Table 5-1: The correlation coefficients (r) and significant levels (p-value) of UMP

	CI	Dc	FAR	FSR	FVF	FVFe	FVFn	FVFs	FVFW	SCR	SF	SVF	SVFe	SVFn	SVFs
CI															
Dc	0.75														
	0.007														
FAR	0.79	0.91													
	0.004	0													
FSR	0.74	0.8	0.95												
	0.01	0.003	0												
FVF	0.7	0.66	0.82	0.81											
	0.016	0.028	0.002	0.003											
FVFe	0.114	0.194	-0.07	-0.08	0.088										
	0.738	0.569	0.843	0.819	0.797										
FVFn	0.159	0.279	0.479	0.54	0.388	-0.22									
	0.64	0.407	0.136	0.086	0.239	0.512									
FVFs	0.297	0.247	0.332	0.22	0.462	-0.32	-0.41								
	0.375	0.464	0.319	0.516	0.152	0.335	0.215								
FVFW	0.62	0.304	0.63	0.72	0.694	-0.5	0.427	0.401							
	0.042	0.364	0.038	0.013	0.018	0.115	0.19	0.221							
SCR	0.004	0.53	0.62	0.579	0.411	-0.28	0.505	0.22	0.222						
	0.99	0.094	0.043	0.062	0.209	0.405	0.113	0.516	0.511						
SF	-0.52	-0.5	-0.45	-0.21	-0.198	0.003	-0.05	-0.19	-0.05	-0.069					
	0.102	0.12	0.167	0.531	0.56	0.993	0.891	0.579	0.894	0.84					
SVF	0.088	-0.2	-0.36	-0.38	-0.579	-0.11	-0.3	-0.27	-0.2	-0.666	-0.16				
	0.797	0.562	0.283	0.255	0.062	0.757	0.37	0.42	0.562	0.025	0.642				
SVFe	0.363	0.058	0.272	0.255	0.194	-0.8	0.004	0.58	0.69	0.01	-0.21	0.3			
	0.272	0.865	0.418	0.45	0.567	0.003	0.992	0.061	0.019	0.977	0.529	0.4			
SVFn	0.105	0.035	-0.22	-0.4	-0.306	0.205	-0.7	0.282	-0.45	-0.457	-0.47	0.6	0.143		
	0.758	0.918	0.509	0.224	0.36	0.545	0.016	0.402	0.171	0.158	0.144	0.1	0.675		
SVFs	0.054	-0.13	-0.15	-0.03	-0.344	0.007	0.394	-0.79	0.018	-0.336	0.171	0.6	-0.1	-0.28	
	0.876	0.711	0.655	0.924	0.301	0.984	0.231	0.004	0.958	0.313	0.615	0.1	0.763	0.399	
SVFW	-0.44	-0.38	-0.66	-0.62	-0.727	0.528	-0.3	-0.7	-0.79	-0.525	0.26	0.5	-0.65	0.235	0.475
	0.176	0.248	0.026	0.041	0.011	0.095	0.363	0.017	0.004	0.097	0.441	0.1	0.03	0.487	0.14

All significant correlations showed good values that exceeded the barrier of 60%. Some of these parameters had many linkages, like Floor Area Ratio (FAR), while some of them showed solo correlation, like SVF. The trends of these correlations may be positive or negative.

The correlation value ($r = -0.66$, $p = 0.025$) show that the sky view factor (SVF) had a negative morphological relationship with the site coverage ratio (SCR). Increasing SCR led to a decrease in the intra-spaces between the urban blocks and, therefore, the openness to sky will shrink and be followed by diminishing SVF value. SVF had no linkages with the other urban morphological parameters that are affected by the height of buildings, like FAR, the degree of compactness (Dc) and the façade to site ratio (FSR), although the skyline that control SVF is affected by the high. This may own to the nature of SVF that counts just the visible surfaces around the observation point, while the other parameters take into account the urban blocks' heights for the site irrespective the measurement point. The negative acceptable correlation between SVF and FVF ($r = -0.58$, $p = 0.062$) may support this suggestion although it is insignificant. Both of them are affected by only the visible surfaces in addition to the location of measurement point.

The façade to site ratio (FSR) has strong significant correlations with each of the parameters: FAR ($r = 0.945$, $p = 0$), Dc ($r = 0.798$, $p = 0.003$), FVF ($r = 0.798$, $p = 0.003$) and CI ($r = 0.735$, $p = 0.01$). Where the façade area is affected by the height of building and dimensions of floors and these two factors in addition to the site area which affect the values of the other parameters.

The total façade view factor (FVF) has positive correlation with CI, Dc, FAR and FSR due to it considering the facade area; however, its correlations with FAR and Dc were weaker than correlations of FSR with the same parameter due to FVF dealing with the visible facades to the measurement point compared to FSR that counts all the façade areas in the urban site regardless the point.

It is worth noting that the values of some UMP were subjected to the configuration of western sides of the urban spaces. The western subdivisions of the partial sky view factor (SVFw) and the façade view factor (FVFw) have positive correlations with FAR,

FSR, FVF, CI and negative correlation between them because SVFw expresses the void and FVFw expresses the solid. The other subdivisions (SVFn, SVFe and SVFs) also have negative links with their counterparts (FVF_n, FVF_e and FVF_s) for the same reason.

The positive correlation has been noticed between SVFe and FVFw and this may be owing to the statistical process where the locations that show dominance of the western surfaces like H3 and H11 have high values of FVFw and low values of SVFw and vice versa for the eastern sectors while the locations that show dominance of eastern walls like H7 and H10 have high values of FVFe and low values of SVFe and vice versa for the western sectors

The compactness index (CI) and SCR did not show a significant correlation ($r=0.004$, $p=0.99$) although SCR is a part of calculation method of the CI and this may be because there is no real difference between the area of ground floor and the area of each upper floor for the same building or block. Therefore, CI, depending on its calculation method, will represent the average number of floors that describes the vertical configuration of urban area and this causes the lack of relationship with SCR that describe the horizontal configuration. However, SCR had a significant positive correlation with FAR ($r=0.62$, $p=0.043$) because these two parameters change in similar tendency for locations H4, H5, H7, H9, H10 and H11.

The urban morphological parameters (FAR, CI and Dc) have positive correlations with each other due to the common factors in their calculation methods, such as the site area, the ground floor area and the number of floors however the similarity of ground floors and the upper floors, in terms the area, for the most buildings in the site contributes in these correlations. Therefore, these parameters witnessed a convergence in their changes from one location to another.

Despite these linkages, there is no guarantee that parameters with strong bonds will contribute to the interpretation of air temperature variations in the same efficiency, which may be revealed by the results of the statistical analyses.

5.7 Conclusion

This chapter was devoted to the review and discussion of field measurement results in terms of the variation of air temperatures in the hot and cold seasons under the temperate maritime climate of the city of Liverpool, UK.

These results, for the hot season, revealed that the behaviours of on-site measured air temperatures were notably modified compared to the ambient air temperatures that were recorded about 700m from the residential compound in the weather station of Liverpool University. Although there were variations of sky conditions of the hot season days, the locations with convergent urban characteristics showed, in general, convergent behaviours. H3, H11 and H13 represented the most active locations throughout the morning period from 6 am till midday - maybe owing to the configuration of the western sides of the urban spaces. The air temperatures at locations H7, H8 and H1 dominated the afternoon period from midday till 6 pm due to the likely effect of eastern sides configuration for the spaces around these measurement points. For the most part, H8 appeared as the hottest location till sunrise because of the compact configuration of its space that supported the effect of western surfaces. Generally, H1, H2 and H4 represented the coolest locations owing to the role of buildings on the southern side of urban spaces in blocking the direct solar radiation throughout the day. Although H5 and H9 were similar, the former was usually warmer than the latter because of the space around the measurement point. H5 was more compact than H9. Their activities increased after sunrise and were distinguished at the afternoon period, especially under the sunny sky. As a rule, the air temperatures of all locations be more moderate and be more convergent with absence of solar radiation.

Regarding the cold season results, some behaviours that were noticed in the hot season continued in the cold season, especially in locations H7, H8 and H10. However, the behaviours of most locations were submissive to the ambient air temperature variation because of the weakness of the urban configuration role in affecting the temperatures as a result for shortness of daytime duration and weakness of solar radiation intensity in the cold season.

This study, therefore, recommends the hot season data as inputs for the statistical analyses to explore the relationships between the urban configuration parameter and the air temperature. These behaviours in the hot season are likely to have been modified by the impact of the urban environment surrounding the measurement points.

The last part of this chapter aimed to reveal and discuss the correlations of the urban morphological parameters with each other. Some parameters had no correlation at all with others like the shape factor (SF), while some of them had correlations with many parameters at the same time, like the total façade view factor (FVF). The linkages between the urban parameters may be an important step to discussing the statistical analyses results, where these parameters represented another input of this analyses.

Chapter Six

6 Results and Analyses

6.1 Introduction

This chapter explores the stepwise multi-linear regression analysis that was conducted to identify any relationships between the urban morphological parameters (UMP) and thermal microclimate indicators in terms of variations in on-site measured air temperatures (T_a) on three levels: hourly average (average- T_a or AVG), hourly maximum (maximum- T_a or MAX) and hourly minimum (minimum- T_a or MIN), and, depending on the dissimilarity of daily periods (night, morning, afternoon and evening) under each of the sky conditions (sunny, partial cloudy and cloudy) throughout a set duration of the hot season. Utilizing a statistical approach and, especially, linear regression is common in urban environmental research (Unger et al. 2001; Eliasson & Svensson 2003; Al-sudani & Sharples 2016; JUSUF et al. 2016; Hien et al. 2012; Ng 2010). The description and analyses of results were done relying on values of Adjusted R-squared ($R\text{-Sq}(\text{adj})$) for the models that showed significant levels (P-value) lower than or equal to 0.05. Also, the standard error of the regression (S) will be referred to investigate the increasing accuracy of the statistical models after adding the urban morphological parameters (UMP). S is similar to $R\text{-Sq}(\text{adj})$ in terms of the adjustment for the number of predictors in a regression model (Frost 2014), where both of them do not change unless the new independent variable has a real impact on the statistical model.

The first group of analysis used two datasets: the on-site measured air temperatures (T_a) as the dependent variable and the weather station measurements (ambient air temperature (a. T_a) and solar radiation) as independent variables to produce Basic Models (B.M) for the three thermal microclimate indicators (AVG, MAX and MIN) for each of the four daily periods under any of the three skies circumstances. The second group of analysis follows a similar approach by utilizing the same datasets but increasing the independent variables to be three by adding one of the urban morphological parameter (UMP) each time to produce Modified Models (M.M). The Modified Models (M.M) represent the combined influence of the climatic factors (ambient air temperature (a. T_a) and SOLAR) and each one of the urban morphological

parameters, [Compactness index (CI), Degree of compactness (Dc), floor area ratio (FAR), Façade to site ratio (FSR), total façade view factor (FVF), façade view factor (FVFX), Site Coverage Ratio (SCR), shape factor (SF), sky view factor (SVF) and partial sky view factor (SVFX)], on in-situ measured air temperature.

The R-Sq(adj) values for the 369 statistical models represent the basis of the comparison between B.M and M.M. The augmentation of the R-Sq(adj) values, after adding the urban parameters (UMP), revealed the role of the UMP in the variation of air temperature (Ta) as AVG, MAX and MIN. The convergent values of R-Sq(adj) for B.M and M.M indicated that the on-site air temperature was almost completely affected by the climatic factors (a.Ta and solar), with the UMP having no substantial influence on Ta. Contrariwise, the divergent R-Sq(adj) values between B.M and M.M refers to the effects of the UMP on the Ta, where this influence increased by increasing the R-Sq(adj) values for the modified models (M.M). To investigate the accuracy of the models and to explore more benefits of UMP, the decreasing value of the standard error of the regression (S) values for the modified models (M.M) compared to the basic models (B.M) revealed the contribution of the UMP in ameliorating the accuracy of models.

The mathematical signs for the independent variables of the statistical models (B.M and M.M) will be considered to reveal the effects of these variables in terms of raising or lowering the on-site air temperature and the contribution of a.Ta and solar in this regard.

A set of 19 days of data, from the field measurements that were conducted in the hot season between 29th July 2014 and 3rd September 2014, were selected and categorised, according to the sky conditions, in to sunny days, partial cloudy days and cloudy days.

6.2 Sunny days analyses (su-hot)

A group of five days (4th, 7th, 9th, 15th August and 2nd September) were chosen as sunny calm days. The sunrise times of these days ranged from 5:32 for the first day to 6:22 for the last day, while the sunset times moved from 21:02 to 19:59. The

datasets of these days have been distributed and processed as four daily periods that can be defined as:

6.2.1 Night period: midnight to 6.00 am (ni-su-hot)

It is the first period of the sunny days, the night time extended from midnight to 6.00am. This period involved 33 models [see Figure 6.1]. Three of them represent the basic models (B.M) that clarifies the influence of climate factors (ambient air temperature (aT.a) and solar) on the three indicators of thermal microclimate (AVG, MAX and MIN). The B.M explained about 88% of the Ta variation, and this leaves around 12% to be interpreted by all other variables, which include the urban morphological parameters (UMP). Each of FSR, FVF and SCR did not succeeded in explaining the variation; on the contrary, the highest improvement of R-Sq(adj) was achieved by adding the novel parameter (SVFx) as AVG. 91.2%, MAX. 90.0% and MIN. 90.5%. The addition of SF gave enhancement rates close to the SVFs rates (91.1%, 90.0% and 90.3%). SVF, FVFX (the novel parameter), CI, FAR and DC respectively added less than 1% in approving R-Sq(adj) compared to values of the B.M. In general, AVG witnessed the highest values of R-Sq(adj) compared to MAX and MIN, while the (MAX and MIN) had very similar values.

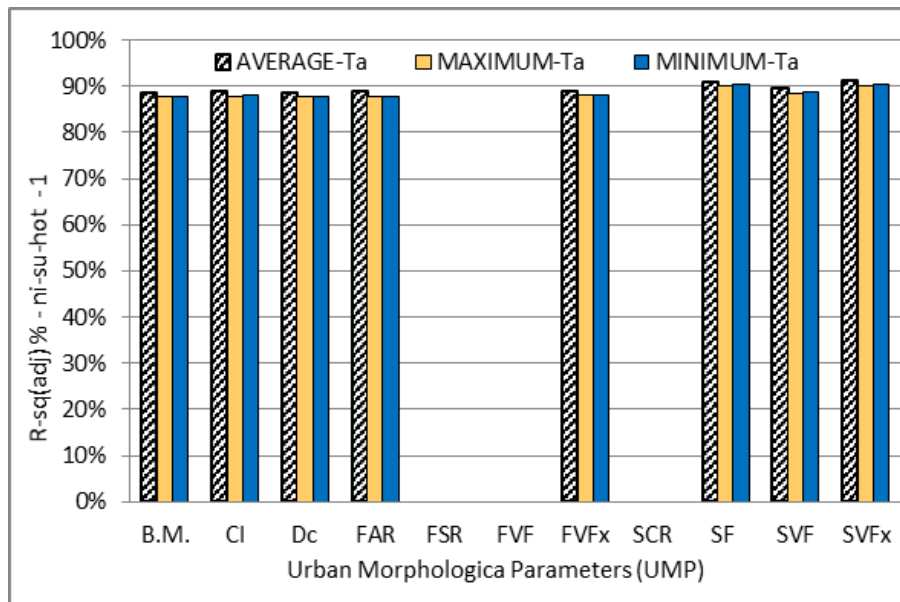
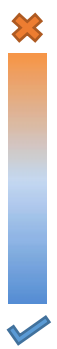


Figure 6.1 Percentages of R-Sq(adj) for the basic and modified air temperature models in (ni-su-hot)

In terms of the standard error of regression (**S**) of the ni-su-hot period, the accuracy of the models generally improved by adding UMP; the shift of colour scale from the orange colour to the blue colour is a sign of this improvement with a decline in the **S** values as shown in the **Table 6-1**. The models with SVFx and SF showed the best rates of accuracy respectively; while Dc and FAR displayed a lowest reduction of **S** compared to other parameters.

Table 6-1 the values of standard error of the regression (**S**) for (ni-su-hot)

S	<i>ni su hot</i>	1	
	avg	max	min
B.M.	0.419067	0.440274	0.435205
CI	0.4151	0.43568	0.431881
Dc	0.417762	0.43879	0.433981
FAR	0.417162	0.43787	0.433731
FSR	x	x	x
FVF	x	x	x
FVFX	0.41191	0.434702	0.427581
SCR	x	x	x
SF	0.371868	0.396596	0.389466
SVF	0.403637	0.427326	0.418633
SVFx	0.36939	0.395805	0.384715



In terms of fluctuating the on-site measured air temperature (T_a), the independent variables (solar, $a.T_a$ and UPM) may have influence that can be elucidated relying on the mathematical signs of these variables in the regression models. The plus sign (+) refers to the ability of the variable to increase T_a and the minus sign (-) refers to the ability of the variable to decrease T_a . Therefore, the basic models (B.M) of (ni-su-hot), according to **Equations 6-1**, show that the increasing of ambient air temperature ($a.T_a$) leads to an elevation in T_a in a direct relationship, while increasing solar radiation has an opposite effect that leads to a reducing T_a in an inverse relationship. While the signs of modified models (M.M) for a one period are gathered in a one symbolic table and the complete details of these models are shown in Appendices (A, B and C).

$$\text{AVERAGE-Ta} = -1.513 - 0.01968 \text{ avg solar} + 1.1143 \text{ avg a.Ta}$$

$$\text{MAXIMUM-Ta} = -1.214 - 0.01471 \text{ max solar} + 1.0960 \text{ max a.Ta}$$

$$\text{MINIMUM-Ta} = -1.762 - 0.0514 \text{ min solar} + 1.1303 \text{ min a.Ta}$$

Equations 6-1 Basic models (B.M.) of (ni-su-hot)

In **Table 6-2** is divided into three main horizontal sections according to the three independent variables (solar, a.Ta and UMP) and each section is divided into three rows according to the air temperature indicators (AVG, MAX and MIN). The titles of the ten columns represent the ten urban morphological parameters (UMP). Two of these parameters (FVFX and SVFX) have subdivisions, therefore the statistical models of each of them include six variables instead of the three variables like the others. For example, FVFX models include (aTa, solar, FVFN, FVFE, FVFS and FVFW). In terms of symbols, dark cells refer to the failed models where the adding of UMP did not contribute in improving the explanatory power ($R\text{-Sq}(\text{adj})$) for a one or more of the three indicators of thermal microclimate. The star symbol (*) refers to failure a one or more of the following independent variables (solar, a.Ta and subdivisions), while; Plus and minus signs (+ & -) refer to increasing and decreasing the on-site measured air temperature (Ta) respectively.

Table 6-2, as a sample, shows an inverse relationship between solar radiation and Ta which, at the same time, had a direct relationship with a.Ta. A group of UMP like CI, Dc, FAR and SVF show a counteractive behaviour to Ta where the increase of their values leads to a reduction in the values of AVG, MAX and MIN; conversely, the variable (SF) showed positive signs. In terms of FVFX and SVFX, they displayed a contradictory behaviour. While the subdivisions of FVFX (FVFE and partially FVFW) elevate the Ta, the subdivisions of SVFX (SVFN and SVFE) have a negative effect on it. The other subdivisions of FVFX and SVFX may have no real effect on thermal microclimate in this period.

Table 6-2 The signs of modified models (M.M.) for (ni-su-hot)

		The Details of Urban Morphological Parameters (UMP)																
		CI	Dc	FAR	FSR	FVF	FVFX				SCR	SF	SVF	SVFX				
							FVFn	FVFe	FVFs	FVFw				SVFn	SVFe	SVFs	SVFw	
Independent variables of modified models (M.M.) / ni- su- hot	UMP	AVG	-	-	-	X	X	*	+	*	+	X	+	-	-	-	*	*
		MAX	-	-	-	X	X	*	+	*	*	X	+	-	-	-	*	*
		MIN	-	-	-	X	X	*	+	*	+	X	+	-	-	-	*	*
	a. Ta	AVG	+	+	+	X	X			+		X	+	+				+
		MAX	+	+	+	X	X			+		X	+	+				+
		MIN	+	+	+	X	X			+		X	+	+				+
	SOLAR	AVG	-	-	-	X	X			-		X	-	-				-
		MAX	-	-	-	X	X			-		X	-	-				-
		MIN	-	-	-	X	X			-		X	-	-				-

6.2.2 Morning period: 6.00 am to 12.00 noon (mo-su-hot)

The morning period covers the time between 6.00 am and 12.00 noon as a second period of the sunny days group. R-Sq(adj) values for the B.M, (43.3%, 42.3%, and 45.4%) as AVG, MAX and MIN respectively, indicated that the ambient air temperature and solar radiation, as independent variables, account for less than 50% of the variance in the measured air temperature, as the dependent variable. The UMP may contribute partly in explaining the rest of the change, but SF fails in that respect, according to [Figure 6.2](#).

The novel parameter FVFX showed a greater potential to improve the ability of the statistical models (60.1%, 63.4% and 57.5% for AVG, MAX and MIN respectively). Furthermore, the other novel parameter, SVFX, was second, with values very close to the first.

Both show the same behaviour in terms of AVG, MAX and MIN, where MAX models show higher rates of R-Sq(adj) compared to the AVG and MIN models respectively.

Although CI, SCR, Dc and SVF have promoted their models, the explanatory powers of these models were under 50%, while the third novel parameter, FVF, elevated this ability to exceed the midline and settled at 51%, with no real difference between the

three indicators. Both FSR and FAR exceeded the ceiling of 50% also to be the third and the fourth in the order of UMP affecting the thermal microclimate in this period.

The standard error of the estimate (**S**) completes the image of how well the models fit the data, where **Table 6-3** shows that the accuracy tracks the same steps of R-Sq (adj). The **S** values recorded their lowest levels with the FVFX and SVFX models respectively; while the SVF models occupied the opposite position. Generally, adding the UMP leads to expand the precision of the MAX models compared to the AVG and MIN models.

The independent variables (solar, a.Ta) connected to the on-site measured air temperature for the morning period from 6am to 12pm in a positive relationship, although, a.Ta has not contributed to explain the fluctuation of the on-site maximum air temperature according to **Equations 6-2**.

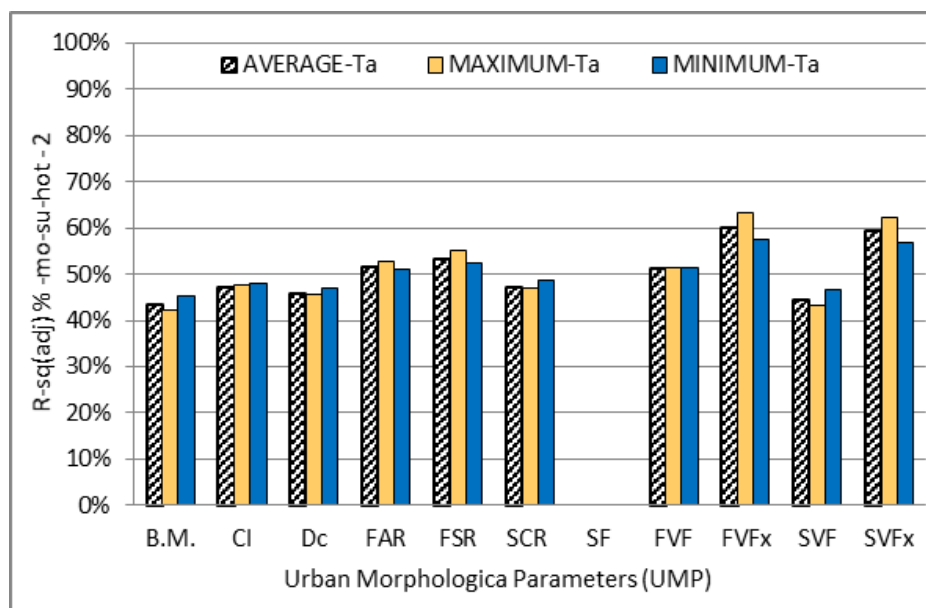


Figure 6.2 Percentages of R-Sq(adj) for the basic and modified air temperature models in (mo-su-hot)

Table 6-3 The values of standard error of the regression (S) for (mo-su-hot)

S	mo su hot		
	avg	max	min
B.M.	1.88653	2.01601	1.73642
CI	1.82019	1.91797	1.69666
Dc	1.84636	1.95784	1.7103
FAR	1.74562	1.82497	1.6426
FSR	1.71215	1.77942	1.62083
SCR	1.81947	1.93235	1.68506
SF	x	x	x
FVF	1.75208	1.85011	1.63561
FVFX	1.58294	1.60668	1.53249
SVF	1.86782	1.99765	1.71589
SVFX	1.6002	1.63202	1.54565



$$\text{AVERAGE-Ta} = 5.67 + 0.003435 \text{ avg solar} + 0.559 \text{ avg a.Ta}$$

$$\text{MAXIMUM-Ta} = 13.517 + 0.006722 \text{ max solar}$$

$$\text{MINIMUM-Ta} = 2.03 + 0.001310 \text{ min solar} + 0.8317 \text{ min a.Ta}$$

Equations 6-2 Basic models (B.M.) of (mo-su-hot)

Table 6-4 shows that both the climatic variables (a.Ta and SOLAR) had a positive impact on thermal microclimate. SVF displayed negative relations with AVG, MAX and MIN in contrast to other UMPs (CI, Dc, FAR, FSR, FVF and SCR), while SF failed completely in explaining the variation of Ta.

The subdivisions of FVFX might have no impact on some indicators like AVG and MIN for FVFe and MAX for FVFs also SVFe as a part of SVFX fail, with MIN. FVFe affecting negatively on MAX. However, the positive trend dominated the influence of other subdivisions (FVF_n, FVFs and FVFW). SVFe and SVFs as two quarters of SVFX show a concordant behaviour to Ta, where the increase of their values leads to a growth in the values of its indicators; conversely, the other quarters (SVFe and SVFs) that displayed the negative signs.

It is worth noting that the development of structure of the MAX model, where the effect of a.Ta was considered after adding the UMP, unlike the basic model of MAX.

Table 6-4 the signs of modified models (M.M.) for (mo-su-hot)

		The Details of Urban Morphological Parameters (UMP)																
		CI	Dc	FAR	FSR	FVF	FVFX				SCR	SF	SVF	SVFX				
							FVFn	FVFe	FVFs	FVFW				SVFn	SVFe	SVFs	SVFW	
Independent variables of modified models (M.M.) / mo-su-hot	UMP	AVG	+	+	+	+	+	+	*	+	+	+	x	-	-	+	+	-
		MAX	+	+	+	+	+	+	-	*	+	+	x	-	-	+	+	-
		MIN	+	+	+	+	+	+	+	*	+	+	+	x	-	-	*	+
	Ta	AVG	+	+	+	+	+			+		+	x	+			+	
		MAX	+	+	+	+	+			+		+	x	+			+	
		MIN	+	+	+	+	+			+		+	x	+			+	
	SOLAR	AVG	+	+	+	+	+			+		+	x	+			+	
		MAX	+	+	+	+	+			+		+	x	+			+	
		MIN	+	+	+	+	+			+		+	x	+			+	

6.2.3 Afternoon period: 12.00 noon to 6.00 pm (no-su-hot)

Figure 6.3 shows the basic model fit (10.8%, 9.1% and 13.9%) of the data for AVG, MAX and MIN respectively throughout the third period of the sunny days from 12.00 noon to 6.00 pm. In addition to the failure of the nine models for FAR, FSR and FVF, more than 80% of air temperature variation can be justified partially by the UMP. Dramatic increases occurred for R-Sq(adj) by adding SVFx and FVFX. The model of hourly maximum air temperature (MAX), in this period, reached its peak (57.1%) with SVFx, while AVG (53.4 %) and MIN (49.9%) came lower. FVFX occupied the second position with the same arrangement as SVFx, where MAX, AVG and MIN values settled at 41.5%, 38.4% and 36.2% respectively. A similarity in conduct and values can be noticed between B.M. and the rest of UMP, except for the values of SF models that crossed the barrier of 20%.

According to Table 6-5, the standard error of regression for the thermal microclimate indicators was decreased as a result of adding the urban morphological parameters. The improvement of S values have followed the same trends for R-Sq(adj). Therefore,

the models of SVFx and FVFx respectively are the most accurate in comparison to the others. The Equations 6-3 showed that a.Ta and solar have different effects on air temperature indicators. While the increasing of ambient air temperature (a.Ta) leads to raising Ta, the growing of solar leads to reduce Ta. However solar did not contributed in formation the MAX model for the (no-su-hot) period.

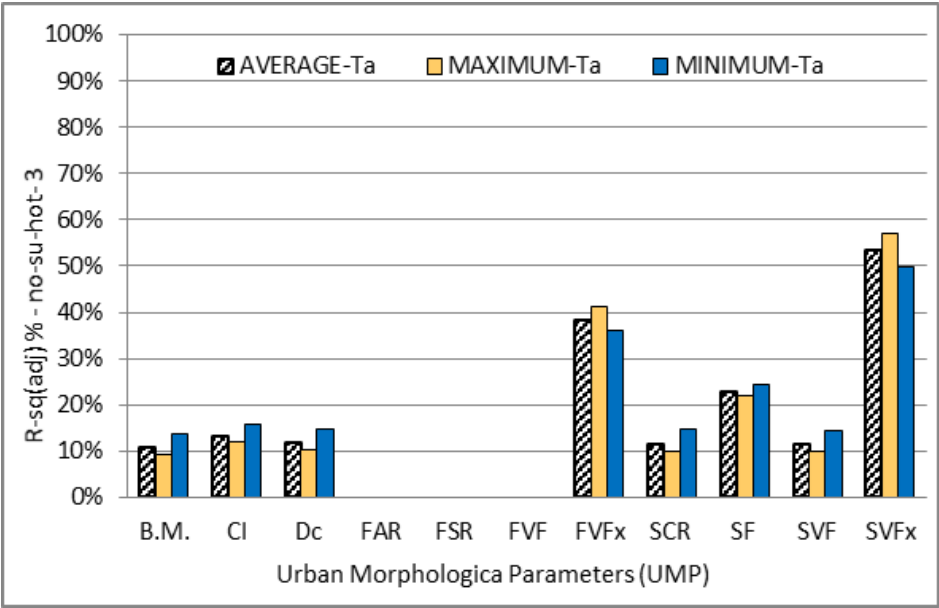


Figure 6.3 Percentages of R-Sq(adj) for the basic and modified air temperature models in (no-su-hot)

$$\text{AVERAGE-Ta} = 5.07 - 0.001450 \text{ avg solar} + 0.848 \text{ avg a.Ta}$$

$$\text{MAXIMUM-Ta} = 5.77 + 0.782 \text{ max a.Ta}$$

$$\text{MINIMUM-Ta} = 3.52 - 0.002080 \text{ min solar} + 0.930 \text{ min a.Ta}$$

Equations 6-3 Bbasic models (B.M.) of (no-su-hot)

Table 6-5 The values of standard error of the regression (*S*) for (no-su-hot)

<i>S</i>	<i>no su hot</i>	<i>3</i>	
	avg	max	min
B.M.	2.81623	3.11574	2.53436
CI	2.77815	3.06537	2.50709
Dc	2.79872	3.0945	2.52202
FAR	x	x	x
FSR	x	x	x
FVF	x	x	x
FVfx	2.3399	2.50266	2.18078
SCR	2.80343	3.09924	2.52265
SF	2.62086	2.8838	2.37326
SVF	2.8044	3.10111	2.52527
SVfx	2.03588	2.13987	1.9328

The signs of modified model variables elucidated that the solar radiation had a negative effect on two thermal microclimate indicators (AVG and MIN) and had no effect on MAX model, as shown in Table 6-6, while ambient air temperature had positive relationships with the three indicators.

In relation to the role of UMP, some of them (CI, Dc and SVF) showed minus signs, demonstrating their negative influences on air temperature in contrast of the positive behaviours for SCR and SF. FAR, FSR and FVF, statistically, had no effect on the thermal microclimate. FVfx witnessed different roles for its subdivisions, while FVfn and FVfw had positive effects on the three indicators, while FVfs displayed minus signs. FVfe failed to be an effective variable with AVG and MAX although it had a negative role with MIN. Any growth in openness to the sky for one or more of the three subdivisions of SVfx (SVfe, SVfs and SVfw) led to affect the thermal indicators positively, although AVG and MAX were not stimulated by SVfe. Also, MIN by SVfs. SVfs showed negative relationships with all indicators.

The adding of urban morphological parameters (UMP) did not improve the composition of the MAX model in terms of solar effect on air temperature. Solar as one of the climatic variables was excluded statistically from the basic models (B.M) and the modified models (M.M) for this period.

Table 6-6 The signs of modified models (M.M.) for (no-su-hot)

Independent variables of modified models (M.M.) / no-su-hot		The Details of Urban Morphological Parameters (UMP)																
		CI	Dc	FAR	FSR	FVF	FVFX				SCR	SF	SVF	SVFX				
							FVFn	FVFe	FVFs	FVFw				SVFn	SVFe	SVFs	SVFw	
UMP	AVG	-	-	X	X	X	+	*	-	+	+	+	-	-	*	+	+	
	MAX	-	-	X	X	X	+	*	-	+	+	-	-	-	*	+	+	
	MIN	-	-	X	X	X	+	-	-	+	+	-	-	-	+	*	+	
	a.Ta	AVG	+	+	X	X	X	+				+	+	+	+			
		MAX	+	+	X	X	X	+				+	+	+	+			
		MIN	+	+	X	X	X	+				+	+	+	+			
	SOLAR	AVG	-	-	X	X	X	-				-	-	-	-			
		MAX	*	*	X	X	X	*				*	*	*	*			
		MIN	-	-	X	X	X	-				-	-	-	-			

6.2.4 Evening period: 6.00 pm to midnight (ev-su-hot)

Between 65% to 70% of the variation in the on-site measured air temperature data sets, throughout the evening period of the sunny days group, could be explained as a direct response to climate factors in the basic models, [see Figure 6.4]. UMP contributed about 12% to improving the explanatory power, to reach more than 82% in the best cases with some of SVF_x models. In addition to the failure of SCR, all the modified models have similar behaviours to the basic models, where the values of MIN and AVG were almost equal and MAX regressed to be the last for the parameter itself. At the same time, there is some convergence in values between most parameters and, in particular, Dc, FAR, FSR and SVF. The general comparison between the parameters has revealed that CI overtakes FVFX to be the third after SF, which ranged between about 71% and 77%. The novel parameter FVF came last with range (69.8% AVG -65.7% MAX); also, it failed to explain the variation of the MIN data set.

The accuracy of the modified models (M.M) increased compared to the basic models (B.M), where the values of the standard error of the regression (**S**) followed an opposite inclination of R-Sq(adj) values in varying up and down. The M.M that had the highest values of R-Sq(adj) displayed the lowest values of **S** like SVF_x, SF and CI respectively; in contrast, the models of FVF showed that values were o close to B.M

values, as illustrated in Table 6-7. According to the liner regression models that are shown in Equations 6-4 as the basic models (B.M), the solar radiation may have no effect on thermal microclimate for the last period of sunny days for the hot season under the maritime temperate climate of the city of Liverpool, while the ambient air temperature affects positively to increase the on-site measured air temperature (Ta).

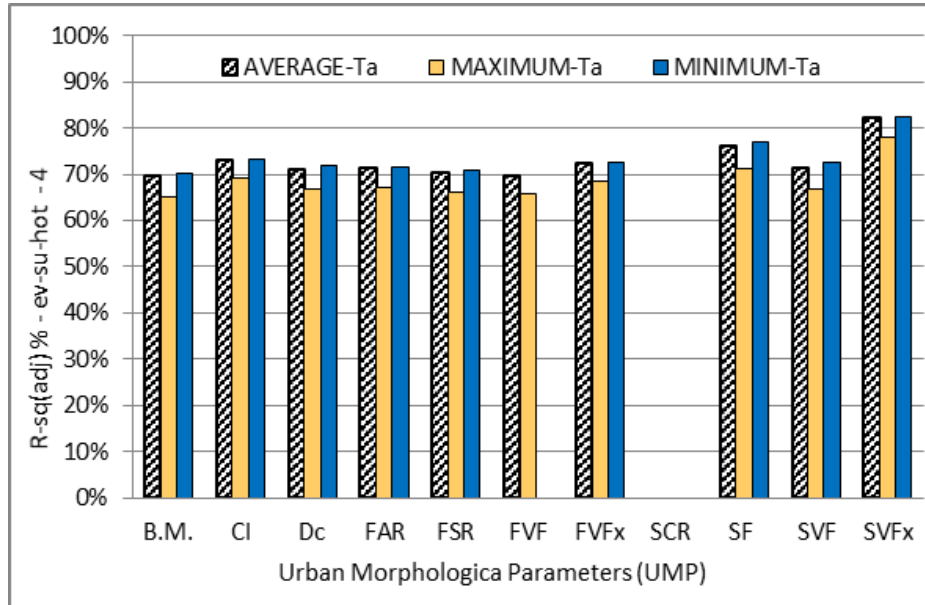


Figure 6.4 Percentages of R-Sq(adj) for the basic and modified air temperature models in (ev-su-hot)

Table 6-7 The values of standard error of the regression (*S*) for (ev-su-hot)

<i>S</i>	<i>ev su hot</i>		
	avg	max	min
B.M.	1.16113	1.40243	1.04185
CI	1.09097	1.32029	0.988471
Dc	1.12985	1.37016	1.01478
FAR	1.12769	1.36285	1.01678
FSR	1.14794	1.38532	1.03365
FVF	1.15558	1.39066	x
FVFX	1.10483	1.33548	0.999556
SCR	x	x	x
SF	1.0312	1.27333	0.918428
SVF	1.12304	1.369	1.0033
SVFX	0.88496	1.10989	0.803211



$$\text{AVERAGE-Ta} = -2.440 + 1.2061 \text{ avg a.Ta}$$

$$\text{MAXIMUM-Ta} = -2.120 + 1.1908 \text{ max a.Ta}$$

$$\text{MINIMUM-Ta} = -2.673 + 1.2176 \text{ min a.Ta}$$

Equations 6-4 Basic models (B.M.) of (ev-su-hot)

It appears that the total surface area of buildings to their total volume (SF) and the openness degree to the sky depending on the cardinal directions (SVFx) promoted the role of solar radiation in relation to the MIN models, compared to the basic models and the other modified models. However, this role limits the air temperature increase as shown in [Table 6-8](#). Generally, the mounting trend of the thermal microclimate indicators was boosted by the ambient air temperature (a.Ta). By increasing the values of following parameters [compactness index (CI), degree of compactness (Dc), floor area ratio (FAR), façade to site ratio (FSR), façade view factor (FVF) and sky view factor (SVF)] that serve as independent variables for the statistical models, the onsite air temperature (Ta) will decline, although the MIN model did not respond to FVF. Conversely, shape factor (SF) took part positively in stimulating Ta. In relation to the FVFX and SVFX, some of their subdivisions (FVFN, FVFW and SVFE) did not participate in determining the Ta tendency. The limits of Ta may be subject to the conflicting effects of FVFE and FVFs in positive and negative influences respectively. Increasing openness to the sky towards the north direction (SVFN) or south direction (SVFS) may participate in reducing e Ta in contrast to the west direction (SVFW) that possibly elevate the onsite measured air temperature indicators (AVG, MAX and MIN).

Table 6-8 The signs of modified models (M.M.) for (ev-su-hot)

		The Details of Urban Morphological Parameters (UMP)																
		CI	Dc	FAR	FSR	FVF	FVFX				SCR	SF	SVF	SVFX				
							FVFn	FVFe	FVFs	FVFw				SVFn	SVFe	SVFs	SVFw	
Independent variables of modified models (M.M.) / ev-su-hot	UMP	AVG	-	-	-	-	-	*	+	-	*	x	+	-	-	*	-	+
		MAX	-	-	-	-	-	*	+	-	*	x	+	-	-	*	-	+
		MIN	-	-	-	-	x	*	+	-	*	x	+	-	-	*	-	+
	a.Ta	AVG	+	+	+	+	+		+			x	+	+			+	
		MAX	+	+	+	+	+		+			x	+	+			+	
		MIN	+	+	+	+	x		+			x	+	+			+	
	SOLAR	AVG	*	*	*	*	*		*			x	*	*			*	
		MAX	*	*	*	*	*		*			x	*	*			*	
		MIN	*	*	*	*	x		*			x	-	*			-	

6.3 Partially cloudy days analysis (pr-hot)

The group of partially cloudy days covered ten days of the hot season (31st July, 3rd 5th, 12th, 14th, 20th, 22nd, 23rd, 24th and 31st August) where the sunshine hours ranged from 30% to 60% of the daylight length. The sunrise time for the first and the last days in this group changed from 05:26 to 06:19 while the sunset times went from 21:09 to 20:04. Therefore, the daylight length declined from 15:43 hours to 13:44 hours.

6.3.1 Night period: midnight to 6.00 am (ni-pr-hot)

The domination of climatic factors in air temperature variances from 12.00 midnight to 6.00 am was very strong, with around 91% of the variance explained, as shown by B.M. in Figure 6.5. About 9% of disparities may be explained by other factors; the addition of UMP did not contribute much in improving rates that were lower than 1% in the best cases with SF, SVFX, FVFX and FAR respectively. Nine models belonging to CI, Dc and FVF did not succeed completely to clarify a part of the variation; while the parameters FSR, SCR and SVF succeed partially as a result to fail AVG and MAX for the first two and MIN for SVF. The small differences between the R-Sq(adj) values

for AVG and MAX models with retreat MIN slightly from them lead to appearing all M.M. have similar behaviour to the B.M.

The standard error of regression is inversely proportional to the R-Sq(adj) values according to Table 6-9, where the ascending order of urban parameters SF, SVFx, FVx and FAR are similar in the three columns of the table AVG, MAX and MIN. Consequently, the accuracy of the statistical models increased after adding the parameters as independent variables to these models, although the MIN is the solo model for SVF and show R-Sq(adj) value equal to that for FAR as 90.4%, S value for SVF is lower than that for FAR.

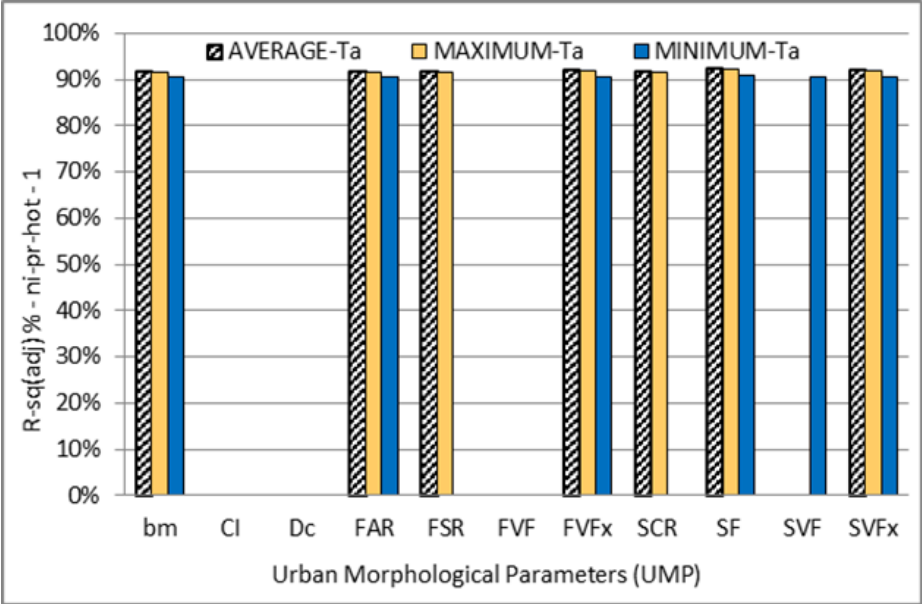


Figure 6.5 Percentages of R-Sq(adj) for the basic and modified air temperature models in (ni-pr-hot)

Equations 6-5 showed that the solar radiation as a climatic variable affected negatively just on the basic model MAX while all the basic models were affected positively by the ambient air temperature (a.Ta).

Table 6-9 The values of standard error of the regression (S) for (ni-pr-hot)

S	ni pr hot		
	AVG	MAX	MIN
B.M.	0.488205	0.487746	0.53191
CI	x	x	x
Dc	x	x	x
FAR	0.486797	0.485885	0.531301
FSR	0.487744	0.486947	X
FVF	x	x	x
FVFX	0.480094	0.479905	0.525015
SCR	0.487172	0.486648	x
SF	0.471694	0.471436	0.51652
SVF	x	x	0.531211
SVFX	0.479372	0.479377	0.523802



$$\text{AVERAGE-Ta} = -0.587 + 1.0457 \text{ avg a.Ta}$$

$$\text{MAXIMUM-Ta} = -0.639 - 0.001530 \text{ max solar} + 1.0484 \text{ max a.Ta}$$

$$\text{MINIMUM-Ta} = -0.183 + 1.0187 \text{ min a.Ta}$$

Equations 6-5 Basic models (B.M.) of (ni-pr-hot)

Although the sun had risen about half hour before ending this period for some of the partially cloudy days, the solar radiation had a negative impact on the MAX models, while a.Ta kept its positive impact on all indicators, as shown in Table 6-10. The FAR and a group of the urban morphological parameters (UMP) that supported one indicator like SVF or two indicators like FSR and SCR, showed inverse relationships with air temperature (Ta) variances. As for the subdivisions of FVFX, it seemed to be each both opposite directions had the same effect on thermal microclimate indicators. Where FVFn and FVFs had the negative influences opposite of the positive effects of FVFe and FVfw. The two quarters of SVFX (SVFn and SVFw) had conflicting effects on the indicators, while the openness on the other half of sky (SVFe and SVFs) may has no effect on (AVG, MAX and MIN) from a statistical point of view. In terms

of the dark cells, they refer to the failure of thirteen models under effect of partially cloudy sky for the hot season at the night period.

Table 6-10 The signs of modified models (M.M.) for (ni-pr-hot)

		The Details of Urban Morphological Parameters (UMP)																
		CI	Dc	FAR	FSR	FVF	FVFX				SCR	SF	SVF	SVFX				
							FVFn	FVFe	FVFs	FVFw				SVFn	SVFe	SVFs	SVFw	
Independent variables of modified models (M.M.) / ni-pr-hot	UMP	AVG	X	X	-	-	X	-	+	-	+	-	+	X	-	*	*	+
		MAX	X	X	-	-	X	-	+	-	+	-	+	X	-	*	*	+
		MIN	X	X	-	X	X	-	+	-	+	X	+	-	-	*	*	+
	a.Ta	AVG	X	X	+	+	X		+		+	+	X					+
		MAX	X	X	+	+	X		+		+	+	X					+
		MIN	X	X	+	X	X		+		X	+	+					+
	SOLAR	AVG	X	X	*	*	X		*		*	*	X					*
		MAX	X	X	-	-	X		-		-	-	X					-
		MIN	X	X	*	X	X		*		X	*	*					*

6.3.2 Morning period: 6.00 am to 12.00 noon (mo-su-hot)

Come along with increasing the sun height during the specified period (6.00 am to 12.00 noon), the contribution of the ambient climatic variables (a.Ta and solar) to the interpretation of air temperature variation was reduced as shown in [Figure 6.6](#) compared to the previous period. The basic models (B.M) showed 81.62%, 77.13% and 83.10% as R-Sq(adj) values for the statistical models of the thermal microclimate indicators respectively (AVG, MAX and MIN). The best improvement rates after adding the urban morphological parameters (UMP) were by AVG and MAX to be about 3% for façade view factor (FVFX) and partial sky view factor (SVFX) respectively. For the same factors the MIN models recorded about 1.5% as improvement rates. The other modified models (M.M) witnessed lower rates except for the shape factor (SF) that did not succeed to increase the explanatory power of the indicators models. The M.M have a pattern similar to the B.M where MAX settled the last and AVG and MIN came in the middle and the first respectively.

The turning colour from orange to blue shown in Table 6-11 refers to an increase in the accuracy of statistical model by decreasing the standard error of the regression (S) after adding the UMP especially FVFX and SVFX

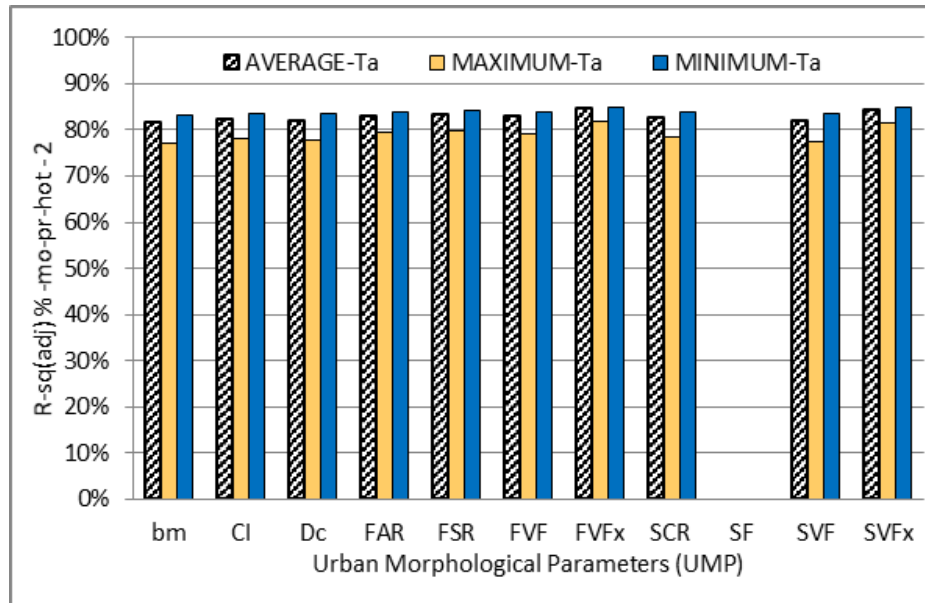


Figure 6.6 Percentages of R-Sq(adj) for the basic and modified air temperature models in (mo-pr-hot)

Table 6-11 The values of standard error of the regression (S) for (mo-pr-hot)

S	<i>mo pr hot</i>	2	
	AVG	MAX	MIN
B.M.	1.14873	1.3151	1.09195
CI	1.13189	1.28726	1.08355
Dc	1.13382	1.29371	1.08308
FAR	1.10191	1.24634	1.06435
FSR	1.09548	1.23498	1.06109
FVF	1.10578	1.25765	1.06354
FVFX	1.04797	1.16926	1.03146
SCR	1.11611	1.27365	1.06943
SF	x	x	x
SVF	1.14014	1.30694	1.08391
SVFX	1.05454	1.17955	1.0345

The basic models (B.M) of (mo-pr-hot), according to Equations 6-6, show that the negative role of solar radiation affected the three indicators instead of just the MAX,

as had happened in the period from midnight to 6.00 am (night period). Also the direct relationship between the ambient air temperature (a.Ta) and the indicators leads to elevated Ta values.

$$\text{AVERAGE-Ta} = -1.345 - 0.001125 \text{ avg solar} + 1.1178 \text{ avg a.T}$$

$$\text{MAXIMUM-Ta} = -2.011 - 0.000253 \text{ max solar} + 1.1451 \text{ max a.Ta}$$

$$\text{MINIMUM-Ta} = -0.405 - 0.001830 \text{ min solar} + 1.0596 \text{ min a.Ta}$$

Equations 6-6 Basic models (B.M.) of (mo-pr-hot)

Table 6-12 shows that the solar radiation had a negative influences on the three indicators, contrary to the ambient air temperature (a.Ta) that affected positively on AVG, MAX and MIN. In terms of urban morphological parameters (UMP), the thermal microclimate of the period may be adversely affected by the sky view factor (SVF). Contrariwise, the other parameters (CI, Dc, FAR, FSR, FVF and SCR) could have direct relationships with the air temperature indicators. Concerning the façade view factor (FVFx), three of its subdivisions (FVF_n, FVF_s and FVF_w) affected positively on Ta, but with negative signs of FVF_e. With regard to the SVF_x, two quarters of it (SVF_n and SVF_w) was affected negatively on the indicators while the other parts (SVF_e and SVF_s) showed positive influences except the MIN, which experienced lower values by increasing the openness to the sky on the southern side (SVF_s).

Table 6-12 The signs of modified models (M.M.) for (mo-pr-hot)

		The Details of Urban Morphological Parameters (UMP)															
		CI	Dc	FAR	FSR	FVF	FVFX				SCR	SF	SVF	SVFX			
							FVFn	FVFe	FVFs	FVFw				SVFn	SVFe	SVFs	SVFw
Independent variables of modified models (M.M.) / mo-pr-hot	UMP	AVG	+	+	+	+	+	-	+	+	+	x	-	-	+	+	-
		MAX	+	+	+	+	+	-	+	+	+	x	-	-	+	+	-
		MIN	+	+	+	+	+	-	+	+	+	x	-	-	+	-	-
	a.Ta	AVG	+	+	+	+		+			+	x	+		+		
		MAX	+	+	+	+		+			+	x	+		+		
		MIN	+	+	+	+		+			+	x	+		+		
	SOLAR	AVG	-	-	-	-	-	-			-	x	-		-		
		MAX	-	-	-	-	-	-			-	x	-		-		
		MIN	-	-	-	-	-	-			-	x	-		-		

6.3.3 Afternoon period: 12.00 noon to 6.00 pm (no-pr-hot)

The variation of air temperature (Ta) from 12:00 noon to 6:00 pm can be explained partially by considering the direct effects of solar and ambient air temperature (a.Ta) as shown by the basic model (B.M) bars in Figure 6.7 where a wide range can be noticed between MAX model (50%) and MIN model (70%) while AVG settled at about 60%. The editing processes of the basic models to produce the modified models (M.M) by adding urban morphological parameters, one by one, revealed that the façade to site ratio (FSR) may have had no effect on thermal microclimate indicators, unlike SVFx, SF, FVFX and CI which contributed effectively in justifying the air temperature variability compared to the rest of UMP. AVG, MAX and MIN recorded upswings after adding the partial sky view factor (SVFx) to 73.42%, 69.21% and 77.2% respectively. The façade view factor (FVFX) and the shape factor (SF) showed almost similar values, which exceeded the values of the compactness index (CI) by about 3% for each indicator where the R-Sq(adj) values of CI were 62.9% as AVG, 53.61% as MAX and 70.86% as MIN. The models of the rest UMP recorded slight improvements against the basic models.

The values of standard error of the regression (S) in Table 6-13 support the previous results by giving the lowest values for the models of SVFx, SF, FVFX and CI respectively

compared to other models where the minimal accuracy is for the basic models as usual. The solar radiation as a one of the two variables in the basic models (B.M) had the opposite effect of increasing the onsite measured air temperature (Ta) by showing minus signs in the three models as shown in Equations 6-7, while the ambient air temperature (a.Ta) kept its the positive influence on Ta.

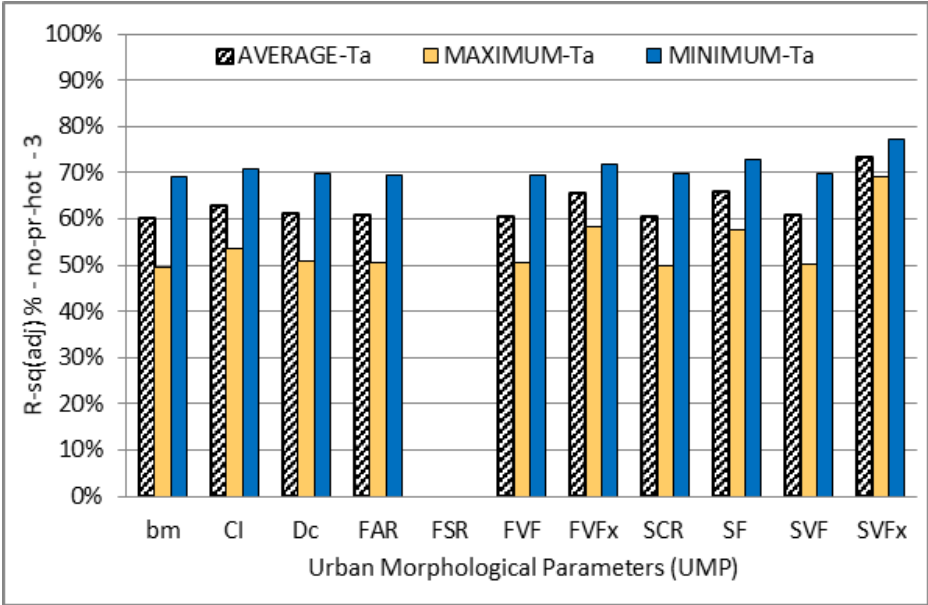


Figure 6.7 Percentages of R-Sq(adj) for the basic and modified air temperature models in (no-pr-hot)

Table 6-13 The values of standard error of the regression (S) for (no-pr-hot)

S	<i>no pr hot</i>	3	
	AVG	MAX	MIN
B.M.	1.80861	2.16119	1.53739
CI	1.74529	2.07172	1.49574
Dc	1.78788	2.12928	1.52541
FAR	1.7954	2.13802	1.5315
FSR	x	x	x
FVF	1.7975	2.14045	1.53344
FVFX	1.68381	1.96228	1.46932
SCR	1.79762	2.15166	1.52499
SF	1.67352	1.98179	1.44245
SVF	1.79214	2.1438	1.52107
SVFX	1.47731	1.68792	1.32316

$$\text{AVERAGE-Ta} = 0.973 - 0.001847 \text{ avg solar} + 1.0491 \text{ avg a.Ta}$$

$$\text{MAXIMUM-Ta} = 2.144 - 0.001328 \text{ max solar} + 0.9902 \text{ max a.Ta}$$

$$\text{MINIMUM-Ta} = 0.396 - 0.002561 \text{ min solar} + 1.0751 \text{ min a.Ta}$$

Equations 6-7 Basic models (B.M.) of (no-pr-hot)

The signs of the modified models in Table 6-14 revealed that some urban morphological parameters (CI, Dc, FAR, FVF and SVF) worked on the reduction of (Ta) while SCR and SF influenced positively on Ta. With regard to the FVFX it appears that the façade that faced the east direction from their positions on the west side of the urban spaces (FVFw) had no effects on Ta. FVFe and FVFs had negative effects in contrary to the influence of FVFn, which showed plus signs. Each of the two opposite subdivisions of SVF_x had the same effect where any increase in the values of SVFn and SVFs leads to reduce the air temperature. In contrast SVFe and SVFw have positive influence on the air temperature (Ta).

Table 6-14 The signs of modified models (M.M.) for (no-pr-hot)

		The Details of Urban Morphological Parameters (UMP)																
		CI	Dc	FAR	FSR	FVF	FVFX				SCR	SF	SVF	SVF _x				
							FVF _n	FVFe	FVFs	FVF _w				SVFn	SVFe	SVFs	SVF _w	
Independent variables of modified models (M.M.) / no-pr-hot	UMP	AVG	-	-	-	X	-	+	-	-	*	+	+	-	-	+	-	+
		MAX	-	-	-	X	-	+	-	-	*	+	+	-	-	+	-	+
		MIN	-	-	-	X	-	+	-	-	*	+	+	-	-	+	-	+
	a.Ta	AVG	+	+	+	X	+		+			+	+	+			+	
		MAX	+	+	+	X	+		+			+	+	+			+	
		MIN	+	+	+	X	+		+			+	+	+			+	
	SOLAR	AVG	-	-	-	X	-		-			-	-	-			-	
		MAX	-	-	-	X	-		-			-	-	-			-	
		MIN	-	-	-	X	-		-			-	-	-			-	

6.3.4 Evening period: 6.00 pm to midnight (ev-pr-hot)

This period covers the last six hours of the partially cloudy days. As for the R-Sq(adj) values of the B.M, they were 91.71%, 88.69% and 91.62% for the three indicators (AVG, MAX and MIN) [see Figure 6.8]. The adding of UMP did not lead to any remarkable changes to the graph bars. The highest improvement of the explanatory power was less than 3% for the MAX model after adding SVFx ; however, MAX models came last compared to AVG and MIN models. The modified models of the urban parameters SVFx, SF and CI respectively came to the foreground relative to others while SCR did not improve R-Sq(adj) value at all.

In terms of the standard error of regression (S), the turning up the colour scale to the blue colour refers to decline the S values and increase the accuracy of models especially with SVFx, SF and CI as shown in the Table 6-15.

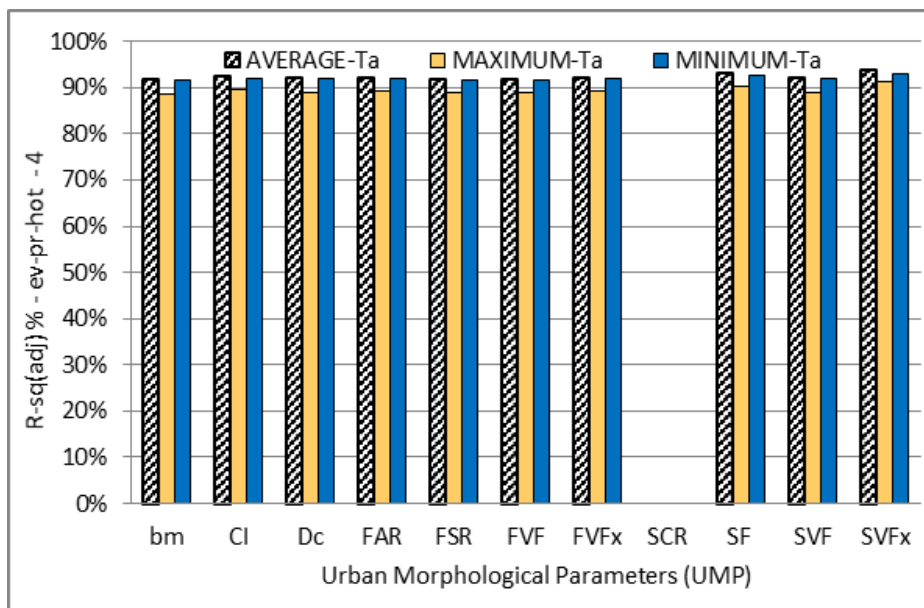


Figure 6.8 Percentages of R-Sq(adj) for the basic and modified air temperature models in (ev-pr-hot)

The liner regression models that shown in Equations 6-8, as the basic models (B.M), indicated that the solar radiation and ambient air temperature have positive influences on the three air temperature indicators for the last period of the partial cloudy days in the hot season.

Table 6-15 The values of standard error of the regression (**S**) for (ev-pr-hot)

S	ev pr hot	4	
	AVG	MAX	MIN
B.M.	0.727457	0.875691	0.726349
CI	0.697694	0.835895	0.707108
Dc	0.716624	0.86154	0.718927
FAR	0.711811	0.854751	0.716024
FSR	0.719244	0.863658	0.721536
FVF	0.72386	0.869155	0.725018
FVFX	0.71322	0.854076	0.718416
SCR	x	x	x
SF	0.667768	0.813564	0.676811
SVF	0.714556	0.862349	0.715601
SVFX	0.633684	0.762769	0.658235

$$\text{AVERAGE-Ta} = -0.345 + 0.003839 \text{ avg solar} + 1.0661 \text{ avg a.Ta}$$

$$\text{MAXIMUM-Ta} = -0.407 + 0.001961 \text{ max solar} + 1.0722 \text{ max a.Ta}$$

$$\text{MINIMUM-Ta} = -0.076 + 0.00703 \text{ min solar} + 1.0496 \text{ min a.Ta}$$

Equations 6-8 Basic models (B.M.) of (ev-pr-hot)

The positive effects of a.Ta and SOLAR on thermal microclimate did not change after adding UMP, as shown in [Table 6-16](#). Despite the failure of the SCR, a large part of the urban morphological parameters (CI, Dc, FAR, FAR, VF and SVF) acted as an air temperature inhibitor in this period by showing a minus sign. The shape factor (SF), as usual, kept its positive effect on AVG, MAX and MIN. With respect to the façade view factor (FVFX) and the partial sky view factor (SVFX), their subdivisions that belonged to the east direction had positive effects on measured air temperature, although FVFe and SVFe did not contribute in the MAX model and MIN model respectively. Increasing the values of FVFs and SVFs led to a reduced Ta. FVFn may had no influence thermal microclimate indicators while SVFn had a negative effect, like FVFW, and this is contrary to the effect of the SVFW.

Table 6-16 The signs of modified models (M.M.) for (ev-pr-hot)

		The Details of Urban Morphological Parameters (UMP)																
		CI	Dc	FAR	FSR	FVF	FVFX				SCR	SF	SVF	SVFX				
							FVFn	FVFe	FVFs	FVFw				SVFn	SVFe	SVFs	SVFw	
Independent variables of modified models (M.M.) / ev-pr-hot	UMP	AVG	-	-	-	-	-	*	+	-	-	x	+	-	-	+	-	+
	MAX	-	-	-	-	-	*	*	-	-	x	+	-	-	+	-	+	
	MIN	-	-	-	-	-	*	+	-	*	x	+	-	-	*	-	+	
	a.Ta	AVG	+	+	+	+	+	+	+	+	x	+	+	+	+	+	+	
	MAX	+	+	+	+	+	+	+	+	+	x	+	+	+	+	+	+	
	MIN	+	+	+	+	+	+	+	+	+	x	+	+	+	+	+	+	
	SOLAR	AVG	+	+	+	+	+	+	+	+	x	+	+	+	+	+	+	
	MAX	+	+	+	+	+	+	+	+	+	x	+	+	+	+	+	+	
	MIN	+	+	+	+	+	+	+	+	+	x	+	+	+	+	+	+	

6.4 Cloudy days analysis (cl-hot)

Cloudy days in the hot season were represented by four days (30th July, 8th and 16th august and 3rd September), when the sunshine hours were lower than 30% of the daylight length. The daylight length between the first and the last days in the cloudy days set reduced from 15.46 hours to 13:32 hours. The sunrise time changed from 05:24 to 06:24 while the sunset times moved from 21:11 to 19:57. Four daily periods have been defined depending on the dataset of this group.

6.4.1 Night period: Midnight to 6.00am (ni-cl-hot)

According to [Figure 6.9](#), the basic models (B.M.) showed that the variation of climatic factors throughout the night period explained about 84% of the variability of air temperature. The modified models (M.M.) showed that a group of UMP (CI, Dc and FAR) did not improve R-Sq(adj) value; while the other urban morphological parameters did not add more than 5% as the best improvement rates were about 88% and 87% in SVFX and SF models respectively. FSR and FVF models, in addition to the MAX model of SCR, did not break the 1% barrier. The patterns of thermal indicators of urban microclimate (AVG, MAX and MIN) for UMP were similar to B.M.

The fluctuation between the three indicators was limited, where MAX retreated slightly compared to the convergent levels of AVG and MIN.

Table 6-17 shows that the values of standard error of regression (S) followed an opposite behaviour along with R-Sq(adj) values in general. Therefore, the adding of UMP led to a decrease in the standard error of regression especially (SVF_x, SF, SVF and FVF_x) respectively.

The basic models [see Equations 6-9] show that the ambient air temperature (a.Ta) was the solo climatic factor that dominated the differences of on-site measured air temperature (Ta) in a positive relationship for the period from midnight to 6.00am under a cloudy sky in the hot season.

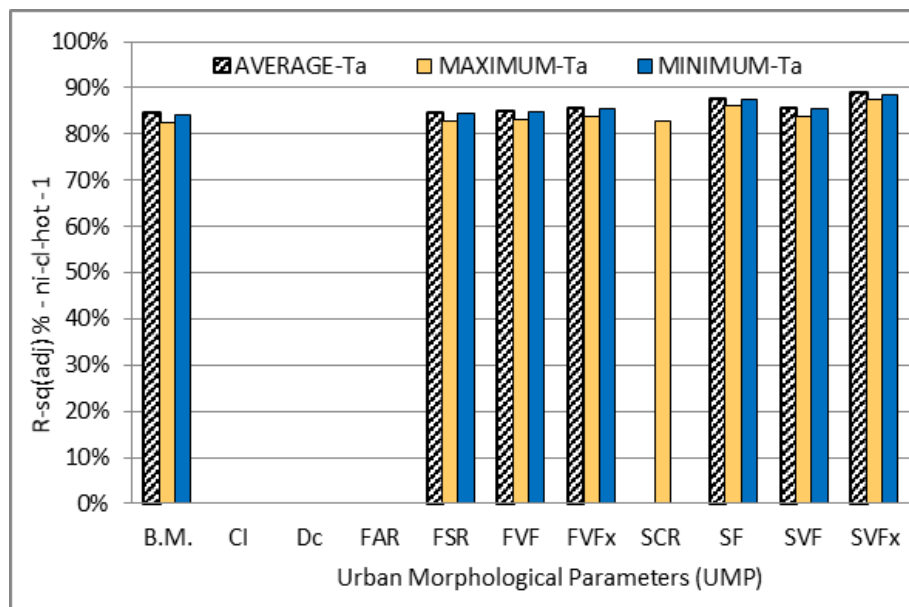


Figure 6.9 Percentages of R-Sq(adj) for the basic and modified air temperature models in (ni-cl-hot)

$$\text{AVG-Ta} = -1.343 + 1.1100 \text{ avg a.Ta}$$

$$\text{MAX-Ta} = -1.560 + 1.1226 \text{ max a.Ta}$$

$$\text{MIN-Ta} = -0.762 + 1.0725 \text{ min a.Ta}$$

Equations 6-9 basic models (B.M.) of (ni-cl-hot)

Table 6-17 The values of standard error of the regression (**S**) for (ni-cl-hot)

S	ni cl hot	1	
	avg	max	min
B.M.	0.434484	0.459804	0.438869
CI	x	x	x
Dc	x	x	x
FAR	x	x	x
FSR	0.43312	0.458077	0.43762
FVF	0.429315	0.454629	0.433219
FVFX	0.41719	0.443935	0.42067
SCR	x	0.458589	x
SF	0.385634	0.411028	0.392336
SVF	0.415842	0.441779	0.420007
SVFX	0.366599	0.392255	0.372924

FSR, FVF, SCR and SF affected positively on thermal indicators of urban microclimate (AVG, MAX and MIN) that represented the hourly measures of on-site air temperature (Ta) while SVF works on the contrary; where, increasing its value leads to a reduction in Ta as shown in [Table 6-18](#). In relation to the other urban morphological parameters (UMP), the subdivision of FVFX showed that FVFn had no effect on Ta while FVFe and FVFW elevated it. At the same time FVFs worked contrariwise by decreasing the air temperature. The subdivision of SVFX showed that SVFn had negative influences on Ta and SVFs had no effect. Simultaneously, SVFe and SVFW had partial contrasting effects on Ta, where SVFe had a negative effect on just MIN while SVFW had a positive relationships with AVG and MAX. Although, the solar radiation have no effect on thermal indicators of most modified models by adding UPM, the statistical models for SF and SVFX showed a negative effect of solar on air temperature values as (hourly MAX) for this period.

Table 6-18 The signs of modified models (M.M.) for (ni-cl-hot)

		The Details of Urban Morphological Parameters (UMP)																
		CI	Dc	FAR	FSR	FVF	FVFX				SCR	SF	SVF	SVFX				
							FVFn	FVFe	FVFs	FVFw				SVFn	SVFe	SVFs	SVFw	
Independent variables of modified models (M.M.) / ni-cl-hot	UMP	AVG	X	X	X	+	+	*	+	-	+	X	+	-	-	*	*	+
		MAX	X	X	X	+	+	*	+	-	+	+	+	-	-	*	*	+
		MIN	X	X	X	+	+	*	+	-	+	X	+	-	-	-	*	*
	a.Ta	AVG	X	X	X	+	+		+			X	+	+				+
		MAX	X	X	X	+	+		+			+	+	+				+
		MIN	X	X	X	+	+		+			X	+	+				+
	SOLAR	AVG	X	X	X	*	*		*			X	*	*			*	
		MAX	X	X	X	*	*		*			*	-	*			-	
		MIN	X	X	X	*	*		*			X	*	*			*	

6.4.2 Morning period: 6.00 am to 12.00 noon (mo-cl-hot)

The dataset of solar and a.Ta may contribute to explaining the variation of thermal microclimate indicators throughout the morning period (AVG 86.52%, MAX 74.52% and MIN 84.36%) [see Figure 6.10], while the urban morphological parameters (UMP) had a slight influence which did not exceed 1.5% in the best case as the AVG model of SVFx. The R-Sq(adj) value of MIN model had not affect by adding the parameters (FAR, FSR and FVF) and also the MAX model of the shape factor (SF). While the compactness index (CI) and the degree of compactness (Dc) may have had no effects totally on the air temperature indicators in this period. The accuracy of models improved after adding the UMP when compare the modified models (M.M) against the basic models (B.M) as shown in Table 6-19.

Although this period ranges from 6.00 am to 12.00 pm at the hot season, the solar radiation had a negative effect on the B.M as shown by Equations 6-10, while the positive effect of ambient air temperature on the three indicators continued in this period as well.

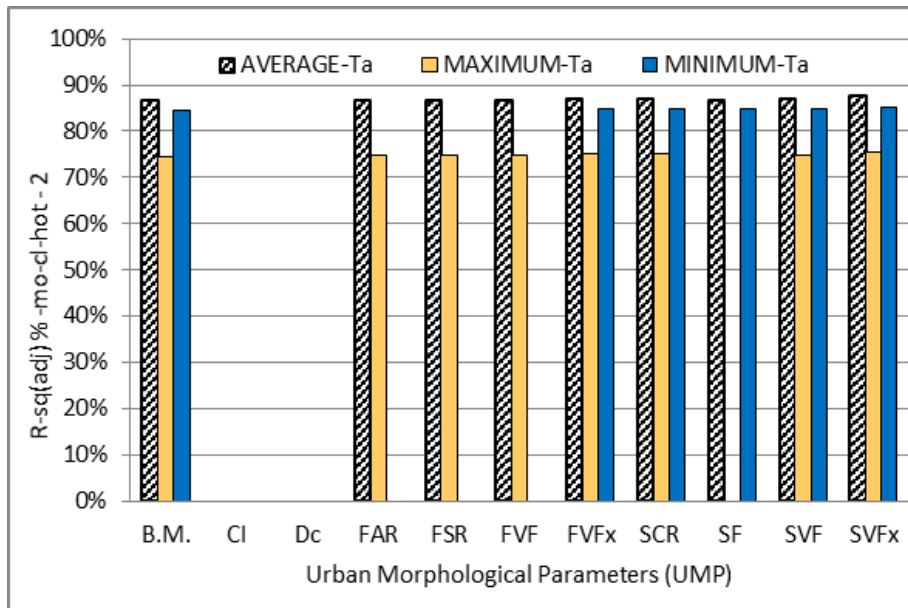


Figure 6.10 Percentages of R-Sq(adj) for the basic and modified air temperature models in (mo-cl-hot)

Table 6-19 The values of standard error of the regression (S) for (mo-cl-hot)

S	mo cl hot		
	avg	max	min
B.M.	0.522655	0.841789	0.511457
CI	x	x	x
Dc	x	x	x
FAR	0.521231	0.838059	x
FSR	0.520195	0.836347	x
FVF	0.520759	0.839418	x
FVFX	0.511761	0.828938	0.505796
SCR	0.511107	0.831114	0.50421
SF	0.51753	x	0.504144
SVF	0.51525	0.838337	0.504061
SVFX	0.50048	0.825976	0.498236

Although the cloudy sky dominated this period, the morphological parameters (FAR, FSR, FVF, SCR and SF) had positive impacts on air temperature in general, as shown

$$\text{AVERAGE-Ta} = -0.291 - 0.001096 \text{ avg solar} + 1.0458 \text{ avg a.Ta}$$

$$\text{MAXIMUM-Ta} = 0.576 - 0.000942 \text{ max solar} + 0.9944 \text{ max a.Ta}$$

$$\text{MINIMUM-Ta} = 0.491 - 0.001372 \text{ min solar} + 0.9916 \text{ min a.Ta}$$

Equations 6-10 Basic models (B.M.) of (mo-cl-hot)

in **Table 6-20**. In contrast, the sky view factor (SVF) showed minus signs for the three indicators (AVG, MAX and MIN). The four subdivisions of façade view factor (FVFX) have not affect simultaneously on the thermal microclimate. While FVFe influence negatively on AVG and MAX, the other subdivisions have positive effects on AVG and MIN models as FVFs, and just MAX model as FVFW. On the other hand, FVFn may has no effect through this time. Regarding the partial sky view factor (SVF_x) each two opposite parts has the same effect where SVFn and SVFs have negative influences on air temperature although SVFs did not contribute in the MAX model. While the positive effects of SVFe and SVFw are clear although the last one did not support MAX and MIN models and the first one did not support MAX model also.

Table 6-20 The signs of modified models (M.M.) for (mo-cl-hot)

		The Details of Urban Morphological Parameters (UMP)																
		CI	Dc	FAR	FSR	FVF	FVFX				SCR	SF	SVF	SVFx				
							FVFn	FVFe	FVFs	FVFW				SVFn	SVFe	SVFs	SVFw	
Independent variables of modified models (M.M.) / mo-cl-hot	UMP	AVG	x	x	+	+	+	*	-	+	*	+	+	-	-	+	-	+
		MAX	x	x	+	+	+	*	-	*	+	+	x	-	-	+	*	*
		MIN	x	x	x	x	x	*	*	+	*	+	+	-	-	*	-	*
	a.Ta	AVG	x	x	+	+	+			+		+	+	+			+	
		MAX	x	x	+	+	+			+		+	x	+			+	
		MIN	x	x	x	x	x			+		+	+	+			+	
	SOLAR	AVG	x	x	-	-	-			-		-	-	-			-	
		MAX	x	x	-	-	-			-		-	x	-			-	
		MIN	x	x	x	x	x			-		-	-	-			-	

6.4.3 Afternoon period: 12.00 noon to 6.00 pm (no-cl-hot)

The changes of the basic model variables (solar and a.Ta) within the afternoon time of the cloudy days fit about (54.51%, 48.4% and 55.16%) of the onsite measured data

variation as AVG, MAX and MIN respectively as shown in Figure 6.11. And this leaves about 50% of air temperature fluctuations to be justified by other factors like the urban morphological parameters (UMP). The best improvements of R-Sq(adj) values were about (8%, 10% and 5%) as AVG, MAX and MIN respectively after adding the partial sky view factor (SVF_x). The rates of compactness index (CI) (56.65%, 51.01% and 56.48%) put it as fourth after the shape factor (SF) and the façade view factor (FVF_x) respectively. The façade-to-site ratio (FSR) may have had no influence on the air temperature (Ta) at this time while the dataset of MAX model was fitted slightly by the variation of parameters FAR, FVF and CI that also supported the AVG model. Although all air temperature indicators are valid with SCR and SVF, they did not contribute effectively in support the explanatory power of these indicators.

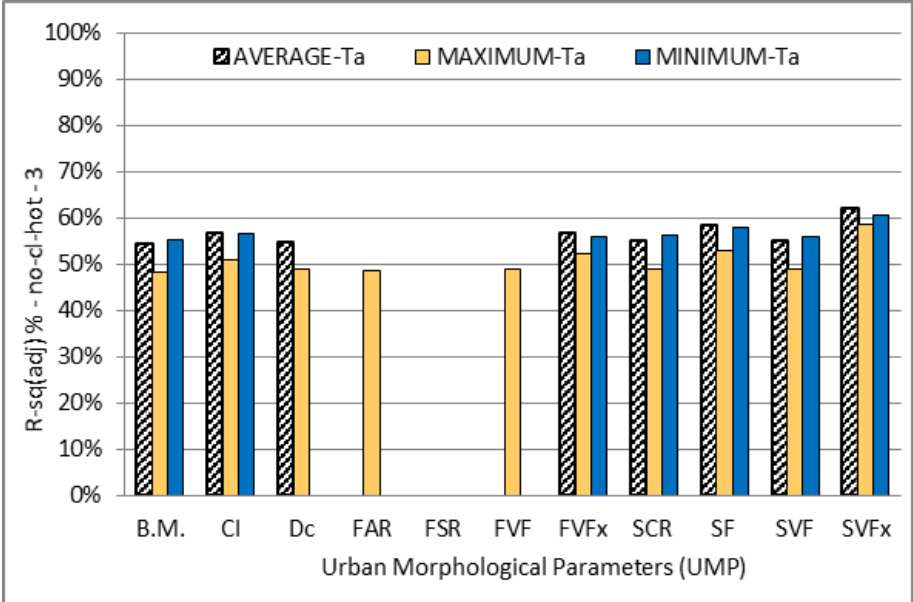


Figure 6.11 Percentages of R-Sq(adj) for the basic and modified air temperature models in (no-cl-hot)

The values of the standard error of the regression (S) went down and turned up into the blue colour as shown in Table 6-21. Therefore, the accuracy of the modified models (M.M) increased compared to the basic models (B.M), especially with parameters SVF_x, SF, FVF_x and CI.

The solar radiation seems to be working against the growth of onsite measured air temperature (Ta) where it showed minus signs in all the basic models, as shown in

Equations 6-11. However, the ambient air temperature still supported the positive trend of Ta by showing the positive signs in all models.

Table 6-21 The values of standard error of the regression (S) for (no-cl-hot)

S	no cl hot	3	
	avg	max	min
B.M.	1.54218	1.84062	1.33075
CI	1.50545	1.79338	1.31108
Dc	1.53575	1.83107	x
FAR	x	1.83459	x
FSR	x	x	x
FVF	x	1.83294	x
FVFX	1.50341	1.77147	1.31742
SCR	1.53038	1.83125	1.3155
SF	1.47481	1.75717	1.28784
SVF	1.53154	1.83324	1.31781
SVFX	1.40717	1.65098	1.24478

$$\text{AVERAGE-Ta} = 4.378 - 0.001298 \text{ avg solar} + 0.8558 \text{ avg a.Ta}$$

$$\text{MAXIMUM-Ta} = 5.873 - 0.000766 \text{ max solar} + 0.7831 \text{ max a.Ta}$$

$$\text{MINIMUM-Ta} = 5.114 - 0.001808 \text{ min solar} + 0.8026 \text{ min a.Ta}$$

Equations 6-11 Basic models (B.M.) of (no-cl-hot)

Table 6-22 shows that some parameters have direct relationship with the air temperature indicators, like SCR and SF, while the sky view factor (SVF) and the compactness index (CI) may reduce the air temperature in this time. The negative effect on the MAX model was noticed by adding the FAR, the FVF and the Dc that also had negative effects on the AVG model. FVFe and FVFs, as the subdivisions of the façade view factor (FVFX), worked on reduction of the air temperature as AVG and MAX while the air temperature as MIN may increase under the effect of FVFn. The fourth subdivision (FVFW) did not affect the air temperature for the afternoon period.

The eastern and the northern parts (SVFe and SVFs) of the partial sky view factor (SVFx) may affect just the MIN model where positive and negative signs were noticed respectively. The northern part (SVFn) showed negative effect against the air temperature indicators in contrary to the positive effect of SVFw. The solar radiation and the ambient air temperature in the modified models (M.M) kept the same behaviour that shown by the basic models (B.M).

Table 6-22 The signs of modified models (M.M.) for (no-cl-hot)

		The Details of Urban Morphological Parameters (UMP)																
		CI	Dc	FAR	FSR	FVF	FVFX				SCR	SF	SVF	SVFX				
							FVFn	FVFe	FVFs	FVFw				SVFn	SVFe	SVFs	SVFw	
Independent variables of modified models (M.M.) / no-cl-hot	UMP	AVG	-	-	X	X	X	*	-	-	*	+	+	-	-	*	*	+
		MAX	-	-		X		*	-	-	*	+	+	-	-	*	*	+
		MIN	-	X	X	X	X	+	*	*	*	+	+	-	-	+	-	+
	a. Ta	AVG	+	+	X	X	X		+			+	+	+				+
		MAX	+	+	+	X	+		+			+	+	+				+
		MIN	+	X	X	X	X		+			+	+	+				+
	SOLAR	AVG	-	-	X	X	X		-			-	-	-				-
		MAX	-	-	-	X	-		-			-	-	-				-
		MIN	-	X	X	X	X		-			-	-	-				-

6.4.4 Evening period: 6.00 pm to midnight (ev-cl-hot)

The R-Sq(adj) values of the three models (AVG, MAX and MIN) explained about (79.15%, 76.72% and 79.63%) of the air temperature variation within the last period of the cloudy days group under the effects of solar and a.Ta as the variables for basic models as shown in Figure 6.12. Although there is about 20% of that variation need to be justified, the urban morphological parameters (UMP) did not contribute efficiently to do that, especially with a total failure for five parameters (Dc, FAR, FSR, FVF and FVFX). The best improvement rates for the AVG and MIN models were done by adding the partial sky view factor (SVFx) to be 81% and 81.5% respectively while the shape factor (SF) supported the MAX model to achieve the best rate with 78.2%. There is no remarkable differences in the explanatory power between the three indicators whether the models are basic or modified. Although the effects of urban

parameters on the air temperature variation is limited, this did not prevent it from improving the accuracy of models and reducing the standard error of the regression (*S*) as shown in [Table 6-23](#).

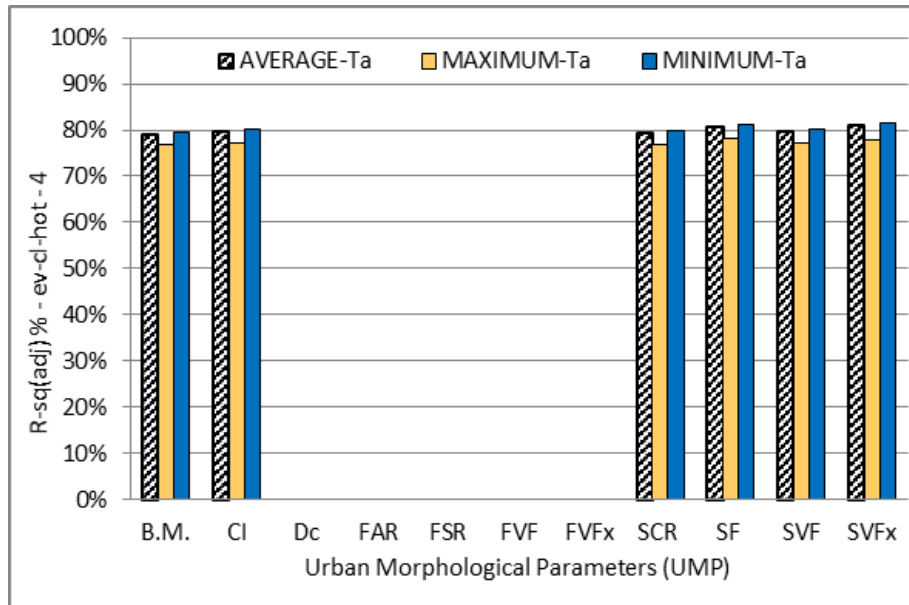


Figure 6.12 Percentages of R-Sq(adj) for the basic and modified air temperature models in (ev-cl-hot)

Table 6-23 The values of standard error of the regression (*S*) for (ev-cl-hot)

<i>S</i>	<i>ev cl hot</i>		
	avg	max	min
B.M.	0.865861	0.955928	0.810526
CI	0.85458	0.94365	0.801234
Dc	X	X	X
FAR	X	X	X
FSR	X	X	X
FVF	X	X	X
FVFx	x	x	x
SCR	0.861652	0.950287	0.807743
SF	0.834526	0.925351	0.779789
SVF	0.856324	0.946008	0.801576
SVFx	0.827299	0.934686	0.772383

As well as the negative role of the solar radiation, as shown in [Equations 6-12](#), it did not have an effect on the MIN model as an indicator for air temperature. While increasing the ambient air temperature (*a.Ta*) led to an increase in the air temperature as (AVG, MAX and MIN) represented the basic models here.

$$\text{AVERAGE-Ta} = -4.237 - 0.00909 \text{ avg solar} + 1.3098 \text{ avg a.Ta}$$

$$\text{MAXIMUM-Ta} = -4.458 - 0.00890 \text{ max solar} + 1.3258 \text{ max a.Ta}$$

$$\text{MINIMUM-Ta} = -3.149 + 1.2403 \text{ min a.Ta}$$

Equations 6-12 Tasic models (B.M.) of (ev-cl-hot)

Although adding of urban morphological parameters (UMP), the roles of the solar radiation and a.Ta did not change, as shown in Table 6-24. The compactness index (CI) and the sky view factor (SVF) showed negative effects on the thermal microclimate indicators (AVG, MAX and MIN); in contrast to this, the influence of the SCR and the shape factor (SF) showed positive signs. In terms of the effect of the partial sky view factor (SVFx) their parts (SVFe, SVFs and SVFw) had no effect on the MAX mode. However, each two opposite parts have similar influence, where SVFn and SVFs have negative relationship with the air temperature indicators while SVFe and SVFw have positive effects on these indicators.

Table 6-24 The signs of modified models (M.M.) for (ev-cl-hot)

		The Details of Urban Morphological Parameters (UMP)																
		CI	Dc	FAR	FSR	FVF	FVFX				SCR	SF	SVF	SVFX				
							FVFn	FVFe	FVFs	FVFw				SVFn	SVFe	SVFs	SVFw	
Independent variables of modified models (M.M.) / ev-cl-hot	UMP	AVG	-	X	X	X	X	X	X	X	X	+	+	-	-	+	-	+
		MAX	-	X	X	X	X	X	X	X	X	+	+	-	-	*	*	*
		MIN	-	X	X	X	X	X	X	X	X	+	+	-	-	+	-	+
	a.Ta	AVG	+	X	X	X	X	X				+	+	+	+			
		MAX	+	X	X	X	X	X				+	+	+	+			
		MIN	+	X	X	X	X	X				+	+	+	+			
	SOLAR	AVG	-	X	X	X	X	X				-	-	-	-			
		MAX	-	X	X	X	X	X				-	-	-	-			
		MIN	*	X	X	X	X	X				*	*	*	*			

6.5 Conclusions

Some 369 statistical models were developed to investigate the connections between the urban morphology and thermal microclimate at a residential building complex in Liverpool. The datasets of ambient air temperature (a.Ta) and solar radiation from

the weather station of Liverpool University were linked to the variations of field measured air temperatures (T_a) for 11 locations around the site as a substantial step to explore the size of the effect of climatic factors independently on air temperature as basic models (B.M). As a second step, the ten parameters that were used to measure the urban configuration for each location (UMP) were used one by one as a third independent variable with aT_a and solar radiation to produce the modified models (M.M) that revealed the integrated impact of climatic factors and urban morphology on air temperature. The analyses process extracted three datasets from the environmental measurements as AVG, MAX and MIN and each of them was divided into three groups of days according to the sky conditions. These, in turn, were subdivided into four periods each representing six hours of the day. The improvement of explanatory power after adding UMP relied on increases in the $R\text{-}Sq(\text{adj})$ value compared to its value with B.M, and revealed the influence and size of an urban morphological parameter on air temperature that may be enhanced or inhibited under this effect.

Although the ten parameters were devoted to quantifying the urban configuration for the same locations, it was found that there were notable differences between them in terms their influence on air temperature. However, their roles fluctuated according to the sky conditions and daily periods, where some of them turned out to be insignificant after appearing to have had a strong effect and vice versa. Regarding the climatic factors, without doubt the ambient air temperature (aT_a) had a positive effect on T_a in all models. However, the solar radiation did impact as expected, where it showed a negative effect and acted as an inhibitor against increases in on-site measured air temperature (T_a) while another group of models witnessed insignificant effects of solar radiation.

An examination of the urban morphological parameters and the climatic factors to explore the reasons for their behaviours will be presented in the next chapter.

Chapter Seven

7 The discussion of statistical approach results

7.1 Introduction

This chapter considers the reasons behind the results that were presented in Chapter Six. It will be divided in to three main sections:

- The climatic factors
- The Urban Morphological Parameters (UMP)
- The total effect of UMP

The aim of this chapter is, firstly, to provide a comprehensive discussion that justifies the behaviours of the in-situ measured air temperature under the effect of climatic factors and urban parameters Secondly, the most influential urban morphological parameters on thermal microclimate under different circumstances of the sky for the hot season in the moderate maritime climate of the city of Liverpool will be identified.

7.2 The Climatic Factors

These factors included the ambient air temperature (a.Ta) and solar radiation, where their effects on air temperature (Ta) are indicated by their signs (+ or -) in the statistical models. The positive sign (+) refers to a positive effect or increase of Ta by increase the factor value in the model, while the minus sign (-) relates to a decrease in Ta as a negative effect of the factor. Statistically insignificant factors have been removed from the models.

The effect of climatic factors on the thermal microclimate did not change notably by developing the basic models (B.M) to be the modified models (M.M) under the influence of urban morphological parameters (UMP). However, the roles of ambient air temperature (a.Ta) and solar radiation were changed, particularly by the sky conditions and the period of the day, as shown in [Table 7-1](#).

As expected, an increase of a.Ta leads to an increase in Ta irrespective the amount of cloud cover and the time of the day. However, the duration from 6am to 12pm under the clear sky witnessed an insignificant role (*) of a.Ta as an independent variable for

the Max model. This underestimation of the a.Ta role may have resulted from the statistical processing of data and the need for more data from more sites or for longer periods and which support this assertion. a.Ta turned up to be a significant variable and with a positive effect on Ta for the same model after adding UMP.

Table 7-1 The signs of climatic factors for the basic models (B.M)

B.M	night		morning		afternoon		evening	
SUNNY	SOLAR	a.Ta	SOLAR	a.Ta	SOLAR	a.Ta	SOLAR	a.Ta
AVG	-	+	+	+	-	+	*	+
MAX	-	+	+	*	*	+	*	+
MIN	-	+	+	+	-	+	*	+
B.M	night		morning		afternoon		evening	
P.CLOUDY	SOLAR	a.Ta	SOLAR	a.Ta	SOLAR	a.Ta	SOLAR	a.Ta
AVG	*	+	-	+	-	+	+	+
MAX	-	+	-	+	-	+	+	+
MIN	*	+	-	+	-	+	+	+
B.M	night		morning		afternoon		evening	
CLOUDY	SOLAR	a.Ta	SOLAR	a.Ta	SOLAR	a.Ta	SOLAR	a.Ta
AVG	*	+	-	+	-	+	-	+
MAX	*	+	-	+	-	+	-	+
MIN	*	+	-	+	-	+	*	+

Regarding solar radiation, it should increase the temperature of surfaces that then lead to an increase in the air temperature. However, unanticipated behaviours have been observed under the different sky conditions and, therefore, this section will be subdivided into three parts for more clarify.

7.2.1 The sunny days

The solar radiation increased at the site of the measured air temperature (Ta) from 6am to 12pm (morning period). However, it led to a decrease in the Ta in the night and afternoon periods while it may have no effect on the Ta for the evening period

after 6pm to midnight [see [Table 7-1](#)]. These unexpected findings may be due to different reasons depending on the daily periods themselves.

According to [Figures 5.1, 5.2 and 5.3](#) in Chapter 5, the comparison between the air temperature graphs and the solar radiation graph for the night period (12am to 6am) revealed that the air temperatures for the five days of the sunny sky declined smoothly, but with the first light of dawn, the devices (pyranometer) of the weather station at Liverpool University started to record the solar radiation, especially for the first three days on solar charts where the sun rose before 6am. Therefore, a negative relationship between the downward trend of air temperature and the upward trend of the solar radiation was defined statistically. Especially, the direct solar radiation may not have yet hit the on-site surfaces to raise their temperature that will affect the air temperature later.

In terms of the afternoon period (12pm to 6pm), the negative relationship between the solar radiation and the air temperature may be interpreted by the contradiction of their changes. While the solar radiation levels have started to decline after midday, the values of on-site air temperatures continued their ascent for most of this period, especially for the locations which were still under the direct sunlight, like H7, H8 and H10. This may be the reason why the solar variable in the Max indicator did not turn out to be significant, where the air temperature measurements of other locations like H1, H2 and H4 followed the track of the ambient air temperature where these locations did not receive the direct solar radiation for all or most of the period while other locations showed different tracks of change like H3, H5, H9 and H12. Therefore, the statistical model did not distinguish the subordination of the air temperature changes to the change of solar radiation regarding the maximum values.

The evening period (6pm - 12am) did not show a real effect of solar radiation with intensities lower than 200 W/m^2 , that declined gradually till disappearing within less than three hours. Furthermore, the measurement locations were shaded early on by urban masses. Therefore, the solar variable became insignificant as shown by the three basic models that could not capture confident relationships between the variation of solar and the variation of in-situ air temperature. Also, the disparity in air temperature levels from one location to another, and the disparity of the rate of

decline during this period leads to a troubled stream of data that was difficult to match with the solar radiation changes. It is noteworthy that some urban morphological parameters like (SF and SVFx) may work as an adjunct to enhance the statistical relationship between the solar and Ta as shown by [Table \(6-8\)](#). The addition of these parameters turned the insignificant solar variable to be influential in the MIN model of the evening period.

7.2.2 The partial cloudy days

The increase of solar radiation led to a decrease in Ta throughout the day time from the start of the morning period to the end of the afternoon period under the partial cloudy sky, However, the solar radiation contributed to elevate the Ta in the evening period while its effect on the Ta at the night period after midnight is unstable where both indicators (AVG and MIN) witnessed insignificant role of solar that influenced negatively on MAX for the same period [see [Table 7-1](#)].

With reference to the solar graph in [Figures 5.12 to 5.17](#), the increase of solar radiation levels from zero to about 30 W/m² within the last half hour of the night period for just four days of the ten partial cloudy days were not enough to act as a significant variable in AVG and MIN models of temperature (Ta). Nevertheless, the maximum changes of solar radiation were linked negatively with the maximum changes of Ta. The contrast between growing solar radiation and the temperature reduction before 6 am is the reason to define negative statistical relationship between the solar and Ta.

Although Ta displayed a rising tendency throughout the morning period for the most partially cloudy days, some of these day experienced a reduction or discontinuity of the increase of solar radiation before midday. This may be the reason behind the negative effect of solar on air temperature models in this period, especially when eight days of the ten witnessed similar changes in solar behaviour.

The levels of solar radiation declined noticeably in the afternoon period. However, the on-site measured air temperature in some locations, like H7, H8 and H10, did not respond immediately, and their temperatures graphics recorded continuous

increases for a long part of this period. Therefore, the statistical models showed that the increase of solar radiation will mitigate the increase air temperature.

The continuous decrease in measured air temperatures in all locations after 6pm until midnight paralleled the gradual shrinkage of solar radiation intensity that reached the zero value within the first three hours of the evening period. Therefore, the positive relationship has been defined between the variables (T_a and solar) because of both were changing in the same way.

7.2.3 The cloudy days

The solar radiation may have had no effect on air temperature at the night period while its increase will lead to a decrease T_a in the other three periods of the day under cloudy skies. The role of solar radiation looks unsteady in the duration from 6 pm to midnight where MIN model experienced insignificant influence of this variable as shown by [Table 7-1](#).

Regarding the morning period, it can be said that, although the increase in solar radiation matched the rise in air temperature for some days, other days witnessed unstable changes of solar radiation that did not match the steady rise in air temperature with the intensity of solar radiation. T_a levels could be higher on these days but also suffered from no rise or a drop as solar radiation levels increased. Consequently, the statistical models gave the negative relationships between solar and T_a for the interval from 6am to 12pm. The continuous decrease in solar radiation for most the afternoon period helped the models to define the negative relationships with T_a where many locations maintained the rising trend for air temperatures for a long time as opposed to the changes in solar radiation levels.

The clear decrease in air temperatures throughout the evening period versus the solar radiation changes may be the reason behind the insignificant effect of solar variable in the MIN model. Furthermore, the negative relationship between solar and T_a in AVG and MAX models may be due to the diversity of air temperature datasets from day to day and from point to point compared to the way the sun disappeared within three hours or less.

During the night period the air temperatures reached their lowest levels in addition to absence the solar radiation for the half number of cloudy days. Therefore, the solar radiation was not a significant variable in the air temperature indicators for this period, especially with the weakness of solar radiation that was recorded in the other half of the cloudy days group. However, the maximum air temperature dataset established a negative relationship with the maximum values of solar radiation under the influence of the urban parameters (SF and SVFx) as shown by [Table \(6-18\)](#). These parameters helped in the changes of the two variables that were moving in opposite directions.

7.3 The Urban Morphological Parameters (UMP)

To discuss the intra-relationships between the urban morphological parameters and the thermal microclimate of the urban space this section will be subdivided into ten parts depending on the number of UMP. Each section will focus on a one of these parameters in terms of the improvement rates and the behaviours of the on-site measured air temperature (Ta).

The improvements rate represents the difference between the values of R-Sq(adj) for the same statistical model before adding the parameter to the basic model (B.M) and after adding the parameter as a modified model (M.M). This approach was to reveal the size of the influence of each parameter on the air temperature indicators (AVG, MAX and MIN) that represent functions for the thermal microclimate of urban space. Although the climatic factor are the dominated variables as shown in the last chapter, the urban parameters work side by side with them to shape the urban microclimate. Adding these variables (climatic variables and UMP) to each other in one model will be more realistic than a model consisting of just an urban parameter. What supports this idea is the increase in the R-Sq(adj) and the accuracy for the M.M against B.M that also improved in terms of the structure of the model. After adding UMPs some insignificant climatic factor turned out to be significant in some models. Therefore, and from the perspective of this study, the improvement rate is more convincing to show the effect size of UMP than a model with a single variable. The contribution of

each UMP throughout the study will gather in one table to show the change of its effectiveness relying on day time and sky conditions.

To get a clear visual comparison, a group of symbols will be utilized to express the improvement rates, as shown in [Figure 7.1](#).

Icons	Rates (%)
	when value is ≥ 40
	when < 40 and ≥ 30
	when < 30 and ≥ 20
	when < 20 and ≥ 10
	when < 10 and ≥ 5
	when < 5 and ≥ 2.5
	when < 2.5 and > 0
	when ≤ 0

Figure 7.1 The symbols of improvement rates (%)

The contribution of urban morphological parameters to increase or decrease the in-situ measured air temperature (T_a) will be the second part of the discussion to draw the whole image for the role of UMP in creating the thermal microclimate. Many other variables, like vegetation and materials are outside of the scope of this study.

7.3.1 Floor Area Ratio (FAR)

This parameter represents the ratio of the total floors areas for all buildings in the buffer zone to the total area of that zone which is defined by 25m as a radius from the measurement point.

Twelve models from 36 modified models (M.M) by FAR as total were not considered statistically to explain the air temperatures variations for the three sky conditions groups throughout the hot season, with the need to note that most of them belong to the cloudy days. An initial comparison between the improvements rates for the three groups of days revealed that the strongest influence of FAR was on the sunny days, as shown by [Table 7-2](#).

Table 7-2 The improvement rates of R-sq(adj) by FAR

SUNNY	Improvement of R-sq(adj) % by FAR - Hot Season			
	UMP	AVERAGE-Ta	MAXIMUM-Ta	MINIMUM-Ta
Night	FAR	0.11	0.13	0.08
Morning	FAR	8.15	10.41	5.74
Afternoon	FAR	0.00	0.00	0.00
Evening	FAR	1.73	1.94	1.42
Total Average		2.50	3.12	1.81
P. CLOUDY	Improvement of R-sq(adj) % by FAR - Hot Season			
	UMP	AVERAGE-Ta	MAXIMUM-Ta	MINIMUM-Ta
Night	FAR	0.05	0.07	0.03
Morning	FAR	1.46	2.33	0.85
Afternoon	FAR	0.58	1.07	0.23
Evening	FAR	0.36	0.54	0.24
Total Average		0.61	1.00	0.34
CLOUDY	Improvement of R-sq(adj) % by FAR - Hot Season			
	UMP	AVERAGE-Ta	MAXIMUM-Ta	MINIMUM-Ta
Night	FAR	0.00	0.00	0.00
Morning	FAR	0.08	0.22	0.00
Afternoon	FAR	0.00	0.33	0.00
Evening	FAR	0.00	0.00	0.00
Total Average		0.02	0.14	0.00

Regarding to the direct effect of FAR on air temperature, a constant behaviour can be noticed between the three groups of days (sunny, partial cloudy and cloudy) as shown by [Table 7-3](#). The floor area ratio has a negative effect on air temperature for

the night, afternoon and evening period, while the morning period witnessed a positive influence by the same parameter.

Table 7-3 the behaviours of air temperature by the effect of FAR

		Sunny days (su)				Partially cloudy days (pr)				cloudy days (cl)			
		ni-su	mo-su	no-su	ev-su	ni-pr	mo-pr	no-pr	ev-pr	ni-cl	mo-cl	no-cl	ev-cl
		FAR	FAR	FAR	FAR	FAR	FAR	FAR	FAR	FAR	FAR	FAR	FAR
INDICATORS	AVG	-	+	X	-	+	-	-	X	+	X	X	
	MAX	-	+	X	-	+	-	-	X	+	-	X	
	MIN	-	+	X	-	+	-	-	X	X	X	X	

Initially, FAR is a well-known measure for urban density and it can be related to the manmade vertical surfaces according to its calculation method. These surfaces have a double behaviour. In the day time, the increase of these surfaces leads to an increase in thermal storage in the urban masses by the direct and diffuse solar radiation. This affects positively and variously on air temperatures from one location to another depending on some circumstances, like the solar duration, the openness to the sky and the surface material, texture and colour. In the night time these accumulations of heat will drop at different speeds depending on the circumstances of each location as a result of emitting longwave radiation and this affects the on-site air temperatures levels.

The positive relationships between FAR and on-site air temperature during the morning period witnessed a rise in air temperature for all measurement points, but the points with the highest rates of FAR saw the highest air temperatures compared to other points due to the increasing of the vertical surfaces areas in those sites. Thus, increasing the radiation received directly and indirectly on these surfaces led to a growth in heat storage and this caused an increase in the air temperature by convection.

Although the afternoon period is still a day time, the on-site air temperatures (Ta) started to drop in most locations, especially that ones with high values of FAR like H11, H12, H3 and H5. In the same period the solar radiation has begun to decline in

general [see [Figures 5.1 to 5.3](#) and [5.12 to 5.20](#)]. Moreover, the direct solar radiation has been blocked from arriving to neighbouring surfaces for most locations with high FAR. The locations with low FAR, like H7, H8 and H10, recorded an upward tendency in air temperature for most of this period. Therefore, it has been seen that there is a negative relationship between FAR and T_a . Increasing FAR causes a decrease in on-site air temperature due to increasing the heat loss from vertical surface areas. Also, the vertical surfaces create shaded areas on the ground and some facades.

The reason of the negative influence of FAR on air temperature in the evening and night periods may be due to the contrasts between the locations that witnessed high values of FAR but low rates of air temperature in these periods, like H11, H4, H12, H3, H5, and the locations that witnessed low values of FAR but high rates of air temperature, like H8, H10, and H7. The early decline of solar radiation from most of the locations with high values of FAR accelerated the pace of heat loss by their vertical surfaces that act as radiators and convectors. Therefore, the statistical models of these period translated these connections as negative relationships with decreasing air temperature due to increasing FAR.

These results do not agree with some studies that detected a different role for FAR, where an increase in FAR may decrease air temperature during the daytime and increase it during the night-time in a tropical climate because of the effect of mutual shading between buildings during the day time. The high FAR may reduce the wind speed that carries heat away from the urban surfaces in the night time (Jin et al. 2018).

7.3.2 Site Coverage Ratio (SCR)

SCR describes the relationship between built and open space for a site. It is calculated as the ratio between the total ground floor area of buildings within the buffer zone and the total area of the zone land. Therefore, it is related to the horizontal allocation of buildings on the site.

Twelve modified models by SCR did not contribute in the statistical analyses of air temperature diversity, especially for the night and evening periods, while the ineffective role of SCR was noticed in the daytime periods (morning and afternoon), as shown by Table 7-4. Although the sunny days group witnessed the largest number of insignificant models, it recorded the better improvement rates compared to other groups. However, SCR did not affect air temperature remarkably where the improvement rates did not cross the barrier of 5% at all.

Table 7-4 The improvement rates of R-sq(adj) by SCR

SUNNY	Improvement of R-sq(adj) % by SCR - Hot Season			
	UMP	AVERAGE-Ta	MAXIMUM-Ta	MINIMUM-Ta
Night	SCR	0.00	0.00	0.00
Morning	SCR	3.96	4.69	3.18
Afternoon	SCR	0.81	0.96	0.79
Evening	SCR	0.00	0.00	0.00
Total Average		1.19	1.41	0.99
P. CLOUDY	Improvement of R-sq(adj) % by SCR - Hot Season			
	UMP	AVERAGE-Ta	MAXIMUM-Ta	MINIMUM-Ta
Night	SCR	0.03	0.04	0.00
Morning	SCR	1.02	1.42	0.69
Afternoon	SCR	0.48	0.44	0.49
Evening	SCR	0.00	0.00	0.00
Total Average		0.38	0.47	0.30
CLOUDY	Improvement of R-sq(adj) % by SCR - Hot Season			
	UMP	AVERAGE-Ta	MAXIMUM-Ta	MINIMUM-Ta
Night	SCR	0.00	0.09	0.00
Morning	SCR	0.59	0.64	0.44
Afternoon	SCR	0.69	0.52	1.02
Evening	SCR	0.20	0.28	0.14
Total Average		0.37	0.38	0.40

According to Table 7-5, the site coverage ratio showed identical effects on in-situ air temperature during the morning and the afternoon periods regardless the state of

the sky. Where increasing the value of SCR leads to increase the air temperature and vice versa. Also, the evening period under the cloudy sky witnessed the same influence of SCR.

Table 7-5 The behaviours of air temperature by the effect of SCR

		Sunny days (su)				Partially cloudy days (pr)				cloudy days (cl)			
		ni-su	mo-su	no-su	ev-su	ni-pr	mo-pr	no-pr	ev-pr	ni-cl	mo-cl	no-cl	ev-cl
		SCR	SCR	SCR	SCR	SCR	SCR	SCR	SCR	SCR	SCR	SCR	SCR
INDICATORS	AVG	X	+	+	X	-	+	+	X	X	+	+	+
	MAX	X	+	+	X	-	+	+	X	+	+	+	+
	MIN	X	+	+	X	X	+	+	X	X	+	+	+

The high values of site coverage ratio include less the intra-spaces and further urban blocks where this binary activity obscures more sky and leads to reduced solar radiation which may reach the ground and the external walls of buildings. It seems that this idea is not controversial - a study in the city of Geneva (Switzerland) showed that SCR had a strong negative correlation with the annual solar irradiation on the building façades because of increasing the mutual shading between buildings (Mohajeri et al. 2016).

This conflict between decreasing the solar radiation and increasing the air temperature as a response to an increasing SCR may be interpreted in several ways. The solar duration on the building façades may also be affected by the degree of horizontal obstruction that controls the incident sun radiation. Any reflected solar radiation will have escaped out due to the narrow spaces in the building’s layout. Consequently, this causes the surfaces and air to be heated. More urban masses means an increase in roof areas, which act as reservoirs of heat for the absorbed solar radiation. The accumulation of heat throughout the daytime is responsible for the elevation of the air temperature as a response to an increase in SCR at the evening period where the outgoing long wave radiation will be trapped.

Strengthening the role of wind movement is a one of countermeasure against the heat island in the urban fabric, where it has been proved that a decrease of SCR increases the urban ventilation (Takebayashi 2015). This study may endorse that

study, as the results from this work indicate that an increase of SCR will lessen the wind speed and increase the air temperature. In terms of decreasing the air temperature by increasing SCR in the night period under the partially cloudy sky, it may also have resulted from the increase of rain rates compared to other two groups (sunny and cloudy) as shown by [Figures 5.12 to 5.17](#).

These results partially agree with a study conducted under a sub-Mediterranean climate in Florence, Italy, where the site coverage ratio had a positive relationship with summer season air temperatures (Petralli et al. 2014). However, the minimum air temperature was affected by SCR more strongly than the maximum air temperature, which contrasts with the results of this study which witnessed something similar only in the afternoon period under the partially cloudy and cloudy skies, where the differences were very small, as shown in [Table 7-4](#). Moreover, a study in Shanghai-China reported that the minimum air temperature will increase as a response to the increasing of SCR values because more heat radiation will be stored in the surfaces of the additional blocks (Wei et al. 2016).

Another study in the centre of Bangkok investigated the relationships between the near-surface air temperature as the average of daytime in the hot season with some parameters, including site coverage ratio and floor area ratio. The results demonstrated that the increasing SCR or FAR values elevated the air temperature. Furthermore, SCR had a stronger influence on the air temperature compared to FAR (Srivanit & Kazunori 2011). However, the role of SCR may support some of this study's results, but its superiority over FAR is consistent only for the cloudy sky results. The predominance of SCR against FAR was reported again but in a different climate area (Seoul, South Korea) where the summer air temperature as a maximum and an average increased in response to escalation of SCR values due to rising building shading and hindered wind movement (Park et al. 2018). On the other hand, FAR had a negative relationship with air temperature and this is contrary to this study's findings for a mild maritime climate.

Salvati, Coch and Morganti, (2017), on the other hand, found that increasing urban compactness, measured as SCR, for a Mediterranean climate, caused a decrease in

building cooling demand due to the narrowness of the spaces between buildings, which blocked solar radiation, thereby lowering the external air temperature.

Overall, although SCR is a one of the urban fabric density measures, it is not easy to evaluate and justify its effect on air temperature, especially as it is possible to get analogous values of SCR for different locations that show a diversity in their configurations in terms of sky line, permeability, layout of buildings and their distribution on site.

7.3.3 Compactness Index (CI)

Compactness index represents the ratio between the floor area ratio (FAR) and the site coverage ratio (SCR) i.e. it is the ratio of total floors area to total ground floors area for buildings inside the buffer zone.

Sunny days did contribute statistically with CI. However, nine models belonging to other groups did not contribute positively in statistical analyses. The distribution of these models was more systematic compared to FAR and SCR and more related to the thermal storage reduction for the urban surfaces. Where they settled in the night period under the partial cloudy sky and both the night and morning periods under the cloudy sky as shown by [Table 7-6](#). CI generally produced better agreement than FAR and SCR, especially in the afternoon and evening periods, by achieving a lower number of insignificant models. This may be because the compactness index represents the relationship between the urban vertical obstructions and their horizontal distribution on a site. Therefore, the urban space configuration around the measurement point was described in more accuracy in terms of the exposure to the direct and diffuse solar radiation from above or from the side depending on the porosity of the buildings layout. Moreover, it affects the long wave radiation exchanges and wind movement.

Disparities in the effectiveness of CI against FAR and SCR have been highlighted by a study in Sao Paulo, Brazil that showed the compactness index is superior versus both FAR and SCR in terms of interpretation of solar radiation and daylight diversities on

the roof of buildings whereas CI came below site coverage ratio and floor cover ratio regarding to the façades of buildings (Cheng et al. 2006).

Table 7-6 The improvement rates of R-sq(adj) by CI

SUNNY	Improvement of R-sq(adj) % by CI - Hot Season			
	UMP	AVERAGE-Ta	MAXIMUM-Ta	MINIMUM-Ta
Night	CI	☺ 0.22	☺ 0.25	☺ 0.18
Morning	CI	☹ 3.92	☹ 5.47	☺ 2.47
Afternoon	CI	☺ 2.40	☹ 2.92	☺ 1.84
Evening	CI	☹ 3.57	☹ 3.97	☹ 2.97
Total Average		2.53	3.15	1.87
P. CLOUDY	Improvement of R-sq(adj) % by CI - Hot Season			
	UMP	AVERAGE-Ta	MAXIMUM-Ta	MINIMUM-Ta
Night	CI	☹ 0.00	☹ 0.00	☹ 0.00
Morning	CI	☺ 0.53	☺ 0.96	☺ 0.26
Afternoon	CI	☹ 2.74	☹ 4.09	☺ 1.64
Evening	CI	☺ 0.67	☺ 1.01	☺ 0.44
Total Average		0.98	1.52	0.58
CLOUDY	Improvement of R-sq(adj) % by CI - Hot Season			
	UMP	AVERAGE-Ta	MAXIMUM-Ta	MINIMUM-Ta
Night	CI	☹ 0.00	☹ 0.00	☹ 0.00
Morning	CI	☹ 0.00	☹ 0.00	☹ 0.00
Afternoon	CI	☺ 2.14	☹ 2.61	☺ 1.32
Evening	CI	☺ 0.54	☺ 0.60	☺ 0.46
Total Average		0.67	0.80	0.44

In terms of the effect on air temperature, the compactness index (CI) showed analogous behaviour to the floor area ratio (FAR), where increasing CI values reduced the air temperature in the night, afternoon and evening periods while having a positive relationship with CI in the morning period, as shown by Table 7-7. This behaviour is because of the values of parameters FAR and CI that describe the spatial configuration around the measurement points have witnessed similarities in the change tendency as shown by Figures 5.24 and 5.26. Therefore, they show a strong correlation between them ($r=0.79$, $p=0.007$) and the statistical models showed about the same influences on the air temperature. Although SCR contributed in the calculation process of the compactness index, there is no correlation between CI and SCR ($r=0.004$, $p=0.99$) and this may be due to the absence of an important difference in the area between the grounds floor and each of the upper floors for the same building. In this case the value of CI may represent the average number of floors that

describes the vertical configuration in each zone more than the horizontal configuration and this had led to the lack of a relationship between CI and SCR that deal with horizontal obstructions.

Table 7-7 The behaviour of air temperature by the effect of CI

		Sunny days (su)				Partially cloudy days (pr)				cloudy days (cl)			
		ni-su	mo-su	no-su	ev-su	ni-pr	mo-pr	no-pr	ev-pr	ni-cl	mo-cl	no-cl	ev-cl
		CI	CI	CI	CI	CI	CI	CI	CI	CI	CI	CI	CI
INDICATORS	AVG	-	+	-	-	X	+	-	-	X	X	-	-
	MAX	-	+	-	-	X	+	-	-	X	X	-	-
	MIN	-	+	-	-	X	+	-	-	X	X	-	-

7.3.4 Degree of Compactness (Dc)

It is the product of multiplication process for the site coverage ratio (SCR) with the average number of floors inside the buffer zone.

Thirteen modified models by Dc did not hold up statistically and they were distributed in a similar pattern to the insignificant models for the compactness index (CI), where most of them were concentrated in the cloudy days and less in the partially cloudy days, as shown by Table 7-8. Maybe this likeness is a result of considering the average number of floors in both of them. Two points may support this claim. Firstly, there is a high correlation between CI and Dc ($r=0.753$, $p=0.007$). Secondly, Dc also has a strong link with FAR and there is no significant correlation with SCR [see Table 5-2], although the latter is a part of the calculation methods for both parameters CI and Dc. The sunny days showed the best improvement rates with no insignificant models compared to the partially cloudy and cloudy days respectively. In general, these rates are lower than their counterparts with the parameters CI, FAR, and SCR. However, some models broke this rule in the afternoon periods against both of SCR and FAR where it can be referred to this behaviour as another point of harmony between Dc and CI.

Table 7-8 The improvement rates of R-sq(adj) by Dc

SUNNY	Improvement of R-sq(adj) % by Dc - Hot Season			
	UMP	AVERAGE-Ta	MAXIMUM-Ta	MINIMUM-Ta
Night	Dc	0.07	0.08	0.07
Morning	Dc	2.39	3.28	1.63
Afternoon	Dc	1.11	1.24	0.83
Evening	Dc	1.62	1.59	1.53
Total Average		1.30	1.55	1.02
P. CLOUDY	Improvement of R-sq(adj) % by Dc - Hot Season			
	UMP	AVERAGE-Ta	MAXIMUM-Ta	MINIMUM-Ta
Night	Dc	0.00	0.00	0.00
Morning	Dc	0.47	0.74	0.28
Afternoon	Dc	0.90	1.48	0.48
Evening	Dc	0.25	0.37	0.17
Total Average		0.40	0.65	0.23
CLOUDY	Improvement of R-sq(adj) % by Dc - Hot Season			
	UMP	AVERAGE-Ta	MAXIMUM-Ta	MINIMUM-Ta
Night	Dc	0.00	0.00	0.00
Morning	Dc	0.00	0.00	0.00
Afternoon	Dc	0.38	0.53	0.00
Evening	Dc	0.00	0.00	0.00
Total Average		0.10	0.13	0.00

The negative influences of Dc on the on-site air temperature throughout the night, afternoon and evening periods in addition to the positive effect in the morning period are shown in [Table 7-9](#).

Table 7-9 the behaviours of air temperature by the effect of Dc

INDICATORS		Sunny days (su)				Partially cloudy days (pr)				cloudy days (cl)			
		ni-su	mo-su	no-su	ev-su	ni-pr	mo-pr	no-pr	ev-pr	ni-cl	mo-cl	no-cl	ev-cl
		Dc	Dc	Dc	Dc	Dc	Dc	Dc	Dc	Dc	Dc	Dc	Dc
AVG	-	+	-	-	X	+	-	-	X	X	-	X	
MAX	-	+	-	-	X	+	-	-	X	X	-	X	
MIN	-	+	-	-	X	+	-	-	X	X	X	X	

The locations with the highest Dc values also have the largest vertical surface areas, like H11, H3 and H12, and this nominates them to receive bigger amounts of direct and diffuse solar radiation that cause an increase in air temperature (Ta), especially

in the morning periods. The afternoon periods witnessed turbulent behaviour of T_a between the different locations and the different days, where T_a increased in some points and decreased in others. But the semi-frequent behaviour that can be observed is the decreasing air temperatures in some sites that have high D_c values due to the changing of sun location and appearing the shadow areas on the walls and grounds as well as the general increasing wind speed in this period, while the air temperatures increase at other sites that have low D_c values because of the direct solar radiation. These behaviours contributed to the negative relationship that suggest that the increasing D_c values may help to decrease the air temperatures in the afternoon period.

After sunset there were differences in terms of the thermal conditions. Some locations with high values of D_c had started to lose their solar gain early compared to other locations that were receiving solar radiation until late even though they recorded the lower values of D_c . Therefore, the graphics of air temperature for the evening period showed two groups of locations where the group with lower air temperatures was, in general, the group with higher D_c values. Therefore, the statistical models showed that the increasing D_c values led to a reduction in the on-site air temperatures in the evening period. What happening in the evening period did continue into the night time but at slower rates because of the stored heat all sites having been reduced. However, some of locations, like H8 and H10, did remain higher than the rest of the sites for most this period and therefore the increasing of D_c led to a decrease of T_a in this period.

An important point should be highlighted here to explain the similarity in behaviours between FAR, CI and D_c . This is due to the absence of big differences between the layout of the ground floors and their related upper floors for the most types of building in the case study. Therefore, the three parameters had convergent patterns of change from one location to other that caused the strong correlation between them as was mentioned before. However, this simple difference in the pattern led to sensible differences in terms of the size effect of each of them on air temperature.

A study under the climate of Cairo, Egypt referred to the role of compactness degree in ameliorating the thermal comfort as a part of approach for hybrid passive urban

form that include the arrangement and dense of trees, orientation and clustered urban forms (Fahmy & Sharples 2009a; Fahmy & Sharples 2011). However, another study in Cairo devoted to the effect of Dc as a solo parameter on thermal comfort under the future scenarios of climate change found a limited potential for Dc as a solo urban parameter, while the increase of Dc did not improve thermal comfort levels under the worse future conditions (Fahmy 2012). Those result support the results from this study in terms of the limited impact of Dc on thermal microclimate.

7.3.5 Façade to Site Ratio (FSR)

FSR represent the ratio between the total summation of façade areas inside the buffer zone and the area of the zone that is defined with a radius that equals 25m.

Seventeen of the 36 modified models by adding FSR were not adopted to explain the air temperature variations throughout the hot season. They were distributed almost equally on the three groups, as shown by [Table 7-10](#).

FSR has some common features that made it show strong correlations with each of the parameters: FAR ($r=0.945$, $p=0$), Dc ($r=0.798$, $p=0.003$) and CI ($r=0.735$, $p=0.01$). Where FSR can be considered as an expression of surface area (skin) for the vertical obstructions against the concept of mass (body) that adopted by these parameters. Therefore, the improvements rates by FSR for the morning period exceeded the mentioned before parameters due to the façades areas of a building may are more accurate to express the outer vertical surfaces that associated with the radiation balance (absorption, emission and reflection) than the mass of the building.

On the other hand, FSR did not success at all with the afternoon periods although the timing is still daytime and perhaps the sun rays still heating some urban surfaces in the study area. This ambivalence can be understood if we realize that the configuration of western sides for the urban spaces influences the values of some urban morphological parameters (UMP) and FSR is one of them where significant correlations were found with other parameters that describe the western side configuration like FVFw ($r=0.719$, $p=0.013$) and SVFw ($r=-0.623$, $p=0.041$). Furthermore, the direct radiation throughout the morning period hits these sides at

H11, H12 and H3 [see Figure 5.1 to 5.3] where most of these locations witnessed high values of FSR while the western surfaces lost this superiority in favour of the eastern surfaces in the afternoon. By time the sun will recede from the western sides to start in illuminate the eastern sides at around midday and continue throughout the afternoon period and beyond, especially at H8, H7 and H10, where these locations recorded lower values of FSR However, they witnessed higher air temperatures than others by an active participation from the northern sides in addition to the eastern sides. Therefore, the improvement rates of FSR were better in the morning period.

Table 7-10 The improvement rates of R-sq(adj) by FSR

SUNNY	Improvement of R-sq(adj) % by FSR - Hot Season			
	UMP	AVERAGE-Ta	MAXIMUM-Ta	MINIMUM-Ta
Night	FSR	☒ 0.00	☒ 0.00	☒ 0.00
Morning	FSR	☺ 9.99	☑ 12.74	☺ 7.03
Afternoon	FSR	☒ 0.00	☒ 0.00	☒ 0.00
Evening	FSR	☺ 0.69	☺ 0.85	☺ 0.47
Total Average		2.67	3.40	1.88
P. CLOUDY	Improvement of R-sq(adj) % by FSR - Hot Season			
	UMP	AVERAGE-Ta	MAXIMUM-Ta	MINIMUM-Ta
Night	FSR	☺ 0.01	☺ 0.03	☒ 0.00
Morning	FSR	☺ 1.66	☺ 2.70	☺ 0.94
Afternoon	FSR	☒ 0.00	☒ 0.00	☒ 0.00
Evening	FSR	☺ 0.19	☺ 0.31	☺ 0.12
Total Average		0.47	0.76	0.27
CLOUDY	Improvement of R-sq(adj) % by FSR - Hot Season			
	UMP	AVERAGE-Ta	MAXIMUM-Ta	MINIMUM-Ta
Night	FSR	☺ 0.10	☺ 0.13	☺ 0.09
Morning	FSR	☺ 0.13	☺ 0.32	☒ 0.00
Afternoon	FSR	☒ 0.00	☒ 0.00	☒ 0.00
Evening	FSR	☒ 0.00	☒ 0.00	☒ 0.00
Total Average		0.06	0.11	0.02

In general, the afternoon period witnessed a lowering of air temperatures at some locations that had high FSR whereas air temperatures grew at other locations with low values of FSR. H4 recorded one of the highest values of FSR and with a modest climb in air temperature, especially in the sunny days; moreover, H5 and H9 logged moderate air temperatures compared to other locations although they recorded high and low values of FSR respectively. All this variability in trends did not help to fit the

variation of FSR with the variation of on-site measured air temperatures for the times between 12pm and 6pm.

In terms of the effect of FSR on the behaviour of in-situ air temperatures, the increasing of FSR caused increasing air temperatures in the morning period, as shown by [Table 7-11](#). All locations at this period, regardless the sky conditions, witnessed an upward trend of air temperature, and especially the ones with high FSR values, where the absorption and reflection rates of solar radiation were heightened by the increasing areas of facades. Therefore, a positive relationship has been statistically identified.

Table 7-11 The behaviours of air temperature by the effect of FSR

		Sunny days (su)				Partially cloudy days (pr)				cloudy days (cl)			
		ni-su	mo-su	no-su	ev-su	ni-pr	mo-pr	no-pr	ev-pr	ni-cl	mo-cl	no-cl	ev-cl
		FSR	FSR	FSR	FSR	FSR	FSR	FSR	FSR	FSR	FSR	FSR	FSR
INDICATORS	AVG	X	+	X	-	-	+	X	-	+	+	X	X
	MAX	X	+	X	-	-	+	X	-	+	+	X	X
	MIN	X	+	X	-	X	+	X	-	+	X	X	X

The air temperatures were dropping with increasing FSR in the evening periods for sunny days and partial cloudy days. From 6pm to 12 am the air temperatures dropped in all measuring points irrespective of the sunset time, but the reduction in some locations that had low FSR values and high thermal capacity, like H8, H7 and H10, was at a faster pace compared to many locations with higher values of FSR and low thermal capacity, like H11 and H12. This inconsistency was translated statistically into negative relationships between Ta and FSR.

Some locations tended to be warmer in the night period for the cloudy days, like H8 [see [Figure 5.18 to 5.20](#)], However, most of the heat stored in the vertical surfaces was dissipated in this period. As a result, the air temperatures graphs look like sloped lines for the longest part of this period and, furthermore, the average wind speed was about 3 m/s in this period. Therefore, it may be that the rate of air temperature lowering at some points that had small FSR values was faster than other sites and this

statistically indicates that the increasing of FSR will limit the air temperature drop. Due to the concurrence of larger values of the FSR with the lower levels of heat dispersion, a positive relationship between them was defined, while a negative effect on air temperature by increasing FSR was noticed for the same period at the partial cloudy sky. The air temperatures differences were mostly negligible, and they were moving in smooth and homogeneous flows. Therefore, the heat losses that led to reduced air temperatures will rise by increasing the wall areas, especially with high levels of rain and a wind movement which typically oscillated between 2 m/s and 4 m/s.

A simulation study that used data from weather stations located in an open area outside of Toulouse, France and Basel, Switzerland (mild climates). This was to simulate air temperatures inside urban canyons by urban weather generator model (UWG) showing that FSR is one of most effective morphological parameters for air temperature variation (UHI) (Bueno et al. 2013). Other studies in Boston, USA (cold climate) (Nakano, Bueno, Norford & C. F. C. F. Reinhart 2015) and Punggol, Singapore (tropical climate) (Bueno et al. 2014) showed that FSR is important for air temperatures in Boston while it is not significant for Punggol, perhaps because the building height variations were too small for the low and high ranges. This research agrees with the results from Toulouse, Basel and Boston but just in morning periods under the sunny and partially cloudy skies, while this study's findings agree with the Punggol results for the other periods.

In terms of annual façade solar gains, FSR showed good negative linear correlation in the urban textures of Rome and Barcelona as Mediterranean cities, where increasing the density of urban site reduced the visible sky from façades (Morganti et al. 2017). For air temperatures this means the increasing of FSR leads to a decrease in air temperature. Conversely, another study for the same cities proved that the increasing of FSR elevated the average difference of air temperatures between rural and urban areas (Salvati et al. 2015). The latter point supports this research, but just in the morning period irrespective of sky conditions, while increases in FSR led to reduced T_a in other periods, except the night period for the cloudy days.

7.3.6 Shape Factor (SF)

SF is the summation of the ratios between the surface area and the volume for each built mass inside the buffer zone.

According to [Table 7-12](#), just seven models of the morning periods did not explain the differentiation of air temperature depending on the shape factor variations, probably because the morning period is the least stable period due to the changes of thermal storage is relatively quick and varied notably from one location to another compared to other periods. Therefore, the necessity for more measuring points, larger number of days or both can be suggested to override failure models, especially the best improve rates were recorded in the afternoon period that represent the second half of the day time and the second least stable period.

Table 7-12 The improvement rates of R-sq(adj) by SF

SUNNY	Improvement of R-sq(adj) % by SF - Hot Season			
	UMP	AVERAGE-Ta	MAXIMUM-Ta	MINIMUM-Ta
Night	SF	2.41	2.33	2.42
Morning	SF	0.00	0.00	0.00
Afternoon	SF	11.95	13.03	10.60
Evening	SF	6.44	6.13	6.64
Total Average		5.20	5.37	4.92
P. CLOUDY	Improvement of R-sq(adj) % by SF - Hot Season			
	UMP	AVERAGE-Ta	MAXIMUM-Ta	MINIMUM-Ta
Night	SF	0.55	0.56	0.55
Morning	SF	0.00	0.00	0.00
Afternoon	SF	5.73	8.03	3.68
Evening	SF	1.31	1.55	1.11
Total Average		1.90	2.54	1.34
CLOUDY	Improvement of R-sq(adj) % by SF - Hot Season			
	UMP	AVERAGE-Ta	MAXIMUM-Ta	MINIMUM-Ta
Night	SF	3.30	3.50	3.17
Morning	SF	0.26	0.00	0.44
Afternoon	SF	3.89	4.57	2.85
Evening	SF	1.48	1.47	1.51
Total Average		2.23	2.39	1.99

However, SF can be considered as one of the best parameters in terms of improvement rates for all periods irrespective the sky types if it is compared to the

other urban morphological parameters (UMP). This amelioration may be because the shape factor represents the more accurate description for built mass within an urban site, especially with the involvement of the roof area that generally has a bigger exposure to the sky. In addition, roofs are less influenced by the urban geometry compared to walls in terms of solar gain (Morganti et al. 2017). The volumes of the buildings affect the size of the shading areas, which increased the uniqueness of the each site compared to another.

The shape factor showed a unique behaviour regarding its effect on air temperature. Increasing SF led to an increasing air temperature irrespective of the period or sky condition, as shown by Table 7-13. The values of SF [see Figure 5.29] did not show a clear rhythm of change that was commensurate with changes in the sun’s position and solar radiation levels like FAR and CI. Therefore, this unique behaviour can be explained depending on the general rules of urban microclimate where increasing the value of SF refers to increased surface area of the building against its volume. Therefore, increasing the thermal gain from direct and diffuse solar radiation increases the heat storage for this surface, and consequently the air temperature will rise. Conversely, decreasing the surface area against volume causes reduced values of SF and air temperature. Therefore, the statistical models will define positive relationships between SF and air temperature in both cases.

Table 7-13 the behaviours of air temperature by the effect of SF

		Sunny days (su)				Partially cloudy days (pr)				cloudy days (cl)			
		ni-su	mo-su	no-su	ev-su	ni-pr	mo-pr	no-pr	ev-pr	ni-cl	mo-cl	no-cl	ev-cl
		SF	SF	SF	SF	SF	SF	SF	SF	SF	SF	SF	SF
INDICATORS	AVG	+	x	+	+	+	x	+	+	+	+	+	+
	MAX	+	x	+	+	+	x	+	+	+	x	+	+
	MIN	+	x	+	+	+	x	+	+	+	+	+	+

For further clarification on the relationships between the air temperature and SF consider that there are two identical buildings, one of which has kept its original size whilst the other was enlarged by double or more. It can be noticed the values of SF for them are not equal. The SF value for the smaller alternative is bigger, although it

has a smaller surface area and smaller volume, and the surface area witnesses a smaller increase compared to the volume increase by enlarging the building size. The change of this ratio leads to changes in the environmental impact of the building. For instance, about 90% of cooling load in houses is because of the weather factors while this percentage drops to 60% in large buildings where the orientation and form are of secondary importance against the effect of the ratio (surface area (SA) / volume (V)) (Olgyay et al. 2015). Increasing SF for houses block compared to multi story building block may cause a rise in air temperature and energy consumption. Therefore, it can say the results of this research supports the findings from the Olgyay work.

7.3.7 Sky View Factor (SVF)

Sky View Factor represents the openness of a site to the sky and is represented as the ratio of the visible sky area to the area of the hemispherical projection that describe the sky border depending on the configurational features of the visible surfaces around the observation point that represents the centre of the projection.

Two modified models of SVF did not take part statistically in on-site air temperature analyses for the night period under the partial cloudy sky. Thus, SVF is better than many parameters in terms of the number of fruitless models as shown in [Table 7-14](#). However, the improvement percentages of SVF did not significantly outperform other parameters, especially SCR, where the latter had a morphological relationship with SVF according to the correlation values ($r = -0.66$, $p = 0.025$). Increasing SCR causes a decrease in the intra-spaces between urban masses and so, consequently, the openness to sky will decrease and be followed by a reduction of the SVF value. It is worth noting that SVF did not correlate to the other parameters that consider the height of buildings, like FAR, DC and FSR, although it is affected by the skyline that varies depending on several factors, the most important of which is the height. This can be attributed to the subordination of SVF values to only the visible objects around the measurement point, while the other parameters take in to consideration the heights of all urban blocks inside the buffer zone regardless of the point. The negative

acceptable correlation between SVF and FVF ($r = -0.58$, $p = 0.062$) may support this suggestion, although it is statistically insignificant. FVF deals exclusively with visible surfaces around the point.

Table 7-14 The improvement rates of R-sq(adj) by SVF

SUNNY	Improvement of R-sq(adj) % by SVF - Hot Season			
	UMP	AVERAGE-Ta	MAXIMUM-Ta	MINIMUM-Ta
Night	SVF	0.82	0.71	0.91
Morning	SVF	1.12	1.05	1.28
Afternoon	SVF	0.75	0.86	0.61
Evening	SVF	1.96	1.64	2.16
Total Average		1.16	1.07	1.24
P. CLOUDY	Improvement of R-sq(adj) % by SVF - Hot Season			
	UMP	AVERAGE-Ta	MAXIMUM-Ta	MINIMUM-Ta
Night	SVF	0.00	0.00	0.03
Morning	SVF	0.27	0.29	0.25
Afternoon	SVF	0.72	0.80	0.65
Evening	SVF	0.30	0.35	0.25
Total Average		0.32	0.36	0.30
CLOUDY	Improvement of R-sq(adj) % by SVF - Hot Season			
	UMP	AVERAGE-Ta	MAXIMUM-Ta	MINIMUM-Ta
Night	SVF	1.31	1.34	1.33
Morning	SVF	0.38	0.20	0.45
Afternoon	SVF	0.63	0.41	0.87
Evening	SVF	0.45	0.48	0.44
Total Average		0.69	0.61	0.77

The best improvement rates were seen in the morning and evening periods for sunny days, where the changes of in-situ air temperature may be affected directly by the solar radiation after sunrise and by the emitted long wave radiation to the sky after sunset. In terms of the period from 6am to 12pm, the amounts, positions and shapes of openness are convergent for the locations H3, H11 and H12, and for H5 and H9. All these locations received direct solar radiation throughout this period. Therefore, they witnessed notable changes in air temperature [see Figures 5.1 to 5.3].

The attributes of SVF regarding to the degree of openness are convergent and the skyline shapes vary between the locations H8, H7 and H10. However, they witnessed the higher air temperatures at the evening period because of the openness positions that caused the high thermal storage by the direct solar gain before the sun set, especially for H8, that kept the heat for a long time and recorded the highest levels

of Ta owing to the ratio between the vertical surfaces and the dimensions of the space. The low air temperatures for some locations that have similar features of SVF, like H1 and H2, in addition to their low levels of radiation, might be affected by the wind speed that rose slightly at the end of the evening period of the sunny days. The night period showed better improvement rates than other periods for the cloudy days. It may be the reason behind that is the discrepancy in the wind speed, that dropped to about 2 m/s in the days with the higher air temperature differences in this period compared to about 3.5 m/s in other days [see Figure 5.18 to 5.20], where the locations H8, H3 and H5 had the highest air temperatures compared to H1, H2, H9 and H12 that mostly showed the lowest air temperatures.

In terms of the effect of SVF on air temperature, the latter decreased in response to increasing SVF values, regardless of the sky conditions and the day hours, as shown by Table 7-15. The bigger value of SVF may cause more heat loss from the surfaces into the sky and more openness may support the influence of air movement as an assistant factor that accelerate the process. However, the inverse effect is also likely due to increasing the radiation levels that reach the urban surfaces, especially during the daylight hours.

Table 7-15 The behaviours of air temperature by the effect of SVF

		Sunny days (su)				Partially cloudy days (pr)				cloudy days (cl)			
		ni-su	mo-su	no-su	ev-su	ni-pr	mo-pr	no-pr	ev-pr	ni-cl	mo-cl	no-cl	ev-cl
		SVF	SVF	SVF	SVF	SVF	SVF	SVF	SVF	SVF	SVF	SVF	SVF
INDICATORS	AVG	-	-	-	-	X	-	-	-	-	-	-	-
	MAX	-	-	-	-	X	-	-	-	-	-	-	-
	MIN	-	-	-	-	-	-	-	-	-	-	-	-

On-site air temperatures generally increased throughout the morning period in all locations regardless the sky conditions, however, some location that had low SVF values, like H3, H12 and H11, showed higher air temperatures compared to the locations with higher SVF, like H1, H2, H5 and H9. So, SVF appeared as to be an inhibitor for air temperature rises. This role of SVF continued in the afternoon period under the influence of the superiority of locations that had small SVF values, like H7,

H8 and H10, versus sites with large SVF values like H1, H2 and H4 in regard to an increase of air temperatures. This role was also repeated at the night and evening periods, where some locations that had low values of SVF recorded higher air temperatures for many reasons, like the hindering of long wave radiation emitted to the sky at night or disruption of the wind influence in heat mitigation and other effects that may be outside the scope of this research. The other locations that had higher values of SVF recorded lower air temperatures.

Similar negative relationships were reported previously in a study that brought together SVF and UHI intensity by investigating the differences of air temperature between the city centre of Manchester, UK and its outskirts, based on 59 sites for clear and calm summer and winter nights. A weak linear relationship was revealed between the two variables ($R^2=32\%$ for summer nights/ $R^2 =36\%$ for winter nights). But these percentages improved to 63% and 53% respectively when the investigation was limited to the city centre canyons with SVFs smaller than 0.65 in general for the ten measurement sites in the summer and the nine sites in the winter (Cheung et al. 2016). These results support this study's findings in terms of the negative effect of SVF. However, the disagreement between the two studies is obvious due to the significant improvement of SVF effects when the study was confined to the city centre of Manchester. This may be attributed to the differences in the configuration of the two study samples where this study adopted urban spaces in a residential complex while the other study adopted streets in a city centre.

Another study used the air temperature data for the first three hours after sunset in 36 clear, calm nights from sixteen stations during two years of measurements in Goteborg, Sweden to examine statistically how changes of SVF heights depending on fish-eye photographs levels (at ground level and 2m above ground) may affect the relationship of SVF/air temperature. The results of simple liner regression indicated a negative fairly relationships between SVF and air temperature where the coefficient of determination was better for ground level SVF ($R^2=0.58$) than 2m over ground SVF ($R^2=0.51$) (Svensson 2004). The results of this study also support this research. However, the Swedish study did suggest some effect of SVF on air temperature against the weak effect that has been introduced here. This may be because of the

time and the length of measurement period that was limited by the three hours after sunset where the thermal heat storage of urban surfaces might still be high.

The influence of SVF on air temperature was investigated statistically depending on outputs of simulation processes based on four urban areas (each 300m x 300m) in Montreal, Canada. The four hours of data after sunset from two days in winter and summer seasons were used in addition to the daytime data of the summer days. Mostly, all receptors were in urban canyons at a height of 1.5m above the ground. The results revealed that higher SVF led to lower air temperatures in the nights of summer and winter, however, it increased with increasing SVF for the summer daytime. However, although this study suggested SVF as a one of the most important factors that influences the urban environment and mitigates UHI in city centres, the coefficient of determination (R^2) ranged from fair to weak - for summer nights it was $R^2= 0.25$, which was lower than for winter night ($R^2= 0.53$) and it was lowest in the summer daytime ($R^2= 0.039$) (Wang & Akbari 2014). In general, the Canadian findings support this study's results, although the positive effect of SVF in the summer daytime may result from the use of the air temperature data as one set from sunrise to sunset for just one day.

7.3.8 Partial Sky View Factor (SVF_x)

The idea of the Partial Sky View Factor is that the sky hemisphere is subdivided diagonally into four quadrants that follow the four cardinal directions of the compass (N, E, S and W) where each subdivision represents the openness degree to sky on that direction. Therefore, there are four values of SVF_x as (SVF_n, SVF_e, SVF_s and SVF_w) and each of them can be calculated as a ratio between the area of sky in the quadrant and the area of the hemisphere.

The use of SVF_x gave results that were an improvement compared to the all UMP. For examples, some of the SVF_x rates crossed the barrier of 40% compared to the nearest competitor (FVF_x) which exceeded the threshold of 30%; furthermore, SVF_x did not display any insignificant models throughout the hot season. The sunny days

recorded the highest rates compared to the partial cloudy and cloudy days respectively, as shown by [Table 7-16](#).

Table 7-16 The improvement rates of R-sq(adj) by SVF_x

SUNNY	Improvement of R-sq(adj) % by SVF _x - Hot Season			
	UMP	AVERAGE-Ta	MAXIMUM-Ta	MINIMUM-Ta
Night	SVF _x	🟡 2.53	🟡 2.37	🟡 2.66
Morning	SVF _x	🟢 15.90	🟢 19.87	🟢 11.34
Afternoon	SVF _x	🟢🟢 42.60	🟢🟢 48.03	🟢🟢 36.04
Evening	SVF _x	🟢 12.77	🟢 13.05	🟢 12.08
Total Average		18.45	20.83	15.53
P. CLOUDY	Improvement of R-sq(adj) % by SVF _x - Hot Season			
	UMP	AVERAGE-Ta	MAXIMUM-Ta	MINIMUM-Ta
Night	SVF _x	🟡 0.29	🟡 0.29	🟡 0.29
Morning	SVF _x	🟡 2.89	🟡 4.47	🟡 1.73
Afternoon	SVF _x	🟢 13.26	🟢 19.69	🟡 7.98
Evening	SVF _x	🟡 2.00	🟡 2.73	🟡 1.50
Total Average		4.61	6.80	2.88
CLOUDY	Improvement of R-sq(adj) % by SVF _x - Hot Season			
	UMP	AVERAGE-Ta	MAXIMUM-Ta	MINIMUM-Ta
Night	SVF _x	🟡 4.48	🟡 4.74	🟡 4.39
Morning	SVF _x	🟡 1.12	🟡 0.94	🟡 0.80
Afternoon	SVF _x	🟡 7.62	🟢 10.08	🟡 5.61
Evening	SVF _x	🟡 1.81	🟡 1.03	🟡 1.87
Total Average		3.76	4.20	3.17

This superiority was due to taking in to account the notion of the direction in SVF_x itself, where SVF_x describes the urban configuration around the monitoring point more accurately by calculating the openness degree to sky on each of the four main directions separately. Therefore, the values of SVF_x will be sensitive to any change in the relationship between the point and the vertical surfaces in terms of heights, positions and distributions of these surfaces depending on a particular direction. The description of the relationships between urban configuration and solar radiation that influences the site-measured temperature will be more precise to explain the air temperature variations for the periods of a day under the different sky circumstances.

The improvement rates by SVF_x change logically, with the lowest rates settled in the night period, and this is consistent with the predominance of ambient climate factors

on temperature changes due to dissipation of the stored heat in the man-made surfaces during this period. By increasing the heat of urban surfaces, amelioration levels were elevated to the highest grade in the afternoon period before then dropping again with the setting sun in the evening period. The latter recorded rates higher than the night period due to the thermal storage of urban surfaces after sunset were higher in general. Nonetheless, the morning period recorded lower rates than the night period under the cloudy sky because air temperatures in the night periods for some days had recorded large changes while the morning period experienced smaller changes of air temperature [see Figure 5.18 to 5.20]. Some parameters like SF, and others that will be mentioned later like FVFX and FVF, witnessed similar tendencies in the cloudy days.

In terms of the influence on air temperature, increasing the exposure to the sky on the northern orientation by increase SVFn led to a reduction in air temperature regardless of the day periods and sky conditions, as shown by Table 7-17. This is due to shrink the thermal reservoirs that store the heat from the direct solar radiation of the morning and afternoon periods. Furthermore, the heat may dissipate more quickly especially after sunset by increasing SVFn where the thermal radiation that was emitted from the surfaces was not held between the urban blocks for a long time.

Table 7-17 The behaviours of air temperature by the effect of SVFn

		Sunny days (su)				Partially cloudy days (pr)				cloudy days (cl)			
		ni-su	mo-su	no-su	ev-su	ni-pr	mo-pr	no-pr	ev-pr	ni-cl	mo-cl	no-cl	ev-cl
		SVFn	SVFn	SVFn	SVFn	SVFn	SVFn	SVFn	SVFn	SVFn	SVFn	SVFn	SVFn
INDICATORS	AVG	-	-	-	-	-	-	-	-	-	-	-	-
	MAX	-	-	-	-	-	-	-	-	-	-	-	-
	MIN	-	-	-	-	-	-	-	-	-	-	-	-

The increase of eastern quadrant of sky view factor (SVFe) decreased Ta in the night period generally, as shown by Table 7-18. The vertical surfaces involved in SVFe were on the eastern side of the urban space and faced the west, thus the heat from the sun was absorbed by them during the course from midday till sunset and after that

they acted as heat radiators. Consequently, decreasing the area of these surfaces leads to a reduction in the air temperature for the period after midnight.

The air temperature has positive relationships with SVFe at the evening period and this look discordant. The increase of SVFe means a decrease in the vertical surfaces areas and an increase in the openness on the eastern side of the urban spaces where these surfaces stored the direct solar gain before sunset and blocked the sky on the east, like locations H7, H8 and H10, that were thermally active in this period, thus the reduction of temperature was expected. But on the other hand, the increase of SVFe will increase the amount and duration of solar radiation that irradiates the ground and vertical surfaces in the morning and afternoon periods. This will enhance the thermal storage which will affect the air temperatures for longer and support the statistical models to show the positive relationships between the variables (SVFe and Ta) in the evening period.

The on-site air temperatures will be elevated for the increase in the value of SVFe during the morning and the afternoon periods and it is an expected behaviour where all locations displayed an upward tendency in the morning period and a number of them kept this trend in the afternoon period. Any direct or indirect increase of solar radiation through these days periods will support air temperature rises, especially the locations with higher SVFe like H11, H12 and H3, which frequently recorded higher levels of Ta.

Table 7-18 The behaviours of air temperature by the effect of SVFe

		Sunny days (su)				Partially cloudy days (pr)				cloudy days (cl)			
		ni-su	mo-su	no-su	ev-su	ni-pr	mo-pr	no-pr	ev-pr	ni-cl	mo-cl	no-cl	ev-cl
		SVFe	SVFe	SVFe	SVFe	SVFe	SVFe	SVFe	SVFe	SVFe	SVFe	SVFe	SVFe
INDICATORS	AVG	-	+	*	*	*	+	+	+	*	+	*	+
	MAX	-	+	*	*	*	+	+	+	*	+	*	*
	MIN	-	*	+	*	*	+	+	*	-	*	+	+

Increasing the sky openness in the southern quadrant (SVFs) may increase long wave emissions to the sky, especially after dusk, and so the air temperature may reduce in the evening period regardless of the sky conditions, as shown by [Table 7-19](#).

Table 7-19 The behaviours of air temperature by the effect of SVFs

		Sunny days (su)				Partially cloudy days (pr)				cloudy days (cl)			
		ni-su	mo-su	no-su	ev-su	ni-pr	mo-pr	no-pr	ev-pr	ni-cl	mo-cl	no-cl	ev-cl
		SVFs	SVFs	SVFs	SVFs	SVFs	SVFs	SVFs	SVFs	SVFs	SVFs	SVFs	SVFs
INDICATORS	AVG	*	+	+	-	*	+	-	-	*	-	*	-
	MAX	*	+	+	-	*	+	-	-	*	*	*	*
	MIN	*	+	*	-	*	-	-	-	*	-	-	-

This sector of the sky hemisphere may not have the impact on the air temperature variation at the night period due to retention of the thermal storage of the urban surfaces. The increase of SVFs elevates the air temperature in the morning period under the sunny and partial cloudy skies due to exposure to higher levels of direct solar radiation from the south and reduction in the shading areas. However, one of the thermal microclimate indicators (MIN) showed a negative relationship with SVFs under the partially cloudy sky condition. This unfamiliar behaviour may be due to a decrease in the intensity of the solar radiation compared to the sunny days and an increase in the wind speed for this period [see [Figures 5.12 to 5.17](#)]. The dataset of MIN fitted the changes of SVFs negatively, which supports this justification of the negative relationships between air temperature and SVFs in the morning period for the cloudy days, which also witnessed higher wind speeds compared to other periods of the cloudy days [see [Figure 5.18 to 5.20](#)] but with bigger decrease of solar radiation compared to partial cloudy days. The role of SVFs in the morning and the afternoon periods seems similar. However, the increase of openness in the southern sector may reduce on-site air temperature in the afternoon period under the partial cloudy sky. This behaviour can be explained by the increases in the wind speed and the decrease in solar radiation. In addition, the upward trend of air temperatures was noticed in the morning period regardless of the sky conditions did not continue throughout the afternoon period owing to the combined effect of blocking the direct radiation by urban blocks and the big drop in solar radiation before and after the time of sunset. Increased SVFw in the western quarter of the sky dome led to alleviation of temperatures in the morning period under the sunny and partial cloudy skies because

of the downscaling of the façades areas that act as thermal tanks and diffusers for the solar radiation, as shown by Table 7-20. Nevertheless, the same change of sky line may cause an increase in air temperature for the same duration from 6am to 12pm under the cloudy sky because some locations with low values of SVFw did not take the lead regarding the air temperature levels in this period although they had larger areas of vertical surfaces on the western side, like H11 and H12. Conversely, other locations recorded high values of SVFw and high temperatures, like H8. Therefore, the statistical relationships became positive. Increasing SVFw in the other periods (afternoon, evening and night) regardless of the sky conditions elevated the air temperatures as a result of the effect of higher solar radiation levels from the western side, starting about midday till sunset, where the northern and eastern surfaces will store heat and reflect the solar radiation in the daytime and re-radiate it during the night time, causing higher temperature for some locations.

Table 7-20 The behaviours of air temperature by the effect of SVFw

		Sunny days (su)				Partially cloudy days (pr)				cloudy days (cl)			
		ni-su	mo-su	no-su	ev-su	ni-pr	mo-pr	no-pr	ev-pr	ni-cl	mo-cl	no-cl	ev-cl
		SVFw	SVFw	SVFw	SVFw	SVFw	SVFw	SVFw	SVFw	SVFw	SVFw	SVFw	SVFw
INDICATORS	AVG	*	-	+	+	+	-	+	+	+	+	+	+
	MAX	*	-	+	+	+	-	+	+	+	*	+	*
	MIN	*	-	+	+	+	-	+	+	*	*	+	+

It should be noted that there is no clear reason for why SVFn did show a significant role in all the statistical models compared to other subdivisions of SVFx which showed different behaviours in this regard. Therefore, this point may need further investigation to reveal it in detail as a part of future perspective for this study.

7.3.9 Façade View Factor (FVFX)

The Façade View Factor is a numerical description for the façade area depending on its projection for the observation point that sees this façade, with the values for facades that are connected to the same point and face the same direction are accumulated to give one value for that point. Therefore, there are eight values or less to express the surroundings around the point in relation to the four cardinal directions and their four subdivisions.

Although there is no congruence between FVFX and the on-site air temperature throughout the evening period for the cloudy days, the improvement rates by FVFX reached outstanding levels compared to other parameters. The improvement rates were highest for the sunny days compared to the partial cloudy and cloudy days respectively where the range was between 12% and 21% for the morning period and from 22% to 32% in the afternoon period to be more than 2% to more than 3% in the evening period and lower from the latter in the night period, as shown in [Table 7-21](#).

Table 7-21 The improvement rates of R-sq(adj) by FVFX

SUNNY	Improvement of R-sq(adj) % by FVFX - Hot Season			
	UMP	AVERAGE-Ta	MAXIMUM-Ta	MINIMUM-Ta
Night	FVFX	☹️ 0.39	☹️ 0.31	☹️ 0.42
Morning	FVFX	✅ 16.77	📈 21.04	✅ 12.07
Afternoon	FVFX	📈 27.64	✅📈 32.26	📈 22.36
Evening	FVFX	⚠️ 2.88	⚠️ 3.25	☹️ 2.37
Total Average		11.92	14.22	9.31
P. CLOUDY	Improvement of R-sq(adj) % by FVFX - Hot Season			
	UMP	AVERAGE-Ta	MAXIMUM-Ta	MINIMUM-Ta
Night	FVFX	☹️ 0.27	☹️ 0.27	☹️ 0.25
Morning	FVFX	⚠️ 3.08	⚠️ 4.79	☹️ 1.82
Afternoon	FVFX	☹️ 5.30	☹️ 8.86	⚠️ 2.66
Evening	FVFX	☹️ 0.33	☹️ 0.56	☹️ 0.19
Total Average		2.25	3.62	1.23
CLOUDY	Improvement of R-sq(adj) % by FVFX - Hot Season			
	UMP	AVERAGE-Ta	MAXIMUM-Ta	MINIMUM-Ta
Night	FVFX	☹️ 1.22	☹️ 1.18	☹️ 1.28
Morning	FVFX	☹️ 0.56	☹️ 0.77	☹️ 0.34
Afternoon	FVFX	☹️ 2.26	⚠️ 3.80	☹️ 0.89
Evening	FVFX	❌ 0.00	❌ 0.00	❌ 0.00
Total Average		1.01	1.44	0.63

The significant increase of improvement rates by FV_{Fx} is attributed to its embedded orientation concept in the parameter itself. The façade view factor (FV_{Fx}) that measures the configuration of an urban space around the observation point may have no more than eight subdivisions (FV_{Fn}, FV_{Fne}, FV_{Fe}, FV_{Fse}, FV_{Fs}, FV_{Fsw}, FV_{Fw}) depending on the number, distribution and the angle of rotation of vertical surfaces. Therefore, the interaction between the sun's trajectory and the urban morphology, that controls the radiation balance throughout the day, may be expressed more accurately by FV_{Fx} than most UMP in terms of influence on air temperatures.

Furthermore, the improvement rates changed logically with FV_{Fx} compared to most UMP. They increased in the morning period from their lowest levels in the night period to reach their highest values at the afternoon period, which considered as the most varying period. These rates decrease again in the evening period. However, the night period under the cloudy sky witnessed notable significance rates higher than the morning periods, where the same feature was noticed with some of the urban morphological parameters like FV_F, SF, SV_F and SV_{Fx}. This may be attributed to the dramatic change of the air temperatures throughout the night period for some days of the cloudy sky. This is in comparison to the morning period, as shown by [Figures 5.18 to 5.20](#), where the cloudy skies at night are not a good absorber of radiant heat like clear dark sky that, theoretically, behave as a black body which may be of affect here (McMullan, 2007).

Regarding the influence of FV_{Fx} on air temperatures, increasing the subdivision values of FV_{Fx} led to a boost in the degree of enclosure and reduced the openness degree to the sky for the urban space. Therefore, these subdivisions had negative correlations with their counterparts from the partial sky view factor (SV_{Fx}), as shown by [Table 5-2](#). As a result, on-site air temperatures will increase with increasing FV_{Fn} values in the morning and afternoon periods under both sunny and partial cloudy skies in addition to afternoon period under the cloudy sky, as shown by [Table 7-22](#). Because an increase in the façades areas is associated with an increase in the thermal storage on the northern side of urban space this side, especially, receives direct solar radiation for most of the day. Nevertheless, the air temperature in the night period under the partial cloudy sky showed a counter tendency to increased FV_{Fn}. The

relatively low air temperature at H11 showed the highest value of FVFn. Location H10 came second and both recorded lower temperatures than H8, which kept the heat longer owing to its compact space, although it came third in terms of FVFn. Therefore, the statistical models have defined a negative relationships between air temperature and FVFn.

Table 7-22 The behaviours of air temperature by the effect of FVFn

INDICATORS		Sunny days (su)				Partially cloudy days (pr)				cloudy days (cl)			
		ni-su	mo-su	no-su	ev-su	ni-pr	mo-pr	no-pr	ev-pr	ni-cl	mo-cl	no-cl	ev-cl
		FVFn	FVFn	FVFn	FVFn	FVFn	FVFn	FVFn	FVFn	FVFn	FVFn	FVFn	FVFn
AVG	*	+	+	*	-	+	+	*	*	*	*	X	
MAX	*	+	+	*	-	+	+	*	*	*	*	X	
MIN	*	+	+	*	-	+	+	*	*	*	+	X	

The enlargement of FVFe led to elevated air temperatures in the night and evening periods, especially under the sunny and partially cloudy skies, because of increasing the effect of vertical surfaces that received the solar radiation from midday till late on the eastern side of urban space by increasing the surfaces area, decreasing the distance between the surfaces and measurement point or increasing the exposure of that point to these surfaces. This effect was reversed in the morning period due to the blocking of the solar radiation that came from the eastern side of the site under the effect of an increased FVFe, as shown by [Table 7-23](#), and this led to a decrease in the temperatures as a response to reduced thermal storage. The negative influence of FVFe on the air temperature in the afternoon period may looks perplexing because of the increase the air temperatures in most of the locations, especially H7, H8 and H10. This may be due to the contrast in temperature changes versus change in FVFe values. H4 has the higher value of FVFe but the lower air temperature compared to H7, H8 and H10, and the same thing occurs between H9 and H5, where the latter has the lower value of FVFe but, in general, the higher air temperature compared to H9. This was because of the urban space more enclosing and more compact around H5, leading to reduced wind effects and heat being stored in the surfaces for a longer time - the same thing happens between H8 and H7.

Table 7-23 the behaviours of air temperature by the effect of FVFe

		Sunny days (su)				Partially cloudy days (pr)				cloudy days (cl)			
		ni-su	mo-su	no-su	ev-su	ni-pr	mo-pr	no-pr	ev-pr	ni-cl	mo-cl	no-cl	ev-cl
		FVFe	FVFe	FVFe	FVFe	FVFe	FVFe	FVFe	FVFe	FVFe	FVFe	FVFe	FVFe
INDICATORS	AVG	+	*	*	+	+	-	-	+	+	-	-	X
	MAX	+	-	*	+	+	-	-	*	+	-	-	X
	MIN	+	*	-	+	+	-	-	+	+	*	*	X

The increase of FVFs will block more direct solar radiation, consequently reducing the thermal storage in urban surfaces and lessening the air temperature, especially in the afternoon period, regardless of the sky conditions - see Table 7-24. The possible cause behind the negative relationships at night and the evening periods may be the contrast, where the locations with high FVFs values, like H1, H2, H3, H4 and H12, witnessed low air temperatures compared to the locations that recorded generally higher air temperatures with low values of FVFs, like H7, H8 and H10. The effect of FVFs has reversed in the morning period, where nearly all locations witnessed increased air temperatures in this period. Some of the locations with high values of FVFs, like H3 and H12, witnessed higher increases of air temperature due to the potential impact of neighbouring vertical surfaces on the western sides, while H1 sometimes recorded tangible increases of temperature in this period resulting, probably, from the influence of the ground around the sensor. The low building heights of the southern side of H1 generated short shadows on the grass area while around H1 asphalt was the predominant area exposed to the direct solar radiation throughout this period. On the other hand, the locations with lower values of FVFs recorded air temperatures lower than the first group. Therefore, the statistical models highlighted a positive relationship between FVFs and air temperature.

The vertical surfaces on the western side of the site show binary behaviour according to the day periods where they work as convectors of adjacent air and as diffusers for the direct radiation from sunrise till midday then act as radiators of long wave radiation for the rest of the day. Therefore, the air temperature will rise in the night,

Table 7-24 The behaviours of air temperature by the effect of FVFs

INDICATORS		Sunny days (su)				Partially cloudy days (pr)				cloudy days (cl)			
		ni-su	mo-su	no-su	ev-su	ni-pr	mo-pr	no-pr	ev-pr	ni-cl	mo-cl	no-cl	ev-cl
		FVFs	FVFs	FVFs	FVFs	FVFs	FVFs	FVFs	FVFs	FVFs	FVFs	FVFs	FVFs
AVG	*	+	-	-	-	+	-	-	-	-	+	-	X
MAX	*	*	-	-	-	+	-	-	-	-	*	-	X
MIN	*	+	-	-	-	+	-	-	-	-	+	*	X

morning and afternoon periods in response to changes in urban configuration by increase the surface area, decreasing the distance to the measure point and increasing the exposure angle, where one or more of these changes led to an increase of FVFW values. However, the differences in air temperatures may not fit the variation of FVFW positively in the evening period under the partial cloudy sky, as shown by Table 7-25, because the direct solar radiation has been blocked from access to the most sites from about 6 pm under the increase of FVFW. Furthermore, the air temperatures at locations that recorded the lowest values of FVFW, like H7 and H8, were higher than levels at H11 and H12 that have higher values of FVFW, and, therefore, the air temperatures will drop as a response to augmentation of FVFW.

Table 7-25 The behaviours of air temperature by the effect of FVFW

INDICATORS		Sunny days (su)				Partially cloudy days (pr)				cloudy days (cl)			
		ni-su	mo-su	no-su	ev-su	ni-pr	mo-pr	no-pr	ev-pr	ni-cl	mo-cl	no-cl	ev-cl
		FVFW	FVFW	FVFW	FVFW	FVFW	FVFW	FVFW	FVFW	FVFW	FVFW	FVFW	FVFW
AVG	+	+	+	*	+	+	*	-	+	*	*	X	
MAX	*	+	+	*	+	+	*	-	+	+	*	X	
MIN	+	+	+	*	+	+	*	*	+	*	*	X	

7.3.10 Total Façade View Factor (FVF)

It is the total summation of the individual façade view factor values for all surfaces that are seen by the monitoring point within the buffer zone.

The sunny days witnessed the best improvement rates although it has seven of sixteen as insignificant modified models by FVF. Another three models are in the

partial cloudy days, that showed better amelioration rates than the cloudy sky days, and the last six models were unsuccessful, as shown by [Table 7-26](#).

Table 7-26 The improvement rates of R-sq(adj) by FVF

SUNNY	Improvement of R-sq(adj) % by FVF - Hot Season			
	UMP	AVERAGE-Ta	MAXIMUM-Ta	MINIMUM-Ta
Night	FVF	⊗ 0.00	⊗ 0.00	⊗ 0.00
Morning	FVF	☉ 7.79	☉ 9.10	☉ 6.15
Afternoon	FVF	⊗ 0.00	⊗ 0.00	⊗ 0.00
Evening	FVF	☉ 0.29	☉ 0.58	⊗ 0.00
Total Average		2.02	2.42	1.54
P. CLOUDY	Improvement of R-sq(adj) % by FVF - Hot Season			
	UMP	AVERAGE-Ta	MAXIMUM-Ta	MINIMUM-Ta
Night	FVF	⊗ 0.00	⊗ 0.00	⊗ 0.00
Morning	FVF	☉ 1.34	☉ 1.96	☉ 0.87
Afternoon	FVF	☉ 0.48	☉ 0.96	☉ 0.16
Evening	FVF	☉ 0.09	☉ 0.17	☉ 0.04
Total Average		0.48	0.77	0.27
CLOUDY	Improvement of R-sq(adj) % by FVF - Hot Season			
	UMP	AVERAGE-Ta	MAXIMUM-Ta	MINIMUM-Ta
Night	FVF	☉ 0.37	☉ 0.39	☉ 0.41
Morning	FVF	☉ 0.10	☉ 0.14	⊗ 0.00
Afternoon	FVF	⊗ 0.00	☉ 0.43	⊗ 0.00
Evening	FVF	⊗ 0.00	⊗ 0.00	⊗ 0.00
Total Average		0.12	0.24	0.10

The improvement rates reveal that the ability of FVF to explain the air temperature differences was not impressive, although the parameter itself as an urban metric can be considered trustworthy. Due to its strong shared features with many parameters like the compactness index (CI), the degree of compactness (Dc), the floor area ratio (FAR), the façade to site ratio (FSR) and the western subdivisions of both FVFX and SVFX, as shown by the correlation coefficient values in [Table 5-2](#).

Despite FVF being developed as a part of this study, the point that counts against this parameter is that it does not consider the effect of the invisible facades that are working with the visible ones in forming the urban space around the measurement point. Maybe this is the reason its abilities were limited regarding the changes of air temperature. This opinion can be supported by the improvement rates of sky view factor (SVF) that came in close to those of FVF, where both depended on the location of the measurement point and they had the same problem in terms of the invisible

surfaces. What has been mentioned above cannot be refuted by the results of the parameter of facade to site ratio (FSR) that took in to account all vertical surfaces inside the buffer zone (visible and invisible), yet it did not record remarkable improvement rates. Not taking the relationship between the measurement point and the façade regarding to the position and the projection into consideration may be the most likely cause of the weakness of the FSR role. In return, the results of FVFX and SVFX can support all this discussion, where their outstanding improvement rates alleviated the disadvantage of not considering the effects of invisible façades on air temperature. The direction concept that is embodied in these parameters gives a more accurate description for the space around the measurement point.

In terms of the influences on air temperature, generally the increase of FVF values elevate the air temperatures in the morning periods regardless of the sky conditions, while the afternoon periods under the partial cloudy and cloudy skies and the evening periods under the sunny and the partial cloudy skies will be cooler for any augmentation in FVF. This is not the case for the night period under the cloudy days, as shown in [Table 7-27](#).

Table 7-27 the behaviours of air temperature by the effect of FVF

		Sunny days (su)				Partially cloudy days (pr)				cloudy days (cl)			
		ni-su	mo-su	no-su	ev-su	ni-pr	mo-pr	no-pr	ev-pr	ni-cl	mo-cl	no-cl	ev-cl
		FVF	FVF	FVF	FVF	FVF	FVF	FVF	FVF	FVF	FVF	FVF	FVF
INDICATORS	AVG	X	+	X	-	X	+	-	-	+	+	X	X
	MAX	X	+	X	-	X	+	-	-	+	+	-	X
	MIN	X	+	X	X	X	+	-	-	+	X	X	X

The notable increase of air temperature throughout the morning periods in the sites that had high values of FVF, like H3, H11 and H12, irrespective the sky conditions, helped to define the positive relationship between FVF and the in-situ air temperatures, especially for the other locations that also witnessed an increase in Ta. The continuity of air temperature rising in the locations with low values of FVF, like H8, H7 and H10, versus its decreasing in the high FVF locations enhanced the role of FVF as a calming agent for temperature in the afternoon period for the partial cloudy

and cloudy days. The behaviour of measured air temperatures in the evening periods was, in general, opposite to the morning periods, where all locations experienced a reduction of air temperatures that were in a low level at H3, H11 and H12 against high levels at H8, H7 and H10. Thus, the statistical models show that air temperature may decrease for increasing FVF in this period under the sunny and partial cloudy skies.

The increase of FVF led to an increase in T_a during the night period under the cloudy sky. The slight increase of wind speed in this period [see [Figures 5.18 to 5.20](#)] may have accelerated the dissipation of stored heat. Therefore, the locations with higher T_a and lower FVF, like H8, might experience bigger and faster cooling rates than other locations with higher values of FVF. In addition, the slight increase of ambient air temperature led to more convergence between the on-site measured temperatures in the last part of the period, where the temperatures of locations with higher FVF had started to climb again like H3, H4 and H11. It is difficult to see these changes because of the scale of the figure. However, evidence from the subsequent period can be noticed easily, where the air temperature in these locations witnessed an upswing immediately, despite there being no direct solar radiation.

7.4 The total effect of UMP

The total effect of each parameter (UMP) was determined using the summation of the total average of improvement rates for its three indicators (AVG, MAX and MIN) as shown by [Tables 7-28, 7-29 and 7-30](#). Furthermore, the summation of the average of improvement rates for all parameters under each indicator of the three reveals the importance of each one of them in regard to response to the urban parameters.

The above mentioned tables were transferred into a type of visual graph called a chord graph, which will be utilized to deliver an easy-to-visualise comparison between the urban morphological parameters as air temperature indicators. The effect of UMP on indicators will be expressed as chords that have different sizes according to the size of that influence.

[Figure 7.2](#) shows the total effect of UMP on air temperature (T_a) under the sunny sky. The partial sky view factor (SVF_x) and the façade view factor (FVF_x) respectively take the lead. The shape factor (SF) and the façade to site ratio (FSR) ranked as the third and the fourth in the row, with a clear gap from the first ranks as well as between them. The well-known parameters of the sky view factor (SVF) and the site coverage ratio (SCR) occupy the last two positions with a tiny difference between them where they came after the degree of compactness (Dc) that lies beneath the total façade view factor (FVF), which came seventh. The other well-known parameter, the floor area ratio (FAR), came sixth after the compactness index (CI).

It can be seen that the urban morphological parameters (UMP) affect more on the maximum air temperature (MAX) than average (AVG) and minimum (MIN) respectively. However, the differences between the air temperature indicators are not big under the sunny sky.

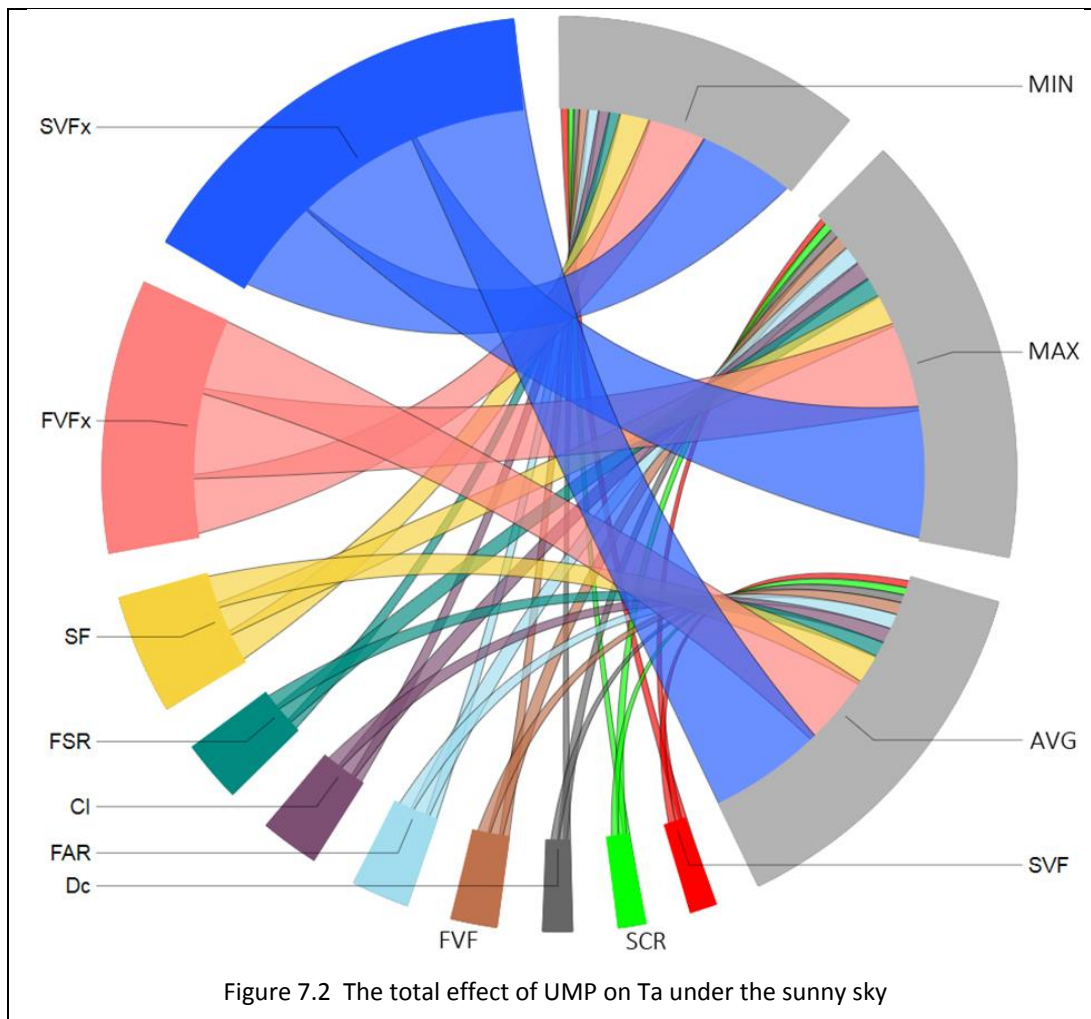


Table 7-28 The total effect of UMP on Ta under the sunny sky

SUNNY	Total Average of improvement rates			SUM
	AVG	MAX	MIN	
CI	2.53	3.15	1.87	7.55
Dc	1.30	1.55	1.02	3.86
FAR	2.50	3.12	1.81	7.43
FSR	2.67	3.40	1.88	7.94
FV	2.02	2.42	1.54	5.98
FVx	11.92	14.22	9.31	35.44
SCR	1.19	1.41	0.99	3.60
SF	5.20	5.37	4.92	15.49
SVF	1.16	1.07	1.24	3.47
SVFx	18.45	20.83	15.53	54.81
SUM	48.94	56.53	40.09	

Although the average of improvement rates at the partial cloudy days was scaled-down compared to the sunny days, and the rates of improvement for UMP had changed compared to each other, the various UMP kept the same ranking in general. SVF_x, FVF_x, SF and CI respectively stay at the foreground with a clear improvement of SF versus a reduced effect of FVF_x, as shown by Figure 7.3. D_c, SCR and SVF occupied the last three positions where SVF settled in the bottom after the SCR. FVF came sixth rank after FAR compared to seventh in the sunny days, while FSR settled under FVF with a small difference in their values. Although the air temperatures under the partially cloudy sky were lower in general, compared to the sunny days, the sensitivity of maximum air temperature (MAX) to the UMP increased compared to the sunny days and the minimum air temperature (MIN) became less affected by UMP while AVG came in the middle with notable differences from both MAX and MIN.

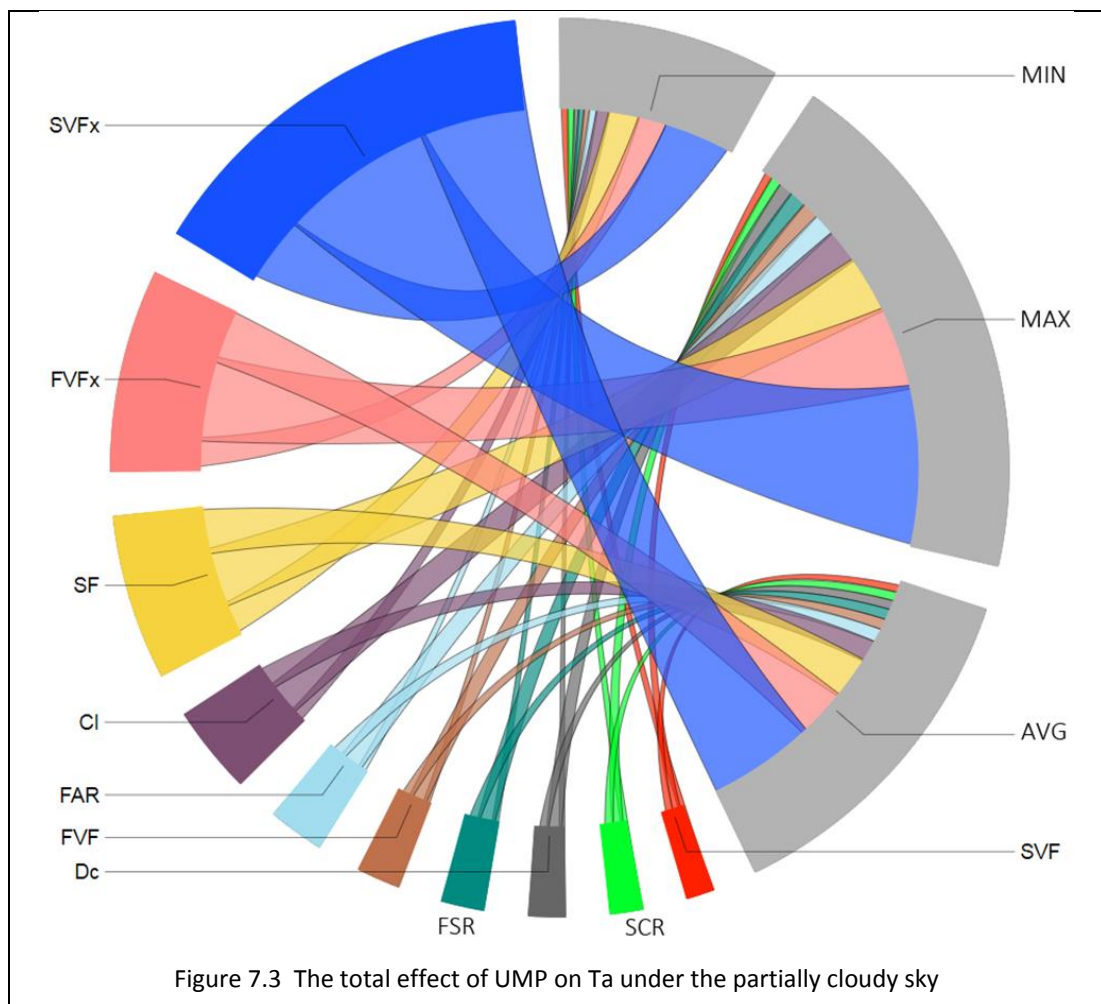


Table 7-29 The total effect of UMP on Ta under the partially cloudy sky

P. CLOUDY	Total Average of improvement rates			SUM
	AVG	MAX	MIN	
CI	0.98	1.52	0.58	3.09
Dc	0.40	0.65	0.23	1.28
FAR	0.61	1.00	0.34	1.95
FSR	0.47	0.76	0.27	1.49
FVF	0.48	0.77	0.27	1.52
FVFX	2.25	3.62	1.23	7.10
SCR	0.38	0.47	0.30	1.15
SF	1.90	2.54	1.34	5.77
SVF	0.32	0.36	0.30	0.98
SVFX	4.61	6.80	2.88	14.28
SUM	12.40	18.48	7.72	

The effect of UMP on air temperature changed dramatically, to the lowest level for the cloudy days, with the reduction of solar radiation. Although the first three positions have been reserved for the same parameters, the shape factor (SF) passed FVFX by a big margin to become in the second rank after SVFX, as shown in [Figure 7.4](#). The effect of SVF increased prominently to be fourth, followed directly by CI. SCR rose to be the sixth compared to the last two positions under sunny and partially cloudy skies. FVF came seventh while the rest of the parameters went down to occupy the bottom places. The renowned parameter (FAR) came the last with the lowest influence on air temperature under the cloudy sky after FSR, while Dc was at the eighth position. Although MAX is the most influenced by the urban morphological parameters (UMP), there is no big differences compared to AVG and MIN versus the partial cloudy days. Consequently, the thermal microclimate indicators kept the same classification regardless of the sky conditions.

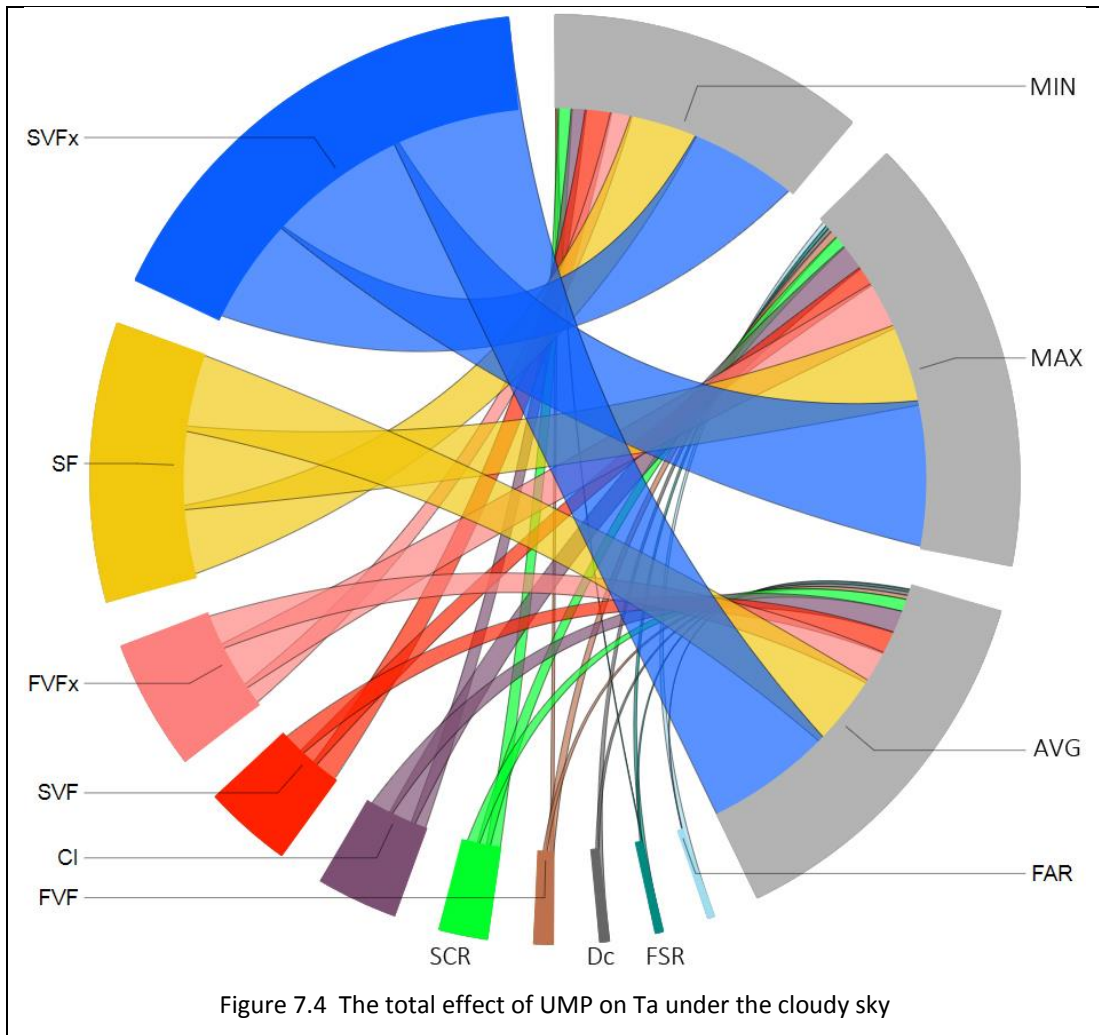
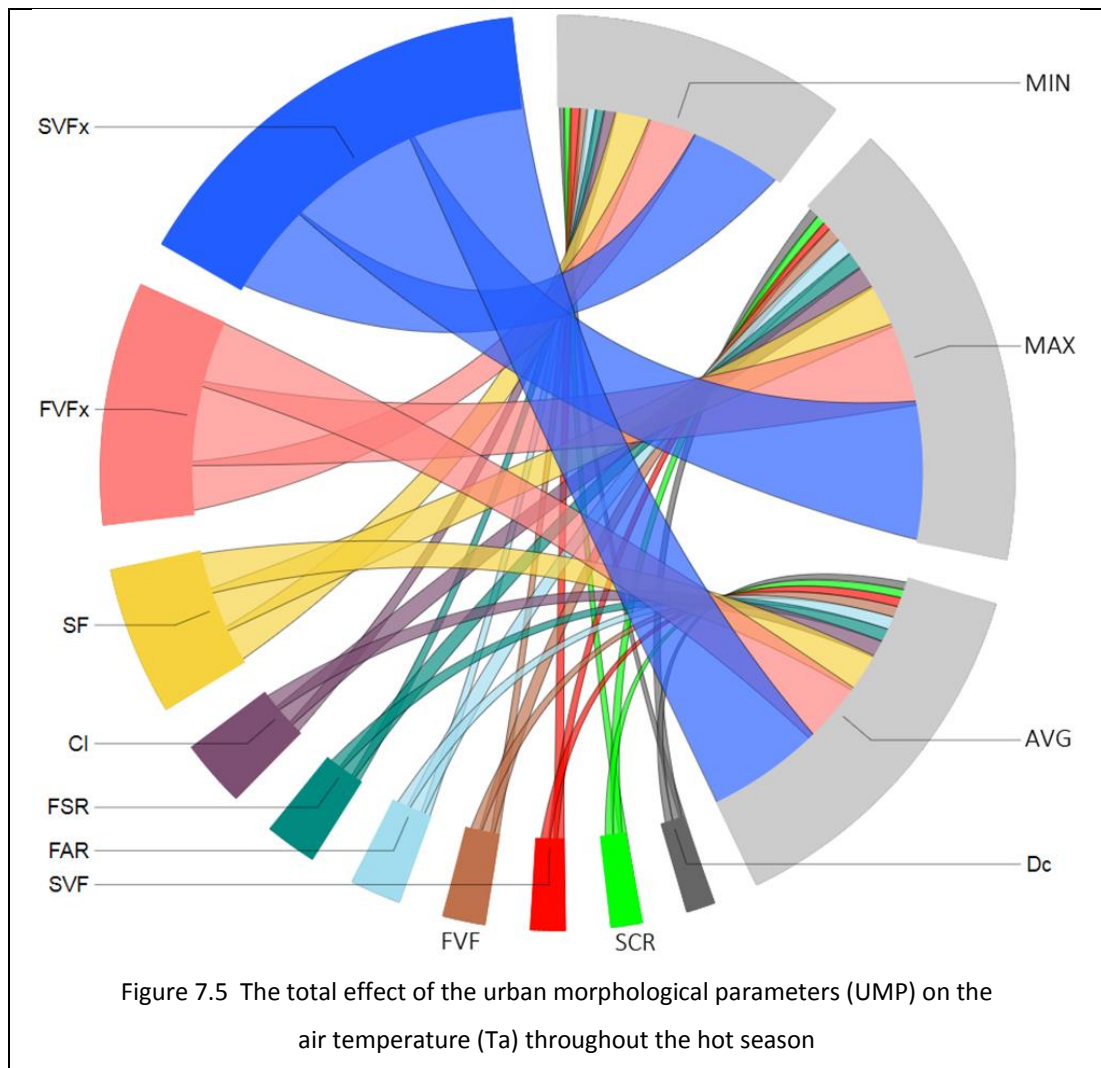


Table 7-30 The total effect of UMP on Ta under the cloudy sky

CLOUDY	Total Average of improvement rates			SUM
	AVG	MAX	MIN	
CI	0.67	0.80	0.44	1.92
Dc	0.10	0.13	0.00	0.23
FAR	0.02	0.14	0.00	0.16
FSR	0.06	0.11	0.02	0.19
FV	0.12	0.24	0.10	0.46
FVx	1.01	1.44	0.63	3.08
SCR	0.37	0.38	0.40	1.15
SF	2.23	2.39	1.99	6.61
SV	0.69	0.61	0.77	2.07
SVx	3.76	4.20	3.17	11.12
SUM	9.02	10.44	7.53	

The total effect of the urban morphological parameters throughout the hot season was revealed as the summation of total effect for each parameter under the three sky conditions, as shown by **Figure 7.5**. The partial sky view factor (SVF_x) and the façade view factor (FVF_x) occupied the summit in terms of their effect on thermal microclimate indicators (AVG, MAX and MIN), where they considered the directions concept as an approach to link between the change of the sun location and the configuration of the urban space depending on the periods of the day. The shape factor (SF), that is used mostly in the studies of building radiation due to its consideration for the ratio between the total surface area of the building and its total volume, showed an impressive role in this urban environmental study by occupying the third rank with considerable differences compared to the parameter that precedes it and the parameter that follows it. The compactness index (CI), that represent the ratio between two famed parameters (floor area ratio (FAR) and site coverage ratio (SCR)), was fourth. However, each of its two components showed less importance. The ratio of total façades area to the site area as (FSR) and the ratio of total floors area to the ground floor area as (FAR) have about the same effect size on the air temperature, and they occupied the fifth and the sixth positions respectively before the total façade view factor (FVF), which came seventh. The sky view factor (SVF) did not achieve a prominent position, reaching eighth place, followed by the ratio of the total ground floor area to the site area (SCR) and, last, the degree of compactness (Dc).



To determine the size effect of each subdivision of SVFx and FVFX on air temperature variation, the simple linear regression was used to show the correlation of subdivisions with the differences of maximum air temperature between the site and the reference weather station. The data of hottest time during the day (afternoon period) at the most ideal day in terms of its ambient climate circumstances throughout the hot season (2nd September) was considered for this analysis. In addition to, the correlations of other urban parameters with the differences of maximum air temperature between the site and the reference weather station for the same day were revealed.

Figures 7.6, 7.7, 7.8 and 7.9 reveal that the subdivisions SVFn and SVFs respectively have the stronger effect on air temperature compared to SVFw and SVFe respectively as shown by R-Sq(adj) values (30.1%, 26.3%, 14.4% and 12.8%). The differences

between Ta and a.Ta will decrease for increasing SVFn and SVFe, on the contrary the effect of both SVFs and SVFw.

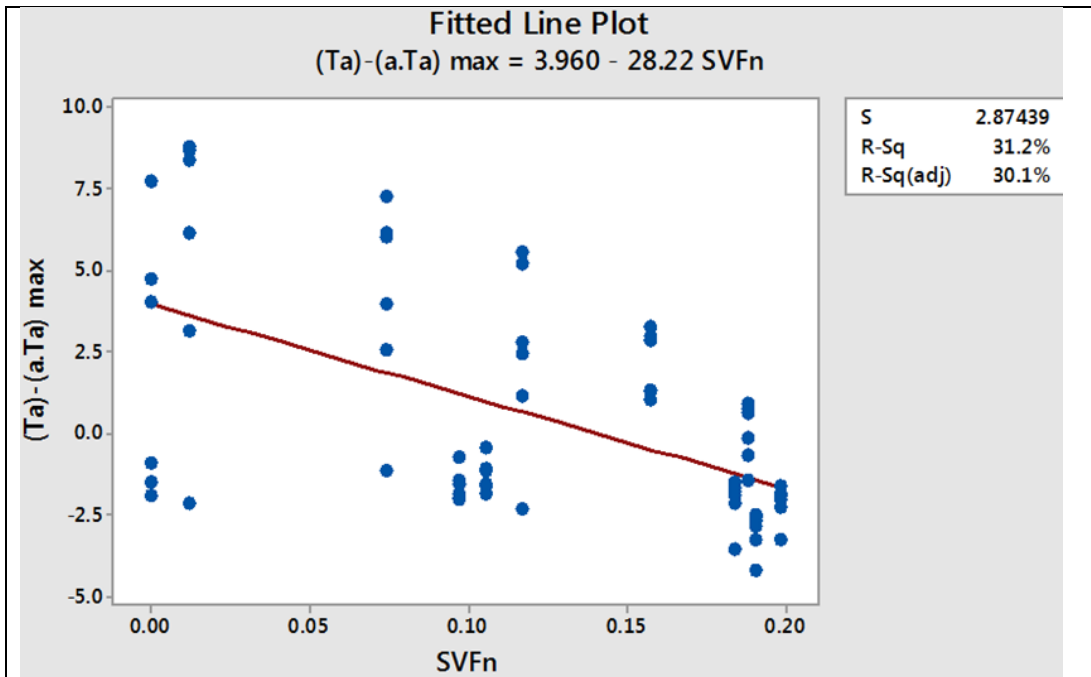


Figure 7.6 the correlation of SVFn with the differences of maximum air temperature between the site (Ta) and the reference weather station (a.Ta)

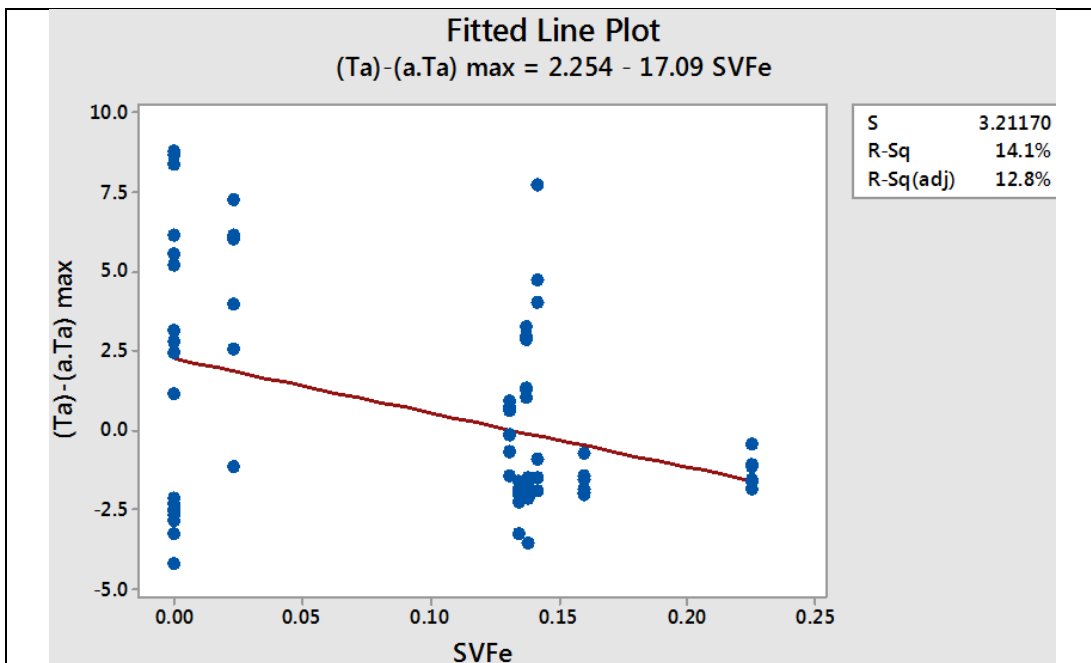


Figure 7.7 the correlation of SVFe with the differences of maximum air temperature between the site (Ta) and the reference weather station (a.Ta)

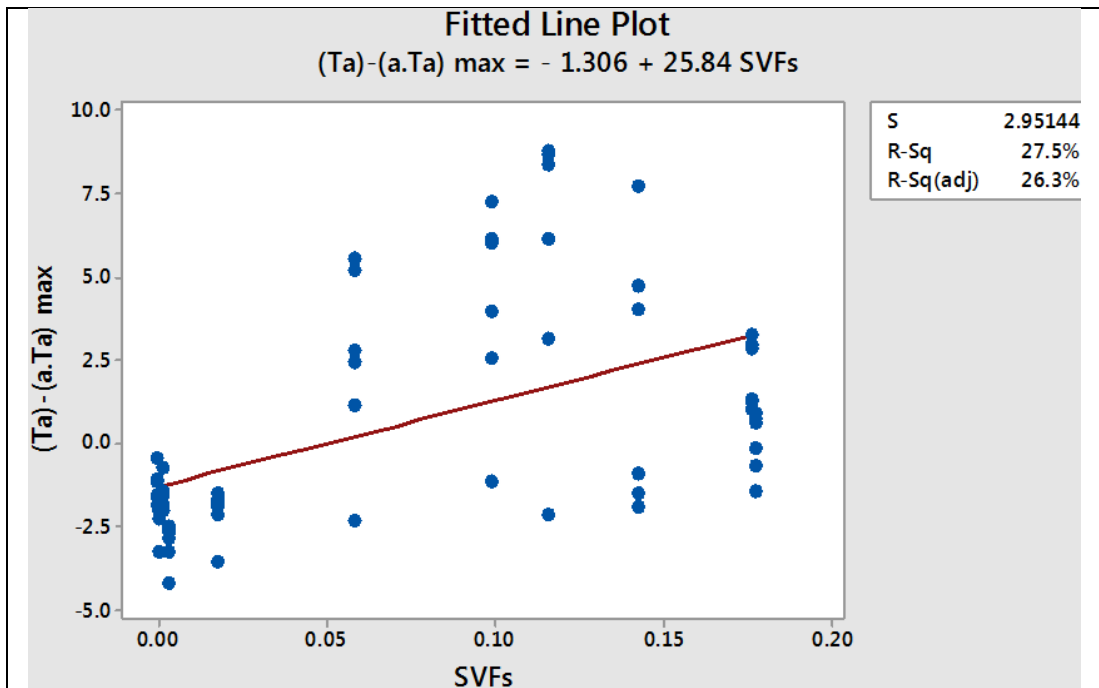


Figure 7.8 the correlation of SVFs with the differences of maximum air temperature between the site (Ta) and the reference weather station (a.Ta)

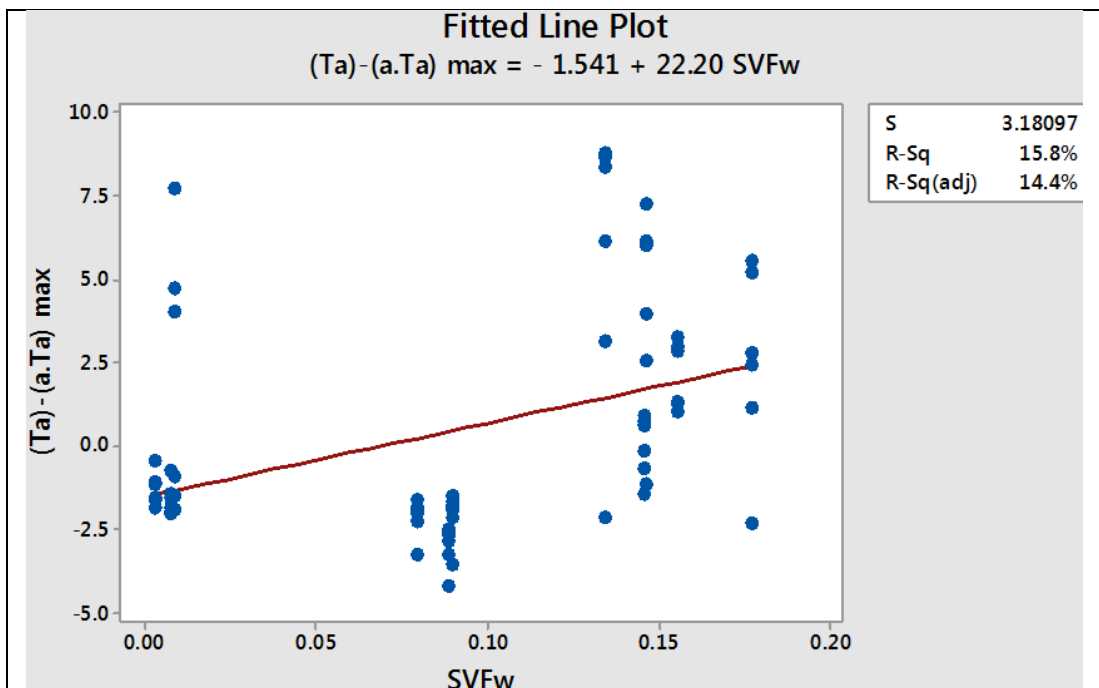
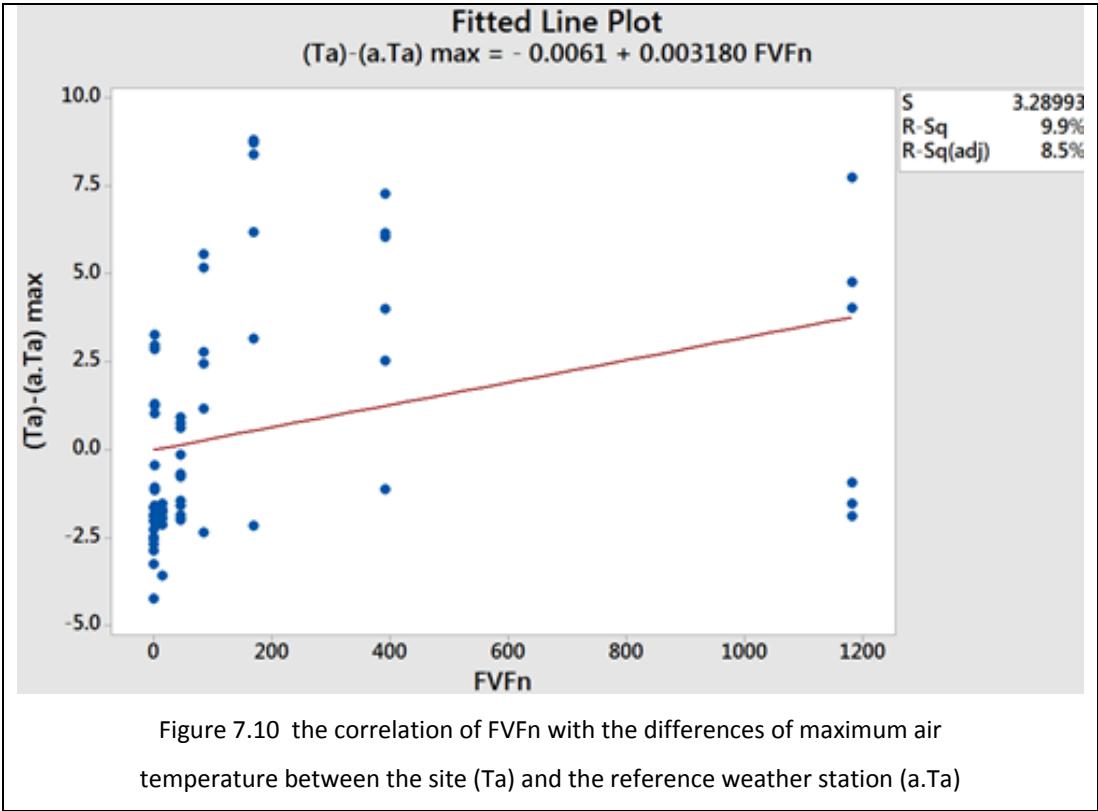


Figure 7.9 the correlation of SVFw with the differences of maximum air temperature between the site (Ta) and the reference weather station (a.Ta)

It can be noticed that the subdivisions of SVFx have better ability to explain the air temperature differences than the subdivisions of FVfx especially for eastern and western directions where $R\text{-Sq}(\text{adj}) = \text{zero}$ for both FVFe and FVFW as shown by [Figures 7.10, 7.11, 7.12 and 7.13](#). While FVFs contribute effectively compared to FVFn in regard to explain the air temperature differences ($R\text{-Sq}(\text{adj}) = 31.3\%$ and 8.5% respectively). Increasing FVFn leads to increase the differences between T_a and $a.T_a$, in contrast to the effect of FVFs.



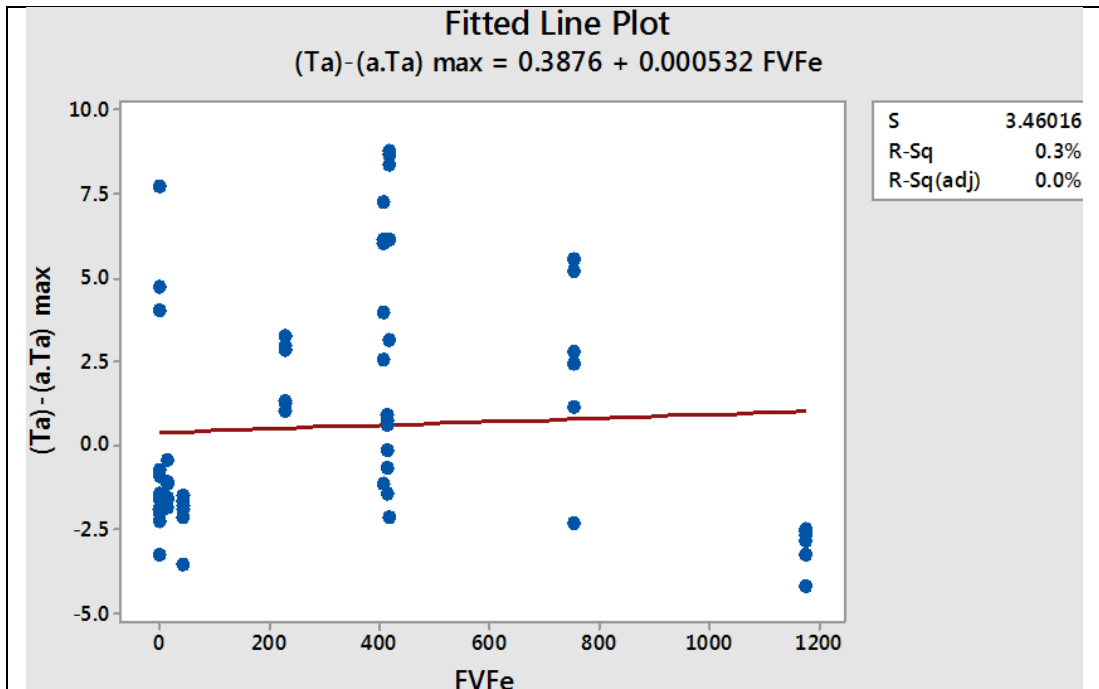


Figure 7.11 the correlation of FVFe with the differences of maximum air temperature between the site (Ta) and the reference weather station (a.Ta)

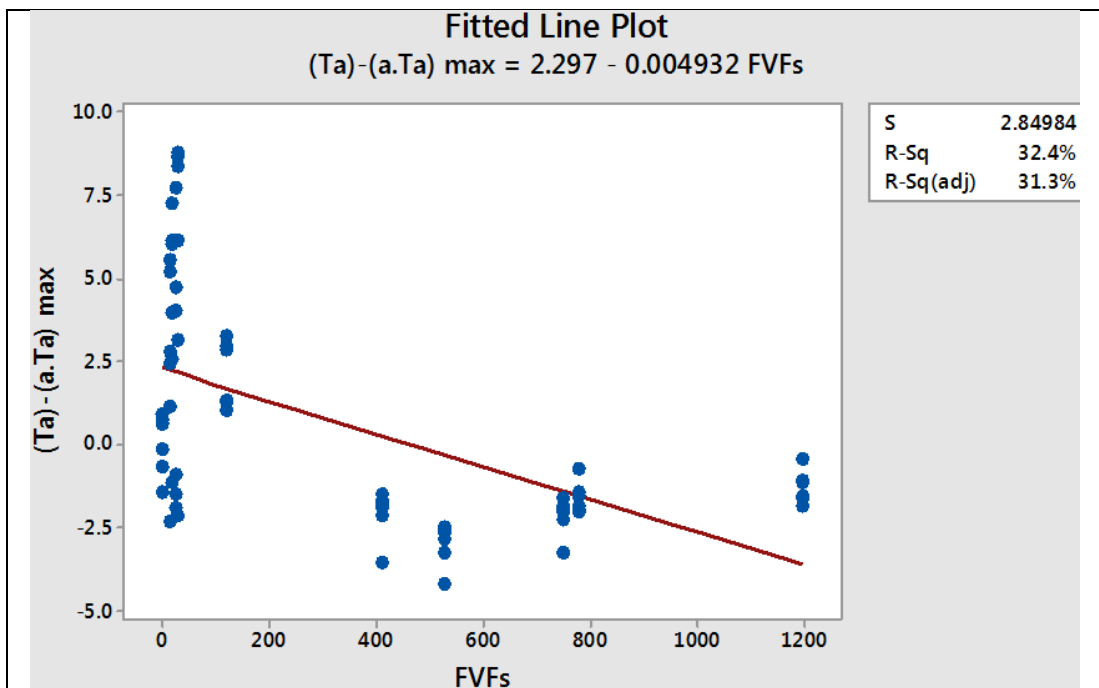
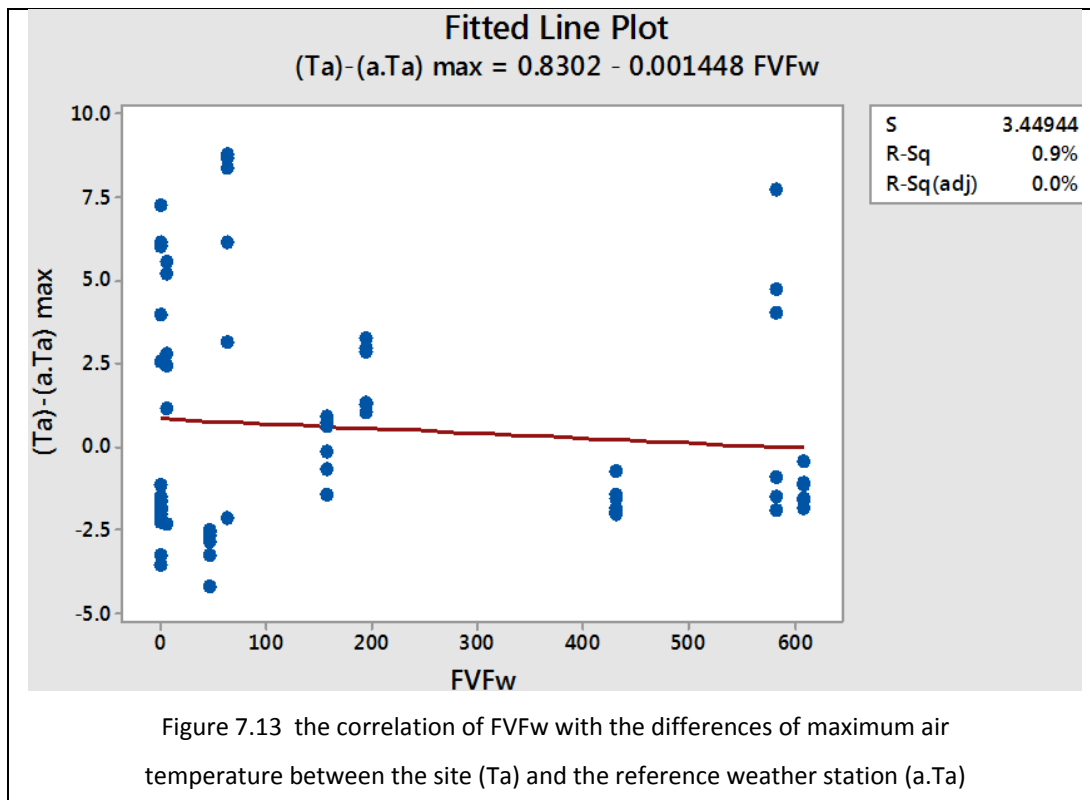


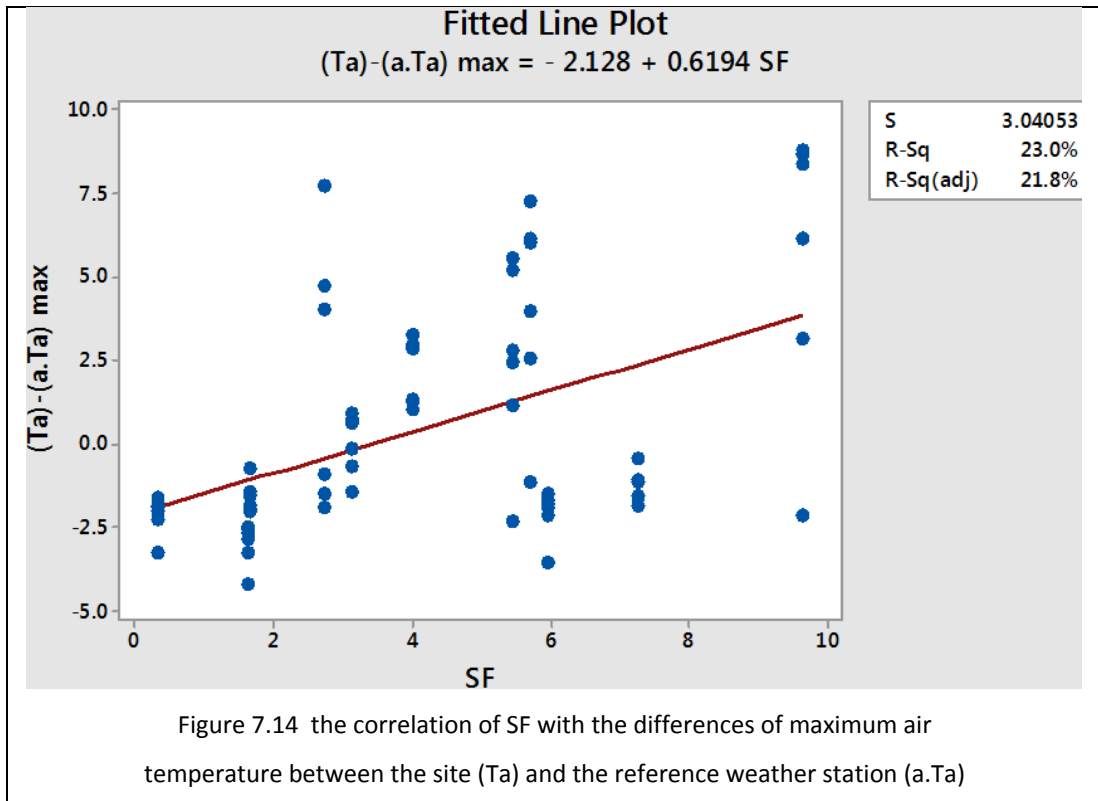
Figure 7.12 the correlation of FVFs with the differences of maximum air temperature between the site (Ta) and the reference weather station (a.Ta)



The results of simple linear regression analysis for both urban morphological parameters (SVFx and FVFx) support the findings of the maximum multilinear regression models for the same parameters as modified model (M.M) for the afternoon period, especially in terms of increasing and decreasing the air temperature [see Appendix A].

The correlations of other urban parameters with the differences of maximum air temperature between the site and the reference weather station ($Ta - a.Ta$) were explored for the same data set.

The shape factor (SF) kept its position as the one of the most influential parameter on air temperature differences with $R-Sq(adj) = 21.8\%$. These differences will increase for any increasing in Sf value. These outputs are compatible with the improvement rates [see Figure 7.2] and the maximum modified model of SF [see Appendix A].



The sky view factor (SVF) and the site coverage ratio (SCR) have no real correlations with air temperature as shown by [Figures 7.15 and 7.16](#) and this in line with their total effects as the parameters that came the last compared to other parameters as shown by [Figure 7.2](#), while the façade to site ratio (FSR), that occupied the fourth position according to the latter figure, showed no correlation with air temperature as shown by [Figure 7.17](#). The most likely cause for this mismatch is the limited of data that used with the simple linear regression.

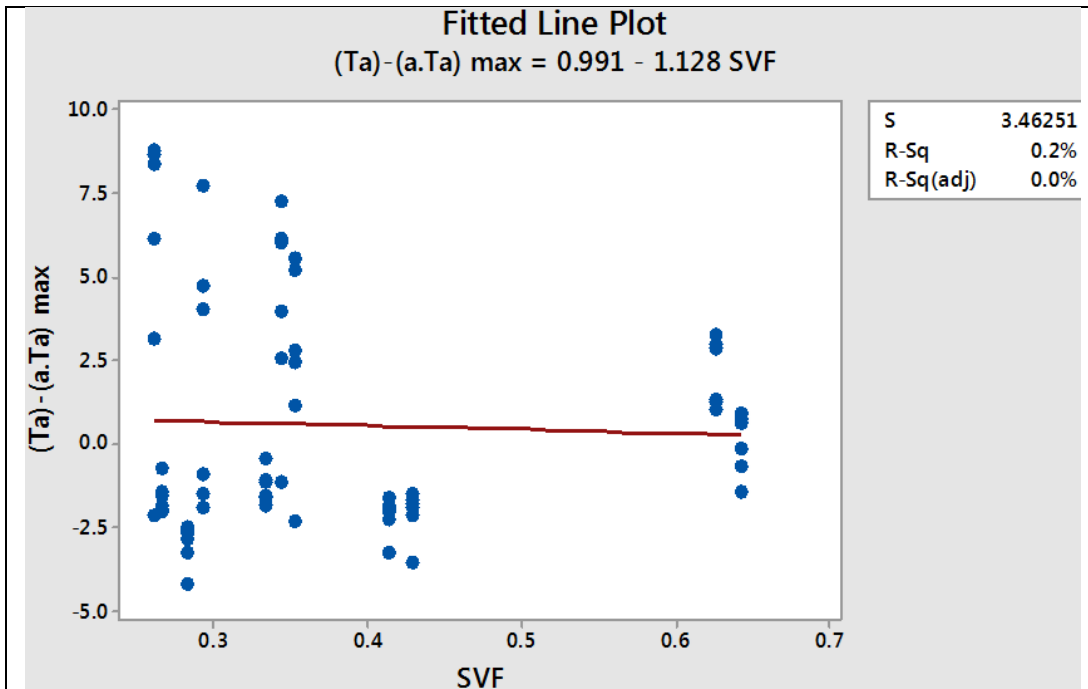


Figure 7.15 the correlation of SVF with the differences of maximum air temperature between the site (Ta) and the reference weather station (a.Ta)

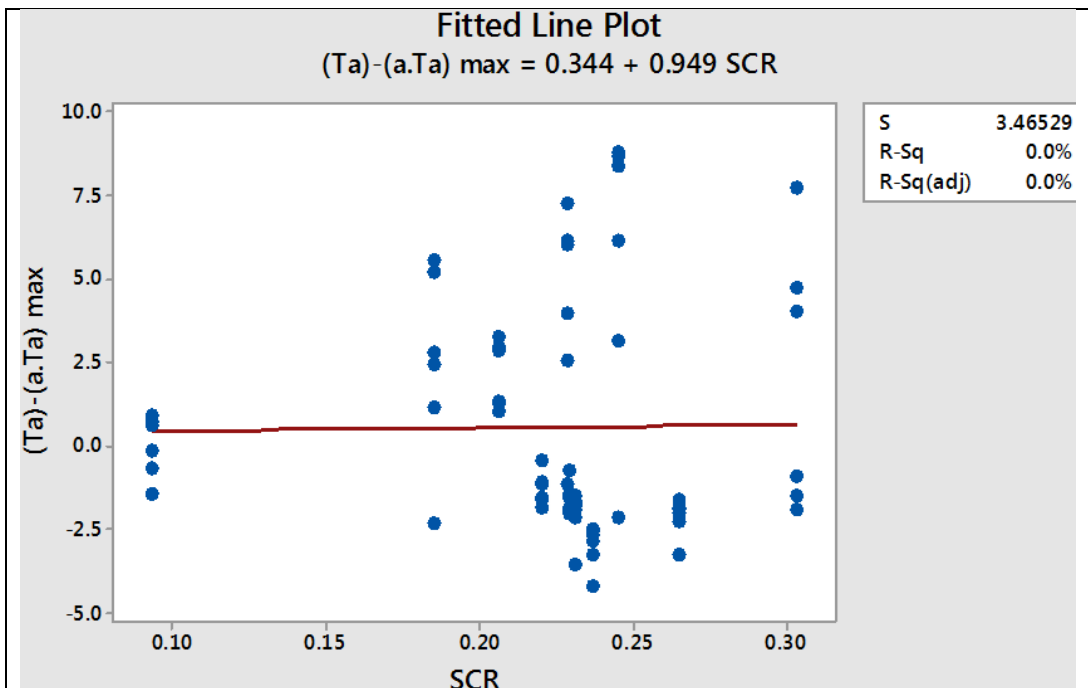
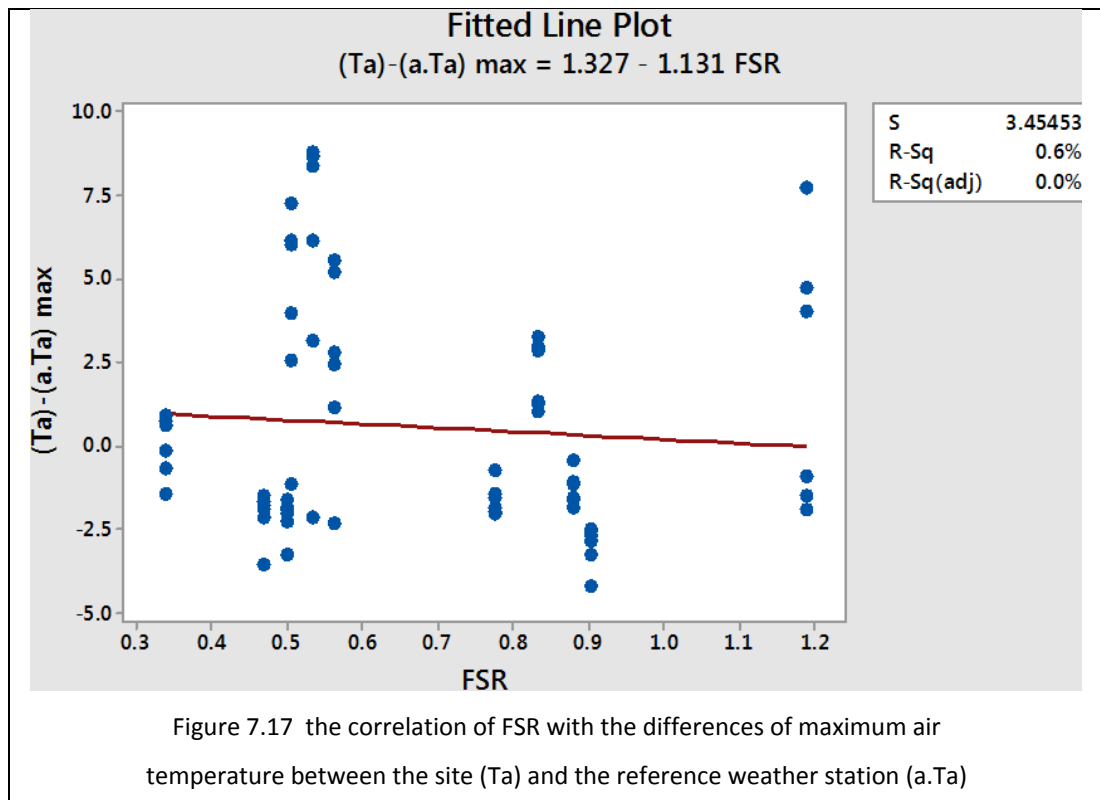


Figure 7.16 the correlation of SCR with the differences of maximum air temperature between the site (Ta) and the reference weather station (a.Ta)



Figures 7.18, 7.19, 7.20 and 7.21 show that the parameters compactness index (CI), degree of compactness (Dc), total façade view factor (FVF) and floor area ratio (FAR) respectively have a moderate effects on the differences between Ta and a.Ta. These results in line with the other findings that were showed by Figure 7.2, where these parameters occupied the intermediate ranks between SVFx, FVFX and SF as the most influential parameters and the parameters SVF, SCR and FSR as the lowest influential parameters. In terms of increasing or decreasing the gap between Ta and a.Ta, both of CI and Dc showed negative relationships with air temperature similarly to the findings of the maximum multilinear regression models for the same parameters as modified model (M.M) for the afternoon period as shown by Appendix A. FVF and FAR affect negatively on differences between Ta and a.Ta as shown by Figures 7.20 and 7.21, however they were insignificant to affect air temperature as shown by their modified models [see Appendix A] due to the difference of dataset size between the simple liner regression analysis and multiple liner regression analysis.

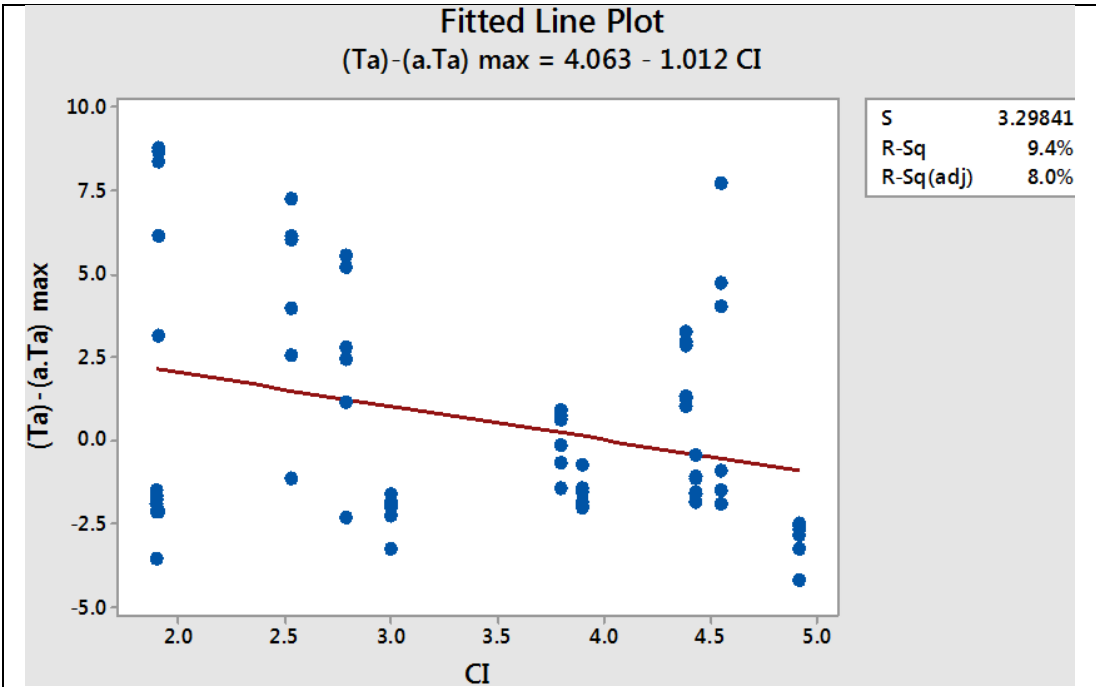


Figure 7.18 the correlation of CI with the differences of maximum air temperature between the site (Ta) and the reference weather station (a.Ta)

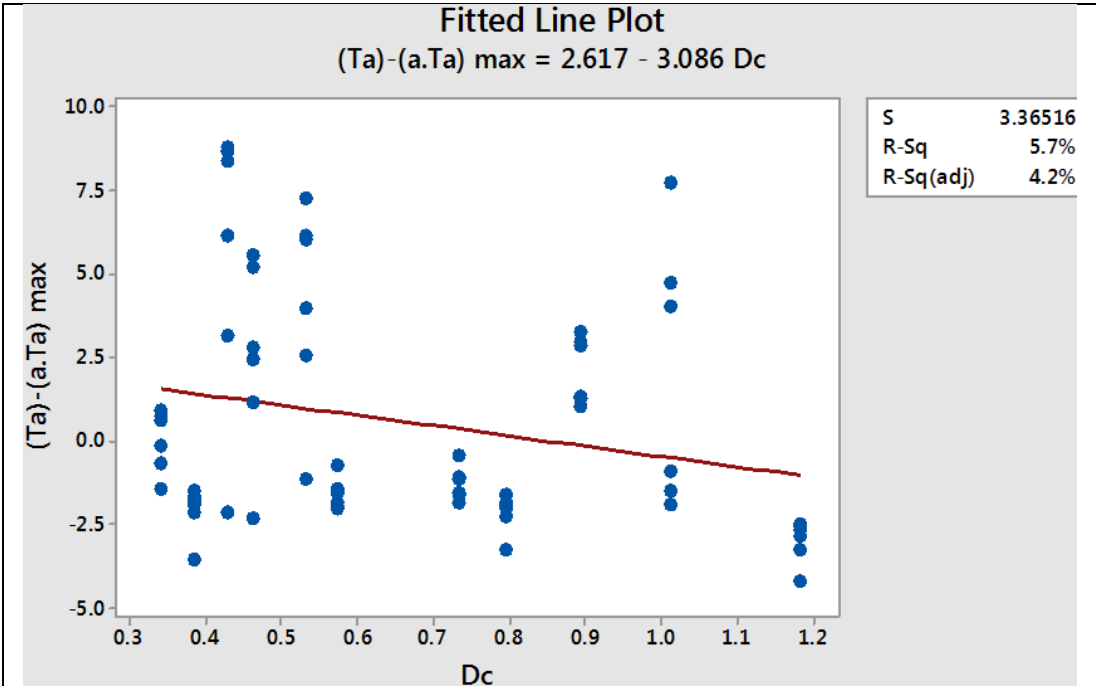
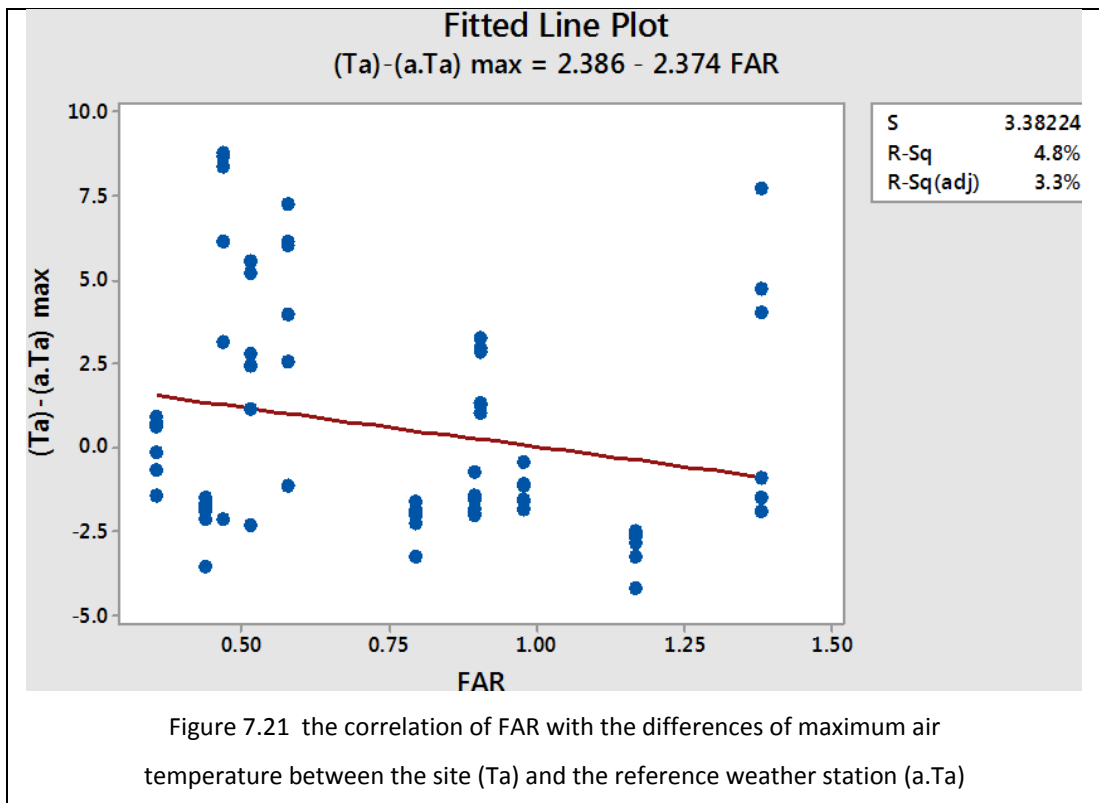
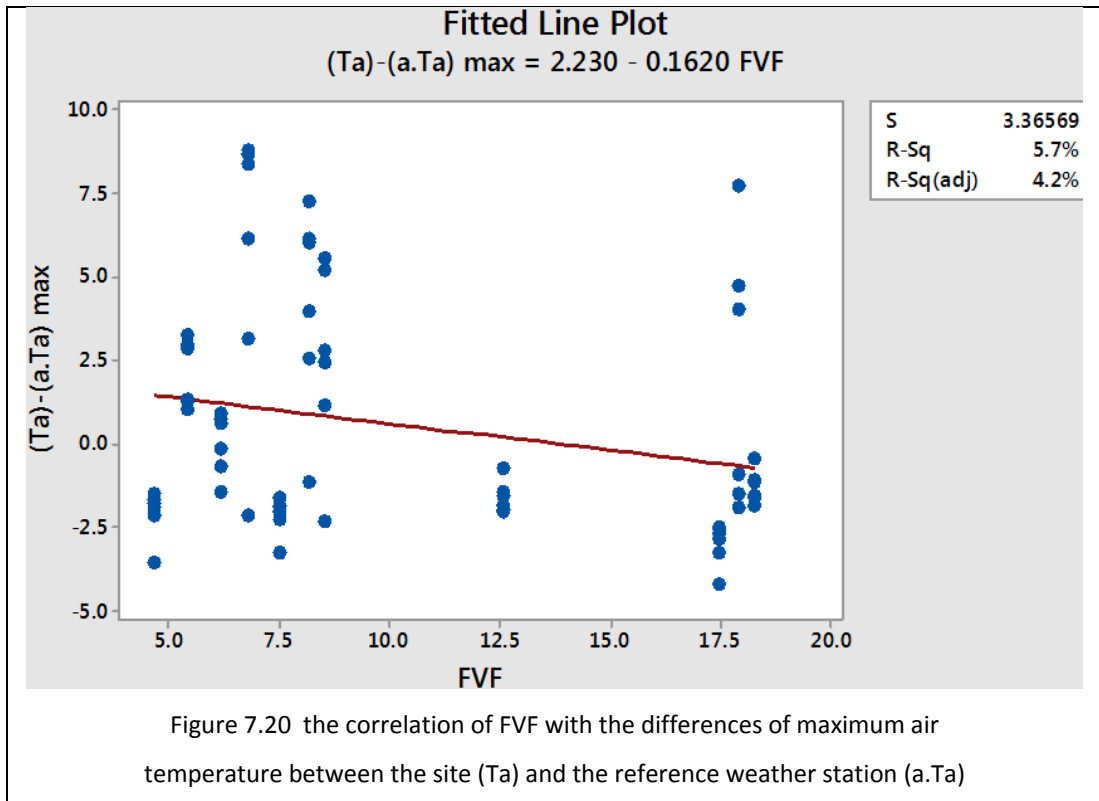


Figure 7.19 the correlation of Dc with the differences of maximum air temperature between the site (Ta) and the reference weather station (a.Ta)



7.5 Conclusions

This chapter was devoted to a comprehensive discussion about the results of the statistical analyses between the climatic factors and the urban morphological parameters (UMP) on the one hand and the on-site measured air temperatures (T_a) on the other hand to reveal the effect of each UMP and its role in terms of increasing or decreasing T_a .

The effects of the climatic factors (the ambient air temperature ($a.T_a$) and the solar radiation) on the indicators of T_a (AVG, MAX and MIN) were discussed without contribution of UMP in the basic models (B.M). As expected, the increase of $a.T_a$ led to a rise in T_a regardless of the sky condition and the periods of day. In terms of the solar radiation, unanticipated negative relationships with T_a were noticed under the different sky conditions because of the nature of the statistical process. Therefore, it was not a real effect where an increase of the solar radiation will not lead to a decrease the air temperature. Mostly, the influences of $a.T_a$ and solar radiation on T_a did not change notably by the influence of UMP. However, the roles of $a.T_a$ and the solar radiation were changed particularly by the sky conditions and the period of the day.

Although the climatic factor were the dominant variables compared to the UMP, the latter showed a significant role regarding thermal microclimate indicators, as reflected in the rates of improvement. These rates represented the differences between the $R-Sq(adj)$ for models with just the climatic factors as independent variables (B.M) versus the modified models (M.M) that utilized both the climatic factors and UMP as independent variables. This approach revealed the size effect of each UMP on the air temperature indicators.

Regarding the effect of UMP on air temperature behaviours, it has been noticed that these behaviours may differ from one parameter to another, where increasing SVF can lead to a reduction in T_a regardless of the sky conditions and daily periods as opposed to the SF that, in general, had positive relationships with T_a . The rest of the parameters showed mixed behaviours that varied depending on the daily periods. It is worth noting that these mixed daily behaviours were not often influenced by the

sky conditions. In other words, they mostly remain constant between the sunny, partially cloudy and cloudy skies – as seen for FSR, Dc, CI and FVF. In addition, these behaviours were not affected by the different datasets for the three indicators of air temperature. In terms of the novel parameters SVFx and FVFx, although the increase of SVFn led to a reduced Ta irrespective the sky conditions and daily periods, the rest of the subdivisions for both parameters showed mixed behaviours that were mostly not affected by sky conditions or the variant datasets of AVG, MAX and MIN. However, the diversity of these behaviours was subject to the differences of the daily periods and the cardinal directions.

Unexpected air temperature behaviours by the effects of UMP were observed under the different sky conditions owing to the nature of the statistical process that just dealt numerical values and relationships. The statistical analyses witnessed insignificant models which were not neglected, and they were used as a weighting factor in the process of assessing the size of the effect of each UMP on the thermal microclimate indicators. The improvement rates for the indicators AVG, MAX and MIN were weighted and summed into a one value to represent the influence size of each parameter under the determined sky condition. Finally, the total effect of each UMP on Ta throughout the hot season could be calculated as the total summation of effect size values for each UMP in the three sky conditions.

In general, the partial sky view factor (SVFx) and the façade view factor (FVFx) have the biggest effect, respectively, on in-situ measured air temperature owing to adopting the directions approach to link between the sun's position and the urban space configuration, depending on the daily periods. The shape factor (SF) occupied the third rank above the compactness index (CI). The total façade view factor (FVF) which came seventh after the floor area ratio (FAR) and the façade to site ratio (FSR) respectively. The sky view factor (SVF) was in eighth place, above the site cover ratio (SCR) and the degree of compactness (Dc), which came last.

These results and discussions cannot be categorical or indisputable because the behaviours of air temperature are complex due to the diversity and interdependence of the influential factors and the morphology of the urban space is a one of them. However, statistical analyses have shown much about the relationships between the

urban morphology and the climatic factors as independent variables and the indicators of air temperature as dependent variables.

Chapter Eight

8 Conclusions

8.1 Introduction

This chapter summarises the answers of research questions and addresses the conclusions that relates to them. While the research objectives were reviewed in terms of their direct relations with thesis chapters that mentioned the most important outcomes of this study. Future research work and limitations were revealed at the end of this chapter.

8.2 Answering the research questions

There are many research questions that were asked in chapter one and this section is devoted to answering them.

Firstly, ‘to what extent does the urban morphology influences the thermal microclimate of an urban space under the hot season condition of a maritime temperate climate?’

This is perhaps one of the most common questions that was asked in the urban-microclimate studies taking into account the diversity of climatic conditions and cases studied. However, there is no typical answer to this question. Due to the effect of urban morphology on air temperature, as shown in this study, is related to the method that was used to measure the urban morphology. In the other words, the effect depends on the parameter where some of them contributed significantly in explaining the air temperature variation irrespective of the sky conditions such as partial sky view factor (SVF_x), façade view factor (FVF) and shape factor (SF). This is in contrast to the role of sky view factor (SVF) which significantly improved in the cloudy days in comparison with the sunny days. However, its effect remained weak in all cases [see Figures 7.3, 7.4 and 7.5]. Therefore, the effect of the urban morphology that is expressed by SVF on thermal microclimate is very weak in the hot season of the maritime temperate climate, whereas the effect of urban morphology that expressed by SVF_x for the same climatic conditions and the studied sites is very strong. This indicates the following conclusion: in regard to understanding the urban-microclimate relationship, a set of urban morphological parameters may be suitable

for using in a specific urban environment to understand this relationship effectively and the same parameters are not suitable for other environments or climates. Consequently, promising a potential to utilize these parameters to issue planning regulations and to prepare urban designs for more sustainable urban environments in terms of employing the urban form.

The second question, **'does the role of an urban morphological parameter vary by changing the sky conditions and day intervals?'**

In terms of the size of effect of urban parameters this variation is clear for all parameters, however, the novel parameter SVFx did not notably change in comparison with the others for the same sky condition. In addition, it kept the lead position irrespective of the sky conditions in all cases. Whilst some parameters such as degree of compactness (Dc), facade to site ratio (FSR), total façade view factor (FVF) and floor area ratio (FAR) became virtually ineffective in the cloudy days [see Figure 7.5]. One conclusion that may be drawn from this suggests that some urban morphological parameters may need a limited range of sky conditions to be effective in explaining the variation of thermal microclimate, and this limits their potential regarding understanding and applying the sustainability concept by the urban morphology on a micro-scale. In return, this study developed two novel parameters (SVFx and FVF) and presented the third (SF) to overcome this disadvantage, at least in temperate climates. These three parameters contribute quite substantially in the explanation of the variation of air temperature weather for each sky condition, or for the hot season as a whole [see Figure 7.6].

Another segment to the answer of the second question, in terms of the role of parameters in decreasing or increasing the air temperature, is that the change of sky condition showed a very limited effect on most of the parameters [see Tables 7-3, 7-5 and 7-7 as samples]. However, the day periods had important influences on the role of parameters, mostly the increase of parameter values increase the air temperature throughout the morning period from 6am to 12pm, in contrast to the evening period from 6pm to 12am. Both parameters (SF and SVF) shifted our view to another possibility that the urban morphology may have a constant role that is not affected by daily periods in regard to the air temperature behaviours, where the

increase of SF leads to increase the air temperature irrespective of the sky condition and daily intervals, completely in contrast to the role of SVF [see Tables 7-13, 7-15].

Third, 'Is there a mechanism to improve the ability of urban morphological parameter in regard to the interpretation of air temperature variation?'

A numerical comparison between SVFx and FVx on the one hand and SVF and FVF on the other hand reveals significant differences in the parameter's ability to explain the change in air temperature irrespective of the conditions of the sky [see Tables 7-29, 7-30 and 7-31]. This is due to involving the direction concept in the calculation method of parameter which helped to create greater privacy for the urban morphology around the point of measurement compared to other points, which in turn helped statistical models in the diagnosis of a stronger relationship between the parameter and air temperature indicators.

A Promising mechanism to understand the air temperature irrespective of the sky conditions can be inferred by the parameters that describe the building configuration itself such as SF and CI instead of the parameters that describe the building configuration in relation with the urban space, such as: FVF, FSR and SCR.

The conclusion that can be drawn here is that many effective mechanisms are available to support the sustainable urban design practice by measuring or describing the urban morphology in greater particularity, and this opens the door to further scientific research on this point.

The last research question answers the question, **'Does the behaviour of air temperature, in terms of increase and decrease, subjected to the method of urban morphology expression?'**

The calculation methods of urban morphology that use the similar inputs such as site area and ground floor area, mostly, have similar effects on the behaviours of air temperature although the dealing with the inputs vary from one method to another for example CI, Dc, FAR, FSR and FVF [see Tables 7-3, 7-7, 7-9, 7-11 and 7-27]. On the other hand the urban morphological parameters that depend on different inputs compared to the aforementioned parameters such as SVF and SF affected the air temperature behaviours in completely different ways where an increase of SVF

leads to a decrease in air temperature irrespective of both the daily periods and sky conditions, this is in contrast with the role of SF FVF [see Tables 7-13, 7-15]. Regarding the novel parameter FVFX, its subdivisions were calculated by the same method, however, each one affected the air temperature behaviour differently due to involving the direction idea as an input by calculating FVFX for each side separately and this defines the urban configuration of each side around the measuring point and contribute to showing the unique role of each side. The thermal behaviours changed according to the daily periods and limitedly changed depending to the sky conditions [see Tables 7-22 to 7-25]. The same thing happened with SVFX that also took into account the effect of direction as previously mentioned [see Tables 7-17 to 7-20].

8.3 Aim and Objectives

The aim of this research was defined as **the need to deepen our understanding of the relationship between urban morphology and thermal environment on a micro urban scale in order to contribute to endeavours to minimize the negative effects of urbanization.** Depending on the analysis and evaluation of the statistical relationship between the parameters that describe the urban morphology numerically and the indicators of air temperature (AVG., MAX. and MIN) under three types of sky in the hot season, and within an urban area that experiences the maritime temperate climate.

Five applicable objectives were determined to help achieve the research aim, they were met through the successive chapters of this study as shown below.

The first objective is, **to explore briefly the basic knowledge that is related to the nature of this research.**

Chapter two sought to achieve this objective by defining and exploring the urban morphology in terms of the concepts of configuration, the types of urban spaces and the analysis and description of urban form. On the other hand, the urban climate was explored regarding the surface temperature and air temperature, where both of them mainly control the micro thermal environment of urban space. The relationship

between the urban morphology and climate was explored by reviewing a number of previous studies that have been conducted mostly in temperate climates. Consequently, the concept of urban morphological parameter as a measure or descriptor of physical part of urban morphology (urban form) was highlighted with its effect on climatic factors concerning an understanding of the urban-climate relationship on micro urban scale.

With reference to the second objective, **exploring the existing methods to measure the urban morphology.**

This was achieved part of the research methodology, chapter three presented seven methods (parameters) to measure the urban morphology. The reasons to select them are various, where floor area ratio (FAR) and site coverage ratio (SCR) were used as a part of planning regulations in many countries, sky view factor (SVF) is a well-known parameter in the urban climate studies from about forty years, shape factor (SF) is a well-known parameter in the energy consumption studies in relation to the effect of building form. While the remaining parameters (compactness index (CI), degree of compactness (Dc) and façade-to-site ratio (FSR)) were used in many studies and showed good potentials. The urban morphology for twelve locations within a residential compound were measured by these methods and the results were revealed in chapter five. Other methods describe the urban morphology depending on a relationship of some parameter together were mentioned briefly in chapter two such as spacemate and space syntax.

Regarding the third objective, **measuring the air temperatures within urban spaces of a case study under a maritime temperate climate.**

The accomplishment of this objective was distributed throughout two chapters (three and five). Chapter three discussed, in detail, the case study in terms of climate conditions and design features in addition to discussion of field measurements in terms of measuring points, measuring tools, seasons of measurement and the validity of measurements. Chapter five presented the results of air temperature measurements along with some of climatic factors including (ambient air temperature, solar radiation, wind speed and rain rates) to get enough conception

about the conditions that associated the measuring process. The results was introduced in groups in accordance with seasons, sky conditions and day periods.

The fourth objective is, **developing a statistical approach to assess and analyse the relationships between urban morphological parameters and air temperature.**

As a main part of research methodology, statistical approach was developed and introduced within chapter three. This approach consists of two parts, data sorting and statistical framework. The first part is to minimize the effect of other climatic factors on air temperature variation by distributing the inputs of statistical models (field measurements) into hot and cold seasons which in turn were divided into three groups, each of them in accordance to sky conditions (sunny, partially cloudy and cloudy) which, in turn, were divided into four groups for each of them in accordance to day periods (night, morning, afternoon and evening). Following this, the data of each group was distributed into three indicators of air temperature (AVG, MAX and MIN).

The second part of this approach used multiple regression models on two levels. Firstly, to assess only the climatic factors effects (ambient air temperature and solar radiation) on on-site measured air temperatures. Secondly, to assess the effect of the same climatic factors with urban morphological parameters on on-site measured air temperatures.

The statistical analysis depended on the output of regression models including (p-value, R-Sq(adj), the standard error of the regression (S) and mathematical signs of regression coefficients). In general, the augmentation of the R-Sq(adj) values for the same models before and after adding the urban parameters reveals the role of that parameters in the variation of air temperatures. While the coefficients signs show the role of parameters in terms of raising or lowering the on-site air temperature. The results of statistical approach and their analysis were revealed in chapter six.

The last objective of the study, **determining the size of effect of each parameter and its role in terms of increasing or decreasing the air temperature.**

Chapter seven was set out to achieve this objective by providing a comprehensive discussion of the statistical approach results that was presented in chapter six in

order to understanding the behaviours of the in-situ measured air temperature, in terms of increasing or decreasing, under the effect of urban parameters and to define the most influential urban morphological parameters on thermal microclimate.

The effect of urban parameters on the air temperature behaviours was previously mentioned earlier in this chapter.

Regarding the size of effect of each parameter, four of the ten parameters kept their positions at the top as the most influential in air temperature, irrespective of sky conditions. The first position was reserved permanently for the novel parameter (SVFx) [see Figures 7.3, 7.4 and 7.3] and, therefore, was labelled as the most influential throughout the hot season [see Figure 7.6]. The second novel parameter (FVFX) reserved its position as the second most influential parameter under the sunny and partially cloudy conditions of the sky, however, taking third place under the condition of cloudy sky. Hence, FVFX settled on the second rank for the hot season after SVFx. The pioneer parameter (SF) in the urban microclimate studies come second under the cloudy sky and third under the sunny and partially cloudy skies, thus SF represented the third most influential parameter on air temperature throughout the hot season. CI ranked fourth under the three sky conditions and for the hot season also. Concerning the third novel parameter (FVF), it surpassed all of SVF, SCR and Dc to be ranked seventh under the sunny sky, and it came sixth before each SVF, SCR, Dc and FSR under the partially cloudy sky, and again to be the seventh under the cloudy sky before all of Dc, FSR and FAR. In regard to the hot season, it came seventh before each of SVF, SCR, Dc.

8.4 Future research

This study was conducted with a small number of measuring points for a relatively short time scale and its scope was limited to the temperate climate, particularly in the maritime type. Future research could utilize a larger number of measuring points for longer period of time to test the reliability of its outcomes.

As a matter of generalization for the results of this research, further studies can be done under different types of temperate climate or with different climate zones such as hot climate.

Further urban morphological parameters can be investigated on different urban scale, especially under the maritime temperate climate to compensate the lack of similar studies highlighted by this research.

The parameters that were developed by this study can be used to investigate the urban-climate relationship in regard to other climatic factors, for instance the on-site measured wind speed or on-site measured solar radiation in addition to the thermal comfort within urban spaces and so on. Furthermore, these parameter can be used together to develop predictive statistical model of air temperature or other climate factors depending on the urban morphology on micro scale.

8.5 Limitations of the research

A portion of the research limitations lies in the description and measuring of morphology of urban area within any of its spatial scales, since it is a complex entity with unlimited number of choices. Therefore, there is no comprehensive method to describe urban morphology and understand its effect on microclimate especially with diversity of climate factors that add further limitations for this research.

The dynamic processes between the urban area and atmosphere that occur in the real world, every second, cannot be represented accurately by any statistical approach which, in turn, suffers from a limitation of its inputs and outputs in terms of their ability to describe the case study comprehensively.

Other limitations can be highlighted by the scope of the study that covers only a small number of measuring points on a short time scale and in regard to the filed measurement duration under one type of climate within a small case study in terms of its spatial scale.

A limited contribution of the programming in the urban-climate studies a result of the gap between the specialists, where this study tried to contribute in this side by developing a plugin to calculate SVF_x.

Appendices

Appendix A: The modified models (M.M) of the sunny days

The Night Period

Façade View Factor (FV_{Fx})

AVERAGE-Ta = -1.634 - 0.01968 avg solar + 1.1143 avg a.Ta + 0.000267 FVFe + 0.000195 FVw

MAXIMUM-Ta = -1.279 - 0.01471 max solar + 1.0960 max a.Ta + 0.000204 FVFe

MINIMUM-Ta = -1.895 - 0.0514 min solar + 1.1303 min a.Ta + 0.000280 FVFe + 0.000235 FVw

Partial Sky View Factor (SV_{Fx})

AVERAGE-Ta = -1.098 - 0.01968 avg solar + 1.1143 avg a.Ta - 2.275 SVFn - 1.419 SVFe

MAXIMUM-Ta = -0.809 - 0.01471 max solar + 1.0960 max a.Ta - 2.165 SVFn - 1.451 SVFe

MINIMUM-Ta = -1.335 - 0.05140 min solar + 1.1303 min a.Ta - 2.385 SVFn - 1.404 SVFe

Total Façade View Factor (FVF)

AVERAGE-Ta = -1.513 - 0.01968 avg solar + 1.1143 avg a.Ta

MAXIMUM-Ta = -1.214 - 0.01471 max solar + 1.0960 max a.Ta

MINIMUM-Ta = -1.762 - 0.0514 min solar + 1.1303 min a.Ta

Site Coverage Ratio (SCR)

AVERAGE-Ta = -1.513 - 0.01968 avg solar + 1.1143 avg a.Ta

MAXIMUM-Ta = -1.214 - 0.01471 max solar + 1.0960 max a.Ta

MINIMUM-Ta = -1.762 - 0.0514 min solar + 1.1303 min a.Ta

Floor Area Ratio (FAR)

AVERAGE-Ta = -1.401 - 0.01968 avg solar + 1.1143 avg a.Ta - 0.1464 FAR

MAXIMUM-Ta = -1.087 - 0.01471 max solar + 1.0960 max a.Ta - 0.1649 FAR

MINIMUM-Ta = -1.657 - 0.0514 min solar + 1.1303 min a.Ta - 0.1368 FAR

Façade to Site Ratio (FSR)

AVERAGE-Ta = -1.513 - 0.01968 avg solar + 1.1143 avg a.Ta

MAXIMUM-Ta = -1.214 - 0.01471 max solar + 1.0960 max a.Ta

MINIMUM-Ta = -1.762 - 0.0514 min solar + 1.1303 min a.Ta

Compactness Index (CI)

AVERAGE-Ta = -1.307 - 0.01968 avg solar + 1.1143 avg a.Ta - 0.0596 CI

MAXIMUM-Ta = -0.988 - 0.01471 max solar + 1.0960 max a.Ta - 0.0653 CI

MINIMUM-Ta = -1.566 - 0.0514 min solar + 1.1303 min a.Ta - 0.0565 CI

Degree of Compactness (Dc)

AVERAGE-Ta = -1.412 - 0.01968 avg solar + 1.1143 avg a.Ta - 0.1518 Dc

MAXIMUM-Ta = -1.105 - 0.01471 max solar + 1.0960 max a.Ta - 0.1638 Dc

MINIMUM-Ta = -1.660 - 0.0514 min solar + 1.1303 min a.Ta - 0.1525 Dc

Shape Factor (SF)

AVERAGE-Ta = -1.830 - 0.01968 avg solar + 1.1143 avg a.Ta + 0.07315 SF

MAXIMUM-Ta = -1.528 - 0.01471 max solar + 1.0960 max a.Ta + 0.07245 SF

MINIMUM-Ta = -2.081 - 0.05140 min solar + 1.1303 min a.Ta + 0.07357 SF

Sky View Factor (SVF)

AVERAGE-Ta = -1.169 - 0.01968 avg solar + 1.1143 avg a.Ta - 0.891 SVF

MAXIMUM-Ta = -0.889 - 0.01471 max solar + 1.0960 max a.Ta - 0.843 SVF

MINIMUM-Ta = -1.399 - 0.0514 min solar + 1.1303 min a.Ta - 0.940 SVF

The Morning Period

Façade View Factor (FV_{Fx})

AVERAGE-Ta = 4.62 + 0.003435 avg solar + 0.5588 avg a.Ta + 0.001568 FV_{Fn} + 0.000651 FV_{Fs} + 0.002815 FV_{Fw}

MAXIMUM-Ta = 10.29 + 0.005738 max solar + 0.1725 max a.Ta + 0.001269 FV_{Fn} - 0.000581 FV_{Fe} + 0.003739 FV_{Fw}

MINIMUM-Ta = 1.16 + 0.001310 min solar + 0.8317 min a.Ta + 0.001312 FV_{Fn} + 0.000682 FV_{Fs} + 0.002096 FV_{Fw}

Partial Sky View Factor (SV_{Fx})

AVERAGE-Ta = 6.75 + 0.003435 avg solar + 0.5588 avg a.Ta - 5.09 SV_{Fn} + 3.34 SV_{Fe} + 5.17 SV_{Fs} - 12.41 SV_{Fw}

MAXIMUM-Ta = 12.17 + 0.005738 max solar + 0.1725 max a.Ta - 5.20 SV_{Fn} + 4.00 SV_{Fe} + 7.19 SV_{Fs} - 14.96 SV_{Fw}

MINIMUM-Ta = 3.30 + 0.001310 min solar + 0.8317 min a.Ta - 3.24 SV_{Fn} + 4.61 SV_{Fs} - 12.79 SV_{Fw}

Sky View Factor (SVF)

AVERAGE-Ta = 6.52 + 0.003435 avg solar + 0.559 avg a.Ta - 2.207 SVF

MAXIMUM-Ta = 11.86 + 0.005738 max solar + 0.173 max a.Ta - 2.094 SVF

MINIMUM-Ta = 2.88 + 0.001310 min solar + 0.8317 min a.Ta - 2.193 SVF

Total Façade View Factor (FVF)

AVERAGE-Ta = 4.22 + 0.003435 avg solar + 0.5588 avg a.Ta + 0.1399 FVF

MAXIMUM-Ta = 9.41 + 0.005738 max solar + 0.173 max a.Ta + 0.1584 FVF

MINIMUM-Ta = 0.82 + 0.001310 min solar + 0.8317 min a.Ta + 0.1169 FVF

Site Coverage Ratio (SCR)

AVERAGE-Ta = 3.42 + 0.003435 avg solar + 0.559 avg a.Ta + 10.10 SCR

MAXIMUM-Ta = 8.51 + 0.005738 max solar + 0.173 max a.Ta + 11.39 SCR

MINIMUM-Ta = 0.13 + 0.001310 min solar + 0.8317 min a.Ta + 8.53 SCR

Floor Area Ratio (FAR)

AVERAGE-Ta = 3.90 + 0.003435 avg solar + 0.5588 avg a.Ta + 2.292 FAR

MAXIMUM-Ta = 8.95 + 0.005738 max solar + 0.173 max a.Ta + 2.715 FAR

MINIMUM-Ta = 0.63 + 0.001310 min solar + 0.8317 min a.Ta + 1.811 FAR

Façade to Site Ratio (FSR)

AVERAGE-Ta = 3.42 + 0.003435 avg solar + 0.5588 avg a.Ta + 3.293 FSR

MAXIMUM-Ta = 8.38 + 0.005738 max solar + 0.173 max a.Ta + 3.903 FSR

MINIMUM-Ta = 0.26 + 0.001310 min solar + 0.8317 min a.Ta + 2.597 FSR

Compactness Index (CI)

AVERAGE-Ta = 3.98 + 0.003435 avg solar + 0.559 avg a.Ta + 0.4868 CI

MAXIMUM-Ta = 8.98 + 0.005738 max solar + 0.173 max a.Ta + 0.596 CI

MINIMUM-Ta = 0.76 + 0.001310 min solar + 0.8317 min a.Ta + 0.3667 CI

Degree of Compactness (Dc)

AVERAGE-Ta = 4.66 + 0.003435 avg solar + 0.559 avg a.Ta + 1.508 Dc

MAXIMUM-Ta = 9.84 + 0.005738 max solar + 0.173 max a.Ta + 1.805 Dc

MINIMUM-Ta = 1.24 + 0.001310 min solar + 0.8317 min a.Ta + 1.185 Dc

Shape Factor (SF)

AVERAGE-Ta = 5.67 + 0.003435 avg solar + 0.559 avg a.Ta

MAXIMUM-Ta = 13.517 + 0.006722 max solar

MINIMUM-Ta = 2.03 + 0.001310 min solar + 0.8317 min a.Ta

The Afternoon Period

Façade View Factor (FV_{Fx})

AVERAGE-Ta = 5.56 - 0.001450 avg solar + 0.848 avg a.Ta + 0.001510 FV_{Fn} - 0.003347 FV_{Fs} + 0.002234 FV_{Fw}

MAXIMUM-Ta = 6.38 + 0.782 max a.Ta + 0.001874 FV_{Fn} - 0.003916 FV_{Fs} + 0.002338 FV_{Fw}

MINIMUM-Ta = 4.20 - 0.002080 min solar + 0.930 min a.Ta + 0.001087 FV_{Fn} - 0.000586 FV_{Fe} - 0.002902 FV_{Fs} + 0.001773 FV_{Fw}

Partial Sky View Factor (SV_{Fx})

AVERAGE-Ta = 6.46 - 0.001450 avg solar + 0.8483 avg a.Ta - 24.87 SV_{Fn} + 6.97 SV_{Fs} + 11.74 SV_{Fw}

MAXIMUM-Ta = 7.33 + 0.7824 max a.Ta - 28.85 SV_{Fn} + 8.03 SV_{Fs} + 14.24 SV_{Fw}

MINIMUM-Ta = 4.22 - 0.002080 min solar + 0.9299 min a.Ta - 25.83 SV_{Fn} + 6.41 SV_{Fe} + 18.85 SV_{Fw}

Total Façade View Factor (FVF)

AVERAGE-Ta = 5.07 - 0.001450 avg solar + 0.848 avg a.Ta

MAXIMUM-Ta = 5.77 + 0.782 max a.Ta

MINIMUM-Ta = 3.52 - 0.002080 min solar + 0.930 min a.Ta

Site Coverage Ratio (SCR)

AVERAGE-Ta = 3.70 - 0.001450 avg solar + 0.848 avg a.Ta + 6.16 SCR

MAXIMUM-Ta = 4.17 + 0.782 max a.Ta + 7.22 SCR

MINIMUM-Ta = 2.28 - 0.002080 min solar + 0.930 min a.Ta + 5.57 SCR

Floor Area Ratio (FAR)

AVERAGE-Ta = 5.07 - 0.001450 avg solar + 0.848 avg a.Ta

MAXIMUM-Ta = 5.77 + 0.782 max a.Ta

MINIMUM-Ta = 3.52 - 0.002080 min solar + 0.930 min a.Ta

Façade to Site Ratio (FSR)

AVERAGE-Ta = 5.07 - 0.001450 avg solar + 0.848 avg a.Ta

MAXIMUM-Ta = 5.77 + 0.782 max a.Ta

MINIMUM-Ta = 3.52 - 0.002080 min solar + 0.930 min a.Ta

Compactness Index (CI)

AVERAGE-Ta = 6.69 - 0.001450 avg solar + 0.848 avg a.Ta - 0.468 CI

MAXIMUM-Ta = 7.72 + 0.782 max a.Ta - 0.562 CI

MINIMUM-Ta = 4.84 - 0.002080 min solar + 0.930 min a.Ta - 0.381 CI

Degree of Compactness (Dc)

AVERAGE-Ta = 5.95 - 0.001450 avg solar + 0.848 avg a.Ta - 1.317 Dc

MAXIMUM-Ta = 6.79 + 0.782 max a.Ta - 1.514 Dc

MINIMUM-Ta = 4.24 - 0.002080 min solar + 0.930 min a.Ta - 1.077 Dc

Shape Factor (SF)

AVERAGE-Ta = 3.37 - 0.001450 avg solar + 0.848 avg a.Ta + 0.3918 SF

MAXIMUM-Ta = 3.83 + 0.782 max a.Ta + 0.4488 SF

MINIMUM-Ta = 2.05 - 0.002080 min solar + 0.930 min a.Ta + 0.3384 SF

Sky View Factor (SVF)

AVERAGE-Ta = 5.97 - 0.001450 avg solar + 0.848 avg a.Ta - 2.34 SVF

MAXIMUM-Ta = 6.82 + 0.782 max a.Ta - 2.70 SVF

MINIMUM-Ta = 4.29 - 0.002080 min solar + 0.930 min a.Ta - 1.99 SVF

The Evening Period

Façade View Factor (FV_{Fx})

AVERAGE-Ta = -2.287 + 1.2061 avg a.Ta + 0.000369 FV_{Fe} - 0.000765 FV_{Fs}

MAXIMUM-Ta = -1.941 + 1.1908 max a.Ta + 0.000453 FV_{Fe} - 0.000911 FV_{Fs}

MINIMUM-Ta = -2.541 + 1.2176 min a.Ta + 0.000297 FV_{Fe} - 0.000638 FV_{Fs}

Partial Sky View Factor (SV_{Fx})

AVERAGE-Ta = -1.781 + 1.2061 avg a.Ta - 11.396 SV_{Fn} - 5.566 SV_{Fs} + 11.83 SV_{Fw}

MAXIMUM-Ta = -1.473 + 1.1908 max a.Ta - 12.57 SV_{Fn} - 6.60 SV_{Fs} + 14.25 SV_{Fw}

MINIMUM-Ta = -2.633 - 0.00360 min solar + 1.2582 min a.Ta - 10.328 SV_{Fn} - 4.592 SV_{Fs} + 9.710 SV_{Fw}

Total Façade View Factor (FVF)

AVERAGE-Ta = -2.174 + 1.2061 avg a.Ta - 0.0258 FVF

MAXIMUM-Ta = -1.716 + 1.1908 max a.Ta - 0.0391 FVF

MINIMUM-Ta = -2.673 + 1.2176 min a.Ta

Site Coverage Ratio (SCR)

AVERAGE-Ta = -2.440 + 1.2061 avg a.Ta

MAXIMUM-Ta = -2.120 + 1.1908 max a.Ta

MINIMUM-Ta = -2.673 + 1.2176 min a.Ta

Floor Area Ratio (FAR)

AVERAGE-Ta = -1.745 + 1.2061 avg a.Ta - 0.902 FAR

MAXIMUM-Ta = -1.288 + 1.1908 max a.Ta - 1.079 FAR

MINIMUM-Ta = -2.099 + 1.2176 min a.Ta - 0.744 FAR

Façade to Site Ratio (FSR)

AVERAGE-Ta = -1.917 + 1.2061 avg a.Ta - 0.767 FSR

MAXIMUM-Ta = -1.467 + 1.1908 max a.Ta - 0.957 FSR

MINIMUM-Ta = -2.271 + 1.2176 min a.Ta - 0.589 FSR

Compactness Index (CI)

AVERAGE-Ta = -1.098 + 1.2061 avg a.Ta - 0.3874 CI

MAXIMUM-Ta = -0.522 + 1.1908 max a.Ta - 0.4610 CI

MINIMUM-Ta = -1.559 + 1.2176 min a.Ta - 0.3215 CI

Degree of Compactness (Dc)

AVERAGE-Ta = -1.748 + 1.2061 avg a.Ta - 1.037 Dc

MAXIMUM-Ta = -1.342 + 1.1908 max a.Ta - 1.164 Dc

MINIMUM-Ta = -2.062 + 1.2176 min a.Ta - 0.915 Dc

Shape Factor (SF)

AVERAGE-Ta = -3.317 + 1.2061 avg a.Ta + 0.2024 SF

MAXIMUM-Ta = -3.087 + 1.1908 max a.Ta + 0.2232 SF

MINIMUM-Ta = -4.097 - 0.00360 min solar + 1.2582 min a.Ta + 0.1854 SF

Sky View Factor (SVF)

AVERAGE-Ta = -1.535 + 1.2061 avg a.Ta - 2.343 SVF

MAXIMUM-Ta = -1.178 + 1.1908 max a.Ta - 2.438 SVF

MINIMUM-Ta = -1.813 + 1.2176 min a.Ta - 2.224 SVF

Appendix B: The modified models (M.M) of the partially cloudy days

The Night Period

Façade View Factor (FV_{Fx})

AVERAGE-Ta = -0.601 + 1.0457 avg a.Ta - 0.000333 FV_{Fn} + 0.000168 FV_{Fe} - 0.000189 FV_{Fs} + 0.000454 FV_{Fw}

MAXIMUM-Ta = -0.635 - 0.001530 max solar + 1.0484 max a.Ta - 0.000343 FV_{Fn} + 0.000147 FV_{Fe} - 0.000193 FV_{Fs} + 0.000412 FV_{Fw}

MINIMUM-Ta = -0.222 + 1.0187 min a.Ta - 0.000302 FV_{Fn} + 0.000187 FV_{Fe} - 0.000163 FV_{Fs} + 0.000477 FV_{Fw}

Partial Sky View Factor (SV_{Fx})

AVERAGE-Ta = -0.543 + 1.0457 avg a.Ta - 1.254 SV_{Fn} + 1.135 SV_{Fw}

MAXIMUM-Ta = -0.613 - 0.001530 max solar + 1.0484 max a.Ta - 1.152 SV_{Fn} + 1.202 SV_{Fw}

MINIMUM-Ta = -0.111 + 1.0187 min a.Ta - 1.356 SV_{Fn} + 0.973 SV_{Fw}

Total Façade View Factor (FVF)

AVERAGE-Ta = -0.587 + 1.0457 avg a.Ta

MAXIMUM-Ta = -0.639 - 0.001530 max solar + 1.0484 max a.Ta

MINIMUM-Ta = -0.183 + 1.0187 min a.Ta

Sky View Factor (SVF)

AVERAGE-Ta = -0.587 + 1.0457 avg a.Ta

MAXIMUM-Ta = -0.639 - 0.001530 max solar + 1.0484 max a.Ta

MINIMUM-Ta = -0.080 + 1.0187 min a.Ta - 0.266 SVF

Site Coverage Ratio (SCR)

AVERAGE-Ta = -0.423 + 1.0457 avg a.Ta - 0.737 SCR

MAXIMUM-Ta = -0.471 - 0.001530 max solar + 1.0484 max a.Ta - 0.753 SCR

MINIMUM-Ta = -0.183 + 1.0187 min a.Ta

Floor Area Ratio (FAR)

AVERAGE-Ta = -0.485 + 1.0457 avg a.Ta - 0.1326 FAR

MAXIMUM-Ta = -0.524 - 0.001530 max solar + 1.0484 max a.Ta - 0.1483 PR

MINIMUM-Ta = -0.103 + 1.0187 min a.Ta - 0.1045 PR

Façade to Site Ratio (FSR)

AVERAGE-Ta = -0.507 + 1.0457 avg a.Ta - 0.1179 FSR

MAXIMUM-Ta = -0.543 - 0.001530 max solar + 1.0484 max a.Ta - 0.1397 FSR

MINIMUM-Ta = -0.183 + 1.0187 min a.Ta

Compactness Index (CI)

AVERAGE-Ta = -0.587 + 1.0457 avg a.Ta

MAXIMUM-Ta = -0.639 - 0.001530 max solar + 1.0484 max a.Ta

MINIMUM-Ta = -0.183 + 1.0187 min a.Ta

Degree of Compactness (Dc)

AVERAGE-Ta = -0.587 + 1.0457 avg a.Ta

MAXIMUM-Ta = -0.639 - 0.001530 max solar + 1.0484 max a.Ta

MINIMUM-Ta = -0.183 + 1.0187 min a.Ta

Shape Factor (SF)

AVERAGE-Ta = -0.795 + 1.0457 avg a.Ta + 0.04805 SF

MAXIMUM-Ta = -0.845 - 0.001530 max solar + 1.0484 max a.Ta + 0.04771 SF

MINIMUM-Ta = -0.394 + 1.0187 min a.Ta + 0.04857 SF

The Morning Period

Façade View Factor (FV_{Fx})

AVERAGE-Ta = -1.724 - 0.001125 avg solar + 1.1178 avg a.Ta + 0.000746 FV_{Fn} - 0.000290 FV_{Fe} + 0.000507 FV_{Fs} + 0.000841 FV_{Fw}

MAXIMUM-Ta = -2.452 - 0.000253 max solar + 1.1451 max a.Ta + 0.000905 FV_{Fn} - 0.000389 FV_{Fe} + 0.000485 FV_{Fs} + 0.001219 FV_{Fw}

MINIMUM-Ta = -0.728 - 0.001830 min solar + 1.0596 min a.Ta + 0.000599 FV_{Fn} - 0.000196 FV_{Fe} + 0.000480 FV_{Fs} + 0.000575 FV_{Fw}

Partial Sky View Factor (SV_{Fx})

AVERAGE-Ta = -0.934 - 0.001125 avg solar + 1.1178 avg a.Ta - 3.230 SV_{Fn} + 2.888 SV_{Fe} + 0.516 SV_{Fs} - 3.66 SV_{Fw}

MAXIMUM-Ta = -1.528 - 0.000253 max solar + 1.1451 max a.Ta - 3.52 SV_{Fn} + 3.36 SV_{Fe} + 1.67 SV_{Fs} - 5.44 SV_{Fw}

MINIMUM-Ta = -0.043 - 0.001830 min solar + 1.0596 min a.Ta - 2.965 SV_{Fn} + 2.337 SV_{Fe} - 0.218 SV_{Fs} - 2.33 SV_{Fw}

Sky View Factor (SVF)

AVERAGE-Ta = -0.903 - 0.001125 avg solar + 1.1178 avg a.Ta - 1.144 SVF

MAXIMUM-Ta = -1.546 - 0.000253 max solar + 1.1451 max a.Ta - 1.205 SVF

MINIMUM-Ta = 0.013 - 0.001830 min solar + 1.0596 min a.Ta - 1.080 SVF

Total Façade View Factor (FVF)

AVERAGE-Ta = -1.990 - 0.001125 avg solar + 1.1178 avg a.Ta + 0.06240 FVF

MAXIMUM-Ta = -2.808 - 0.000253 max solar + 1.1451 max a.Ta + 0.07698 FVF

MINIMUM-Ta = -0.921 - 0.001830 min solar + 1.0596 min a.Ta + 0.04984 FVF

Site Coverage Ratio (SCR)

AVERAGE-Ta = -2.564 - 0.001125 avg solar + 1.1178 avg a.Ta + 5.481 SCR

MAXIMUM-Ta = -3.479 - 0.000253 max solar + 1.1451 max a.Ta + 6.597 SCR

MINIMUM-Ta = -1.399 - 0.001830 min solar + 1.0596 min a.Ta + 4.471 SCR

Floor Area Ratio (FAR)

AVERAGE-Ta = -2.149 - 0.001125 avg solar + 1.1178 avg a.Ta + 1.042 FAR

MAXIMUM-Ta = -3.048 - 0.000253 max solar + 1.1451 max a.Ta + 1.345 FAR

MINIMUM-Ta = -1.012 - 0.001830 min solar + 1.0596 min a.Ta + 0.788 FAR

Façade to Site Ratio (FSR)

AVERAGE-Ta = -2.328 - 0.001125 avg solar + 1.1178 avg a.Ta + 1.441 FSR

MAXIMUM-Ta = -3.294 - 0.000253 max solar + 1.1451 max a.Ta + 1.880 FSR

MINIMUM-Ta = -1.142 - 0.001830 min solar + 1.0596 min a.Ta + 1.080 FSR

Compactness Index (CI)

AVERAGE-Ta = -2.016 - 0.001125 avg solar + 1.1178 avg a.Ta + 0.1937 CI

MAXIMUM-Ta = -2.927 - 0.000253 max solar + 1.1451 max a.Ta + 0.2640 CI

MINIMUM-Ta = -0.878 - 0.001830 min solar + 1.0596 min a.Ta + 0.1366 CI

Degree of Compactness (Dc)

AVERAGE-Ta = -1.824 - 0.001125 avg solar + 1.1178 avg a.Ta + 0.716 Dc

MAXIMUM-Ta = -2.621 - 0.000253 max solar + 1.1451 max a.Ta + 0.912 Dc

MINIMUM-Ta = -0.771 - 0.001830 min solar + 1.0596 min a.Ta + 0.548 Dc

Shape Factor (SF)

AVERAGE-Ta = -1.345 - 0.001125 avg solar + 1.1178 avg a.Ta

MAXIMUM-Ta = -2.011 - 0.000253 max solar + 1.1451 max a.Ta

MINIMUM-Ta = -0.405 - 0.001830 min solar + 1.0596 min a.Ta

The Afternoon Period

Façade View Factor (FV_{Fx})

AVERAGE-Ta = 1.510 - 0.001847 avg solar + 1.0491 avg a.Ta + 0.000596 FV_{Fn} - 0.000398 FV_{Fe} - 0.001463 FV_{Fs}

MAXIMUM-Ta = 2.886 - 0.001328 max solar + 0.9902 max a.Ta + 0.000701 FV_{Fn} - 0.000429 FV_{Fe} - 0.002067 FV_{Fs}

MINIMUM-Ta = 0.749 - 0.002561 min solar + 1.0751 min a.Ta + 0.000513 FV_{Fn} - 0.000358 FV_{Fe} - 0.000936 FV_{Fs}

Partial Sky View Factor (SV_{Fx})

AVERAGE-Ta = 1.403 - 0.001847 avg solar + 1.0491 avg a.Ta - 17.51 SV_{Fn} + 4.09 SV_{Fe} - 3.78 SV_{Fs} + 16.41 SV_{Fw}

MAXIMUM-Ta = 2.663 - 0.001328 max solar + 0.9902 max a.Ta - 21.46 SV_{Fn} + 4.17 SV_{Fe} - 3.72 SV_{Fs} + 20.39 SV_{Fw}

MINIMUM-Ta = 0.773 - 0.002561 min solar + 1.0751 min a.Ta - 14.05 SV_{Fn} + 3.87 SV_{Fe} - 3.82 SV_{Fs} + 12.81 SV_{Fw}

Sky View Factor (SVF)

AVERAGE-Ta = 1.735 - 0.001847 avg solar + 1.0491 avg a.Ta - 1.971 SVF

MAXIMUM-Ta = 3.004 - 0.001328 max solar + 0.9902 max a.Ta - 2.225 SVF

MINIMUM-Ta = 1.091 - 0.002561 min solar + 1.0751 min a.Ta - 1.798 SVF

Total Façade View Factor (FVF)

AVERAGE-Ta = 1.409 - 0.001847 avg solar + 1.0491 avg a.Ta - 0.0421 FVF

MAXIMUM-Ta = 2.781 - 0.001328 max solar + 0.9902 max a.Ta - 0.0616 FVF

MINIMUM-Ta = 0.654 - 0.002561 min solar + 1.0751 min a.Ta - 0.0249 FVF

Site Coverage Ratio (SCR)

AVERAGE-Ta = 0.038 - 0.001847 avg solar + 1.0491 avg a.Ta + 4.20 SCR

MAXIMUM-Ta = 1.172 - 0.001328 max solar + 0.9902 max a.Ta + 4.37 SCR

MINIMUM-Ta = -0.506 - 0.002561 min solar + 1.0751 min a.Ta + 4.06 SCR

Floor Area Ratio (FAR)

AVERAGE-Ta = 1.536 - 0.001847 avg solar + 1.0491 avg a.Ta - 0.729 FAR

MAXIMUM-Ta = 2.946 - 0.001328 max solar + 0.9902 max a.Ta - 1.039 FAR

MINIMUM-Ta = 0.758 - 0.002561 min solar + 1.0751 min a.Ta - 0.468 FAR

Façade to Site Ratio (FSR)

AVERAGE-Ta = 0.973 - 0.001847 avg solar + 1.0491 avg a.Ta

MAXIMUM-Ta = 2.144 - 0.001328 max solar + 0.9902 max a.Ta

MINIMUM-Ta = 0.396 - 0.002561 min solar + 1.0751 min a.Ta

Compactness Index (CI)

AVERAGE-Ta = 2.575 - 0.001847 avg solar + 1.0491 avg a.Ta - 0.4621 CI

MAXIMUM-Ta = 4.219 - 0.001328 max solar + 0.9902 max a.Ta - 0.5985 CI

MINIMUM-Ta = 1.600 - 0.002561 min solar + 1.0751 min a.Ta - 0.3473 CI

Degree of Compactness (Dc)

AVERAGE-Ta = 1.684 - 0.001847 avg solar + 1.0491 avg a.Ta - 1.064 Dc

MAXIMUM-Ta = 3.101 - 0.001328 max solar + 0.9902 max a.Ta - 1.431 Dc

MINIMUM-Ta = 0.902 - 0.002561 min solar + 1.0751 min a.Ta - 0.757 Dc

Shape Factor (SF)

AVERAGE-Ta = -0.153 - 0.001847 avg solar + 1.0491 avg a.Ta + 0.2600 SF

MAXIMUM-Ta = 0.729 - 0.001328 max solar + 0.9902 max a.Ta + 0.3266 SF

MINIMUM-Ta = -0.478 - 0.002561 min solar + 1.0751 min a.Ta + 0.2018 SF

The Evening Period

Façade View Factor (FV_{Fx})

AVERAGE-Ta = -0.271 + 0.003839 avg solar + 1.0661 avg a.Ta + 0.000150 FV_{Fe} - 0.000187 FV_{Fs} - 0.000290 FV_{Fw}

MAXIMUM-Ta = -0.203 + 0.001961 max solar + 1.0722 max a.Ta - 0.000270 FV_{Fs} - 0.000574 FV_{Fw}

MINIMUM-Ta = -0.077 + 0.00703 min solar + 1.0496 min a.Ta + 0.000199 FV_{Fe} - 0.000174 FV_{Fs}

Partial Sky View Factor (SV_{Fx})

AVERAGE-Ta = -0.145 + 0.003839 avg solar + 1.0661 avg a.Ta - 5.842 SV_{Fn} + 0.933 SV_{Fe} - 3.737 SV_{Fs} + 7.220 SV_{Fw}

MAXIMUM-Ta = -0.210 + 0.001961 max solar + 1.0722 max a.Ta - 6.810 SV_{Fn} + 1.110 SV_{Fe} - 4.627 SV_{Fs} + 8.98 SV_{Fw}

MINIMUM-Ta = 0.211 + 0.00703 min solar + 1.0496 min a.Ta - 4.708 SV_{Fn} - 2.614 SV_{Fs} + 4.974 SV_{Fw}

Sky View Factor (SVF)

AVERAGE-Ta = 0.073 + 0.003839 avg solar + 1.0661 avg a.Ta - 1.083 SVF

MAXIMUM-Ta = 0.062 + 0.001961 max solar + 1.0722 max a.Ta - 1.213 SVF

MINIMUM-Ta = 0.307 + 0.00703 min solar + 1.0496 min a.Ta - 0.992 SVF

Total Façade View Factor (FVF)

AVERAGE-Ta = -0.186 + 0.003839 avg solar + 1.0661 avg a.Ta - 0.01541 FVF

MAXIMUM-Ta = -0.177 + 0.001961 max solar + 1.0722 max a.Ta - 0.02225 FVF

MINIMUM-Ta = 0.031 + 0.00703 min solar + 1.0496 min a.Ta - 0.01038 FVF

Site Coverage Ratio (SCR)

AVERAGE-Ta = -0.345 + 0.003839 avg solar + 1.0661 avg a.Ta

MAXIMUM-Ta = -0.407 + 0.001961 max solar + 1.0722 max a.Ta

MINIMUM-Ta = -0.076 + 0.00703 min solar + 1.0496 min a.Ta

Floor Area Ratio (FAR)

AVERAGE-Ta = 0.029 + 0.003839 avg solar + 1.0661 avg a.Ta - 0.4857 FAR

MAXIMUM-Ta = 0.067 + 0.001961 max solar + 1.0722 max a.Ta - 0.615 FAR

MINIMUM-Ta = 0.231 + 0.00703 min solar + 1.0496 min a.Ta - 0.3984 FAR

Façade to Site Ratio (FSR)

AVERAGE-Ta = -0.028 + 0.003839 avg solar + 1.0661 avg a.Ta - 0.466 FSR

MAXIMUM-Ta = 0.012 + 0.001961 max solar + 1.0722 max a.Ta - 0.614 FSR

MINIMUM-Ta = 0.172 + 0.00703 min solar + 1.0496 min a.Ta - 0.364 FSR

Compactness Index (CI)

AVERAGE-Ta = 0.349 + 0.003839 avg solar + 1.0661 avg a.Ta - 0.2003 CI

MAXIMUM-Ta = 0.472 + 0.001961 max solar + 1.0722 max a.Ta - 0.2536 CI

MINIMUM-Ta = 0.486 + 0.00703 min solar + 1.0496 min a.Ta - 0.1623 CI

Degree of Compactness (Dc)

AVERAGE-Ta = -0.022 + 0.003839 avg solar + 1.0661 avg a.Ta - 0.484 Dc

MAXIMUM-Ta = -0.003 + 0.001961 max solar + 1.0722 max a.Ta - 0.605 Dc

MINIMUM-Ta = 0.194 + 0.00703 min solar + 1.0496 min a.Ta - 0.405 Dc

Shape Factor (SF)

AVERAGE-Ta = -0.819 + 0.003839 avg solar + 1.0661 avg a.Ta + 0.10934 SF

MAXIMUM-Ta = -0.939 + 0.001961 max solar + 1.0722 max a.Ta + 0.1228 SF

MINIMUM-Ta = -0.509 + 0.00703 min solar + 1.0496 min a.Ta + 0.09998 SF

Appendix C: The modified models (M.M) of the cloudy days

The Night Period

Façade View Factor (FV_{Fx})

$$\text{AVERAGE-Ta} = -1.488 + 1.1100 \text{ avg a.Ta} + 0.000248 \text{ FVFe} - 0.000159 \text{ FVFs} + 0.000649 \text{ FVFw}$$

$$\text{MAXIMUM-Ta} = -1.698 + 1.1226 \text{ max a.Ta} + 0.000224 \text{ FVFe} - 0.000163 \text{ FVFs} + 0.000657 \text{ FVFw}$$

$$\text{MINIMUM-Ta} = -0.916 + 1.0725 \text{ min a.Ta} + 0.000265 \text{ FVFe} - 0.000156 \text{ FVFs} + 0.000664 \text{ FVFw}$$

Partial Sky View Factor (SV_{Fx})

$$\text{AVERAGE-Ta} = -0.999 + 1.1100 \text{ avg a.Ta} - 3.571 \text{ SVFn} + 0.921 \text{ SVFw}$$

$$\text{MAXIMUM-Ta} = -1.061 - 0.00416 \text{ max solar} + 1.1140 \text{ max a.Ta} - 3.649 \text{ SVFn} + 0.861 \text{ SVFw}$$

$$\text{MINIMUM-Ta} = -0.298 + 1.0725 \text{ min a.Ta} - 3.228 \text{ SVFn} - 0.745 \text{ SVFe}$$

Sky View Factor (SVF)

$$\text{AVERAGE-Ta} = -0.957 + 1.1100 \text{ avg a.Ta} - 0.998 \text{ SVF}$$

$$\text{MAXIMUM-Ta} = -1.169 + 1.1226 \text{ max a.Ta} - 1.012 \text{ SVF}$$

$$\text{MINIMUM-Ta} = -0.372 + 1.0725 \text{ min a.Ta} - 1.009 \text{ SVF}$$

Total Façade View Factor (FVF)

$$\text{AVERAGE-Ta} = -1.490 + 1.1100 \text{ avg a.Ta} + 0.01426 \text{ FVF}$$

$$\text{MAXIMUM-Ta} = -1.713 + 1.1226 \text{ max a.Ta} + 0.01474 \text{ FVF}$$

$$\text{MINIMUM-Ta} = -0.916 + 1.0725 \text{ min a.Ta} + 0.01490 \text{ FVF}$$

Site Coverage Ratio (SCR)

$$\text{AVERAGE-Ta} = -1.343 + 1.1100 \text{ avg a.Ta}$$

$$\text{MAXIMUM-Ta} = -1.754 + 1.1226 \text{ max a.Ta} + 0.871 \text{ SCR}$$

$$\text{MINIMUM-Ta} = -0.762 + 1.0725 \text{ min a.Ta}$$

Floor Area Ratio (FAR)

$$\text{AVERAGE-Ta} = -1.343 + 1.1100 \text{ avg a.Ta}$$

$$\text{MAXIMUM-Ta} = -1.560 + 1.1226 \text{ max a.Ta}$$

$$\text{MINIMUM-Ta} = -0.762 + 1.0725 \text{ min a.Ta}$$

Façade to Site Ratio (FSR)

$$\text{AVERAGE-Ta} = -1.465 + 1.1100 \text{ avg a.Ta} + 0.180 \text{ FSR}$$

$$\text{MAXIMUM-Ta} = -1.698 + 1.1226 \text{ max a.Ta} + 0.202 \text{ FSR}$$

$$\text{MINIMUM-Ta} = -0.882 + 1.0725 \text{ min a.Ta} + 0.176 \text{ FSR}$$

Compactness Index (CI)

$$\text{AVERAGE-Ta} = -1.343 + 1.1100 \text{ avg a.Ta}$$

$$\text{MAXIMUM-Ta} = -1.560 + 1.1226 \text{ max a.Ta}$$

$$\text{MINIMUM-Ta} = -0.762 + 1.0725 \text{ min a.Ta}$$

Degree of Compactness (Dc)

$$\text{AVERAGE-Ta} = -1.343 + 1.1100 \text{ avg a.Ta}$$

$$\text{MAXIMUM-Ta} = -1.560 + 1.1226 \text{ max a.Ta}$$

$$\text{MINIMUM-Ta} = -0.762 + 1.0725 \text{ min a.Ta}$$

Shape Factor (SF)

$$\text{AVERAGE-Ta} = -1.672 + 1.1100 \text{ avg a.Ta} + 0.07595 \text{ SF}$$

$$\text{MAXIMUM-Ta} = -1.756 - 0.00416 \text{ max solar} + 1.1140 \text{ max a.Ta} + 0.07754 \text{ SF}$$

$$\text{MINIMUM-Ta} = -1.085 + 1.0725 \text{ min a.Ta} + 0.07466 \text{ SF}$$

The Morning Period

Façade View Factor (FV_{Fx})

AVERAGE-Ta = -0.282 - 0.001096 avg solar + 1.0458 avg a.Ta - 0.000211 FV_{Fe} + 0.000164 FV_{Fs}

MAXIMUM-Ta = 0.590 - 0.000942 max solar + 0.9944 max a.Ta - 0.000276 FV_{Fe} + 0.000387 FV_{Fw}

MINIMUM-Ta = 0.417 - 0.001372 min solar + 0.9916 min a.Ta + 0.000207 FV_{Fs}

Partial Sky View Factor (SV_{Fx})

AVERAGE-Ta = -0.189 - 0.001096 avg solar + 1.0458 avg a.Ta - 3.053 SV_{Fn} + 2.145 SV_{Fe} - 2.378 SV_{Fs} + 2.38 SV_{Fw}

MAXIMUM-Ta = 0.677 - 0.000942 max solar + 0.9944 max a.Ta - 2.173 SV_{Fn} + 1.621 SV_{Fe}

MINIMUM-Ta = 0.786 - 0.001372 min solar + 0.9916 min a.Ta - 1.695 SV_{Fn} - 1.260 SV_{Fs}

Sky View Factor (SVF)

AVERAGE-Ta = -0.011 - 0.001096 avg solar + 1.0458 avg a.Ta - 0.723 SVF

MAXIMUM-Ta = 0.852 - 0.000942 max solar + 0.9944 max a.Ta - 0.714 SVF

MINIMUM-Ta = 0.766 - 0.001372 min solar + 0.9916 min a.Ta - 0.714 SVF

Total Façade View Factor (FVF)

AVERAGE-Ta = -0.403 - 0.001096 avg solar + 1.0458 avg a.Ta + 0.01087 FVF

MAXIMUM-Ta = 0.409 - 0.000942 max solar + 0.9944 max a.Ta + 0.0162 FVF

MINIMUM-Ta = 0.491 - 0.001372 min solar + 0.9916 min a.Ta

Site Coverage Ratio (SCR)

AVERAGE-Ta = -0.793 - 0.001096 avg solar + 1.0458 avg a.Ta + 2.257 SCR

MAXIMUM-Ta = -0.056 - 0.000942 max solar + 0.9944 max a.Ta + 2.84 SCR

MINIMUM-Ta = 0.088 - 0.001372 min solar + 0.9916 min a.Ta + 1.812 SCR

Floor Area Ratio (FAR)

AVERAGE-Ta = -0.414 + 1.0458 avg a.Ta - 0.001096 avg solar + 0.159 FAR

MAXIMUM-Ta = 0.345 - 0.000942 max solar + 0.9944 max a.Ta + 0.300 FAR

MINIMUM-Ta = 0.491 - 0.001372 min solar + 0.9916 min a.Ta

Façade to Site Ratio (FSR)

AVERAGE-Ta = -0.459 - 0.001096 avg solar + 1.0458 avg a.Ta + 0.247 FSR

MAXIMUM-Ta = 0.271 - 0.000942 max solar + 0.9944 max a.Ta + 0.448 FSR

MINIMUM-Ta = 0.491 - 0.001372 min solar + 0.9916 min a.Ta

Compactness Index (CI)

AVERAGE-Ta = -0.291 - 0.001096 avg solar + 1.0458 avg a.Ta

MAXIMUM-Ta = 0.576 - 0.000942 max solar + 0.9944 max a.Ta

MINIMUM-Ta = 0.491 - 0.001372 min solar + 0.9916 min a.Ta

Degree of Compactness (Dc)

AVERAGE-Ta = -0.291 - 0.001096 avg solar + 1.0458 avg a.Ta

MAXIMUM-Ta = 0.576 - 0.000942 max solar + 0.9944 max a.Ta

MINIMUM-Ta = 0.491 - 0.001372 min solar + 0.9916 min a.Ta

Shape Factor (SF)

AVERAGE-Ta = -0.421 - 0.001096 avg solar + 1.0458 avg a.Ta + 0.0300 SF

MAXIMUM-Ta = 0.576 - 0.000942 max solar + 0.9944 max a.Ta

MINIMUM-Ta = 0.341 - 0.001372 min solar + 0.9916 min a.Ta + 0.0345 SF

The Afternoon Period

Façade View Factor (FV_{Fx})

AVERAGE-Ta = 4.879 - 0.001298 avg solar + 0.8558 avg a.Ta - 0.000507 FV_{Fe} - 0.000968 FV_{Fs}

MAXIMUM-Ta = 6.544 - 0.000766 max solar + 0.7831 max a.Ta - 0.000571 FV_{Fe} - 0.001393 FV_{Fs}

MINIMUM-Ta = 5.008 - 0.001808 min solar + 0.8026 min a.Ta + 0.000604 FV_{Fn}

Partial Sky View Factor (SV_{Fx})

AVERAGE-Ta = 4.917 - 0.001298 avg solar + 0.8558 avg a.Ta - 9.14 SV_{Fn} + 5.97 SV_{Fw}

MAXIMUM-Ta = 6.438 - 0.000766 max solar + 0.7831 max a.Ta - 11.38 SV_{Fn} + 8.56 SV_{Fw}

MINIMUM-Ta = 5.347 - 0.001808 min solar + 0.8026 min a.Ta - 10.16 SV_{Fn} + 4.15 SV_{Fe} - 4.89 SV_{Fs} + 9.88 SV_{Fw}

Sky View Factor (SVF)

AVERAGE-Ta = 4.989 - 0.001298 avg solar + 0.8558 avg a.Ta - 1.583 SVF

MAXIMUM-Ta = 6.47 - 0.000766 max solar + 0.7831 max a.Ta - 1.550 SVF

MINIMUM-Ta = 5.720 - 0.001808 min solar + 0.8026 min a.Ta - 1.568 SVF

Total Façade View Factor (FVF)

AVERAGE-Ta = 4.378 - 0.001298 avg solar + 0.8558 avg a.Ta

MAXIMUM-Ta = 6.287 - 0.000766 max solar + 0.7831 max a.Ta - 0.0401 FVF

MINIMUM-Ta = 5.114 - 0.001808 min solar + 0.8026 min a.Ta

Site Coverage Ratio (SCR)

AVERAGE-Ta = 3.439 - 0.001298 avg solar + 0.8558 avg a.Ta + 4.22 SCR

MAXIMUM-Ta = 4.91 - 0.000766 max solar + 0.7831 max a.Ta + 4.31 SCR

MINIMUM-Ta = 4.157 - 0.001808 min solar + 0.8026 min a.Ta + 4.30 SCR

Floor Area Ratio (FAR)

AVERAGE-Ta = 4.378 - 0.001298 avg solar + 0.8558 avg a.Ta

MAXIMUM-Ta = 6.33 - 0.000766 max solar + 0.7831 max a.Ta - 0.594 FAR

MINIMUM-Ta = 5.114 - 0.001808 min solar + 0.8026 min a.Ta

Façade to Site Ratio (FSR)

AVERAGE-Ta = 4.378 - 0.001298 avg solar + 0.8558 avg a.Ta

MAXIMUM-Ta = 5.873 - 0.000766 max solar + 0.7831 max a.Ta

MINIMUM-Ta = 5.114 - 0.001808 min solar + 0.8026 min a.Ta

Compactness Index (CI)

AVERAGE-Ta = 5.534 - 0.001298 avg solar + 0.8558 avg a.Ta - 0.3337 CI

MAXIMUM-Ta = 7.30 - 0.000766 max solar + 0.7831 max a.Ta - 0.412 CI

MINIMUM-Ta = 5.920 - 0.001808 min solar + 0.8026 min a.Ta - 0.2325 CI

Degree of Compactness (Dc)

AVERAGE-Ta = 4.804 - 0.001298 avg solar + 0.8558 avg a.Ta - 0.639 Dc

MAXIMUM-Ta = 6.42 - 0.000766 max solar + 0.7831 max a.Ta - 0.823 Dc

MINIMUM-Ta = 5.114 - 0.001808 min solar + 0.8026 min a.Ta

Shape Factor (SF)

AVERAGE-Ta = 3.628 - 0.001298 avg solar + 0.8558 avg a.Ta + 0.1730 SF

MAXIMUM-Ta = 4.962 - 0.000766 max solar + 0.7831 max a.Ta + 0.2101 SF

MINIMUM-Ta = 4.553 - 0.001808 min solar + 0.8026 min a.Ta + 0.1296 SF

The Evening Period

Façade View Factor (FV_{Fx})

AVERAGE-Ta = -4.237 - 0.00909 avg solar + 1.3098 avg a.Ta

MAXIMUM-Ta = -4.458 - 0.00890 max solar + 1.3258 max a.Ta

MINIMUM-Ta = -3.149 + 1.2403 min a.Ta

Partial Sky View Factor (SV_{Fx})

AVERAGE-Ta = -4.084 - 0.00909 avg solar + 1.3098 avg a.Ta - 5.81 SV_{Fn} + 2.50 SV_{Fe} - 3.77 SV_{Fs} + 6.05 SV_{Fw}

MAXIMUM-Ta = -4.088 - 0.00890 max solar + 1.3258 max a.Ta - 3.070 SV_{Fn}

MINIMUM-Ta = -2.996 + 1.2403 min a.Ta - 5.54 SV_{Fn} + 2.30 SV_{Fe} - 3.38 SV_{Fs} + 5.62 SV_{Fw}

Sky View Factor (SVF)

AVERAGE-Ta = -3.822 - 0.00909 avg solar + 1.3098 avg a.Ta - 1.075 SVF

MAXIMUM-Ta = -4.011 - 0.00890 max solar + 1.3258 max a.Ta - 1.157 SVF

MINIMUM-Ta = -2.759 + 1.2403 min a.Ta - 1.009 SVF

Total Façade View Factor (FVF)

AVERAGE-Ta = -4.237 - 0.00909 avg solar + 1.3098 avg a.Ta

MAXIMUM-Ta = -4.458 - 0.00890 max solar + 1.3258 max a.Ta

MINIMUM-Ta = 3.149 + 1.2403 min a.Ta

Site Coverage Ratio (SCR)

AVERAGE-Ta = -4.681 - 0.00909 avg solar + 1.3098 avg a.Ta + 2.00 SCR

MAXIMUM-Ta = -4.985 - 0.00890 max solar + 1.3258 max a.Ta + 2.37 SCR

MINIMUM-Ta = -3.519 + 1.2403 min a.Ta + 1.663 SCR

Floor Area Ratio (FAR)

$$\text{AVERAGE-Ta} = -4.237 - 0.00909 \text{ avg solar} + 1.3098 \text{ avg a.Ta}$$

$$\text{MAXIMUM-Ta} = -4.458 - 0.00890 \text{ max solar} + 1.3258 \text{ max a.Ta}$$

$$\text{MINIMUM-Ta} = -3.149 + 1.2403 \text{ min a.Ta}$$

Façade to Site Ratio (FSR)

$$\text{AVERAGE-Ta} = -4.237 - 0.00909 \text{ avg solar} + 1.3098 \text{ avg a.Ta}$$

$$\text{MAXIMUM-Ta} = -4.458 - 0.00890 \text{ max solar} + 1.3258 \text{ max a.Ta}$$

$$\text{MINIMUM-Ta} = -3.149 + 1.2403 \text{ min a.Ta}$$

Compactness Index (CI)

$$\text{AVERAGE-Ta} = -3.741 - 0.00909 \text{ avg solar} + 1.3098 \text{ avg a.Ta} - 0.1432 \text{ CI}$$

$$\text{MAXIMUM-Ta} = -3.914 - 0.00890 \text{ max solar} + 1.3258 \text{ max a.Ta} - 0.1571 \text{ CI}$$

$$\text{MINIMUM-Ta} = -2.708 + 1.2403 \text{ min a.Ta} - 0.1271 \text{ CI}$$

Degree of Compactness (Dc)

$$\text{AVERAGE-Ta} = -4.237 - 0.00909 \text{ avg solar} + 1.3098 \text{ avg a.Ta}$$

$$\text{MAXIMUM-Ta} = -4.458 - 0.00890 \text{ max solar} + 1.3258 \text{ max a.Ta}$$

$$\text{MINIMUM-Ta} = -3.149 + 1.2403 \text{ min a.Ta}$$

Shape Factor (SF)

$$\text{AVERAGE-Ta} = -4.622 - 0.00909 \text{ avg solar} + 1.3098 \text{ avg a.Ta} + 0.0889 \text{ SF}$$

$$\text{MAXIMUM-Ta} = -4.860 - 0.00890 \text{ max solar} + 1.3258 \text{ max a.Ta} + 0.0927 \text{ SF}$$

$$\text{MINIMUM-Ta} = -3.518 + 1.2403 \text{ min a.Ta} + 0.0853 \text{ SF}$$

References

- Agathokleous, R.A. & Kalogirou, S.A., 2016. Double skin facades (DSF) and building integrated photovoltaics (BIPV): A review of configurations and heat transfer characteristics. *Renewable Energy*, 89, pp.743–756. Available at: <http://dx.doi.org/10.1016/j.renene.2015.12.043>.
- Al_Sayed, K., 2018. *SPACE SYNTAX METHODOLOGY*, London: Bartlett School of Architecture, UCL.
- Al-Sudani, A., Hussein, H. & Sharples, S., 2017. Sky View Factor Calculation A computational-geometrical approach. In *Space Syntax and Ontologies-Volume 2-eCAADe 35*. Rome, Italy: Sapienza University of Rome, pp. 673–682.
- Al-sudani, A. & Sharples, S., 2016. Analyzing urban microclimate air temperature measurements using a novel parameter - the partial sky view factor. In *PLEA 2016 - Proceedings of the 32nd International Conference on Passive and Low Energy Architecture*; Los Angeles, pp. 1239–1245.
- Alberto J. Fernández de Trocóniz y Revuelta, Miguel Ángel Gálvez Huerta, T.G.L., 2012. A Simple Way to Assess and Compare the Thermal Efficacy in Elongated Building Designs Alberto. In L. C. (Eds. . M'Sirdi, N., Namaane, A., Howlett, R.J., Jain, ed. *Sustainability in Energy and Buildings Proceedings of the 3rd International Conference on Sustainability in Energy and Buildings (SEB'11)*. Springer, pp. 285–294.
- Ali-Toudert, F. & Mayer, H., 2006. Numerical study on the effects of aspect ratio and orientation of an urban street canyon on outdoor thermal comfort in hot and dry climate. *Building and Environment*, 41(2), pp.94–108. Available at: <http://linkinghub.elsevier.com/retrieve/pii/S0360132305000120>.
- Ali-Toudert, F. & Mayer, H., 2007. Thermal comfort in an east-west oriented street canyon in Freiburg (Germany) under hot summer conditions. *Theoretical and Applied Climatology*, 87(1–4), pp.223–237.
- Alsabry, A. et al., 2017. THERMAL-MODERNIZATION IN RESIDENTIAL BUILDINGS IN

- POLAND CASE STUDY : THE TOWN OF ZIELONA GÓRA. *Int. J. of Applied Mechanics and Engineering*, 22(4), pp.1083–1095.
- Andreou, E., 2014. The effect of urban layout, street geometry and orientation on shading conditions in urban canyons in the Mediterranean. *Renewable Energy*, 63.
- Arnfield, A.J., 2003. Two decades of urban climate research: A review of turbulence, exchanges of energy and water, and the urban heat island. *International Journal of Climatology*, 23(1), pp.1–26.
- Berghauser Pont, M. et al., 2015. Connectivity, density and built form: integrating 'Spacemate' with space syntax. *22nd ISUF Conference: City as organism. New visions for urban life*, (April).
- Berghauser Pont, M.Y. & Haupt, P.A., 2007. The relation between urban form and density. *Urban Morphology*, 11(1), pp.62–65.
- Bottyan, Z. & Unger, J., 2003. A multiple linear statistical model for estimating the mean maximum urban heat island. *Theoretical and Applied Climatology*, 75(3–4), pp.233–243.
- Bueno, B. et al., 2013. The urban weather generator. *Journal of Building Performance Simulation*, 6(4), pp.269–281.
- Bueno, B. et al., 2014. *Urban Climate Computationally efficient prediction of canopy level urban air temperature at the neighbourhood scale*. Elsevier Ltd. Available at: <http://dx.doi.org/10.1016/j.uclim.2014.05.005>.
- CAG Consultants, 2009. *Climate Impacts and Vulnerabilities Framework for Liverpool City*, London.
- Cao, A., Li, Q. & Meng, Q., 2015. Effects of Orientation of Urban Roads on the Local Thermal Environment in Guangzhou City. *Procedia Engineering*, 121, pp.2075–2082. Available at: <http://dx.doi.org/10.1016/j.proeng.2015.09.209>.
- Carmona, M. et al., 2010. *Public Places, Urban Spaces: The Dimensions of Urban Design* 2nd ed.,

- Carneiro, C. et al., 2010. Urban environment quality indicators: Application to solar radiation and morphological analysis on built area. In *Proceedings of the 3rd WSEAS international conference on Visualization, imaging and simulation*. Faro, Portugal, pp. 141–148. Available at: <https://www.scopus.com/inward/record.uri?eid=2-s2.0-79959868371&partnerID=40&md5=a3582f73bd01dde6cc26766c94673352>.
- Chatzidimitriou, A. & Yannas, S., 2017. Street canyon design and improvement potential for urban open spaces; the influence of canyon aspect ratio and orientation on microclimate and outdoor comfort. *Sustainable Cities and Society*, 33(May), pp.85–101. Available at: <http://dx.doi.org/10.1016/j.scs.2017.05.019>.
- Chatzipoulka, C., Compagnon, R. & Nikolopoulou, M., 2016. Urban geometry and solar availability on façades and ground of real urban forms: using London as a case study. *Solar Energy*, 138, pp.53–66. Available at: <http://linkinghub.elsevier.com/retrieve/pii/S0038092X16304005>.
- Chen, L. et al., 2012. Sky view factor analysis of street canyons and its implications for daytime intra-urban air temperature differentials in high-rise, high-density urban areas of Hong Kong: A GIS-based simulation approach. *International Journal of Climatology*, 32(1), pp.121–136.
- Chen, L. & Ng, E., 2011. Quantitative urban climate mapping based on a geographical database: A simulation approach using Hong Kong as a case study. *International Journal of Applied Earth Observation and Geoinformation*, 13(4), pp.586–594. Available at: <http://dx.doi.org/10.1016/j.jag.2011.03.003>.
- Cheng, V. et al., 2006. Compact cities in a sustainable manner. *2nd International Solar Cities Congress*, 44(April), pp.1–11.
- Cheung, H.K.W., Coles, D. & Levermore, G.J., 2016. Urban heat island analysis of Greater Manchester, UK using sky view factor analysis. *Building Services Engineering Research and Technology*, 37(1), pp.5–17.
- Clifton, K. et al., 2008. Quantitative analysis of urban form: a multidisciplinary review.

Journal of Urbanism: International Research on Placemaking and Urban Sustainability, 1(1), pp.17–45.

Collier, C.G., 2006. The impact of urban areas on weather. *Quarterly Journal of the Royal Meteorological Society*, 132(614), pp.1–25. Available at: <http://doi.wiley.com/10.1256/qj.05.199>.

Compagnon, R., 2004. Solar and daylight availability in the urban fabric. *Energy and Buildings*, 36(4), pp.321–328. Available at: <http://linkinghub.elsevier.com/retrieve/pii/S0378778804000398>.

Cortese, J.G. et al., 2009. The climatic skin of urban spaces. *International Journal for Housing Science and Its Applications*, 33(2), pp.105–115.

Dahab, G.M. et al., 2004. Digital quantification of fibrosis in liver biopsy sections: Description of a new method by Photoshop software. *Journal of Gastroenterology and Hepatology (Australia)*, 19(1), pp.78–85.

Danielski, I., Fröling, M. & Joelsson, A., 2012. The Impact of the Shape Factor on Final Energy Demand in. In *World Renewable Energy Forum*. Denver, USA, pp. 4260–4264. Available at: <http://www.wref2012.ases.org/>.

DAS, 2010. Effects of Cloud Cover on forecasted temperatures. *WW2010. Department of Atmospheric Sciences (DAS) at the University of Illinois at Urbana-Champaign*. Available at: [http://ww2010.atmos.uiuc.edu/\(Gh\)/guides/mtr/fcst/tmps/cld.rxml](http://ww2010.atmos.uiuc.edu/(Gh)/guides/mtr/fcst/tmps/cld.rxml) [Accessed May 26, 2018].

De, B. & Mukherjee, M., 2017. “Optimisation of canyon orientation and aspect ratio in warm-humid climate: Case of Rajarhat Newtown, India.” *Urban Climate*, 24(November 2017), pp.887–920. Available at: <https://doi.org/10.1016/j.uclim.2017.11.003>.

Drach, P., Krüger, E.L. & Emmanuel, R., 2018. Effects of atmospheric stability and urban morphology on daytime intra-urban temperature variability for Glasgow, UK. *Science of the Total Environment*, 627, pp.782–791.

- Ealing Council, 2004. *Plot ratios*,
- Edwards, R.F., 2016. Myrtle Gardens. Available at: www.liverpoolpicturebook.com/2015/05/myrtle-gardens.html [Accessed June 23, 2018].
- Eliasson, I. & Svensson, M.K., 2003. Spatial air temperature variations and urban land use — a statistical approach. *Meteorological Applications*, 10(2), pp.135–149. Available at: <http://doi.wiley.com/10.1017/S1350482703002056>.
- Erell, E., Pearlmutter, D. & Williamson, T., 2011. *Urban Microclimate – Designing the Spaces between Buildings*, London: Earthscan.
- Fahmy, Mohamad; Sharples, S., 2008. Passive design for urban thermal comfort: a comparison between different urban forms in Cairo, Egypt. *25th Conference on Passive and Low Energy Architecture*, (October), pp.1–6.
- Fahmy, M., 2012. Climate change adaptation for mid-latitude urban developments. *Proceedings - 28th International PLEA Conference on Sustainable Architecture + Urban Design: Opportunities, Limits and Needs - Towards an Environmentally Responsible Architecture, PLEA 2012*, 2012–January(November 2012).
- Fahmy, M. & Sharples, S., 2009a. On the development of an urban passive thermal comfort system in Cairo, Egypt. *Building and Environment*, 44(9), pp.1907–1916. Available at: <http://dx.doi.org/10.1016/j.buildenv.2009.01.010>.
- Fahmy, M. & Sharples, S., 2009b. Once upon a climate: arid urban utopia of passive cooling and the diversity of sustainable forms. In *2nd International Conference on Whole Life Urban Sustainability and its Assessment*. Loughborough, UK, pp. 134–138. Available at: www.sue-mot.org/conference/.
- Fahmy, M. & Sharples, S., 2011. Urban form, thermal comfort and building CO₂ emissions - a numerical analysis in Cairo. *Building Services Engineering Research and Technology*, 32(1), pp.73–84. Available at: <http://journals.sagepub.com/doi/10.1177/0143624410394536>.
- FAREHAM Council, 2009. Protocol for dealing with variations to planning permissions.

Available at:
www.fareham.gov.uk/planning/applications_and_advice/protocol.aspx
[Accessed June 19, 2018].

Ferrante, A., 2016. *Towards nearly zero energy : urban settings in the Mediterranean climate*, Elsevier Ltd.

Flores, S., Rengifo, L. & Filippín, C., 2015. Double skin glazed facades in sunny Mediterranean climates. *Energy & Buildings*, 102, pp.18–31. Available at:
<http://dx.doi.org/10.1016/j.enbuild.2015.05.019>.

Franck, U. et al., 2013. Heat stress in urban areas : Indoor and outdoor temperatures in different urban structure types and subjectively reported well-being during a heat wave in the city of Leipzig. *Meteorologische Zeitschrift*, 22(2), pp.167–177.

Frost, J., 2017. Regression coefficients. *Statistics By Jim: Making statistics intuitive*. Available at: <http://statisticsbyjim.com/glossary/regression-coefficient/>
[Accessed June 5, 2018].

Galloway, R. & Kang, B., 2009. *Space Node Place*, USA - Texas. Available at:
https://repositories.lib.utexas.edu/bitstream/handle/2152/13088/3-Galloway_Kang-Space_Node_Place.pdf?sequence=2.

Geletka, V. & Sedláková, A., 2012. Shape of buildings and energy consumption. *Czasopismo Techniczne*, 109(3), pp.124–128. Available at:
<http://suw.biblos.pk.edu.pl/resourceDetails&rId=4745%7D%7D%3C/opinion&rId=14488>.

Giovannini, L., Zardi, D. & Franceschi, M. de, 2013. Characterization of the thermal structure inside an urban canyon: Field measurements and validation of a simple model. *Journal of Applied Meteorology and Climatology*, 52(1), pp.64–81.

Giridharan, R. et al., 2007. Urban design factors influencing heat island intensity in high-rise high-density environments of Hong Kong. *Building and Environment*, 42(10), pp.3669–3684.

Givoni, B., 1998. *Climate considerations in building and urban design*, New York: John

Wiley & Sons. Available at:
http://books.google.com/books?id=MGkArZ_berAC&pgis=1.

Glasgow city council, 2014. *PROPOSED CITY DEVELOPMENT PLAN 2014: Office Business and Industrial Development*,

GOV.UK, 2014. Climate change explained. *Department for Business, Energy & Industrial Strategy*.

Grimmond, C.S.B. et al., 2010. Climate and More Sustainable Cities : Climate Information for Improved Planning and Management of Cities (Producers / Capabilities Perspective). *Procedia Environmental Sciences*, 1, pp.247–274.

Hammersmith & Fulham Council, 2013. *London Borough of Hammersmith & Fulham*,

Hien, W.N. et al., 2012. Comparison of STEVE and ENVI-met as temperature prediction models for Singapore context. *International Journal of Sustainable Building Technology and Urban Development*, 3(3), pp.197–209. Available at:
<http://www.tandfonline.com/doi/abs/10.1080/2093761X.2012.720224>.

Hien, W.N. & Jusuf, S.K., 2010. Air Temperature Distribution and the Influence of Sky View Factor in a Green Singapore Estate. *Journal of Urban Planning and Development*, 136(3), pp.261–272.

Hillier, B., 2007. *Space is the machine: A configurational theory of architecture*, London: University College London (UCL).

Hughes, K., 2006. The impact of urban areas on climate in the UK: a spatial and temporal analysis, with an emphasis on temperature and precipitation effects. *Earth & Environment*, (2), pp.54–83.

Hwang, R. & Shu, S., 2011. Building envelope regulations on thermal comfort in glass facade buildings and energy-saving potential for PMV-based comfort control. *Building and Environment*, 46(4), pp.824–834. Available at:
<http://dx.doi.org/10.1016/j.buildenv.2010.10.009>.

Ignatius, M., Wong, N.H. & Jusuf, S.K., 2015. Urban microclimate analysis with consideration of local ambient temperature, external heat gain, urban

ventilation, and outdoor thermal comfort in the tropics. *Sustainable Cities and Society*, 19, pp.121–135. Available at: <http://dx.doi.org/10.1016/j.scs.2015.07.016>.

Irger, M., 2014. *THE EFFECT OF URBAN FORM ON URBAN MICROCLIMATE*. The University of New South Wales.

Jänicke, B. et al., 2015. Evaluating the Effects of Façade Greening on Human Bioclimate in a Complex Urban Environment. *Advances in Meteorology*, 2015, pp.1–15.

Jiang, B., Claramunt, C. & Klarqvist, B., 2000. An Integration of Space Syntax into GIS for Urban Planning and Design. *International Journal of Applied Earth Observation and Geoinformation*, 2, pp.1–18.

Jim Frost, 2015. How to Choose the Best Regression Model. *The Minitab Blog*. Available at: <http://blog.minitab.com/blog/adventures-in-statistics-2/how-to-choose-the-best-regression-model> [Accessed July 15, 2017].

Jim Frost, 2014. Regression Analysis: How to Interpret S, the Standard Error of the Regression. *The Minitab Blog*. Available at: <http://blog.minitab.com/blog/adventures-in-statistics-2/regression-analysis-how-to-interpret-s-the-standard-error-of-the-regression> [Accessed July 15, 2017].

Jin, H. et al., 2018. Assessing the Effects of Urban Morphology Parameters on Microclimate in Singapore to Control the Urban Heat Island Effect. *Sustainability*, 10(1), p.206. Available at: <http://www.mdpi.com/2071-1050/10/1/206>.

Johnson, G.T. & Watson, I.D., 1984. The determination of View-Factors in Urban Canyons. *Journal of Applied Meteorology and Climatology*, 23(2), pp.329–335.

Jusuf, S.K. & Hien, W.N., 2009. Development of empirical models for an estate level air temperature prediction in Singapore. In T. S. I. C. on C. to U. H. I. (SICCUHI), ed. *The Second International Conference on Countermeasures to Urban Heat Islands (SICCUHI)*. California: The Second International Conference on

Countermeasures to Urban Heat Islands (SICCUHI). Available at: <http://heatisland2009.lbl.gov/papers.html>.

JUSUF, S.K., IGNATIUS, M. & Hien, W.N., 2016. Urban climatic mapping using prediction models for ambient temperature and outdoor thermal comfort : a Singapore case study. In *4th International Conference on Countermeasures to Urban Heat Island*. pp. 1–14.

Kickert, C.C., Pont, M.B. & Nefs, M., 2014. Surveying density, urban characteristics, and development capacity of station areas in the delta metropolis. *Environment and Planning B: Planning and Design*, 41(1), pp.69–92.

Kleerekoper, L. et al., 2015. Urban Climate Creating drafts in urban settings through coloured façades : Exploring a new climate adaptation measure based on thermal stratification. *Urban Climate*, 14, pp.290–300. Available at: <http://dx.doi.org/10.1016/j.uclim.2015.09.002>.

Kotharkar, R., Bahadure, P. & Sarda, N., 2014. Measuring compact urban form: A case of Nagpur city, India. *Sustainability (Switzerland)*, 6(7), pp.4246–4272.

Krier, R., 1979. *Urban Space*, New York: Rizzoli.

Kropf, K., 2014. Ambiguity in the definition of built form. *Urban Morphology*, 18(1), pp.41–57.

Kropf, K., 2009. Aspects of urban form. *Urban Morphology*, 13(2), pp.105–20.

Krüger, E. & Emmanuel, R., 2013. Landscape and Urban Planning Accounting for atmospheric stability conditions in urban heat island studies : The case of Glasgow , UK. *Landscape and Urban Planning*, 117, pp.112–121.

Krüger, E. & Givoni, B., 2007. Outdoor measurements and temperature comparisons of seven monitoring stations: Preliminary studies in Curitiba, Brazil. *Building and Environment*, 42(4), pp.1685–1698.

Krüger, E., Pearlmutter, D. & Rasia, F., 2010. Evaluating the impact of canyon geometry and orientation on cooling loads in a high-mass building in a hot dry environment. *Applied Energy*, 87(6), pp.2068–2078. Available at:

<http://dx.doi.org/10.1016/j.apenergy.2009.11.034>.

Krüger, E.L., Minella, F.O. & Rasia, F., 2011. Impact of urban geometry on outdoor thermal comfort and air quality from field measurements in Curitiba, Brazil. *Building and Environment*, 46(3), pp.621–634. Available at: <http://dx.doi.org/10.1016/j.buildenv.2010.09.006>.

Lau, K.K. et al., 2014. Street Geometry Design and its Effect on Mean Radiant Temperature : A Parametric Study based on Numerical Modelling. , pp.0–5.

Liu, C. et al., 2013. Canopy leaf area index for apple tree using hemispherical photography in arid region. *Scientia Horticulturae*, 164, pp.610–615.

Liu, Z. et al., 2014. How much of the world’s land has been urbanized, really? A hierarchical framework for avoiding confusion. *Landscape Ecology*, 29(5), pp.763–771.

Liverpool City Council, 2009. *City of Liverpool Climate Change Strategic Framework : A Prospectus for Action*, Liverpool.

Liverpool City Council, 2018. Population statistics. Available at: liverpool.gov.uk/council/key-statistics-and-data/data/population/ [Accessed May 31, 2018].

Lylykangas, K., 2009. Shape Factor as an Indicator of Heating Energy Demand. In *Internationales Holzbau-Forum 09*. pp. 1–8. Available at: http://www.forum-holzbau.com/pdf/ihf09_Lylykangas.pdf.

Macfarlane, C., Grigg, A. & Evangelista, C., 2007. Estimating forest leaf area using cover and fullframe fisheye photography: Thinking inside the circle. *Agricultural and Forest Meteorology*, 146(1–2), pp.1–12.

Maciel, C.D.R. et al., 2013. The impact of surface characteristics on ambient temperature at urban micro scale: comparative field study in two climates. *International Journal of Low-Carbon Technologies*, 10(3), pp.165–175.

Mao, J. et al., 2017. Global sensitivity analysis of an urban microclimate system under uncertainty: Design and case study. *Building and Environment*, 124, pp.153–170.

Available at: <http://dx.doi.org/10.1016/j.buildenv.2017.08.011>.

Maoh, H. & Kanaroglou, P., 2009. A tool for evaluating urban sustainability via integrated transportation and land use simulation models. *Environnement Urbain / Urban Environment*, 3. Available at: eue.revues.org/957.

Margaritis, E. & Kang, J., 2016. Relationship between urban green spaces and other features of urban morphology with traffic noise distribution. *Urban Forestry and Urban Greening*, 15, pp.174–185. Available at: <http://dx.doi.org/10.1016/j.ufug.2015.12.009>.

Martins, T., Adolphe, L. & Bastos, L., 2014. DOE sensitivity analysis of urban morphology factors regarding solar irradiation on buildings envelope in the Brazilian tropical context. In *30th International PLEA Conference SUSTAINABLE HABITAT FOR DEVELOPING SOCIETIES Choosing the way forward*. Ahmedabad, pp. 1–8.

Matzarakis, A., 2015. Developments and applications of thermal indices in urban structures by RayMan and SkyHelios model. *9th International Conference on Urban Climate*.

Mavrogianni, A. et al., 2009. Space heating demand and heatwave vulnerability: London domestic stock. *Building Research and Information*, 37(5–6), pp.583–597.

Mcmullan, R., 2007. *Environmental Science in Building* sixth edit., New York: PALGRAVE MACMILLAN.

Md Din, M.F. et al., 2012. Investigation of thermal effect on exterior wall surface of building material at urban city area. *International Journal of Energy and Environment*, 3(4), pp.531–540. Available at: <http://www.omicsgroup.org/journals/2165-784X/2165-784X-2-110.pdf>.

Met Office, 2016a. Beaufort wind force scale. Available at: <https://www.metoffice.gov.uk/guide/weather/marine/beaufort-scale> [Accessed May 17, 2018].

Met Office, 2018. Liverpool climate. Available at: <https://www.metoffice.gov.uk/public/weather/climate/gcmzggpxq> [Accessed May 31, 2018].

Met Office, 2016b. North West England & Isle of Man: climate. Available at: www.metoffice.gov.uk/climate/uk/regional-climates/nw [Accessed May 31, 2018].

Met Office, 2015. The heatwave of 2003.

Met Office, 2016c. UK regional climates. Available at: www.metoffice.gov.uk/climate/uk/regional-climates [Accessed May 31, 2018].

Met Office, 2012. *Weather and climate*,

Middel, A. et al., 2014. Impact of urban form and design on mid-afternoon microclimate in Phoenix Local Climate Zones. *Landscape and Urban Planning*, 122, pp.16–28. Available at: <http://dx.doi.org/10.1016/j.landurbplan.2013.11.004>.

Mills, G., 2014. Urban climatology : History , status and prospects. *Urban Climate*, 10, pp.479–489.

Minitab, 2014a. How to Correctly Interpret P Values. Available at: <http://blog.minitab.com/blog/adventures-in-statistics-2/how-to-correctly-interpret-p-values> [Accessed June 3, 2018].

Minitab, 2013a. Multiple Regression Analysis: Use Adjusted R-Squared and Predicted R-Squared to Include the Correct Number of Variables. Available at: <http://blog.minitab.com/blog/adventures-in-statistics-2/multiple-regression-analysis-use-adjusted-r-squared-and-predicted-r-squared-to-include-the-correct-number-of-variables> [Accessed June 4, 2018].

Minitab, 2013b. Regression Analysis: How Do I Interpret R-squared and Assess the Goodness-of-Fit? Available at: <http://blog.minitab.com/blog/adventures-in-statistics-2/regression-analysis-how-do-i-interpret-r-squared-and-assess-the-goodness-of-fit> [Accessed June 4, 2018].

- Minitab, 2014b. Regression Analysis: How to Interpret S, the Standard Error of the Regression. Available at: <http://blog.minitab.com/blog/adventures-in-statistics-2/regression-analysis-how-to-interpret-s-the-standard-error-of-the-regression> [Accessed June 4, 2018].
- Minitab, 2014c. Which Is Better, Stepwise Regression or Best Subsets Regression? Available at: <http://blog.minitab.com/blog/adventures-in-statistics-2/which-is-better-stepwise-regression-or-best-subsets-regression> [Accessed June 5, 2018].
- MIT, 2018. Urban Weather Generator 4.1: urban heat island effect modeling software. *Massachusetts Institute of Technology*. Available at: <http://urbanmicroclimate.scripts.mit.edu/uwg.php> [Accessed May 2, 2018].
- Mohajeri, N. et al., 2016. Effects of urban compactness on solar energy potential. *Renewable Energy*, 93, pp.469–482.
- Morganti, M. et al., 2017. Urban morphology indicators for solar energy analysis. *Energy Procedia*, 134, pp.807–814. Available at: <https://doi.org/10.1016/j.egypro.2017.09.533>.
- Morganti, M., Coch Roura, H. & Cecere, C., 2012. THE EFFECT OF URBAN OBSTRUCTIONS IN MEDITERRANEAN CLIMATES: BUILT FORM TYPOLOGY, DENSITY AND ENERGY. *Architecture, city and environment*, (19), pp.13–26.
- Moughtin, C., 2003. *URBAN DESIGN: STREET AND SQUARE* third edit., Oxford: Architectural Press, Elsevier.
- Mumovic, D. & Santamouris, M. eds., 2009. *A Handbook of Sustainable Building Design and Engineering: An Integrated Approach to Energy, Health and Operational Performance*, London: Earthscan.
- Municipal Dreams, 2015. Liverpool’s Interwar Multi-Storey Housing: Building an ‘A1 community in a properly planned township of flats.’ Available at: <https://municipaldreams.wordpress.com/2015/02/10/liverpools-interwar-multi-storey-tenements-building-an-a1-community-in-a-properly-planned-township-of-flats/> [Accessed June 23, 2018].

Nakano, A., 2015. *URBAN WEATHER GENERATOR, USER INTERFACE DEVELOPMENT*. MIT.

Nakano, A., Bueno, B., Norford, L. & Reinhart, C.F.C.F., 2015. URBAN WEATHER GENERATOR – A NOVEL WORKFLOW FOR INTEGRATING URBAN HEAT ISLAND EFFECT WITHIN URBAN DESIGN PROCESS. In *Proceedings of BS2015: 14th Conference of International Building Performance Simulation Association*. Hyderabad, India, pp. 1901–1908.

Nakano, A., Bueno, B., Norford, L. & Reinhart, C.F., 2015. URBAN WEATHER GENERATOR – A NOVEL WORKFLOW FOR INTEGRATING URBAN HEAT ISLAND EFFECT WITHIN URBAN DESIGN PROCESS Massachusetts Institute of Technology , Cambridge , USA Fraunhofer Institute for Solar Energy Systems ISE , Germany SIMULATION ENGINE & PLATFOR. *Building Simulation Conference*, pp.1901–1908.

Nasrollahi, N. & Shokri, E., 2016. Daylight illuminance in urban environments for visual comfort and energy performance. *Renewable and Sustainable Energy Reviews*, 66, pp.861–874. Available at: <http://dx.doi.org/10.1016/j.rser.2016.08.052>.

NES, A. van, PONT, M.B. & MASHHOODI, B., 2012. COMBINATION OF SPACE SYNTAX WITH SPACEMATRIX AND THE MIXED USE INDEX . The Rotterdam South test case. *Eighth International Space Syntax Symposium*, (October 2015).

Ng, E. ed., 2010. Designing high-density cities for social and environmental sustainability. In London: Earthscan.

Nichol, J. & Wong, M.S., 2005. Modeling urban environmental quality in a tropical city. *Landscape and Urban Planning*, 73(1), pp.49–58.

Nikolopoulou, D.M. ed., 2004. *Designing Open Spaces in the Urban Environment: a Biolimatic Approach*, Centre for Renewable Energy Sources (C.R.E.S.). Available at: <http://www.ncbi.nlm.nih.gov/pubmed/15003161><http://cid.oxfordjournals.org/lookup/doi/10.1093/cid/cir991><http://www.scielo.cl/pdf/udecada/v>

15n26/art06.pdf%5Cnhttp://www.scopus.com/inward/record.url?eid=2-s2.0-84861150233&partnerID=tZOtx3y1.

Nouri, A.S., Costa, J.P. & Matzarakis, A., 2017. Examining default urban-aspect-ratios and sky-view-factors to identify priorities for thermal-sensitive public space design in hot-summer Mediterranean climates: The Lisbon case. *Building and Environment*, 126(July), pp.442–456. Available at: <https://doi.org/10.1016/j.buildenv.2017.10.027>.

Nourian, P., Rezvani, S. & Sariyildiz, S., 2013. Designing with Space Syntax. In *eCAADe 31*. Netherlands, Delft, pp. 357–366.

Nunez, M. & Oke, T.R., 1977. The Energy Balance of an Urban Canyon. *Journal of Applied Meteorology*, 16(1), pp.11–19.

Oke, T.R., 2004. Initial guidance to obtain representative meteorological observations at urban sites. *World Meteorological Organization*, (81), p.51.

Oke, T.R., 1988. The urban energy balance. *Progress in Physical Geography*, 12(4), pp.471–508.

Olgyay, V., Olgyay, A. & Lyndon, D., 2015. *Design with climate : bioclimatic approach to architectural regionalism* New and ex., Princeton University Press- New Jersey- USA.

Oliveira, V., 2016. *Urban Morphology: An Introduction to the Study of the Physical Form of Cities*, Switzerland: Springer International Publishing.

Orme, J.G. & Orme, T.C., 2009. Multiple Regression with Discrete Dependent Variables. Available at: <http://ebookcentral.proquest.com/lib/liverpool/reader.action?docID=415559&ppg=22>.

Ozkeresteci, I. et al., 2003. Use and Evaluation of the Envi-Met Model for Environmental Design and Planning: an Experiment on Linear Parks. *Catographic Renaissance*, (August), pp.402–409.

Pan, X. et al., 2008. Analyzing the Variation of Building Density Using High Spatial

- Resolution Satellite Images the Example of Shanghai City. *sensors*, 8, pp.2541–2550.
- Paramita, B. et al., 2016. Optimization of Design and Planing VHS Building Using Chronolux. *Indonesian Journal of Science & Technology*, 1(2), pp.170–184.
- Park, B., Oh, K. & Hong, S., 2018. Analysis of the Changes in Urban Thermal Environments Considering Development Densities (FAR and BCR). *International Journal of Environmental Science and Development*, 9(2), pp.32–37.
- Petralli, M. et al., 2014. Urban planning indicators: useful tools to measure the effect of urbanization and vegetation on summer air temperatures. *International Journal of Climatology*, 34(4), pp.1236–1244. Available at: <http://doi.wiley.com/10.1002/joc.3760>.
- Polo, C.S. et al., 2016. Solar radiation and daylighting assessment using the Sky-View Factor (SVF) analysis as method to evaluate urban planning densification policies impacts. *Energy Procedia*, 91(0), pp.989–996. Available at: <http://dx.doi.org/10.1016/j.egypro.2016.06.266>.
- Pont, M.B. & Haupt, P., 2009. *Space, Density and Urban Form*. Delft University of Technology. Available at: repository.tudelft.nl/islandora/object/uuid:0e8cdd4d-80d0-4c4c-97dc-dbb9e5eee7c2/.
- Pont, M.B. & Haupt, P., 1900. The Spacemate : Density and the Typomorphology of the Urban Fabric. , pp.55–68.
- Population Reference Bureau, 2016. 2016 World Population Data Sheet. Available at: <http://www.prb.org/pdf16/prb-wpds2016-web-2016.pdf>.
- Rehman, N.U. & Uzair, M., 2017. The proper interpretation of analytical sky view factors for isotropic diffuse solar irradiance on tilted planes. , 053702.
- Robinson, D., 2006. Urban morphology and indicators of radiation availability. *Solar Energy*, 80(12), pp.1643–1648.
- Rodríguez-Algeciras, J. et al., 2018. Influence of aspect ratio and orientation on large courtyard thermal conditions in the historical centre of Camagüey-Cuba.

- Renewable Energy*, 125, pp.840–856.
- Roth, M. et al., 2011. ICUC-7 Urban Climate Special Issue. *International Journal of Climatology*, 31(2), pp.159–161.
- Rzepa, M., 2009. The map of sky view factor in the center of lodz. In *The 7th International Conference on Urban Climate*. Yokohama, Japan, p. 4.
- Salingaros, N.A., 2000. Complexity and Urban Coherence. *Journal of Urban Design*, 5(3), pp.291–316.
- Salingaros, N.A., 1999. Urban Space and its Information Field. *Journal of Urban Design*, 4(1), pp.29–49.
- Salvati, A., Cecere, C. & Coch, H., 2015. Microclimatic response of urban form in the Mediterranean context. In *City as organism. New vision for urban life, 22nd ISUF International Conference*. Rome, Italy, pp. 719–728. Available at: <https://www.urbanform.it/city-as-organism-isuf-rome-2015/>.
- Salvati, A., Coch, H. & Morganti, M., 2017. Effects of urban compactness on the building energy performance in Mediterranean climate. *Energy Procedia*, 122(September), pp.499–504. Available at: <http://dx.doi.org/10.1016/j.egypro.2017.07.303>.
- Salvati, A., Palme, M. & Inostroza, L., 2017. Key Parameters for Urban Heat Island Assessment in A Mediterranean Context: A Sensitivity Analysis Using the Urban Weather Generator Model. In *IOP Conference Series: Materials Science and Engineering*.
- Sarralde, J.J. et al., 2015. Solar energy and urban morphology: Scenarios for increasing the renewable energy potential of neighbourhoods in London. *Renewable Energy*, 73, pp.10–17.
- Shaker, R.R. & Drezner, T.D., 2010. A New Technique for Predicting the Sky-View Factor for Urban Heat Island Assessment. , (Oke 1987), pp.85–96.
- Shishegar, N., 2013. Street Design and Urban Microclimate: Analyzing the Effects of Street Geometry and Orientation on Airflow and Solar Access in Urban Canyons.

- Journal of Clean Energy Technologies*, 1(1), pp.52–56. Available at: <http://www.jocet.org/show-7-273-1.html>.
- Silva, J.P., 2017. Solar radiation and street temperature as function of street orientation. An analysis of the status quo and simulation of future scenarios towards sustainability in Bahrain. *E3S Web of Conferences*, 23, p.02002. Available at: <http://www.e3s-conferences.org/10.1051/e3sconf/20172302002>.
- Sinou, M., 2007. *Design and Thermal Diversity of Semi-enclosed Spaces* first edit., Cambridgeshire - UK: MELROSE BOOKS.
- Srivanit, M. & Kazunori, H., 2011. The influence of urban morphology indicators on summer diurnal range of urban climate in Bangkok Metropolitan Area, Thailand. *International Journal of Civil & Environmental Engineering*, 11(5), pp.34–46.
- Steadman, P., 2014. Density and built form: Integrating “Spacemate” with the work of Martin and March. *Environment and Planning B: Planning and Design*, 41(2), pp.341–358.
- Steadman, P., Evans, S. & Batty, M., 2009. Wall area, volume and plan depth in the building stock. *Building Research and Information*, 37(5–6), pp.455–467.
- Stewart, I.D. & Oke, T.R., 2012. Local climate zones for urban temperature studies. *Bulletin of the American Meteorological Society*, 93(12), pp.1879–1900.
- Stewart, I.D., Oke, T.R. & Krayenhoff, E.S., 2014. Evaluation of the “local climate zone” scheme using temperature observations and model simulations. *International Journal of Climatology*, 34(4), pp.1062–1080.
- Steyn, D.G., 1980. The calculation of view factors from fisheye-lens photographs: Research note. *Atmosphere-Ocean*, 18(april 2015), pp.254–258.
- Street, M. et al., 2013. URBAN HEAT ISLAND IN BOSTON – AN EVALUATION OF URBAN AIR- TEMPERATURE MODELS FOR PREDICTING BUILDING ENERGY USE Massachusetts Institute of Technology , Cambridge , MA. In *Proceedings of BS2013: 13th Conference of International Building Performance Simulation Association*. Chambéry, France, pp. 1022–1029.

- Strømmandersen, J. & Sattrup, P.A., 2011. The urban canyon and building energy use: Urban density versus daylight and passive solar gains. *Energy and Buildings*, 43(8), pp.2011–2020.
- Sun, C.Y., 2011. A street thermal environment study in summer by the mobile transect technique. *Theoretical and Applied Climatology*, 106(3–4), pp.433–442.
- Svensson, M.K., 2004. Sky-view factor analysis – implications for urban air temperature differences. *Meteorological Applications*, 11(3), pp.201–211. Available at: <http://doi.wiley.com/10.1017/S1350482704001288>.
- Svensson, M.K. & Eliasson, I., 2002. Diurnal air temperatures in built-up areas in relation to urban planning. *Landscape and Urban Planning*, 61(1), pp.37–54.
- Sykes, O. et al., 2013. City profile A City Profile of Liverpool. *Cities*, 35, pp.299–318. Available at: <http://dx.doi.org/10.1016/j.cities.2013.03.013>.
- Szokolay, S.V., 2014. *Introduction to architectural science : the basis of sustainable design* 3rd ed.,
- T.R.OKE, *Boundary Layer Climates* Second edi., London: Routledge,.
- Taesler, R., 1991. The bioclimate in temperate and northern cities. *International Journal of Biometeorology*, 35(3), pp.161–168.
- Takebayashi, H., 2015. *Improvement measures of urban thermal environment*,
- Taleghani, M., 2014. *Dwelling on Courtyards: Exploring the energy efficiency and comfort potential of courtyards for dwellings in the Netherlands*, Rotterdam: Delft University of Technology.
- Taleghani, M., Tenpierik, M., van den Dobbelsteen, A., et al., 2014. Heat mitigation strategies in winter and summer: Field measurements in temperate climates. *Building and Environment*, 81, pp.309–319. Available at: <http://dx.doi.org/10.1016/j.buildenv.2014.07.010>.
- Taleghani, M. et al., 2015. Outdoor thermal comfort within five different urban forms in the Netherlands. *Building and Environment*, 83, pp.65–78. Available at: <http://linkinghub.elsevier.com/retrieve/pii/S0360132314000730>.

- Taleghani, M., Tenpierik, M. & van den Dobbelsteen, A., 2014. Indoor thermal comfort in urban courtyard block dwellings in the Netherlands. *Building and Environment*, 82, pp.566–579. Available at: <http://dx.doi.org/10.1016/j.buildenv.2014.09.028>.
- Tan, J. et al., 2010. The urban heat island and its impact on heat waves and human health in Shanghai. *International Journal of Biometeorology*, 54(1), pp.75–84.
- The guardian, 2018. Summer 2018 was UK's joint hottest on record, Met Office says. Available at: www.theguardian.com/uk-news/2018/sep/03/summer-2018-uk-joint-hottest-on-record-met-office-says [Accessed October 5, 2018].
- Tong, S. et al., 2018. Study on correlation between air temperature and urban morphology parameters in built environment in northern China. *Building and Environment*, 127(November 2017), pp.239–249.
- Unger, J., 2009. Connection between urban heat island and sky view factor approximated by a software tool on a 3D urban database. *International Journal of Environment and Pollution*, 36(1/2/3), p.59.
- Unger, J. et al., 2001. Land-use and meteorological aspects of the urban heat island. *Meteorological Applications*, 8(2), pp.189–194.
- Unger, J. et al., 2001. Urban temperature excess as a function of urban parameters in szeged, part 1: seasonal patterns. *Acta Climatologica et Chorologica*, 34–35, pp.5–14.
- United Nations, 2015. World Population Prospects The 2015 Revision Key Findings and Advance Tables. *Department of Economic and Social Affairs*,. Available at: https://esa.un.org/unpd/wpp/publications/files/key_findings_wpp_2015.pdf.
- Vanhoutteghem, L. et al., 2015. Impact of facade window design on energy , daylighting and thermal comfort in nearly zero-energy houses. *Energy & Buildings*, 102, pp.149–156. Available at: <http://dx.doi.org/10.1016/j.enbuild.2015.05.018>.
- Venerandi, A., Dibble, J. & Porta, S., 2017. Form and urban change – An urban

- morphometric study of five gentrified neighbourhoods in London. *Environment and Planning B: Urban Analytics and City Science*, 44(6), pp.1056–1076.
- Wang, B. & Kang, J., 2011. Effects of urban morphology on the traffic noise distribution through noise mapping: A comparative study between UK and China. *Applied Acoustics*, 72(8), pp.556–568. Available at: <http://dx.doi.org/10.1016/j.apacoust.2011.01.011>.
- Wang, Y. & Akbari, H., 2014. Effect of Sky View Factor on Outdoor Temperature and Comfort in Montreal. *Environmental Engineering Science*, 31(6), pp.272–287. Available at: <http://online.liebertpub.com/doi/abs/10.1089/ees.2013.0430>.
- Watson, I.D. & Johnson, G.T., 1988. Estimating person view-factors from fish-eye lens photographs. *International Journal of Biometeorology*, pp.123–128.
- Wei, R. et al., 2016. Impact of Urban Morphology Parameters on Microclimate. *Procedia Engineering*, 169, pp.142–149. Available at: <http://dx.doi.org/10.1016/j.proeng.2016.10.017>.
- Wong, N.H. et al., 2011. Evaluation of the impact of the surrounding urban morphology on building energy consumption. *Solar Energy*, 85(1), pp.57–71. Available at: <http://dx.doi.org/10.1016/j.solener.2010.11.002>.
- Y.Nakamura & T.R.Oke, 1988. Wind, temperature and stability conditions in an east-west oriented urban canyon. *Atmospheric Environment*, 22(12), pp.2691–2700.
- Yan, H., Fan, S., Guo, C., Wu, F., et al., 2014. Assessing the effects of landscape design parameters on intra-urban air temperature variability: The case of Beijing, China. *Building and Environment*, 76, pp.44–53. Available at: <http://linkinghub.elsevier.com/retrieve/pii/S0360132314000596>.
- Yan, H., Fan, S., Guo, C., Hu, J., et al., 2014. Quantifying the impact of land cover composition on intra-urban air temperature variations at a mid-latitude city. *PLoS ONE*, 9(7).
- Yang, P.P.J., Putra, S.Y. & Li, W., 2007. Viewsphere: A GIS-based 3D visibility analysis for urban design evaluation. *Environment and Planning B: Planning and Design*,

34(6), pp.971–992.

Young, R. & Sly, F., 2010. *Portrait of the North West*, Available at: www.ons.gov.uk/ons/rel/regional-trends/.../portrait-of-the-north-west.pdf.

Yousuf, M.U., Siddiqui, M. & Rehman, N., 2018. Solar energy potential estimation by calculating sun illumination hours and sky view factor on building rooftops using digital elevation model. , 013703.

Yuan, C. & Chen, L., 2011. Mitigating urban heat island effects in high-density cities based on sky view factor and urban morphological understanding: a study of Hong Kong. *Architectural Science Review*, 54(4), pp.305–315.

Yuan, J. et al., 2016. Application of glass beads as retro-reflective facades for urban heat island mitigation: Experimental investigation and simulation analysis. *Building and Environment*, 105, pp.140–152. Available at: <http://dx.doi.org/10.1016/j.buildenv.2016.05.039>.

Yunitsyna, A. & Shtepani, E., 2017. Urban Pattern Geometry and its Potential Energy Efficiency. *Journal of Contemporary Architecture*, 4(1), pp.29–34.

Zhang, J. et al., 2012. Evaluating environmental implications of density: A comparative case study on the relationship between density, urban block typology and sky exposure. *Automation in Construction*, 22, pp.90–101. Available at: <http://dx.doi.org/10.1016/j.autcon.2011.06.011>.

Zwolinski, a. & Jarzemski, M., 2015. Computing and monitoring potential of public spaces by shading analysis using lidar data in 3D city models. In *ISPRS - International Archives of the Photogrammetry, Remote Sensing and Spatial Information Sciences*. pp. 743–750. Available at: <http://www.int-arch-photogramm-remote-sens-spatial-inf-sci.net/XL-7-W3/743/2015/>.